Purification and characterization of extracellular vesicles released from pluripotent stem cells

Yi Xin Fiona Lee

A thesis submitted for the degree of *Doctor of philosophy* in the division of medical sciences

Department of Physiology, Anatomy and Genetics, University of Oxford

St Hilda's College

Hillary Term 2015

Acknowledgements

Firstly, I would like to thank both of my supervisors, Prof Matthew Wood and Dr Samir El Andaloussi for their constant guidance and supervision on my work, without which any of this would not have been possible. I would also like to mention a huge thank you to A*STAR, Singapore for supporting me in my studies. Next, I would like to thank everyone at Dr Paul Fairchild's lab, especially Mr Tim Davies, Dr Alison Leishmann and Miss Patty Sachmitr for teaching me and providing me their stem cell lines for this study. Also, I am very grateful to both Dr Imre Mäger and Dr Pieter Vader for their useful inputs in our daily discussions.

Next, I would like to mention a special thanks to the following groups of people:

To both old and current members of the Exosome group: Imre, Pieter, Aisling, Caz, Jinghuan, Kariem, Eduard, Aiman, Justin, Kenji, Amr and Chao. Thank you all very much for all the collaborative work on EVs within the Wood lab

To both old and current members of the student's office/Room 109: Tirsa, Sabrina, Karin, Anna, Aisling, Caz, Andrew D. Helen C, Sara, Giulia, Sarah and Lauren. Thank you very much for all the support and fun times both in and out of the office.

To all old and current members of the Wood lab for their help and feedback over the years: Graham, Mary, Kenji, Taeyoung, Tom M. Tom R. Gareth, Miguel, Suzan, Melissa, Corinne, Raquel, Carlo, Katie, Helen O. and everyone else whom I might have missed out.

To all of my collaborators whom have allowed me to participate in their work:

To all members of the Andaloussi lab in Karolinska Institutet (KI), especially to Joel and Oscar for the collaborative work on both the purification and bio-distribution study. Also, thanks for their constant hospitality and kindness during my visits to KI.

To Dr Yiqi Seow (A*STAR, Singapore) for introducing me to the Wood lab and giving me constant guidance regarding EV work during my annual visits back home. To Dr Henrik Johansson and Dr Janne Lethiö (KI) for all the help with processing and analysis of the numerous EV samples in many of the different studies we have started. To Dr Wolf Heusermann and Dr Nicole Meisner-Kober for all the help with the purification paper, especially with the data from FCS. To Dr Jarred Bultema, Dr Jonathan Gilthorpe and Dr Suzanne Gabrielsson for all other collaborative work on the purification paper. To Dr Sarita Panula for all the human ES EV samples.

To Dr Yoshi Aoki for including me in the study of vesicles for his ALS work and also providing me constant guidance and company in the evenings in the lab.

To the following people for their technical help:

To Dr Chris Gardiner for introducing me to the Nanosight and teaching me all the technical know-hows of this machine. To Dr Holger Kramer (OXION) for teaching and helping me with the AKTA machine for LC purification of EVs. To Ms Sheena Lee for teaching me how to operate the RNA bioanalyzer machine.

Apart from my colleagues in the lab, I would like to give special thanks to the following groups of friends:

To all my badminton and tennis buddies, Shermin, Amy, Aiman, Akash, Meijia, Jinquan, Amog, Phil, Yao, Jed and all other members of the Oxford badminton clubnight sessions. Thank you all for the fun game times and weekend gatherings to help me de-stress at work.

To my best friends from college: Mengyun, Kaiwen and Ethan. Thank you for constantly feeding me nutritious food and travels around and outside the UK.

To the group whom has constantly accompanied me for food trips to London: Michelle, Teresa, Xianning, Meijia, Sook Yee, and Yunhwa. Thank you for joining me in my indulgence in every other month. To the rest of the A*STAR family of scholars here in Oxford, especially Shermin, Diane, Kao Chin, Huijia, Sook Yee, thank you for the weekend meeting up and chatting sessions.

Last but not the least, thank you to my family for their continuous support over the last few years.

Abstract

Purification and characterization of extracellular vesicles released from pluripotent stem cells

Yi Xin Fiona Lee
St Hilda's College

DPhil
Hillary term 2015

Extracellular vesicles (EVs) are nano-sized particles constitutively released from cells into biological fluids such as blood, plasma, saliva and urine. Interestingly, these vesicles contain genetic cargoes including proteins, RNA and bioactive lipids that can be functionally delivered and affect recipient cells. Hence, EVs are postulated to be an alternative source of cell-cell communication in both normal physiological systems and pathological situations. Recently, EVs from mesenchymal stem cells have been shown to promote regeneration of injured cells. Induced pluripotent stem cells (iPSCs) are a relative newer type of stem cells that is emerging as useful tools for re-modeling diseases. However, knowledge about EVs from iPSCs is relatively sparse. In initial experiments, we successfully purified EVs from mouse iPSCs using the differential ultracentrifugation (UC) method. However, we noticed a discrepancy between total particle counts and expression of EV markers, across different EV batches. One crucial prerequisite for EV research is the availability of a standardized workflow for collection and purification of EVs from biological sources. Increasing evidence from recent studies has suggested that the original UC method is limited by several shortcomings such as low EV yield, purity and altered biophysical properties. Hence, this has led to a new wave in the development of alternative EV purification strategies. In this thesis, we start with a systematic comparison study between UC and an alternative purification protocol,

size-exclusion liquid chromatography (LC) of EVs from serum-free conditions. We found that LC is better than UC in terms of overall EV yields, purity and vesicle integrity. Subsequently, we demonstrate that LC allowed for the derivation of pure EVs from complex media sources used for growing stem cells like iPSCs, which was previously impossible with UC. Lastly, we describe novel data on the characterization of EVs from pluripotent stem cell sources and discuss the possible roles of these EVs in stem cell biology.

List of abbreviations

AB	Apoptotic body
ACN	Acetonitrile
AFM	Atomic force microscopy
AMPA	α-amino-3-hydroxy-5-methyl-4-isoxazolepropionic acid
APC	Antigen presenting cell
ARF6	ADP ribosylation factor 6
ASCC3	Activating signal co-integrator 1 complex subunit 3
ATP	Adenosine 5'-triphosphate
BCA	Bicinhoninic acid
BMP4	Bone morphogenetic protein-4
CD11c	Cluster of differenitation 11c
CD81	Cluster of differenitation 81
CD9	Cluster of differentiation 9
CM	Conditioned media
DAMP	damage-associated molecular patterns
DC	Dendritic cell
ddH_20	deionized water
DEL-1	Developmental endothelial locus-1
DiR	1,1'-Dioctadecyl-3,3,3',3'-Tetramethylindotricarbocyanine Iodide
DMEM	Dulbecco's modified eagle medium
DNA	Deoxyribonucleic acid
DRF3	Diaphanous-related formin-3
DTT	Dithiothreitol
EDTA	Ethylenediaminetetraacetic acid
EGFR	Epidermal growth factor receptor
ELISA	Enzyme-linked immunosorbent assay
EPHX1	Epoxide hydrolase 1
ERK	Extracellular signal-receptor kinase
ESC	Embryonic stem cell
ESCRT	Endosomal sorting complex required for transport
EV	Extracellular vesicles
FA	Formic acid
FBS	Fetal bovine serum
FCS	Fluorescent correlation spectroscopy
FDR	False discovery rate
FT	Flow-through
GATA-2	GATA binding protein 2
GFP	Green fluorescent protein
GM-CSF	granulocyte-colony stimulating factor
GO	Gene ontology
GTP	Guanosine triphosphate
HDAC2	Histone deacetylase 2
HEK 293T	Human embryonic kidney cell line
HEPES	hydroxyethylpiperazine-*N*'-2-ethanesulfonic acid

HER-2	Human epidermal growth factor receptor-2
HGF	Hepatocyte growth factor
Hh	Hedgehog
HNF3β	Hepatocyte nuclear factor 3β
HoxB4	Homeobox B4
HPC	Haematopoietic progenitor cell
IAA	Iodoacetamide
ICM	Inner cell mass
IDO	Indoleamine2,3-deoxygenase
IFN-γ	interferon-γ
IGF-1	Insulin-like growth factor-1
IL-10	Interleukin-10
IL-4	Interleukin-4
IL-6	Interleukin-6
IL-8	Interleukin-8
ILV	Intraluminal vesicles
iPSC	induced pluripotent stem cell
IVIS	In Vivo Imaging System
KLF4	Kruppel-like factor 4
KOSR	Knockout serum replacement media
LC	Liquid chromatography
LC-MS/MS	Liquid chromatography–tandem mass spectrometry
LRRK2	Leucine-rich repeat kinase 2
MAPK	Mitogen-activated protein kinases
MEF	Mouse embyronic feeder cell
MFG-E8	Milk fat globule-epidermal growth factor 8
MHC	Major histocompatibility complex
MIF	Migration inhibitory factor
miRNA/miR	micro-ribonucleic acid
mLIF	mouse leukaemia inhibitory factor
MLL4	Myeloid/lymphoid or mixed-lineage leukemia 4
MQ	Milli-Q
mRNA	messenger-ribonucleic acid
MRPS25	Mitochondrial ribosomal protein S25
MSC	Mesenchymal stem cell
MVE	Multivesicular endosome
MYG1	melanocyte proliferating gene
N2a	Neuro2a mouse neuroblastoma cell line
NaOH	Sodium hydroxide
NIH	National Institutes of Health
NK	Natural killer
NKG2D	Natural-killer group 2, member D
Notch1-4	Notch receptor ligand Delta-like 4
NSC-34	Spinal cord neuron and neuroblastoma hybrid cell line
NTA	Nanoparticle tracking analysis
OLIG2	Oligodendrocyte lineage transcription factor 2

OM	OptiMEM
P/S	Penicillin/Streptomycin
P2X	Purinoreceptor
PAGE	Polyacrylamide gel electrophoresis
PAMP	Pathogen-associated molecular patterns
PBS	Phosphate buffer saline
PDCD6IP/ALIX	Programmed cell death 6-interacting protein
PEI	Polyethyleneimine
PGE2	Prostaglandin E2
PLD2	Phospholipase D2
POU5F1/OCT-4	POU domain, class 5, transcription factor 1/Octamer-binding transcription factor 4
PS	Phosphatidylserine
PVDF	Polyvinylidene fluoride
qPCR	quantitative real-time Polymerase Chain Reaction
REX-1	zinc finger protein 42
RIPA	Radioimmunoprecipiation assay
RNA	Ribonucleic acid
RT	Room temperature
RT-PCR	Real-time polymerase chain reaction
RVG	Rabie virus glycoprotein
siRNA	Short interfering RNAs
SCF	Stem cell factor
SCL	Stem cell leukaemia
SDS	Sodium dodecyl sulfate
SERPINF1/PEDF	serpin F1/Pigment epithelium-derived factor
SFRP2	Secreted frizzled related protein-2
SHH	Sonic hedgehog
SH-SY5Y	Human neuroblastoma cell line
snoRNA	Small nucleolar ribonucleic acid
SOX2	Sex determining region Y-box 2
TBS	Tris buffer saline
TBS-T	Tris buffer saline with 0.1% Tween-20
TEM	Transmission electron microscopy
TFF	Tangential flow filtration
TGF-β1	Tumour growth factor-beta 1
Th1	Type 1 T helper cells
TIRF	Total internal reflection fluorescence
TNF	Tumour necrosis factor
TNF-α	tumour necrosis factor-α
TRAIL	TNF-related apoptosis-inducing ligand
tRNA	Transfer ribonucleic acid
TSG101	Tumor susceptibility gene 101
UC	Ultracentrifugation
UF	Ultrafiltration
VEGF	Vascular endothelial growth factor
WB	Western blotting

Table of contents

Chapter 1: Introduction

1.1 Extracellular vesicles (EVs)……13

1.1.1 Definition of EVs
1.1.2 Protocols for purification of EVs
1.1.3 Tools for characterisation and analysis of EVs
1.1.4 Applications of EVs in biological and medical sciences

1.1.4.1 EVs in normal physiology
1.1.4.2 EVs in pathogenesis and aiding the spread of diseases
1.1.4.3 EVs as biomarkers of diseases
1.1.4.4 EVs as therapeutic targets and tools

1.2 Preliminary data on pluripotent stem cell EVs

1.3 Aims and outline of this study

Chapter 2: General material and methods

2.1 Cell culture of cells…….....61

2.1.1 Immortalised mouse and human cell lines
2.1.2 Mouse pluripotent stem cell lines and embryonic fibroblasts

2.2 Collection of conditioned media from cell lines

2.2.1 Immortalised mouse and human cell lines
2.2.2 Mouse pluripotent stem cell lines

2.3 Purification of EVs

2.3.1 Differential centrifugation protocol (UC)
2.3.2 Size-exclusion liquid chromatography protocol (LC)

2.4 Quantification and characterization of EVs

2.4.1 Nanoparticle tracking analysis (NTA)
2.4.2 Protein quantification of EVs and cell lysates
2.4.3 Western blotting (WB)
2.4.4 Transmission electron microscopy (TEM)
2.4.5 Trizol extraction of RNA from EVs and cells
2.4.6 RNA profiling with RNA bioanalyzer
2.4.7 LC-MS/MS proteomic analysis

Chapter 3: Optimisation of protocol for collection and purification of EVs from serum-free cultures

3.1 Introduction……..72

3.2 Materials and methods

3.2.1 Investigation on the effect of external culturing factors on EV quantity and content
3.2.2 Comparison study between two different purification methods
3.2.3 Molecular quantification and characterisation of EVs for comparison study
3.2.4 Biophysical characterization of EVs for comparison study
- Fluorescence microscopy
- Fluorescence correlation spectroscopy (FCS)
- Total internal reflection fluorescence microscopy (TIRF)
- EV biodistribution in mice

3.2.5 Statistics

3.3 Results

3.3.1 Proliferation rate and morphology of N2a cells is altered in serum-free culture conditions
3.3.2 Serum-free conditions and increased incubation time prior to EV collection leads to greater EV yields
3.3.3 Serum-free conditions lead to secretion of EVs with an altered proteome
3.3.4 Limitations of the UC protocol for purification of EVs
3.3.5 Ultrafiltration (UF) of CM allows for purification of higher yields of intact EVs than with the UC protocol
3.3.6 UF co-purifies non-vesicular proteins along with EVs
3.3.7 LC separates EVs from non-vesicular proteins
3.3.8 EVs purified by UF-LC maintain their biophysical properties in contrast to EVs purified by UC
3.3.9 LC methodology is applicable for purification of EVs from serum-containing media

3.4 Discussion

3.4.1 Serum-free conditions lead to increased production of EVs with different proteome
3.4.2 The UC protocol is not ideal for EV purification
3.4.3 Ultrafiltration (UF) of sample leads to higher EV yields but with co-purification of proteins
3.4.4 Subsequent LC allows for separation of EVs from contaminating proteins without affect EV yield and integrity

3.5 Conclusion

Chapter 4: Optimisation of protocol for collection and purification of EVs from pluripotent stem cell sources

4.1 Introduction……120

4.2 Material and methods

4.2.1 Evaluation of stem cells in different media types
4.2.2 Comparison study of stem cell EVs purified by UC or UF-LC method
4.2.3 Sucrose gradient density centrifugation of EVs
4.2.4 Molecular and biophysical characterisation of stem cell EVs
4.2.5 Statistics

4,3 Results

4.3.1 Use of alternative types of serum-depleted media is not a viable option for EV collection from stem cells
4.3.2 UF-LC fractionation of stem cell CM allows for the purification of EVs
4.3.3 LC protocol is highly reproducible for EV purification from stem cells
4.3.4 UC purified samples contain more particles, protein and RNA than LC-derived samples
4.3.5 UC pellet displays different molecular characteristics as compared to the LC product
4.3.6 Sucrose gradient floatation of UC pellet shows discrepancy in EV density determination
4.3.7 LC fractionation of UC pellet reveals co-precipitation of proteins
4.3.8 LC samples float at lower densities than UC samples
4.3.9 Additional LC fractionation improves the EV purity marginally

4.4 Discussion

4.4.1The use of serum-replacement media is most ideal for collection of stem cell EVs
4.4.2 LC method highlights the various problems associated with UC purification of EVs from stem cell sources
4.4.3 EVs may function as ‘sponges’ for free proteins in the extracellular environment

4.5 Conclusion

Chapter 5: Characterisation of EVs from pluripotent stem cells

5.1 Introduction……171

5.2 Material and methods

5.2.1 Comparison of EVs from mouse iPSCs and mouse ESCs
5.2.2 Molecular quantification and characterisation of mouse EVs and cell lysates for stem cell comparison study
5.2.3 Characterisation of EVs from human pluripotent stem cell lines
5.2.3.1 Culturing conditions of Human iPSCs
5.2.3.2 Culturing conditions of Human ESCs
5.2.3.3 Molecular quantification and characterisation of human EVs for human stem cell comparison study
5.2.4 Characterisation of EVs from DCs differentiated from human iPSCs
5.2.4.1 Directed differentiation of Human iPSCs into DCs
5.2.4.2 Maturation of DCs differentiated from human iPSCs
5.2.4.3 Collection of EVs and molecular characterisation of EVs from DCs
5.2.5 Statistics

5.3 Results

5.3.1 EVs from mouse iPSCs and ESCs have similar size distribution profiles and expression of EV markers
5.3.2 EVs display very different protein and RNA profile as compared to their parental cells
5.3.3 Preliminary proteomics on stem cell media sample reveal the presence of contaminating proteins
5.3.4 EVs from both cell types contain proteins mapping to similar GO annotations
5.3.5 EVs from mouse iPSCs have fairly different proteome as compared to their parental cells
5.3.6 LC purification EVs shows the presence of relatively few particles from human iPSCs
5.3.7 LC purification of EVs from human ESCs shows the presence of relatively more particles with the detection of EV markers
5.3.8 Differentiation of human iPSCs into DCs shows the presence of particles with EV markers

5.4 Discussion

5.4.1 Proteomics on EVs reveal the presence of contaminating proteins derivative from the media and gelatin
5.4.2 EVs across both stem cell types show little difference in overall proteome
5.4.3 Reduced EV secretion from human iPSCs may be cell type specific

5.5 Conclusion

Chapter 6: General discussion and conclusion

6.1 Summary of findings from the current study……215

6.1.1 LC is a more optimal method for purification of EVs than UC
6.1.2 LC allows for the purification EVs from stem cell sources
6.1.3 EVs from mouse iPSCs and ESCs are similar in both molecular and physical aspects

6.2 Limitations and future directions from the current study

6.2.1 LC method for purification of EVs
6.2.2 Characterisation studies on stem cell vesicles

6.3 Concluding remarks

Chapter 7: References…….227

Chapter 8: Appendix……261

8.1 Abstracts accepted for conferences and seminars
8.2 Manuscripts accepted for publication

Chapter 1

Introduction

1.1 Extracellular vesicles (EVs)

The first report regarding secretory vesicles from cells was in 1967 where Wolf described the presence of minute phospholipid-rich, pro-coagulant material from fresh platelet-free plasma and termed these “platelet-dust” (1). Subsequently, Raz and colleagues demonstrated the release of membrane particles from ascites fluid (2). Interestingly, they found that these vesicles express tumour-specific antigens on their surface and hence the vesicles were suggested to provide protection against detection by the host immune system and further encourage tumourigenicity. A few years later, Trams and colleagues (3) reported the release of two pools of differentially sized vesicles from a variety of cells; a smaller group of around 40nm in diameter and a more heterogeneous pool ranging from 500-1000nm. As these vesicles were collected from the cell supernatant, they initially named both groups of vesicles as “exosomes”. Importantly, one needs to be caution not to confuse these exosomes from cells with the other biological “exosome”, which is used to define an intracellular complex involved in RNA editing (4). Following these early studies, two other groups subsequently described the presence of 50nm-sized vesicles released from reticulocytes (5,6). Based on electron microscopy and biochemical techniques (7,8), the authors specifically proved that these vesicles originated from multivesicular endosomes (MVEs) and were released when MVEs migrated and

fused with the plasma membrane. In 1987, Johnstone et al. re-classified these uniformly nano-sized vesicles of MVE origin as “exosomes”. On the other hand, the more heterogeneous sized vesicles, which directly shed from the plasma membrane, were termed “microvesicles”. A decade later, two studies showed that exosomes from immune cells were functional and could activate the adaptive immune response. In the first study, the authors demonstrated that major histocompatibility complex (MHC) class II was located on the surfaces of exosomes from both human and murine B-lymphocytes (9). Further, these exosomes were able to induce antigen-specific MHC class II-restricted T cell responses. In a subsequent study, the authors showed that dendritic cells (DCs) were also able to secrete exosomes expressing MHC class I and II as well as T-cell co-stimulatory molecules. When these DCs were pulsed with tumor peptide, the resultant exosomes released were able to eradicate or suppress the growth of tumours in a T-cell dependent manner (10). All in all, these early works established the starting point of vesicle research, and laid the foundation for subsequent global interest in exosomes and microvesicles today.

1.1.1 Definition of EVs

Generally, both exosomes and microvesicles are described as membranous vesicles that are released from a variety of different cell types via two distinct mechanisms as depicted in **figure 1.1** (11) and described below.

Figure 1.1

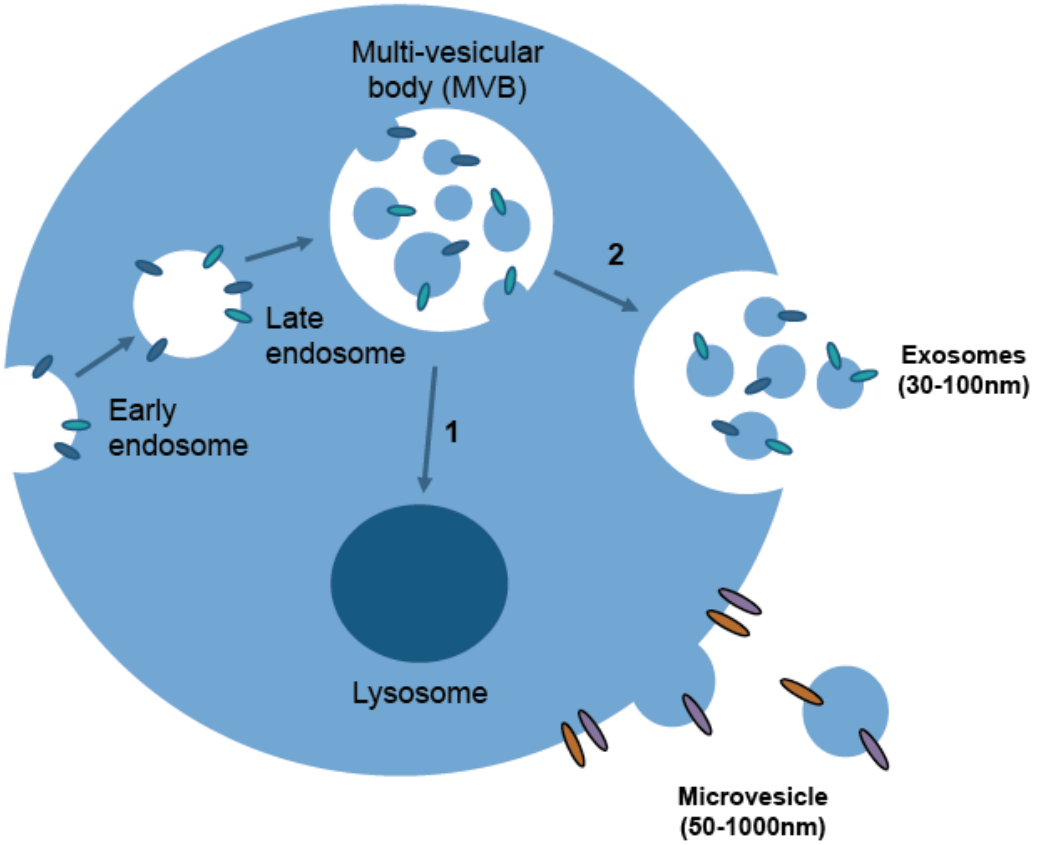

Figure 1.1

Illustration showing how EVs form and are released from cells.
Briefly, during endocytosis, the cell membrane buds inwards and results in the formation of early endosomes. Over time, these endosomes can mature into late endosomes where the endosomal membrane buds inward to form ILVs. The overall endosome carrying these ILVs is termed as the MVE. There are two downstream paths of the MVE: 1) The MVE fuses with lysosomes and the contents are processed for degradation. 2) The MVE migrates to and fuses with the plasma membrane. As a result, exosomes are released into the extracellular environment. Besides exosomes, another type of EV, microvesicles are formed by directly budding off the plasma membrane.

Exosomes are uniformly sized vesicles of around 30-100nm in diameter that emanate from the late endosome pathway. During endocytosis, the cell membrane

buds inwards, taking up a portion of the extracellular environment and resulting in the formation of early endosomes. Over time, these endosomes mature into late endosomes where the endosomal membrane buds inward to form intraluminal vesicles (ILVs). Consequentially, these larger endosomes that carry ILVs are termed MVEs. Recently, this particular cellular process has been shown to be controlled by both endosomal sorting complex required for transport (ESCRT)(12–16) and its associated proteins such as Alix (17,18) and Tsg101 (19). Alternatively, this process can also be regulated by ESCRT-independent machinery like ceramide, G-protein receptors and Rab GTPases (20–22). Following the formation of the MVEs, MVEs can fuse directly with lysosomes, allowing for the degradation of their content. However, we now know that some MVEs can instead migrate towards and fuse with the plasma membrane, which will subsequently lead to the release of exosomes into the extracellular environment. Based on several lines of evidences, the ultimate fate of MVEs can be influenced by Rab GTPases or even bioactive lipids and lipid-associated proteins (15,23,24). Interestingly, most of these mechanisms described are common across the biogenesis of exosomes from different cell sources. Furthermore, during the biogenesis process, some of these proteins can be integrated into EVs. Hence, many groups in the field frequently use the identities of these proteins (e.g. tetraspanins, flotillins, Rabs, Alix and Tsg101) as conserved markers indicative for all exosomes, irrespective of their cellular origin. On the other hand, depending on their parental cell source, exosomes can also contain cell-specific markers as depicted in **figure 1.2** (11).

Figure 1.2

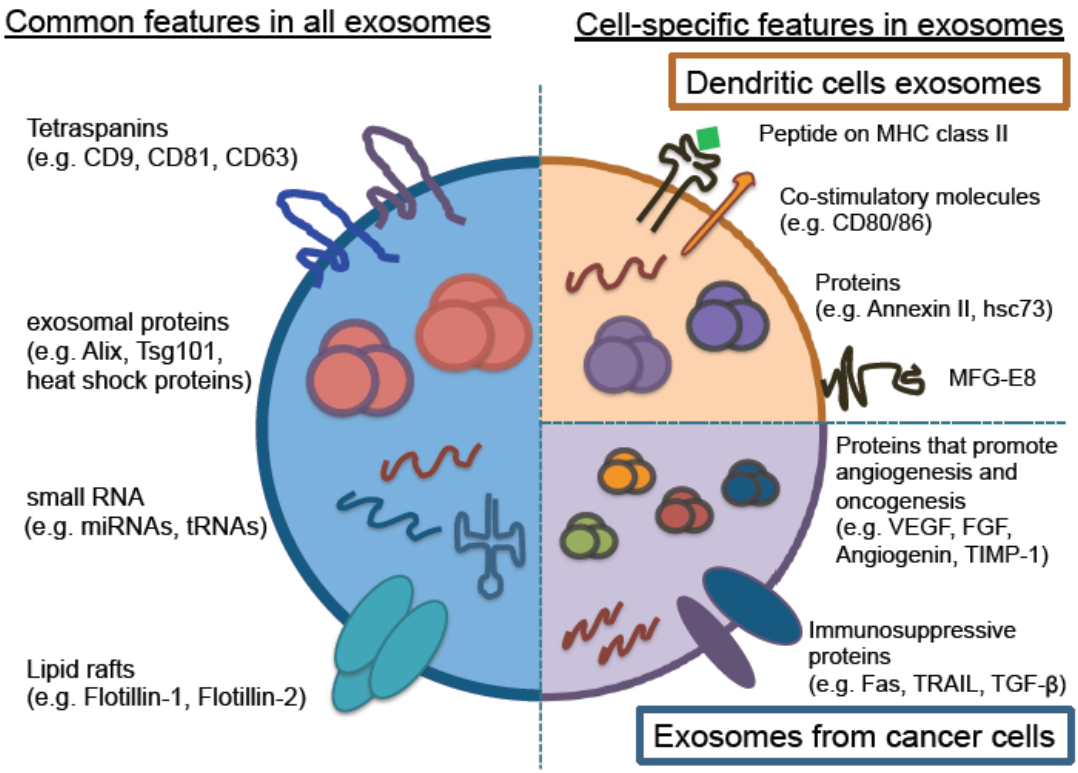

Figure 1.2

Graphic showing the common and cell-specific features reported for exosomes.
Exosomes have been reported to contain different proteins and RNAs that are common in all exosomes regardless of their cellular source, such as surface molecules like tetraspanins and lipid rafts, intra-exosomal proteins like Alix, Tsg101 and heat shock proteins and small RNA identities (left panel). In addition to these molecules, there are some evidences showing the presence of cell-specific molecules dependent on their parental source. Here we illustrate two examples from dendritic cells and cancer cells (right panel).

Unlike exosomes, microvesicles form through direct outward blebbing of the plasma membrane (25). In microglial cells, it has been shown that the activation of ATP-gated ion channels like $P2X_7$, can trigger several intracellular signaling events and result in membrane blebbing and release of microvesicles (26–28). Similarly, in

tumour cells, some studies have suggested that the activation of different signaling pathways can govern the formation of tumour microvesicles at the cell surface. Some examples include the ADP-ribosylation factor 6 (ARF6)-mediated extracellular signal-regulated kinases (ERK) in invasive melanoma cells (29) and the interaction between Diaphanous-related formin-3 (DRF3) and small Rho family GTPases in prostate cancer cells (30,31). Alternatively, others have reported that the microvesicle biogenesis and shedding from monocytes occur at regions on the cell membrane that appear to be enriched in specific lipids such as cholesterol (32,33). Interestingly, one study demonstrated that the ESCRT machinery, previously described in exosome biogenesis, could also stimulate the budding of retrovirus-like vesicles off cell membranes (34,35). As shown here, there are a variety of different mechanisms, which can regulate microvesicle blebbing. With hindsight though, all of these studies were conducted of different cell types. Hence, microvesicles are described as a more heterogeneous population of EVs, with variable sizes (50-1000nm in diameter) and expression of cell-specific cytoplasmic and membrane proteins.

Following the first studies on exosomes derived from reticulocytes (5,6), vesicle research has now rapidly extended across different biological systems. Many studies have described the release of and characteristics of exosomes and microvesicles secreted from most, if not all cells (e.g. dendritic cells (DCs), B-lymphocytes, epithelial cells, neurons, cardiomyocytes and stem cells). Moreover, vesicles can be detected in various biological fluids, including urine, blood, saliva, amniotic fluid, semen, cerebrospinal fluid and breast milk (9,10,36–41). In certain instances, some

have even chosen to adopt new nomenclature and to re-name these cell-type specific vesicles as listed in **Table 1.1** (38,42–62).

Table 1.1

Name	Type of EVs	Origin/Source	Reported biological/medical applications	References
Argosomes	Membrane exo-vesicles	Drosophila imaginal disc epithelium	• Aid in the spread of morphogens (e.g. Wingless protein) for tissue patterning	(42-44)
Cardiosomes	Microvesicles/ exosomes	Cardiomyocytes derived from adult mouse heart	• Facilitate an array of metabolism-related processes and gene expression changes when added to fibroblasts	(38)
Ectosomes	Microvesicles	Polymorphonuclear leucocytes, neutrophils and erythrocytes	• Anti-inflammatory/ immunosuppressive activities	(45-46)
Microparticles	Microvesicles	Platelets and endothelial cells into the blood	• Biomarkers of vascular injury and pro-thrombotic or pro-inflammatory conditions in different diseases (e.g. hypertension, cardiovascular disorders and pre-eclampsia) • Role in rheumatoid arthritis- amplification of inflammation	(47-52)
Prostasomes	Membranous vesicles	Secretions by the acinar epithelial cells of the prostate gland into seminal fluid	• Improvement of sperm motility • Capacitation and acrosome reaction of sperm • Coagulation and liquefaction of seminal fluid • Role in prostate cancer formation	(53-61)
Vexosomes	Exosomes	AAV-transduced	• More potent than conventionally purified AAV vectors, serving as an alternative strategy for better gene delivery	(62)

Table 1.1

Table showing alternative names described for cell-specific EVs.

Apart from exosomes and microvesicles, there is another known type of secretory vesicle that is released under specific cellular circumstances. When the apoptosis cascade is activated in cells, cellular debris and organelles segregate into membrane bound vesicles. These vesicles, also known as apoptotic bodies (ABs), bleb directly from these dying cells (63,64). As ABs are generally larger than exosomes and microvesicles (>1 μm), they are usually eliminated during the initial sample preparation process and are not mentioned in most exosome and microvesicle studies. Importantly though, one should remember that all healthy viable cells can release a mixture of different types of secretory vesicles actively into the extracellular environment. Due to limitations in current technologies and the lack of unique markers for each individual vesicle subpopulation, it is currently still not possible to

accurately differentiate and purify the different subpopulations of EVs (65). Hence, we, like others in the field (66), have chosen to use the collective term “extracellular vesicles (EVs)” to define all of the secretory vesicles described in this thesis.

1.1.2 Protocols for purification of EVs

The most common method for extracting EVs from cell supernatant or biological fluids is the differential ultracentrifugation (UC) method (67). Briefly, the biological sample containing EVs is first subjected to initial low speed spins to remove floating dead cells and larger cell debris and vesicles (e.g. apoptotic bodies). After decanting, the supernatant is subjected to an ultracentrifugation spin to pellet EVs. Usually, the EV pellet will be further treated with additional high-speed wash steps or floating on a sucrose gradient to effectively eliminate any contaminating proteins or RNAs to improve EV purity. As this UC protocol is relatively easy to perform and does not require any specialized equipment apart from an ultracentrifugation unit, which is commonly found in most laboratories, UC has been the most frequently used method to date, in the majority of published reports on EVs.

With the recent improvements in technological characterisation tools for EV phenotyping, it is becoming increasingly evident that the original UC protocol suffers from several drawbacks mainly related to the overall yield, purity and physical integrity of EVs. Concerns have been raised that the resultant EV yields by UC are very low as compared to the starting material and overall particle counts may be highly variable, depending on the individual operator. This low efficiency in EV pelleting has been linked to physical explanations such as the type of centrifugation

rotor (swing-bucket or fixed angle) used, the length of time samples were centrifuged (68) as well as to the viscosity of the sample (69). In addition, there is a need to further subject the derivative UC pellet to additional washes or floating on a sucrose gradient for “cleaning up” the EVs from any contaminants. Although these steps are crucial for improving the purity of the sample, they are often time-consuming and could further compromise the already low EV yields. Lastly, it has been speculated that the high gravitational-forces applied during the final UC steps may damage the integrity of EVs (70), which in turn, may account for the low EV yields measured in the UC pellet. For these reasons, there are several doubts on the reproducibility and reliability of characterisation data of EVs purified with the UC protocol.

In order to resolve this major problem in EV research, some have started developing new methods for EV purification, as summarised in **Table 1.2**. For example, there are various commercially available precipitation-based kits where EVs are captured with polymers (71), based on the expression of specific peptides (e.g. heat shock proteins) (72) or by capitalizing on the negative charge of EV surfaces (73). Although comparison studies have shown that these strategies are less time-consuming and relatively straightforward to conduct, the actual purity and biophysical integrity of EVs purified with precipitation have been found to be of lower quality than those derived by UC (74) .

Table 1.2

Purification strategies	Applications	Advantages	Disadvantages	References
Size bias protocols				
Differential Ultracentrifugation (UC)	• Cell culture supernatants • All types of biological fluids (e.g. urine, serum, saliva, CSF)	• Easy to follow protocol • Most common and established method in the field for comparison of data	• Inefficient pelleting of EVs • Low and operator-dependent yields • Purity of EVs subjective to additional washes or alternative cleaning up strategies (e.g. sucrose-based flotation) • Integrity of EVs compromised • Time consuming process	(67)
Size-exclusion liquid chromatography (LC)/ High performance liquid chromatography (HPLC)	• Cell culture supernatants • Plasma	• Increased purity of EVs✦ • Higher and reproducible yields*✦ • Integrity of EVs preserved✦ • Scalable process for large volume processing of EVs • Re-usable gel filtration column	• Requires a chromatography system with UV280 detection for monitoring of protein peaks • Duration of purification variable depending on type of gel filtration column	(81-85)
Surface marker capture protocols				
Antibody-coated bead capture • ExoCap™ (JSR Micro) • Exo-Flow™ (System Biosciences) Antibody-coated microfluidic chips • ExoChip	• Cell culture supernatants • Serum, plasma	• Quick and easy capture of EVs • Higher yields* • Combination of purification with characterization of EVs • Pre-coated beads available (e.g. tetraspanins: CD9, CD81 and CD63) or as customized request • Small volume sample processing	• Requires prior knowledge of known surface marker on EVs • Requires a FACS machine for characterization of EV capture • Not scalable for large volume processing • Not re-usable beads • Elution of EVs for downstream applications and integrity of EVs is still unknown	(67, 75-80)
Precipitation-based protocols				
PEG-polymer Polymer-based commercial kits: • Total Exosome Isolation Reagent (Life Technologies) • Exo-spin™ (Cell Guidance systems) • ExoQuick™ (System BioSciences)	• Cell culture supernatants • Serum, plasma (blood) and urine	• Fast and easy to follow protocol • Higher yields* • No ultracentrifugation	• Purity of EVs is debatable (especially for complex biological fluids) • Integrity of EVs is still unknown • Costly for large sample volumes	(71)
Peptide-based kit: • The ME™ kit/Vn96 peptide capture (NewEngland peptide)			• Dependent on the expression of heat shock proteins on EVs	(72)
"Charge-neutralisation" precipitation				(73)

*Compared to the UC protocol, ✦data described in chapter 3 and published in Nordin et al. 2015 (Appendix 8.2)

Table 1.2

List of protocols currently used for purification of EVs from in vitro and in vivo sources.

As discussed earlier, there have been multiple reports about the enrichment of specific "exosomal" proteins (e.g. tetraspanins, flotillins and integrins) on the surface of EVs, regardless of their cellular origin. Hence, another newly developed purification strategy is based on capturing EVs directly from the biological sample with antibody-labeled beads or with antibody-coated microfluidic chip devices (75–80). Compared to the UC protocol, this strategy allows for fast and high sensitivity capture of EVs directly from small volume samples, which could be particularly useful for health screening purposes. Furthermore, one can simultaneously purify and phenotype the EVs when these antibody-coupled beads or chips are used in combination with the flow cytometer (67). However, it may be difficult to use this method when purifying and investigating EVs from novel cell lines, as a low readout

signal or a negative result on the flow cytometer may simply be due to low detection of these specific proteins on the EVs. Furthermore, this method is not practical when handling large media volumes for EV purification. Moreover, it is still unknown if EVs can be efficiently eluted from the beads or chips without affecting their biophysical properties for downstream characterization studies or functional purposes.

Next, as EVs are around the size range of 100 nm in diameter, some groups have described the use of size-exclusion liquid chromatography (LC) to separate larger EVs from other smaller non-EV associated protein complexes, in both cell culture and recently, from human biological fluids (81–85). Unlike the UC protocol, the LC methodology does not require any high speed spins and is scalable for large volume samples. However, very little is known about how this method compares to the UC method.

Although, there have been some recent papers cross comparing these alternative techniques (70,74,86–91), many of these studies were conducted on a variety of different sample types. In some instances, reports on EVs from the same cell line had described contradictory findings. Hence, to date, there remains a lack of consensus within the field regarding the most ideal method for purification of EVs from all sources, to ensure the reproducibility and reliability of molecular analysis of EVs.

1.1.3 Tools for characterisation and analysis of EVs

One of the first techniques used for identifying and characterisation of EVs was transmission electron microscopy (TEM)(7,92). In recent years, there has been some criticism related to the traditional TEM methodology as the dehydration step during the sample preparation process may lead to the appearance of artifacts such as cup-shaped vesicles. To circumvent this problem, some have suggested the use of cryo-EM as an alternative tool for visualization of vesicles (93,94) as cryo-EM omits the final dehydration step in sample preparation. Hence, under cryo-EM, all of the vesicles appear like intact bubbles with relatively fewer appearances of those cup-shaped vesicles. Overall though, EM is a laborious process that requires expertise knowledge and equipment to perform systematic studies. Furthermore, the use of EM for determination of the size and quantity of EVs can be relatively subjective. To ensure more reliable and reproducible analysis of EV structure, more quantitative approaches, many of which have been adapted from the liposome field (95), have been extended for use on EVs (**Table 1.3**).

Table 1.3

Research Tool	Description of technique	Applications in EV research:	Limitations:	References
Electron microscopy (EM) • Transmission electron microscopy (TEM) • Scanning electron microscopy (SEM) • Cryo-EM	Transmission of high voltage electron beam through the specimen	• Size distribution of EVs • Number and concentration of EVs • Visualisation of the exact morphology of EVs • Combination with antibody labeling allows for characterization of EVs	• Quantification of size and concentration of EVs is subjective • Labour intensive process • Requires expertise knowledge in instrument handling	(7) (92-94)
Dynamic light scattering (DLS) • Zetasizer Nano S (Malvern) • N5 Submicron Particle Size Analyzer (Beckman-Coulter)	Light based technique	• Absolute size distribution of EVs • High resolution very small vesicles; allowing discrimination between subpopulations of EVs	• Quantification of total amount of EVs	(95-96)
Nanopore-based measurement • qNano (Izon) • Multisizer 4 (Beckman-Coulter)	Tunable resistive pulse sensing/ Coulter principle	• Absolute size distribution of EVs • Resolution of distinct subpopulation of vesicles • Assessment of polydispersity • Number and concentration of differently sized particles	• Limited application for very small vesicles (<30nm)	(97)
Nanoparticle tracking analysis • LM10, NS500 (Nanosight, Malvern) • NS300 (Nanosight, Malvern)	Single particle tracking based on Brownian motion	• Absolute size distribution of EVs • Number and concentration of EVs • Live visualisation of individual particles • Fluorescent NTA of labeled EVs	• Limited application for very small vesicles (<30nm) • Lower camera sensitivity for fluorescent detection as compared to FACS	(98-100) (101)
Atomic force microscopy (AFM)	Scanning of specimen surface	• Absolute size distribution of EVs • Number and concentration of EVs • Visualisation of the morphology of EVs without needing fixation, staining or labeling	• Labour intensive process • Requires expertise knowledge in instrument handling	(102-104)

Table 1.3

Table of common tools used for analyzing the biophysical properties of EVs.

To measure vesicle size, there are currently a variety of different devices available commercially: light-based detection methods such as dynamic light scattering (DLS) (96), tunable resistive pulse sensing such as the qNano (Izon) (97), nanoparticle tracking analysis (NTA) methods based on Brownian motion detection of particles with the Nanosight machine (Malvern) (98–101) or even atomic force microscopy (AFM) (102–104). Apart from DLS, the latter three techniques also allow for the absolute quantification of particles within the sample. Furthermore, unlike TEM, these methods allow for a much faster quantitation of vesicles, without the need for any extra sample preparation steps. Hence, many of these techniques are gradually becoming common tools for characterization in several EV studies.

As for molecular characterization of EVs, common approaches used for cellular analysis such as mass spectrometry based proteomics, western blotting, enzyme-linked immunosorbent assay (ELISA) methods, deep-sequencing of RNA and quantitative real-time polymerase chain reaction (qPCR), can also be applied for evaluating protein and RNA content in the EVs. However, one would need to be careful in the optimization and interpretation of data when using any of these techniques, due to the huge differences in absolute amounts and molecular content in the EVs, as compared to cells in general.

Using the above described techniques; many of the EV characterization studies to date have come to the following conclusions on the molecular content of EVs. Firstly, EVs can contain a number of different functional molecular cargoes, such as messenger RNAs (mRNAs), different species of small RNA types (e.g. microRNAs (miRNAs), transfer ribonucleic acid (tRNAs), small nucleolar ribonucleic acid (snoRNAs), Y-RNAs) and proteins. Secondly, the molecular signatures of EVs are generally different to that of their parent cells, where EVs seem to only contain a specific subset of the general cellular content. Lastly, across all EVs, there appears to be several common traits that are seen, regardless of the cellular origin of EVs. Firstly, all EVs have been found to express a number of proteins that are classified under the Gene Ontology (GO) annotation for extracellular vesicle (GO: 1903561) Secondly, all EVs appear to be enriched in the expression of small RNAs as compared to that in cells. The exact amount of these molecular cargoes in EVs has been debated recently; contrary to literature, some reports have suggested that pure EVs may contain only very low numbers of such cargoes (105,106).

By collating all the high-throughput data that has been generated based on the numerous detailed EV characterization studies, there has been the development of several general databases on the molecular content of EVs, all of which are available freely online. These include EVpedia (http://student4.postech.ac.kr/evpedia2_xe/xe/), ExoCarta (http://www.exocarta.org), Vesiclepedia (http://microvesicles.org/index.html) and the Urinary Exosome Protein Database (http://dir.nhlbi.nih.gov/papers/lkem/exosome/) (107–109). Recently, there has also been the formation of an extracellular RNA communication consortium (ERCC) from the common fund by the National Institutes of Health (NIH), USA (www.exRNA.org), where a part of this consortium is aiming to build up a portal for vesicular RNA data management and resource repository. Hence, all of these databases serve as a platform to provide valuable information on EV content. This then allows for researchers to perform comparative studies on their EV studies to current knowledge about EVs in general.

1.1.4 Applications of EVs in biological and medical sciences

In the 1980s, EVs were thought to function as “waste containers”, serving to expel unwanted cellular material into the extracellular environment and helping to maintain intracellular homeostasis. We now know that these EVs in fact can function as an alternative type of cell-cell communication system through a number of different general mechanisms (110). Firstly, EVs expressing membrane-bound molecules can trigger downstream signaling cascades within the recipient cells through direct receptor-ligand interactions. One such example is the EVs released from platelets

upon activation. These EVs are coated with tissue factors that can interact with macrophages, neutrophils and other platelets by ligation with P-selectin located on recipient cells (111). Alternatively, upon the uptake of EVs into cells via passive fusion, endocytosis, phagocytosis or interaction with phosphatidylserine (PS) which serves as an uptake signal (112–115), cargoes such as mRNAs, miRNAs and proteins within the EVs can be functionally transferred to the recipient cells. Subsequently, this can lead to the translation of mRNA into functional proteins or directly result in epigenetic changes when miRNAs are delivered into the nucleus, both of which may result in molecular changes in recipient cells (116–120). For example, when EVs from GFP-transfected endothelial progenitor cells were added onto endothelial cells, these endothelial cells were subsequently able to produce GFP protein. Interestingly, through RNase pre-treatment experiments on EVs, the authors proved that these RNAs were encapsulated and protected within the lumen of EVs (121). Here, we describe some examples of how EV-mediated communication between cells can play an important role in both normal physiological processes, in the spread of diseases and hence how they can be exploited as biomarkers of diseases or even therapeutic targets and tools in medical treatment (**Figure 1.3**).

Figure 1.3

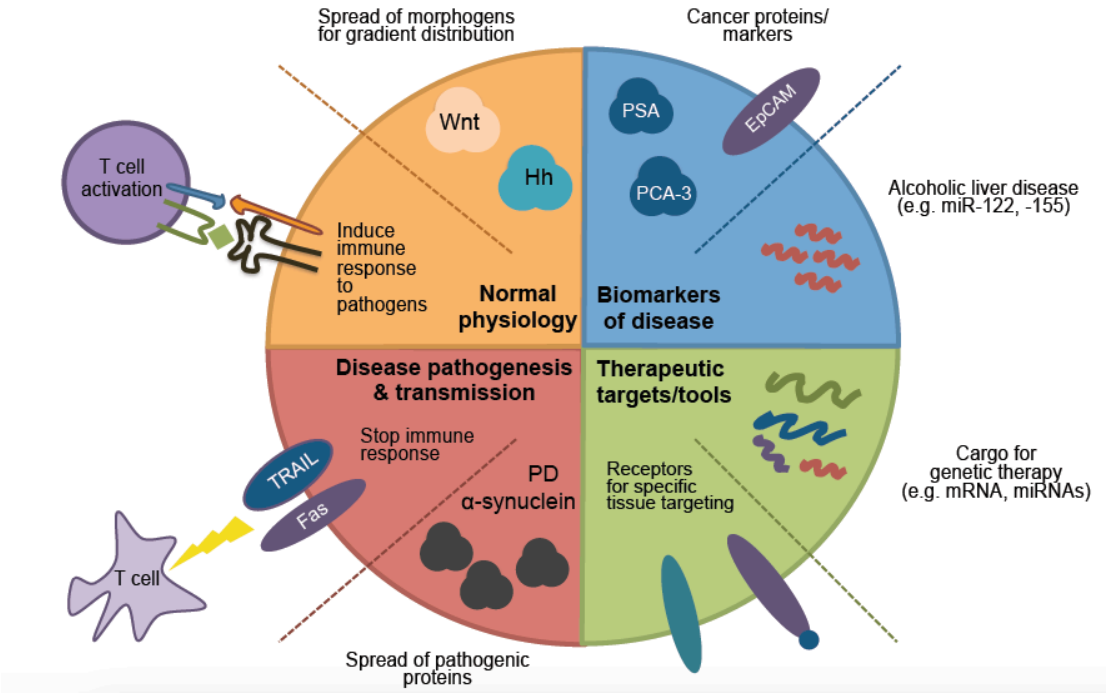

Figure 1.3

Illustration showing the different reported functions of EVs.
There is a wealth of evidence showing the roles of EVs as important cell-cell communicators in different biological systems. Here we show specific examples of EVs in normal physiology and in disease pathogenesis and transmission (left panel). With increasing knowledge about EVs in these processes, have started to investigate the usefulness of EVs in medical sciences, for example as biomarkers of disease and as therapeutic targets or as therapeutic tools (right panel).

1.1.4.1 EVs in normal physiology

Roles of EVs in immunity

There are two known arms of protection against inflammation and pathogen invasion in humans. Firstly, there is the innate immune response where leukocytes expressing pattern recognition receptors (e.g. Toll-like receptors) on immune cells

can recognize the pathogen-associated molecular patterns (PAMPs) or damage-associated molecular patterns (DAMPs) on the foreign entities. Secondly, there is the adaptive immune response, where foreign antigens can be either directly recognised by antigen receptors on adaptive immune cells such as B cells or presented on antigen presenting cells (APCs) such as DCs and macrophages to activate naïve T cells (122) for immune modulation.

Recent evidence strongly supports the finding that immune cells can secrete EVs that elicit specific immune responses, depending on the phenotype of EVs (**Figure 1.4**). For example, when macrophages become infected by pathogens (e.g. mycobacterium or toxoplasma), they secrete EVs containing PAMPs(123–125). In a similar fashion, microglial cells, the immune cells of the brain, shed EVs upon the detection of an inflammation in the brain (28). In both cases, the EVs assist in the recruitment of inflammatory cells to the injured site and hence provide necessary measures to counter the injury. DC-derived EVs, on the other hand, can induce an adaptive immune response through a number of different mechanisms. Depending on their maturation status, the overall quantities and phenotype of EVs released from DCs are strikingly different. Generally, mature DCs secrete fewer EVs than immature DCs (126,127). However, their EVs express higher levels of MHC-II and co-stimulatory molecules such as CD80/86 and Intercellular adhesion molecule-1 (ICAM-1). Hence, these EVs can interact and directly activate T cells, mimicking the role of APCs (9,10,128–131). On the other hand, EVs from immature DCs do not express MHC-II and co-stimulatory molecules, instead they abundantly express milk fat globule-epidermal growth factor 8 (MFG-E8) (127). As a result, it is proposed that these EVs can bind to PS on cell membranes and potentially opsonize apoptotic

cells (132). Furthermore, immature DC EVs can assist in the distribution of foreign antigens to other APCs for antigen presentation.

Figure 1.4

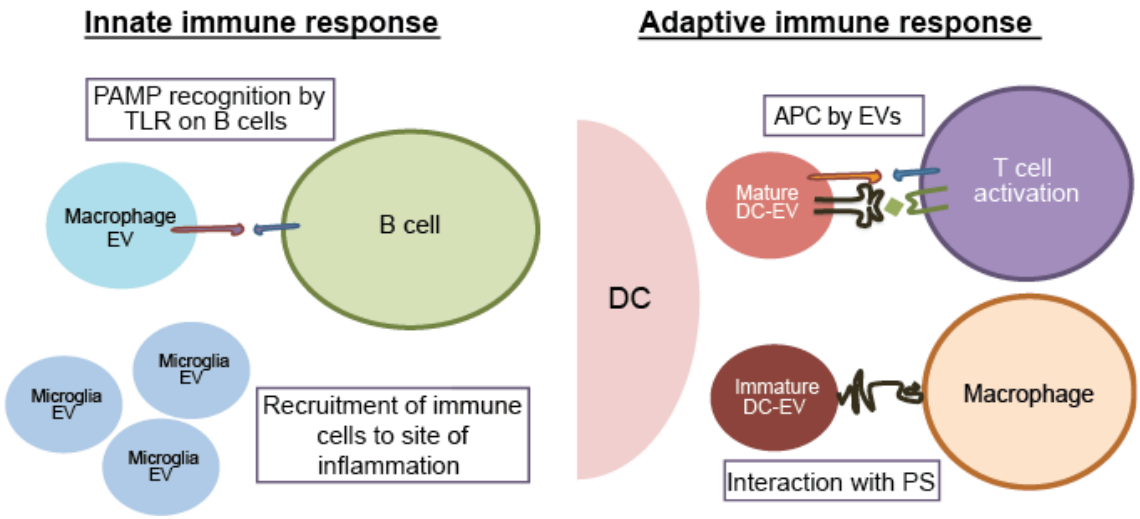

Figure 1.4

Illustration showing the reported roles of EVs in immunity
There is a wealth of evidence showing the roles of EVs as important cell-cell communicators in the immune system. Here we show specific examples of EVs in innate immune response (left panel) and in adaptive immune response (right panel).

Interestingly, the phenotype of EVs from immune cells can be altered for beneficial reasons. For example, genetically modifying immature DCs with interleukin-10 (IL-10) or transforming growth factor-beta1 (TGF-β1) allows for the generation of EVs that promote an anti-inflammatory response and confer immunosuppression, which would be particularly useful for models of transplantation and auto-immune disease (133–138). Similarly, the immunosuppressive phenotype of microparticles released from the semen and placenta are important in preventing any unwanted activation of immune responses during egg fertilization and against the fetus in the duration of the

pregnancy. Unfortunately, the flexibility in switching the EV phenotype might be exploited by pathogens. By pulsing immature DCs with pathogen-associated antigens such as *Toxoplasma gondii* antigen, diphtheria toxin or *Eimeria tenella* antigens (139–141), the resultant EVs released from these cells induced an immune suppression response, which enabled the pathogens to avoid immune detection and modulation by the immune system. Similarly, this mechanism has been shown to be exploited by many other pathogens and viruses (142,143).

Roles of EVs in development

The role of EVs in development was first suggested with the discovery of exo-vesicles budding off the basolateral membranes of Drosophila imaginal disc cells (42). These vesicles, which were termed “argosomes” were derived from basolateral membranes and produced by many different regions of the disc. Interestingly these argosomes were showed to spread at similar rates to the generation of the morphogen gradient for Wingless throughout the disc epithelium. As these argosomes contain Wingless, they were postulated to play a role in development. Recent studies have now confirmed this hypothesis by demonstrating that argosomes carry different morphogens including Hedgehog (Hh) and their related protein, Wnt. When these vesicles were taken up by recipient cells, the Hh and Wnt proteins modulated target gene activation and resulted in Hh-mediated gradients and pattern formation (14,144–149). Interestingly, it was shown that V0-ATPase can mediate secretion of these Hh-related proteins in EVs released from *C. elegans* models. On the other hand, one recent paper demonstrated that vertebrate sonic hedgehog (Shh) is secreted on two types of EVs with different signaling properties,

in both primary chicken notochord cells and in human cell lines (150). Importantly, they demonstrated that only the exosomes co-express Hh and integrins. Subsequently, these exosomes were able to activate the targets of Shh: Hepatocyte nuclear factor 3β (HNF3β) and oligodendrocyte lineage transcription factor 2 (Olig2) during the differentiation of mouse stem cells to ventral neuronal progenitors.

Roles of EVs in the brain

In an organ that requires constant communication across cell types, it is certainly no surprise that EVs play important physiological roles in normal brain functioning. There have been several reports describing the release of EVs from all cell types in the brain including neurons, oligodendrocytes, astrocytes and microglial cells (151–154). Depending on the cell source and the physiological state, the characteristics of EVs can vary accordingly and have different functions in the brain. For example, when mature cortical neurons possess enhanced glutamatergic activity, they secrete EVs that express the α-amino-3-hydroxy-5-methyl-4-isoxazolepropionic acid (AMPA) receptor subunit GluR2. Hence, it is suggested that this activity-dependent regulation of exosome secretion may contribute to the synapse maturation and synaptic plasticity by depleting the neurotransmitter receptors from the postsynaptic compartment (155). Alternatively, EVs from neurons are enriched in syndecans and tetraspanins (e.g. CD81), which coincidentally are important signaling cues. Hence, these EVs could assist in neurite outgrowth and axon path finding in the developing brain and in the neuroplastic adaptations in adult brains (156,157). In other instances, EVs can act as important mechanisms for the cross talk between different cell types in the brain; for example, oligodendrocytes release EVs in response to

neuronal electrical activity. In turn, these EVs carry metabolites or metabolic enzymes such as catalase, which can be delivered back to the neurons for trophic support (158). Similarly, Schwann cells have been shown to release EVs upon axonal damage (153), subsequently these EVs migrate to the site of injury and encourage axonal regeneration.

Role of EVs in stem cell biology

To date, there has only been two studies characterising and showing the horizontal transfer of EV cargoes across pluripotent stem cell lines. In the first study, Ratajczak et al. demonstrated the release of EVs from mouse and human embryonic stem cells (ESCs). Interestingly, they found that EVs from both types of ESC express Wnt-3 protein and are selectively enriched in mRNA for several pluripotent transcription regulatory factors (e.g. Octamer-binding transcription factor 4 (Oct-4), zinc finger protein 42 (Rex-1), Nanog, stem cell leukaemia (Scl) and GATA binding protein 2 (GATA-2)) as compared to their parental cells. Importantly, the authors further demonstrated that these mRNAs could be functionally delivered to other cells and translated into the respective proteins. For example, when mouse ESC-EVs were added onto mouse murine haematopoietic progenitors cells (HPCs), they could enhance the survival and improve the expansion of these HPCs through the transfer of EV mRNA cargoes (e.g. Oct-4, Nanog and Rex-1). Interestingly, some early haematopoietic stem cells markers (Scl, Homeobox B4 (HoxB4) and GATA-2) and the phosphorylation of Mitogen-activated protein kinases (MAPK) p42/44 and serine-threonine kinase AKT were also increased in HPCs that were treated with ESC-EVs (118). A few years later, Yuan et al. published a complementary study, showing the

horizontal transfer of miRNAs via ESC-EVs. Similar to the first study, the authors started off by comparing the levels of different mRNAs and miRNAs in EVs versus that of their parent cells. From RT-PCR analysis, they found that ESCs were more enriched in polyA-containing RNA than the EVs. Furthermore, they probed for the presence of a number of different ESC-specific miRNAs (miR-290, miR-291-3P, miR-292-3p, miR-294 and miR295) as well as two miRNAs that were reported to be upregulated in ESCs undergoing differentiation (miR-21 and miR-22). Overall, all of these miRNAs were found to be less enriched in EVs as compared to their parental cells. However, there was some significant difference in the relative abundance of each individual miRNAs. Subsequently, when these ESC-EVs were added onto mouse embryonic fibroblasts (MEFs), the authors observed an increase in the levels of these ESC-specific miRNAs as early as 1 h after incubation, with the transfer peaking at between 12-36 h, before dropping back to basal levels at 54 h. Interestingly, the authors reported that the miRNAs that appeared to transfer most efficiently were miRNAs found in abundance in ESCs but not in MEFs (120). As a result of the positive transfer results from these two studies, there have been suggestions that EVs derived from other stem cells may have similar functions in the transfer of pluripotency markers and contribute to the maintenance of the stem cell niche.

1.1.4.2 EVs in the pathogenesis and spread of diseases

Roles of EVs in cancer pathogenesis and metastasis

During tumourigenesis, cellular changes within the cancer cells such as an increased expression of GTPase proteins, tumour acidification and increased oxidative stress (159,160) have been shown to contribute to the increased release of EVs as compared to non-tumour cells. Subsequently, these tumour-derived EVs could play a significant role in the communication between cancer cells and other cells in their stromal environment via multiple mechanisms that ultimately encourage the promotion of a pro-tumour phenotype towards tumour progression and metastasis (**Figure 1.5**).

Firstly, some tumour derived EVs contain several pro-survival molecules such as survivin (161). Furthermore, the content of tumour EVs is uniquely enriched for specific mRNAs and miRNAs. For example, miR-1, miR-451 and miR-21 is more abundant in EVs (162) as compared to their parental glioblastoma tumour cells. When these tumour EVs are transferred into non-tumour cells, the proteins and genetic content can be functionally delivered, resulting in both pro-tumourigenic transcriptomic and phenotypic changes in the recipient cells.

Figure 1.5

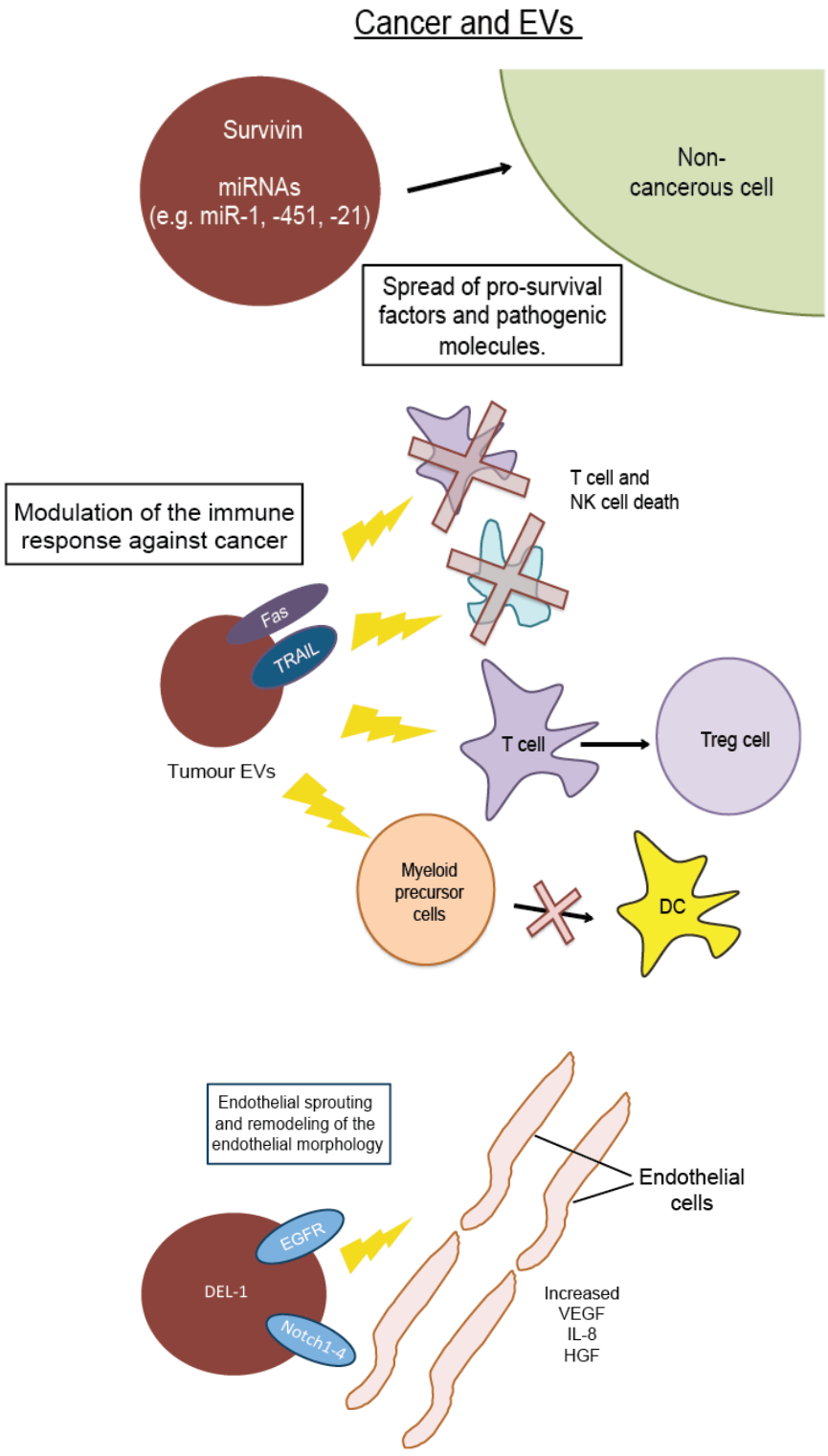

Figure 1.5

Illustration showing the reported roles of EVs in cancer progression
Here we show specific examples of EVs in propagation of pathogenic proteins and miRNAs (top), down-regulating the immune response against the cancer cells (middle) and promoting angiogenesis (bottom).

Next, tumour EVs can intercept the immune response and generate an immunosuppression phenotype against the tumour through a number of mechanisms. For example, colorectal tumour EVs express pro-apoptotic molecules such as Fas and TNF-related apoptosis-inducing ligand (TRAIL) on their surfaces. Upon direct interaction with activated T cells, they can stimulate the apoptosis cascade and kill the immune cells (163,164). Moreover, prostate tumour EVs can down-regulate the cytolytic potential of Natural Killer (NK) cells (165), support the conversion of T cells into regulatory T cells (Treg) cells (166,167) and block the differentiation of DCs from myeloid precursor cells (168). Ultimately, all of these effects would lead to a muted immune response against the tumour and develop peripheral tolerance against the tumour and their tumour antigens. Furthermore, surrounding mast cells could help in the re-organization of the cancer environment, by re-modulating any immune responses against the cancer cells via EVs (169).

In order for cancer to continue flourishing, tumours tend to hijack nutrients from non-tumour cells through angiogenesis of the original vascular system. Interestingly, tumour EVs contribute to this process as they contain potent angiogenic factors such as truncated epidermal growth factor receptor (EGFR), developmental endothelial locus-1 (Del-1) and Notch receptor ligand Delta-like 4 (Notch1-4) (162,170–172). When transferred onto recipient cells, these tumour EVs increased the expression of angiogenic genes (e.g. vascular endothelial growth factor (VEGF), interleukin-8 (IL-8), hepatocyte growth factor (HGF)) and this subsequently led to the stimulation of endothelial sprouting and influenced the endothelial tubule morphology (173).

Besides helping in the local environment, EVs can also assist in the formation of the metastatic niche. Melanoma EVs can induce vascular leakiness at the pre-metastatic site and re-educate bone marrow progenitors towards a pro-vasculogenic phenotype via the transfer of the receptor tyrosine kinase MET (174). Similarly, activated platelets can secrete EVs, which increase the adhesion of cancer cells to endothelial cells and fibrinogen, allowing for the induction of angiogenesis and metastasis (175).

Apart from tumour progression and metastasis formation, some cancers capitalize on the mechanisms of EV secretion to develop chemoresistance against common cancer treatments (e.g. doxorubicin and cisplatin (176)). For example, cancer cells can encourage the specific sorting of cisplatin transporters with cisplatin into the MVEs, which then leads to the clearance of cisplatin from the cancer calls upon release of these EVs (177). In other instances, EVs from human epidermal growth factor receptor 2 (HER-2)-positive breast cancer lines express activated HER-2 on their membranes. Hence, when these EVs interact with Trastuzumab, a monoclonal antibody that interferes with the HER-2 receptor, the EVs function as decoys to inhibit the actual drug activity (178). Recently, drug-resistant breast cancer cells have also been shown to release EVs containing specific miRNAs. Hence, these EVs could encourage the spread of this drug-resistance capacity when they are taken up by other cancer cells (179).

Role of EVs in propagation of Parkinson's disease

Similar to that in cancer, EVs have also been shown to be potential carriers in the progression of neurodegenerative pathologies through the transfer of misfolded

proteins (180) . One example of such a case is in Parkinson's disease (PD). In the last few years, there have been several studies showing the role of EVs assisting in the spread of α-synuclein from neuron-to-neuron. Some studies have demonstrated that α-synuclein deposits are released from affected neurons via EVs. When these EVs get transferred to other neurons, they effectively propagate toxic forms of α-synuclein to other cells (180,181). Alternatively, it has also been shown that the transfer of α-synuclein via EVs ultimately can lead to the formation of aggregates in the recipient cells themselves. Furthermore, Emmanouilidou et al. demonstrated that secreted α-synuclein induced cell death in recipient cells (182–184). Lastly, it has been postulated by Russo et al. that there are some PD related genes that are also involved in various secretory pathways. For example, leucine-rich repeat kinase 2 (LRRK2) is involved in both the secretory and endocytic machinery where it interacts with Rab5b and can colocalise with MVBs. Hence, the authors suggest that LRRK2 can also exploit the EV machinery and get transferred to other cells and propagate PD (185). As the spread of misfolded proteins is common in other neurodegenerative diseases such as Alzheimer's disease and Amyloid lateral sclerosis, there are some emerging evidence indicating that EVs could similarly contribute to the propagation of these pathogenic proteins and spread Alzheimer's disease (186–191).

1.1.4.3 EVs as biomarkers of disease

As discussed in **section 1.1.4.2**, the quantity and content of EVs can vary greatly with the progression of disease (e.g. in cancers). Furthermore, some of these EVs may be released into various biological fluids (e.g. serum, plasma and urine), which are easily acquired via relatively non-invasive procedures during routine health screening. Hence, EVs are beginning to be viewed as attractive alternatives for

disease biomarker discovery, potentially to be used for diagnosis and prognosis in a number of different health conditions and diseases as listed in **Tables 4.1 and 4.2** (87,115,162,192–216).

With hindsight though, it is important to remember that the use of EVs as biomarkers is currently still in its infancy stages for many of the reported diseases. There still needs to be further research on how useful these general biomarkers may be applicable for genetic diseases with various variant subtypes. Furthermore, it would be interesting to analyse if there could be any correlation between EV amounts and content with physical symptoms detected from patients. Unfortunately, there has yet to be the availability of a purification protocol, which allows for fast and accurate capture of EVs from small volume biological samples for such purposes. Nonetheless, it is still exciting to anticipate how EVs might contribute to clinical diagnosis, prognosis or even monitoring of disease states during treatment regimes.

Table 1.4A

Disease type	Source and type of EVs	Reported biomarkers in EVs	References
Cancer			
Ovarian cancer	Plasma exosomes	• ADAM 10, CD24, L1CAM and EMMPRIMN • Claudin-4 and CA125 • miR-21, miR-141, miR-200a, miR-200b, miR -204,miR-205, miR-214, miR-200c, miR -203, miR-205, miR-214	(192-196)
	SKOV-3 & OVCAR-3 cell line exosomes	• MAGE 3/6 and TGF-b1 (levels are higher at advance stages) • let-7 family miRNA (highly invasive cell lines); miR-200 family (less invasive cell lines)	
Bladder cancer	Urinary exosomes	• EGF receptor pathway proteins, retinoic acid-induced protein 3, a-subunit of GTP-binding protein and resistin • LASS2 and GALNT1	(197)
	Urinary and cell lines exosomes	• Basigin, galectin-3 and trophoblast glycoprotein (5T4) • EDIL-3 (high grade cancer)	(198-200)
Glioma/ Glioblastomas	CSF and serum microvesicles	• miR-21 • EGFR, EGFRvIII, TGF-b • Decreased levels of RNAs coding for ribosome production	(162, 201-205)
	Microvesicles from human glioblastoma cells	• small noncoding RNA (RNU6-1), miR-320 and miR-574-3p • Mutant IDH1 • EGFRvIII	
Prostate cancer	Urinary exosomes Plasma microvesicles	• PCA-3, TMPRSS2:ERG, PSA • miR-141 and miR-375 (metastatic prostate cancer); miR-107 and miR-574-3p (prostate cancer in general)	(206-209)
	Plasma/serum exosomes Plasma exosomes	• Survivin • PTEN	

Table 1.4B

Disease type	Source and type of EVs	Reported biomarkers in EVs	References
Neurodegenerative diseases			
Alzheimer's disease	Serum microvesicles	• miRNAs show concordance with neuropsychological and neuroimaging assessments	(210)
Pregnancy			
Pre-eclampsia	Plasma EVs	• Cholera toxin B (CTB)-bound EVs: CD105, IL-6, placental growth factor, tissue inhibitor of metallopeptidase 1 and atrial natriuretic peptide • CTB and annexin V (AV)-bound EVs: Plasminogen activator inhibitor-1, pro-calcitonin, S100b, tumour growth factor B, vascular endothelial growth factor receptor 1, brain natriuretic peptide	(211)
Sperm quality	Seminal plasma vesicles	• Selenoprotein P	(212)
Liver-related diseases			
Alcoholic liver disease	Plasma exosomes	• miR-122 and miR-155	(213)
Renal diseases			
Renal ischemia reperfusion	Urinary exosomes	• Decrease in Aquaporin-1	(214)
Acute kidney injury	Urinary exosomes	• Fetuin-a	(215)
Nephrotic syndrome	Urinary microvesicles	• Neprilysin, aquaporin-2 and podocalyxin	(87)
Diabetic nephropathy	Urinary exosomes (rat)	• Increase in Xaa-Pro dipeptidase; Decrease in Major Urinary Protein 1	(216)

Table 1.4

List of examples where EVs are used as biomarkers in different cancers (A) and diseased states (B).

1.1.4.4 EVs as therapeutic targets and tools

As aforementioned, EVs from diseased cells can contribute to the progression of disease through the delivery of pathogenic proteins and RNAs (**section 1.1.4.2**). Contrary to the negative effects of tumour EVs, it has been recently shown that some tumour EVs are able to induce the opposite effect instead. In these EVs, they found high levels of pro-apoptotic proteins such as Bax. Subsequently, when these EVs were taken up neighbouring prostate tumour cells, the mitochondrial apoptotic cascade was activated within these recipient cells and consequently, the tumour cells were killed (217). Based on this finding, we learn that certain EVs may intrinsically contain beneficial effects and hence can be exploited for therapy.

However, one would need to be extra cautious on the type of EVs to select for such treatments. For example, depending on the type of tumour, the resultant EVs may contain both pro-apoptotic molecules and other viral elements or oncogenic proteins. As a result, if these EVs were used, they may instead induce the opposite negative effect. With this in mind, most of the current successful reports on EV-based therapies have been derived from DCs and Mesenchymal stem cells (MSCs), which have already been used in clinics as cell-based or cell replacement therapies. With hindsight though, there are still several unknown aspects about using EVs for therapy. In this section we describe several examples on how EVs have been applied as both therapeutic tools and targets, and the different challenges that remain with the use of these EVs.

EVs as immunotherapy agents

As described before, EVs released from cells in the natural immune system are able to counter the diseased state directly. For example, tumour EVs expressing the tumour antigens can be endocytosed by DCs. These DCs subsequently can present these tumour antigens via EVs to activate cytotoxic T lymphocytes to act on the cancerous cells (218–220). Hence, some groups have suggested immunotherapy strategies using EVs from immune cells. One such approach is to pulse macrophages or DCs with immune modulatory components like interferon-gamma (IFN-γ). Subsequently, the EVs released from these treated cells can deliver anti-viral proteins and RNAs to hepatocytes and reduce the virus replication ability (221). Similarly, it has been found that EVs from DCs pulsed with pathogen or tumour antigens can induce a Type 1 T helper cells (Th1) biased response when introduced

in naïve animals (10,222) and serve as a form of protection against the infection (139). In line with this idea, there has been a couple of Phase I clinical trials where peptide-pulsed autologous DC-EVs were used as a form of immunization to melanoma and non-small cell lung carcinoma. Generally, the results from these trials indicated that the EVs were well tolerated in patients and had some clinical efficacy (223,224). Hence, with these positive results, some groups further suggest alternative sources of EVs such as ascites (225) and T cells (226) for the same therapeutic purpose, or to use EVs to maintain progression-free survival after chemotherapy in cancer patients (227,228).

EVs in regenerative medicine

Besides the communication between stem cells (**section 1.1.4.2**), there has been some evidence suggesting that secreted EVs could bridge the communication between stem cells and their surrounding differentiated cells via the continuum model of stem cell biology (229) (**Figure 1.6**). In this model as proposed by Quesenberry and Aliotta, stem cells are described as being flexible to cellular changes based on stimuli present in the environment. For example, EVs secreted by differentiated or injured cells can act on stem cells and transfer specific mRNAs. As a result, these stem cells can be directly induced to differentiate and replace the injured cells. Interestingly, this model has been proven in a number of different cell types from lungs, liver, brain, heart and in diseased setting like prostate cancer (230–234). Alternatively, stem cells can secrete ‘regenerative’ EVs that contain specific mRNAs, miRNAs and proteins, which can mediate a more favourable response towards the disease (235). Recently, neural stem cells have been shown

to directly mediate the immune response in target cells through the secretion of EVs containing IFN-γ (236). Of all the different stem cell populations, most of the research to date has been focused primarily on MSC-derived EVs, as they appear to possess an intrinsic potential for use in regenerative medicine.

Figure 1.6

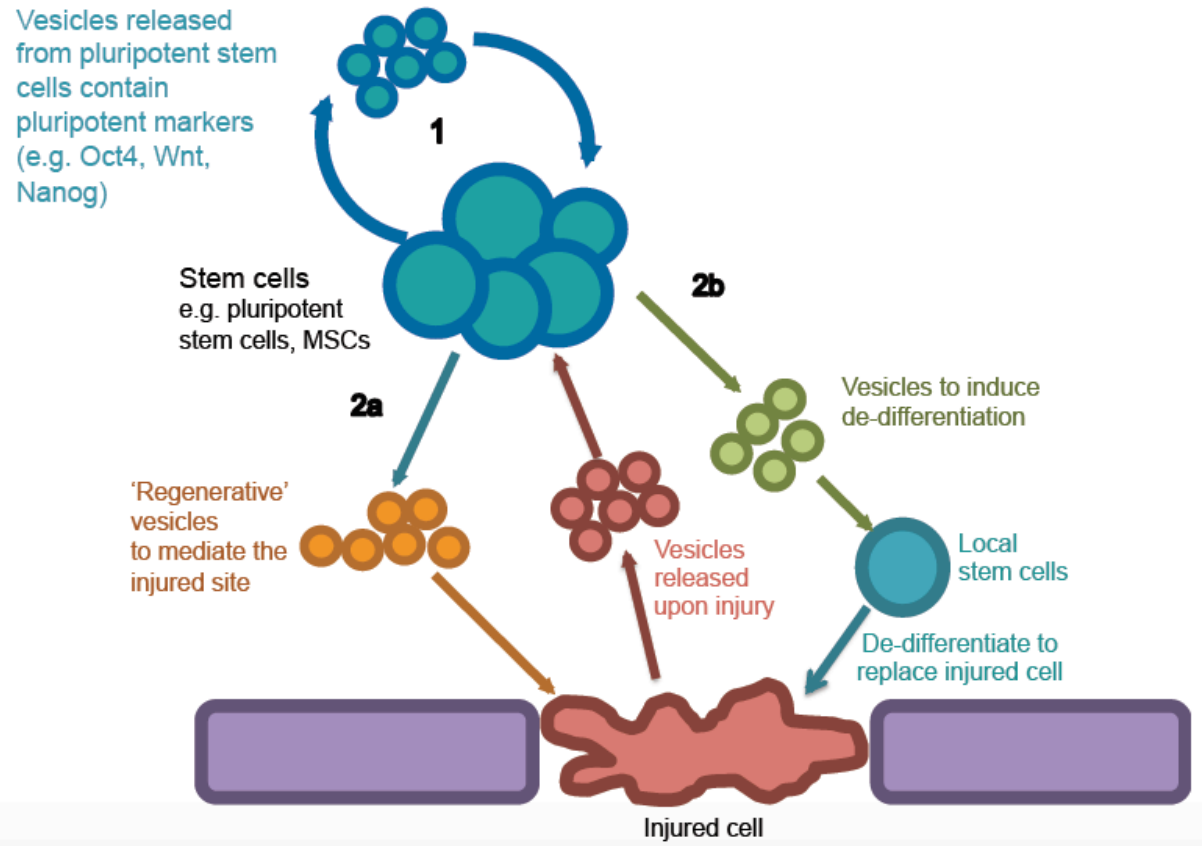

Figure 1.6

Schematic diagram showing the proposed functions of stem cell EVs.
There are two proposed functions of stem cell EVs: 1) EVs released from ESCs have been reported to contain pluripotent markers, which can be functionally delivered to recipient cells (e.g. HPCs). Alternatively, the injured cell releases vesicles upon injury and stem cells and can respond in these two ways: 2a) 'Regenerative' EVs from MSCs contain immuno-modulatory molecules that can mediate the immune response at the site of injury. 2b). MSCs release vesicles that can induce de-differentiation of local stem cells to de-differentiate to replace the injured cell.

MSCs are multipotent precursor cells, which were first described from the bone marrow stroma (237,238). Today, MSCs are viewed as an attractive cell source for cell therapy due to the ease of deriving these cells from a number of different tissues (239–243) and because of their distinct molecular characteristics. Firstly, MSCs express low levels of MHC II and co-stimulatory molecules (B7-1 and B7-2) and secrete soluble molecules to modulate the responses of different immune cells (244–246). For example, MSCs can secrete interleukin-6 (IL-6) to revert the maturation status of DCs (247) or even modify the cytokine production of DCs. Moreover, MSCs can inhibit the proliferation, differentiation and chemotaxis of B-cells (248–250). Furthermore, MSCs can secrete a soluble form of MHC isoform that encourages the expansion of Treg cells (251). Lastly, through the secretion of indoleamine2, 3-deoxygenase (IDO), prostaglandin E2 (PGE2) and TGF-β1, MSCs can downregulate the activity of NK cells (252). In addition to this immuno-modulatory function, MSCs can respond to inflammatory chemokines and home to the sites of injury and disease (253–259). The beneficial effects of MSC-based cell therapies have been confirmed in a number of different pathogenic conditions, such as graft versus host disease (260) and Crohn's disease (261). Furthermore, it has been shown that when used in combination with scaffolds, MSCs promote bone repair and regeneration (262–264). Moreover, MSCs can reverse acute kidney injury via the secretion of factors that stimulate angiogenesis, mitogenesis and a more favourable immune response against the injury site (265).

Despite a wealth of successful reports regarding MSC-based therapies, it has been reported that the majority of the injected MSCs actually get trapped in the lungs (266,267) prior to clearance after a day or two. Furthermore, there have been

numerous studies showing that very few MSCs can integrate, differentiate and remain after the initial engraftment process (268–272). Interestingly, some have found that the direct transfer of conditioned media (CM) from MSCs, which contains a number of different growth factors and proteins, was able to mimic the beneficial effects of MSCs at a comparable level. For example, when co-culturing MSCs with cisplatin-injured proximal tubular epithelial cells, the transfer of insulin-like growth factor (IGF-1) promoted tubular cell proliferation (273). Similarly, AKT-modified MSCs can release secreted frizzled related protein 2 (Sfrp2) which can modulate Wnt signaling, up-regulate the expression of anti-apoptotic genes and mediate myocardial survival and repair (274). Furthermore, Gnecchi et al. showed that after additional pre-treatment of MSCs to hypoxia, the resultant CM was more effective at exerting cytoprotective effects on cardiomyocytes exposed to hypoxia (275). Interestingly, Timmers et al. further demonstrated that the use of MSC-CM was suitable across species; the introduction of CM from human MSCs resulted in a reduction of the myocardial infarct size, an increase in capillary density and an overall improvement in cardiac function in pigs (276).

Besides soluble factors and proteins, the CM of MSCs was found to contain EVs which were found to be enriched in specific miRNAs and ribonucleoproteins that are involved in the regulation of intracellular RNA trafficking (277–280) as compared to their parental cell source. Interestingly, these molecules are linked to pathways involved in immune modulation, self-renewal, differentiation and cell adhesion, indicating the potential role of these MSC-EVs in tissue repair.

The functional effects of MSC-derived EVs has been affirmed in a number of different disease settings such as myocardial infarction (281), acute kidney injury (282,283) and liver disease (284). In many of these cases, EVs were found to promote regeneration mainly through the up-regulation of anti-apoptotic genes and the stimulation of proliferation in remainder of the surviving cells after injury (279,283). Interestingly, one study has even demonstrated that MSC-EVs could deliver miR-133b to astrocytes and neurons and this would encourage neuronal plasticity and functional recovery after stroke (285). Furthermore in a recent proof-of-concept study, it was demonstrated that MSC-EVs could be used successfully for treatment of graft-versus-host disease in humans (71).

Although MSCs have been readily applied as one of the major stem cells for use in numerous Phase I-IV trials in the last decade, there are still some tight regulations concerning the safety and potential immune rejection of stem cell-based therapies (286). For example, depending on the dose and mode of administration, MSCs might get occluded in the vascular system. Alternatively, some MSCs might mal-differentiate and result in the calcification of cells or accumulation of unwanted differentiated fibroblasts in the lungs (287–289). Furthermore, some stem cells might be stimulated to expand and spontaneously transform into tumours (290,291). Importantly, these problems are not applicable to the use of cell-free based therapies such as EVs. Furthermore, EVs can encapsulate several soluble molecules and protect them from degrading enzymes in the circulation, until the EVs reach the site of injury (292). Apart from MSCs, there is new evidence indicating that EVs from other types of stem cells such as liver stem cells could induce functional and morphological recovery of acute kidney injury, similar to that of MSC-EVs (293). For

these reasons, EVs are becoming an attractive cell-free alternative for regenerative medicine.

Designing EVs for personalized medicine

Besides the use of the innate properties of EVs as therapeutic tools, there has been a recent shift in focus towards the engineering of these naturally therapeutic EVs as a combinatorial form of gene therapy. Our lab previously demonstrated in a first proof-of-concept study that synthetic siRNAs can be loaded into immature DC EVs via electroporation and successfully delivered across the blood brain barrier in mice (294). Similarly, others have demonstrated that this method of loading exosomes is applicable to human-derived exosomes (295,296).

Although the idea of engineering EVs for therapy has been shown to be feasible, there are still several steps requiring optimisation in order to increase the efficiency of this form of therapy. Furthermore, one recent paper demonstrated that electroporation was a rather inefficient method for the loading of genetic cargos into EVs, as the electroporation itself led to the aggregation of siRNAs (297). Hence, there have been suggestions on other cargo loading strategies for EVs. For example, by overexpressing specific miRNAs, mRNAs and proteins of interest in the parental cells, it has been shown that these cargoes could be passively loaded into EVs (298,299). Alternatively, one could attach the cargoes of interest to one of the known EV proteins or RNA sequences (e.g. “zip-codes” or specific patterns in the 3’ un-translated regions of the mRNA that was reported to channel mRNAs into EVs (300–302)) and actively load them into EVs. On the other hand, there are some

exogenous loading strategies, where purified EVs could be loaded based on mixing with the drugs of interest (e.g. curcurmin) (303) or with cholesterol-modified oligonucleotides, where the cholesterol tails can bind and interact with the bi-lipid membrane layer of EVs (304). Furthermore, there has been the recent introduction of commercially available transfection reagents specifically for use on EVs (e.g. ExoFect^{TM}, System Biosciences), where one can directly transfect the cargo of interest into purified EVs.

Besides loading, another aspect that would boost the efficiency of EV therapy is to improve the targeting of EVs to their tissue of interest. Generally, knowledge about the natural biodistribution of EVs is rather limited due to technical difficulties of tracking EVs naturally in the blood circulation. Hence, some have tried dissecting this aspect by using labeled EVs that are introduced systematically in mice (305–307). In one recent study, the authors demonstrated that the distribution of EVs could differ slightly depending on the dose of EVs injected, the route of delivery (i.e. intravenous, intramuscular, subcutaneous) or the cellular source of EVs. Interestingly, they also verified that the use of a fusion peptide construct (e.g. Lamp2b-RVG) enabled a significantly higher detection of fluorescence in the brain (308). Similarly, several other papers have also described the use of this strategy when targeting EVs to tumour tissues (299,309). Hence, all of these studies highlighted that the addition of a targeting ligand on EVs could further contribute to the increased efficacy of EV delivery to the site of interest, and additionally minimize the appearance of any side effects.

Previously we discussed the use of therapeutic EVs from immune cells and MSCs, which naturally contain molecules that help in modulation of immune response and tissue regeneration. Recently, some studies have described how to further enhance the beneficial effects of these EVs by engineering additional aspects as a form of combinatorial therapy. For example, Katakowaski and colleagues showed that by loading MSC-derived EVs with an anti-tumour miRNA (miR-146b), there was a decrease in glioma growth in rats after treatment. Similarly, when Munoz and colleagues introduced synthetic anti-miR-9 in EVs, applying EVs resulted in a decrease of resistance of glioblastoma multiforme (GBM) cells to chemotherapy treatment. Furthermore, as MSC-EVs can home to cancer cells, others have suggested the use of MSC-EVs as a delivery agents for anti-cancer drugs or gene therapy (255,310–313).

Targeting the EV biogenesis pathway

Besides using EVs as therapeutic tools, there have been some new ideas about targeting the EV biogenesis pathway instead. The rationale behind this is the observation of higher number of EVs, containing pathogenic proteins and RNAs, from diseased cells than from non-diseased cells. To decrease the overall number of pathogenic EVs released, one suggested therapeutic approach is to use RNA interference to knockdown the expression of proteins involved in EV biogenesis (e.g. Rab GTPases) and down-regulate the release of EVs directly (65). Alternatively, others have recommended performing dialysis to remove circulating diseased EVs from the vascular system (314). On hindsight though, both of these strategies could result in the non-selective removal of both pathogenic and immune cell-derived EVs,

which in turn might help to modulate favourable immune response against the disease. As a result, others suggest switching the phenotype of EVs from diseased cells to a more favourable type for immune detection. For example, one study showed that by decreasing the expression of the natural-killer group 2, member D (NKG2D) ligand on tumour EVs, these EVs were less able to serve as decoys to induce apoptosis of NK cells and dampen the immune response against tumours (315). However, all of these strategies are relatively difficult to pursue, as they require direct access to the specific cells from which the EVs originate, in order to minimize any side effects on non-diseased cells.

Although all of this evidence proves that EVs are highly useful as therapeutic agents, it is currently still very costly and time-consuming to generate large quantities of EVs for therapeutic purposes. Hence, some have tested the possibility of generating artificial exosomes or EV-mimetics by different means (316–319). For example, it has been suggested that coating liposomes with specific peptides that are found on EVs could enhance the uptake of liposomes in targeted cells. Alternatively, others have reported on the use of a cell extruder to manufacture nanovesicles, which carry similar molecular cargoes as EVs from stem cells (320).

1.2 Sequential batches of UC-purified EVs from mouse iPSCs show discrepancy in total particle counts and expression of EV markers

As discussed in **section 1.1.4.2**, ESC-derived EVs are able to transfer functional pluripotency molecules (e.g. protein, mRNA and miRNAs) to their recipient cells and evoke a change in the cellular phenotype. Hence, this led to the suggestion that in the stem cell niche, these EVs may perhaps encourage the maintenance of stem cells in a continuous self-renewal and undifferentiated state. Furthermore, there has been much evidence supporting the natural therapeutic capability of MSC-EVs for different diseases (**section 1.1.4.4**).

With the discovery of induced pluripotent stem cells (iPSCs) by Yamanaka in 2007 (321,322), there began a huge shift of interest into these alternative source of stem cells. Initially, iPSCs were generated by the reprogramming of skin fibroblasts through the introduction of four pluripotency factors (POU5F1/OCT-4, SOX2, c-MYC and KLF4). In the last 8 years, the field on iPSCs has expanded exponentially and there are now several studies describing the generation of these iPSCs from all types of adult cells and tissues, and through a variety of different virus or virus-free mechanisms as reviewed by Malik and Rao (323). Unlike ESCs, iPSCs bypass any ethical debates as they are derived from adult cells. Moreover, as iPSCs can be generated from for each individual, iPSCs could potentially be used for personalized medicine or for the re-modeling of rare diseases. Interestingly, there has yet to be any data on the EVs released from these type of stem cells, which we postulate

could be potentially useful in understanding stem cell biology and for use in regenerative medicine.

For this study, we wanted to investigate the release of EVs from iPSCs and how they could participate in cell-cell communication between the stem cells. Furthermore, we wanted to compare the molecular content of EVs between iPSCs and ESCs, to further understand their role in stem cell biology. Hence, we performed a preliminary study on mouse iPSCs to assess an optimal culturing condition for collection of EVs from these cells. As reported in literature, mouse stem cells are normally cultured on either inactivated MEFs or on gelatin-coated plates. When culturing mouse iPSCs under these two conditions, we observed that the stem cells grew differently. On MEFs, stem cells appeared to grow in clusters while on gelatin-coated plates; the stem cells appeared to be dispersed (**Figure 1.7A**). We proceeded to check for both stem cell and EV marker in the stem cell lysates for the two culture conditions. Interestingly, we detected a higher level of OCT-4 and Alix in the cells cultured on gelatin than those on MEFs (**Figure 1.7B**). From these two cultures, we then collected the CM and purified EVs using the UC method. Generally, the size distribution profiles of particles detected in both sample groups were highly similar, although more particles were detected in the feeder group than in the gelatin group (**Figure 1.7C**). As we were unsure if the MEFs could contribute to the release of some EVs in the CM, we decided to investigate EVs from cells cultured on gelatin-coated plates. For EVs derived from consecutive passages on gelatin, we unexpectedly noticed that there was a discrepancy in the overall number of particles despite having the same cell density at collection. We further performed total protein quantification and western blotting for reported EV markers (Alix and CD9) in these

cultures, based on equal volume loading. Interestingly, all three forms of characterization of EVs did not correspond to each other at all (**Figure 1.7D&E**). Moreover, total protein staining of the membrane with EVs indicated that our purified product contained huge quantities of proteins especially around the 51-76kDa and 17-24kDa size regions (**Figure 1.7F**). Interestingly, the appearance of similarly sized protein bands was previously shown in both stem cell media and EVs purified from mouse ESC (120) However, there was lack of any discussion by the authors on the identities of these proteins and if they were truly vesicle-associated proteins. Based on both our data and this previous study, we postulate that our UC-purified EVs may contain a vast amount of non-vesicular proteins that can skew the protein and NTA quantification of our EVs.

Figure 1.7

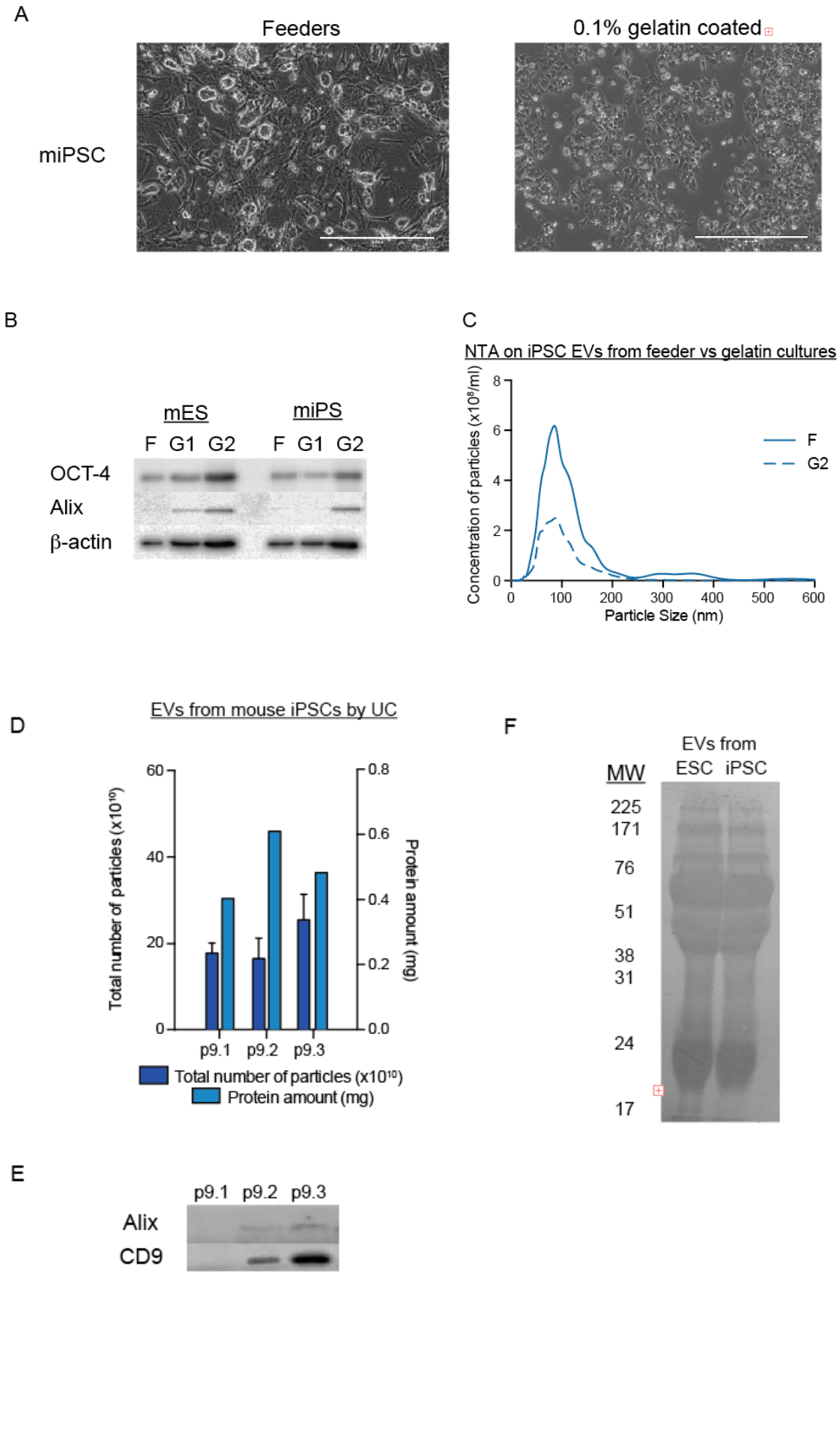
A
Feeders
0.1% gelatin coated
miPSC
B
mES
miPS
F G1 G2 F G1 G2
OCT-4
Alix
β-actin
C
NTA on iPSC EVs from feeder vs gelatin cultures
Concentration of particles (x10⁸/ml)
Particle Size (nm)
F
G2
D
EVs from mouse iPSCs by UC
Total number of particles (x10¹⁰)
Protein amount (mg)
p9.1 p9.2 p9.3
Total number of particles (x10¹⁰)
Protein amount (mg)
F
EVs from
MW
ESC iPSC
225
171
76
51
38
31
24
17
E
p9.1 p9.2 p9.3
Alix
CD9

Figure 1.7

Preliminary data on EVs purified from mouse stem cell sources.
(A) Representative image of mouse iPSCs grown on feeders or 0.1% gelatin-coated plates (scale bar represents 400μm). (B) Representative western blotting of OCT-4, Alix and β-actin in cell lysates derived from mouse ESCs and iPSCs cultured on feeders (F), first-passage on gelatin (G1) and second-passage on gelatin (G2). (C) NTA size distribution graph on the EVs purified from feeder (F) and gelatin-coated (G2) cultures (n=1). (D) Graph showing the total number of particles (dark blue bar) and total protein amounts (light blue bar) of EVs purified from consecutive passages of mouse iPSCs cultures on gelatin. (n=1, bars on the dark blue bar represent mean ±SD of three technical replicates) (E) Representative western blotting of Alix and CD9 on EVs described in (D). (F) Total protein staining of gels with equal volumes of EVs purified from mouse ESCs and iPSCs.

1.3 Aims and outline of this thesis

From our preliminary data as described in **section 1.2**, we showed that we were able to successfully purify EVs from mouse iPSCs. However, our replicate samples demonstrated that there was a huge discrepancy in the quantification of particle numbers with overall protein amounts in the purified EVs. Furthermore, the detection of EV markers in these samples did not correspond to the particle counts or protein amounts. As the appearance of huge protein bands in our EVs did not correspond to proteins that were previously on other EVs (67), we hypothesized that there may have been co-precipitation of proteins with our EVs during the UC process.

From literature, there have been several strategies for collection of EVs in terms of the time length of conditioned media collection or the type of media used, often dependent on the type of cells used. Furthermore, as discussed **in section 1.1.2**, there are a growing number of different EV purification methods, which have emerged in the last decade. As there is currently no consensus on the best method of purifying of EVs across different sample types, this has led to the appearance of varied molecular datasets from EVs of similar origin (108). Based on this understanding, we felt that there was a need to re-evaluate the current methods used for EV collection, before we could derive an optimal workflow for the purification of stem cell EVs for more in-depth characterisation studies.

In **chapter 3** of this thesis, we first investigate how the physical parameters (cell density, length of time for media collection and type of media) affect EV release and content. For practicality purposes, all initial optimization experiments are performed

on immortalized mouse and human cell lines available in the lab. Next, we perform a systematic comparison study between EVs purified by the established UC method versus the LC protocol. As the ultimate aim is to characterise EVs from a novel stem cell source, we chose to use the LC methodology, which was the least biased approach for purification of EVs.

In **chapter 4** in this thesis, we proceed to extend our newly designed LC purification method onto mouse stem cells CM. As stem cell media is known to have additional complexity over regular culture media, we perform a similar systematic comparison study between the UC and LC protocol, to verify our previous findings on EVs from immortalized cell lines from serum-free conditions. Furthermore, we attempt to re-analyse EVs purified by the UC method and account for the discrepancy in quantification as shown in our preliminary data (**Figure 1.7**).

With an optimal method of deriving pure EVs from stem cells, we then perform more in-depth characterization studies in **chapter 5** of this thesis. From current literature, there are only a handful of papers describing EVs released from mouse and human ESCs, whereas there has yet to be any data regarding EVs from iPSCs. We first purify and characterise EVs from different mouse iPSC lines and compare them with EVs from mouse ESCs by both physical and molecular means. To understand the roles of these EVs in stem cell biology, we further compare the molecular traits of EVs with their parental cell source and across both stem cell types. In addition, we conduct some preliminary studies on EVs from human iPSCs and ESCs.

To sum up, the aims of this thesis are firstly, to develop an optimal workflow for the collection and purification of EVs from stem cell cultures and secondly, to characterize EVs derived from pluripotent stem cell sources, including iPSCs and unravel their biological functions in stem cell biology.

Chapter 2

General material and methods

2.1 Cell culture

2.1.1 Immortalised mouse and human cell lines

Immortalised cell lines (mouse neuroblastoma cells, Neuro2a (N2a), mouse neuroblastoma, NSC-34, human embryonic kidney (HEK) and human neuroblastoma (SHSY5Y) were all cultured in complete media comprising of Dulbecco's Modified Eagle Medium (DMEM) (Life Technologies, Carlsbad, CA, USA) supplemented with 10% fetal bovine serum (FBS, Life Technologies) and 50 µg/ml of penicillin/streptomycin (P/S, Life Technologies). All cells were grown at 37°C with 5% CO_2.

2.1.2 Mouse pluripotent stem cell lines and embryonic fibroblasts

Mouse embryonic fibroblasts (MEFs, derived from Dr Paul Fairchild's lab) were grown in complete MEF growth media comprising of DMEM (Life Technologies) supplemented with 15% of FBS and 50 µg/ml of P/S. To prepare feeders for stem cell culture, MEFs were treated with mitomycin-C (Sigma, UK) at 1mg/ml of MEF media for 2 hours. The treated MEFs were then washed 3 times with PBS and re-plated on fresh culture flasks. Mouse stem cell lines (embryonic stem cell (ESC):

ESF121, ESF116 and induced pluripotent stem cell (iPSC): iMEF14, iMEF19; all derived from Dr Paul Fairchild's lab) were first cultured on mitomycin-C treated MEFs feeders. When the cells reached 80% confluence, one-tenth of the cells were plated on fresh feeders while the remainder were plated on 0.1% gelatin-coated plates. For both feeder and feeder-free conditions, cells were cultured in complete mouse stem cell media comprised of DMEM (Lonza, UK) supplemented with 15% knockout serum-replacement supplement (KOSR, Life Technologies, UK), 2mM L-glutamine (Life Technologies), 1 mM sodium pyruvate (Life Technologies), 0.1mM non-essential amino acids (Life Technologies), 50 µg/ml of P/S, 0.2mM 2-mercaptoethanol (Sigma) and 10^6 units of mouse leukaemia inhibitory factor (mLIF, Miltenyi Biotec, UK). All cells were cultured at 37°C with 5% CO_2.

2.2 Collection of conditioned media (CM) for EV purification

2.2.1 Immortalized mouse and human cell lines

24 h after seeding the cells, complete growth media was removed; cells were washed with PBS and replaced with either pre-spun media cleared of EVs or serum-free media (OptiMEM, Life Technologies). Pre-spun media for EV collection is prepared by supplementing DMEM with FBS which was centrifuged at 120,000*g* for 70 min at 4°C. Both pre-spun OptiMEM media is also supplemented with 50 µg/ml P/S. CM from the cells were collected 48 h after the media change; cells were harvested by trypsin and counted with a haemocytometer.

2.2.2 Mouse pluripotent stem cell lines

For both ESC and iPSC cell lines, the stem cells were cultured twice on 0.1% gelatin-coated plates to get rid of any contaminating feeder cells. When stem cells reached 70% confluence (48 h or 72 h after plating), the growth media was removed; cells were washed with PBS and replaced with fresh mouse stem cell media. CM from the cells was collected 48 h after the media change; cells were harvested by trypsin and counted with a haemocytometer.

2.3 Purification of EVs

2.3.1 Differential centrifugation protocol (UC)

The UC protocol used for purification of EVs is based on an established protocol described by Théry et al in 2006 (67). Briefly, CM collected from the cell culture was first centrifuged at 300*g*, 5 min to get rid of cellular debris. The supernatant was decanted and further centrifuged at 2,000*g*, 10 min to get rid of larger particles before subjecting to filtration through a 0.22 μm syringe filter. The filtrate was then spun at 120,000*g*, 70 min to pellet EVs. To eliminate any protein contaminations, the pellet was re-suspended in 25 ml of PBS and spun again at 120,000*g* for 70 min. All centrifugation steps were performed at 4°C. The resultant pellet was then re-suspended in 100 μl and kept at -80°C for further downstream analysis.

2.3.2 Size-exclusion liquid chromatography (LC) protocol

The LC protocol used for purification of EVs was based on the method described by Taylor et al, 2010, with some slight modifications. Briefly, CM collected from cells was first centrifuged at 300*g*, 5 min to get rid of cellular debris. The supernatant was then further centrifuged at 2,000*g*, 10 min to get rid of other large particles before being filtered through a 0.22μm syringe filter. The filtrate was then concentrated using the Amicon 100k-Da molecular weight cut-off (MWCO) filters (Millipore, UK) at 3,500*g* for 15 min. The concentrate retentate was then loaded onto a Sephacryl S-400 16/60 LC column (GE Healthcare, Sweden) and run with PBS at 0.5 ml/min. Fixed-volume 2 ml fractions of the eluted solutions were then collected with a fraction collector. Based on the 280nm LC chromatograph, fractions were pooled and concentrated with Amicon 10-kDa MWCO filters (Millipore) at 3,500*g* for 15 min down to 100 μl and kept at -80°C for further downstream analysis. All centrifugation and LC processes were done at 4°C.

2.4. Quantification and characterisation of EVs

2.4.1 Nanoparticle Tracking Analysis (NTA)

NTA allows for the quantification of total particle amounts and size distribution of particles based on Brownian motion of particles. All NTA was done with the NTA2.3 software on the NS500 Nanosight machine (Nanosight, Malvern, UK). Before each run, the NS500 measurements were calibrated with known concentrations of 100nm silica microspheres to obtain optimum acquisition detector settings and post-

acquisition settings. For all our recordings, we used a camera level of 14 (shutter speed 600, camera gain 250) and automatic function for all post-acquisition settings: detection threshold level 5, blur and minimum expected particle size. EV samples were diluted in PBS prior measurement, starting at an initial dilution of 1:100, and then further adjusted for each sample individually to achieve a particle count of between 2 x 10^8 per ml to 1 x 10^9 per ml. Once the dilution of the sample was determined, the sample was loaded in the sample chamber and the camera focus was adjusted to make the particles appear as sharp dots of light. Using the *script control* facility on the NTA2.3 software, we recorded five 30s videos for each sample; incorporating a sample advance and 5s delay between each recording. The measurements were then analysed using the *batch process* facility and results were exported as Microsoft Excel spreadsheets for further analysis. If the profiles were not in agreement, measurements were then repeated.

2.4.2 Protein quantification of EVs and cell lysates

EVs and cell lysates were quantified using the microBCA or the BCA assay kit (Thermo Scientific, Fisher) respectively as indicated by the manufacturer's instructions.

2.4.3 Western blotting (WB)

Depending on the experimental set-up, either a fixed volume or a set number of particles (as calculated by NTA) from the re-suspension of EV pellet was used. For cells, after trypsin treatment, cells were collected with PBS and spun at 1,500*g*, 5

min to pellet cells. Cells were washed in PBS and pellet at 1,500*g*, 5 min again. The supernatant was decanted and the cell pellet was lysed in radioimmunoprecipitation assay (RIPA) buffer for 1 h at 4°C. The mixture was then spun at 16,000*g*, 20 min. The supernatants were then measured for protein concentration and fixed proteins amounts were used for WB.

The EV/ cell sample was mixed with 2x Laemilli sample buffer (Bio-Rad, UK) containing 5% β-mercaptanol and heated at 100°C for 10 min. Samples were then spun-down briefly before being loaded in 1.5mm, 12% home-made Tris/Glycine SDS-polyacrylamide gels and ran at 170 V for 70 min in running buffer, until the dye front reaches the bottom of the tank. Proteins on the gel were transferred to a polyvinylidene fluoride (PVDF) membrane (Millipore, UK) at 100V for 70 min in transfer buffer containing 20% methanol. Membranes were then incubated in blocking buffer (5% fat free milk in Tris Buffer Saline with 0.1% Tween-20 (TBS-T, Sigma) for 60 min at room temperature (RT) on a rocker with gentle shaking. After blocking, the membrane was incubated with freshly prepared primary antibody solution (**Table 2.1**) overnight at 4°C or 2 h at RT. Membranes were then washed three times 10 min each using washing buffer (TBS-T) with vigorous shaking before adding the secondary antibody solution (**Table 2.2**) and incubating 2 h at RT. After secondary incubation, membranes were washed three times 10 min each with TBS-T and visualized by scanning both 700- and 800nm channels on the LI-COR Odyssey CLx infrared imaging system. For re-probing on the same membrane, the membrane was first washed three times 10 min each before re-incubation with the next primary antibody. For total gel staining, 0.1% Coomassie Blue R250 (Sigma) in 10% acetic acid, 50% methanol and 40% deionized water (ddH_20) was used.

Table 2.1

Primary antibody	Dilution factor	Cat.no/Company
EV marker		
Alix	1: 1000	ab117600, Abcam, UK
Tsg101	1: 1000	ab30871, Abcam, UK
CD9	1: 1000	ab92726, Abcam, UK
CD81 (H-121)	1: 100	sc-9158, Santa Cruz, USA
Endoplasmic reticulum (ER) marker		
Calnexin	1: 1000	ab22595, Abcam, UK
Stem cell marker		
Oct4	1: 1000	ab19857, Abcam, UK
Dendritic cell marker		
CD11c/IGTAX	1: 1000	17342-1-AP, Acris antibodies GmbH, Germany
Cell lysate loading control		
β-actin	1: 200	ab8268, Abcam, UK

Table 2.1

Table showing the list of primary antibodies used.

Table 2.2

Secondary antibody	Type	Dilution	Cat.no/Company
			Li-COR, UK
IRDye® 800CW	Goat anti-mouse IgG	1: 10000	925-32210
IRDye® 800 CW	Goat anti-rabbit IgG	1: 10000	925-32211
IRDye® 680RD	Goat anti-mouse IgG	1: 10000	925-68070
IRDye® 680RD	Goat anti-rabbit IgG	1: 10000	925-68071

Table 2.2

Table showing the list of secondary antibodies used.

2.4.4 Transmission electron microscopy (TEM)

A 200 mesh nickel carbon/formvar grid (AgarScientific) was placed onto a 10µl droplet of the EV suspension for 15 min. The grid was then blotted dry with filter paper, immediately transferred to a 15 µl droplet of 2% uranyl acetate for 1 min and protected from light. The grid was again blotted dry with filter paper before being transferred to a 15 µl droplet of filtered distilled and deionized water (ddH_20) for 1 min. The grid was then blotted dry and left to air dry on the bench top for 15 min. EVs negatively stained on this grid was then visualized with a JEOL 1010 transmission electron microscope (JEOL, Tokyo, Japan).

2.4.5 Trizol extraction of RNA from EVs and cells

Total RNA from EVs and cells were extracted based on the manufacturer's protocol. Briefly, 75 µl of the EV suspension or $2x10^5$ cells were mixed in Trizol LS (Life Technologies) and incubated for 5 min at RT. 60 µl of chloroform was then added and tubes were shaken for 15 sec. The mixed samples were then incubated for 15 min at RT before being centrifuged at 12,000*g* for 15 min at 4°C to derive the 3 distinct phases. The upper colourless phase was transferred to a new tube and 150 µl of isopropanol with 1 µl of glycogen was added. The sample was vortex briefly and incubated at RT for 10 min. The sample was then centrifuged at 12,000*g* for 10 min at 4°C and the supernatant were discarded. The remaining white RNA pellet was washed with 300µl of 75% ethanol and then spun down at 7,500*g* for 5 min at 4°C. The ethanol was then discarded and the pellet was air-dried for 5-10 min, till it turned transparent, and then re-dissolved in 20 µl of RNase-free water. The mixture was

then incubated at 55-60°C for 15 min on a heat block. RNA concentrations of the samples were then measured using the Quant-iT™ RiboGreen® RNA Assay Kit (Life Technologies).

2.4.6 RNA profiling with Agilent Bioanalyzer software

Quality and size of the EV and cellular RNA were detected using capillary electrophoresis with the Agilent RNA 6000 Pico kit and Agilent RNA small RNA kit on an Agilent 2100 Bioanalyzer® (Agilent Technologies, Santa Clara, CA, USA) according to the manufacturer's protocol.

2.4.7 LC/MS/MS Proteomic analysis

All proteomics and bioinformatics analysis were done in collaboration with Dr Henrik Johansson and Dr Janne Lehtiö at Cancer Proteomics Mass Spectrometry Lab located in SciLifeLab, Karolinska Institutet, Stockholm, Sweden.

EVs from UC and UF-LC were concentrated by speedvac and lysed with 1% SDS, 25 mM HEPES, 1 mM DTT. Lysates were heated to 95°C for 5 min followed by sonication for 1 min and centrifugation at 14,000*g* for 15 min. The supernatant was mixed with 1 mM DTT, 8 M urea, 25 mM HEPES, pH 7.6 and transferred to a 10-kDa cut-off centrifugation filtering unit (Pall, Nanosep®), and centrifuged at 14,000*g* for 15 min, followed by an addition of the 8 M urea buffer and centrifugation again. Proteins were alkylated by 50 mM iodoacetamide (IAA) in 8 M urea, 25 mM HEPES for 10 min, The proteins were then centrifuged at 14,000*g* for 15 min followed by 2

more additions and centrifugations with 8 M urea, 25 mM HEPES. Trypsin (Promega) in 250 mM urea, 50 mM HEPES was added to the cell lysate at a ratio of 1:50 trypsin: protein and incubated overnight at 37°C. The filter units were centrifuged at 14,000*g* for 15 min followed by another centrifugation with milli-Q water (MQ) and the flow-through was collected. Peptides were cleaned by a strata-X-C-cartridge (Phenomenex).

Before analysis on the Q Exactive (Thermo Fischer Scientific, San Jose, CA, USA), peptides were separated using an Agilent 1200 nano-LC system. Samples were trapped on a Zorbax 300SB-C18, and separated on a NTCC-360/100-5-153 (Nikkyo Technos. Ltd) column using a gradient of A (3% acetonitrile (ACN), 0.1% formic acid (FA)) and B (95% ACN, 0.1% FA), ranging from 7% to 40% B in 240 min with a flow of 0.4 µl/min. The Q Exactive was operated in a data dependent manner, selecting top 5 precursors for fragmentation by HCD. The survey scan was performed at 70,000 resolution from 300-1700 *m/z,* using lock mass at *m/z* 445.120025, with a max injection time of 100 ms and target of 1×10^6 ions. For generation of HCD fragmentation spectra, a max ion injection time of 500 ms and AGC of 1×10^5 were used before fragmentation at 30% normalized collision energy, 17,500 resolution. Precursors were isolated with a width of 2 *m/z* and put on the exclusion list for 70 s. Single and unassigned charge states were rejected from precursor selection.

Proteome discoverer 1.3 with sequest-percolator was used for protein identification. Precursor mass tolerance was set to 10 ppm and for fragments to 0.02 Da. Oxidized methionine and was set as dynamic modification, and carbamidomethylation as static modification. Spectra were matched to a combined *mus musculus* and *bos taurus* ensembl 72 database, and results were filtered to 1% FDR. Identifications in

bos taurus was considered to originate from FBS and removed. Gene ontology (GO) term enrichment analysis was done using the online Panther software (324).

Chapter 3

Optimisation of method for the collection and purification of EVs from serum-free cultures

3.1 Introduction

Following evidence that strongly support EVs as being potent mediators in cell-cell communication in normal physiological states (118,119) in disease (325) and as natural gene delivery agents (294), research on EVs has grown exponentially in the last decade. However, there still remain incomplete knowledge on the mechanisms controlling EV biogenesis as well as the derivation of an optimal method for EV collection and purification from various biological samples, both of which, are crucial pre-requisites for elucidating the functions of EVs in biology.

In recent years, several groups have demonstrated and highlighted the identities of a number of proteins (e.g. Rab GTPases) that have been shown to control the formation of MVEs and direct the fusion of these MVEs to release EVs into the extracellular environment (as reviewed in **section 1.1.1**). Importantly though, in *in vitro* cell cultures, external cell culture factors such as cell confluence, time of incubation for EV collection and constituents within the growth media could also affect intracellular signaling of cells and subsequently impact on EVs secretion. “Pre-spun” media, which is depleted of serum EVs prior to use, is one commonly used

media for EV collection from cells. Depletion of serum EVs is crucial as they would co-purify with cell-derived EVs during the purification process and subsequently interfere with downstream quantification and analysis of the cellular-derived EVs. However, there have been some doubts if all serum EVs are effectively removed during the preparation process. Hence, in studies investigating EVs derived from MSCs and neurons (281), some have substituted pre-spun media with the use of serum-free media instead for EV harvesting. Knowledge about the relationship between environmental factors and EV production, or how these factors could interplay with reported EV biogenesis mechanisms, remained limited. Therefore, we first conducted a study to elucidate if alterations in culturing conditions could impact on the quantity and content of EVs, focusing on mouse and human neuroblastoma cell lines.

The most established protocol for EV purification from all sample types currently remained to be the UC protocol, as described by Théry et al. in 2006 (67). With the availability of improved techniques for evaluating EVs, it is becoming evident that the UC protocol presents several limitations, particularly with respect to EV yields, purity and integrity. As a result, the reproducibility and reliability of biological data on EVs purified by this UC methodology might be compromised. To resolve this issue, a number of alternative methodologies for the purification of EVs, each with their own technical advantages and disadvantages, have been developed in recent years as discussed in **section 1.1.2**.

One such method is the use of a size-exclusion liquid chromatography column (LC), which has been described for purification of proteins and viruses. Similarly, the LC

fractionation of the CM would allow for the separation of larger EVs from smaller non-associated proteins. Taylor et al. first described the use of LC methodology for EV purification from ovary tumour cell cultures (193). Recently, similar positive results have been shown for plasma samples (83,85). However, it is still relatively unknown how this LC technique compares with UC for EV purification. Similar to others in the field, we also found several limitations when using the original UC protocol and hence we tried to seek an alternative method for our EV purifications. In the latter parts of this chapter, we describe how we came to designing our LC protocol for EV purification. In addition, we outline how we systematically performed a detailed cross comparison study on EVs purified by LC versus that of the traditional UC method.

3.2 Materials and Methodologies

3.2.1 Investigation on the effect of external culturing factors on EV quantity and content

Mouse neuroblastoma cells Neuro2a (N2a) and a fusion of motor neuron enriched embryonic mouse spinal cord with mouse neuroblastoma cells (NSC-34) were plated in each T175cm^2 dishes at three different densities: low, medium and high which correspond to 1.35x10^6, 3x10^6 and 7x10^6 in actual cell numbers. All cells were cultured in complete media comprising of Dulbecco's Modified Eagle Medium (DMEM) (Life Technologies, Carlsbad, CA, USA) supplemented with 10% fetal bovine serum (FBS, Life Technologies) and 50 µg/ml of penicillin/streptomycin (P/S, Life Technologies) and grown at 37°C with 5% CO_2. 24 h after seeding, the growth media was removed; cells were washed with phosphate buffer saline (PBS) and replaced with fresh pre-spun media or serum-free media (OptiMEM, Life Technologies) to generate CM for EV collection. Pre-spun media is DMEM supplemented with 10% FBS that was spun at 120,000*g* for 70 min prior to addition to DMEM. The CM was collected from cells seeded at three indicated starting densities and at five different time points (24h, 48h, 72h, 96h and 120h from the time of media change) for each density type. The CM was subsequently processed for EV purification via the UC protocol (**section 2.3.1**). Following the collection of CM, cells were trypsinised, stained with tryphan blue and counted with a haemocytometer. Each EV sample was then subjected to NTA (**section 2.4.1**) for quantification and determination of the size distribution of particles and western blotting (**section 2.4.2**)

for reported EV markers (Alix, Tsg101 and CD9) as well as Calnexin, which was reported as a good indicator of contamination in EVs. A parallel experiment was conducted on EVs released from human neuroblastoma cells (SHSY5Y). To analyse the proteomic content of EVs from the two growth conditions, CM was collected from post-48h N2a cultures, purified with the UC protocol with an additional PBS wash (**section 2.3.1**) and subjected to LC-MS/MS analysis (**section 2.4.7**). For more details on this study, please refer to **Appendix 8.2**.

3.2.2 Comparison study between two different purification methods

The comparison study was tested on a number of different cell lines; NSC-34, N2a, B16F10, a mouse melanoma and human embryonic kidney (HEK293T). All cells were cultured in complete media (DMEM supplemented with 10% FBS and 50 µg/ml of P/S (all from Life Technologies). For CM collection, complete media were changed 24 h after seeding to OptiMEM (Life Technologies) or pre-spun media as indicated. CM was then collected 48 h after the media change.

To generate GFP-positive EVs, HEK293T cells were pre-transfected with a CD63-EGFP plasmid (pDNA) as described. $6x10^6$ cells were seeded in a 15 cm culture dish in complete media. 24 h later, cells were transfected with polyethyleneimine (PEI, Sigma) at a 1:4 pDNA: PEI ratio; 25 µg of pDNA and 100 µg of PEI were diluted in 500 µl of OptiMEM, each type initially in separate tubes. After 5 min incubation at RT, the pDNA and PEI were mixed and incubated for a further 30 min at RT to form the DNA/PEI complexes. The complexes were then added drop-wise to cells. After 4 h, the complete media containing the complexes was removed, cells

were washed with PBS and fresh OptiMEM, supplemented with P/S was added on cells. 48 h later, the CM was collected for EV isolation.

All CM collected from individual plates were pooled and then equally divided into two equal halves: one for purification by the UC protocol (**section 2.3.1**) and the other for UF with subsequent LC protocol (**section 2.3.2**).

3.2.3 Molecular quantification and characterisation of EVs for comparison study

EVs purified by either method was first analysed by NTA (**section 2.4.1**), quantified for protein and RNA content (**section 2.4.2**) and loaded on a western blotting gel for the detection of EV markers (WB) (**section 2.4.3**). To analyse the overall proteomic content of EVs from the two purification strategies, EVs were subjected to LC-MS/MS (**section 2.4.7**).

3.2.4 Biophysical characterization of EVs for comparison study

The biophysical properties of EVs, such as intactness and aggregation, was analysed using a number of different techniques; TEM (**section 2.4.4**), fluorescence microscopy, fluorescence correlation spectroscopy, total internal reflection fluorescence microscopy and EV biodistribution in mice.

Fluorescence microscopy

Briefly, CD63-EGFP positive EVs were quantified by NTA and the UF-LC and UC samples were diluted to the same concentration of particles/ml. Before any measurements, the EVs were re-suspended with a 27G needle. The samples were positioned on a microscope slide and covered with a coverslip and analysed. Microscopy was performed using Olympus IX-81 inverted microscope (Olympus America, Center Valley PA, USA) equipped with 20X objective. The following fluorescence filter-set (Chroma Technology Corp., Bellows Falls, VT, USA) was used, with the central wavelength and bandwidth of the excitation and emission filters as indicated: GFP (Ex. 470/40 nm; Em. 525/50 nm)

Fluorescence correlation spectroscopy (FCS)

For more quantitative analysis on EV integrity, we collaborated with Dr Wolf Heusermann and Dr Nicole Meisner-Kober (Novartis Institutes for Biomedical Research, Basel, Switzerland) to perform FCS. In FCS, EV hydrodynamic radius, concentration and changes in biophysical properties (e.g. fusion or fragmentation) were determined by measuring diffusion and intensity of CD63-eGFP positive EVs from HEK293T cells. FCS was performed on a Clarina II Reader (Evotec Technologies, Perkin Elmer, Waltham, MA, USA) with 488 nm argon ion laser excitation at 50 µW to minimize photo bleaching, a 40x water emersion 1.15 N.A. objective (UAPO Olympus), a 488/633 nm major dichroic mirror in the excitation path and a HQ535/50m filter in the emission path. In-focus light was collected through a 50 µm pinhole using a SPCM-AQR-13FC avalanche photodiode (Perkin-Elmer Optoelectronics). The confocal volume was calculated in approximation according to(3) using the measured diffusional correlation time τ_{diff} of fluorescent Alexa488 free

dye standard, the known translational diffusion coefficient of Alexa488 (Molecular probes; D = 280 $\mu m^2/s$) and the axis ratio fitted from calibration measurements.

HEK293T and N2a cells were plated in 15 cm dishes and transfected at 50% confluence with CD63-EGFP using Lipofectamine 2000 (Life Technologies) in DMEM supplemented with 10% FBS. After 4 h, cells were washed and medium was replaced with OptiMEM and cultivated for further 48 h. CM was subjected to either UC or UF purification as described in Fig. 2a. The CM (post 0.22 μm), UF retentate, UF flow-through (FT), UC pellet and post-UC supernatant was re-suspended in PBS supplemented with EDTA free Complete Protease inhibitor (Roche, Basel, Switzerland) and analyzed by FCS. For each sample, several dilutions were made and measured in a 96-well glass bottom plate (Whatman, GE Healthcare) with 30 repetitive measurements of 10 s each. NP-40 at 1% v/v (Cambridge Bioscience, Cambridge, UK) was used to induce vesicle disruption. Disruption of vesicles was confirmed by dynamic light scattering. Autocorrelation curves were fitted with a one- or two-component two-dimensional diffusion model (326,327) to extract translational diffusion times, particle numbers and molecular brightness's. For a two-component two-dimensional diffusion model we made the assumption that the two major CD63-EGFP positive components in the isolations are intact EVs/large vesicles and a secondary subpopulation of smaller, potentially disrupted vesicles. We then analyzed all detergent treated samples with a one component fit to derive the translational diffusion time of disrupted vesicles. Alexa488 measurements in an EV sample with and without NP40s confirmed that under these conditions changes in measured translational diffusion times due to viscosity and refractive index changes were negligible (data not shown). Vesicle disruption by NP40s indeed resulted in almost

identical CD63-EGFP translational diffusion times in all samples, including CM. The average value from these measurements was then defined as the translational diffusion time of the putative small, disrupted particles in a two-component fit of the detergent free samples. This allowed to fit the data with significantly improved Chi^2 and delivered a reasonably homogeneous second population with translational diffusion times corresponding to a hydrodynamic radius in the range of ca. 70-100 nm. Data from one experiment representative of at least three independent experiments are shown. Error bars represent Standard deviations from the 30 FCS measurements.

Total internal reflection fluorescence microscopy (TIRF)

For more quantitative analysis on EV aggregation, we collaborated with Dr Mattias Hällbrink (Stockholm University, Stockholm, Sweden) to perform TIRF. TIRF microscopy experiments were performed on a Zeiss Laser TIRF 3 system using a 100x objective. Glass inserts (P35G-1.5-14-C) were from MatTek Ashland, MA, USA. TIRF angle was set at 70 degrees (depth of penetration = 86 nm) Experiments was performed at 37°C. Before assaying, the EVs were mixed with *FAST* DiO™ Solid; DiO$\Delta^{9,12}$-C_{18}(3), ClO_4 (3,3'-Dilinoleyloxacarbocyanine Perchlorate) (Life Technologies). Images were recorded after a brief refocusing.

EV biodistribution in mice

To understand the biological implications of EV integrity, we collaborated with MD Joel Nordin and MD Oscar Wiklander (Karolinska Institutet, Stockholm, Sweden) to

perform biodistribution studies by injecting labeled EVs into mice. Prior to purification with UC (**section 2.3.1**) or LC (**section 2.3.2**), CM was incubated with 1μM (1,1'-Dioctadecyl-3,3,3',3'-Tetramethylindotricarbocyanine Iodide, Life Technologies) DiR dye. Purified EVs were then quantified by NTA (**section 2.4.1**) and equal amounts of particles from both UC and UF-LC preparations were injected in the tail vein of Balb/c mice (n=5). 24 h post injection, the organs were harvested and subjected to imaging using the In Vivo Imaging System (IVIS) (Caliper, CA, USA). The IVIS was set to record the fluorescence for 2 seconds (excitation 710, emission 760) and the data obtained was then analysed with the IVIS software. The Swedish Local Board approved all animal experiments conducted for Laboratory Animals. All experiments were performed in accordance with the ethical permission and designed to minimize the suffering and pain of the animals.

3.2.5 Statistics

A one-way Anova followed by the Dunn's post-test was applied to the molecular brightness data (**Figure 3.3.5M**). The student's t-test was used when comparing EVs derived by the UC versus LC purification (**Figure 3.3.4E, Figure 3.3.5A,B&H, Figure 3.3.7G** and **Figure 3.3.8C**). The biodistribution data was analysed using the nonparametric Krusckal Wallis test followed by the Sidak post-test (**Figure 3.3.8E**). All bars in the graphs represent mean ±SD.

3.3 Results

3.3.1 Proliferation rate and morphology of N2a cells is altered in serum-free culture conditions

N2a cells, like most other in vitro cell cultures, were normally cultured in media supplemented with 10% serum. Hence, we first evaluated how these cells reacted to the rapid switch from complete growth media to pre-spun or serum-free (OptiMEM) media. Interestingly, N2a cells cultured in OptiMEM displayed a different cellular morphology as compared to that prior the media change and to cells in pre-spun media. In serum-free conditions, the cells appeared to have longer outgrowths from the main cell body (**Figure 3.3.1A**). Furthermore, N2a cells proliferated at a slower rate in OptiMEM than in pre-spun media over the course of the 5-day period. This phenomenon appeared to be regardless of the starting cell density (low, medium or high). Moreover, cell death, as indicated by the drop in total number of cells at the time of media collection, was consistently observed a day earlier in OptiMEM cultures than in pre-spun cultures (**Figure 3.3.1B**).

3.3.2 Serum-free conditions and increased incubation time prior to EV collection leads to greater EV yields

Prior to EV purification, both types of media (pre-spun and OptiMEM) were analysed by NTA and found to be rather low in particle counts (data not shown). With NTA, the overall concentration of particles detected was increased across the first 72 h in both

OptiMEM and pre-spun cultures and this was similar across three different starting cell densities. The drop in particle concentration occurred at 96 h for OptiMEM cultures and at 120 h for the pre-spun cultures with the lowest starting cell density. Consistently though, we observed more particles collected from OptiMEM than in pre-spun cultures, where this difference was more obvious in cultures with higher cell density (**Figure 3.3.1C**). To further analyse the kinetics profiles of EV secretion, we plotted the overall EVs released per cell for the low cell density cultures and found that cultures in OptiMEM had a different EV secretion profile to that of pre-spun cultures (**Figure 3.3.1D**).

To verify that our purified particles were indeed EVs, we loaded the same volumes of purified EVs (from low cell density N2a cultures) on a SDS-PAGE gel and tested for the presence of EV markers. Generally, reported EV markers (Alix, CD9 and Tsg101) were consistently detected a day earlier in OptiMEM-derived EVs than in pre-spun samples. On the other hand, Calnexin, an endoplasmic reticulum marker used to indicate the presence of contaminating vesicles in EV preparations, was detected increasingly from post-72h OptiMEM cultures onwards and from post-96h pre-spun cultures onwards (**Figure 3.3.1E**). Moreover, this increasing expression of calnexin expression corresponded to the decrease in overall total number of cells counts in both OptiMEM and pre-spun cultures (N2a-low density plot in **Figure 3.3.1A**).

Figure 3.3.1

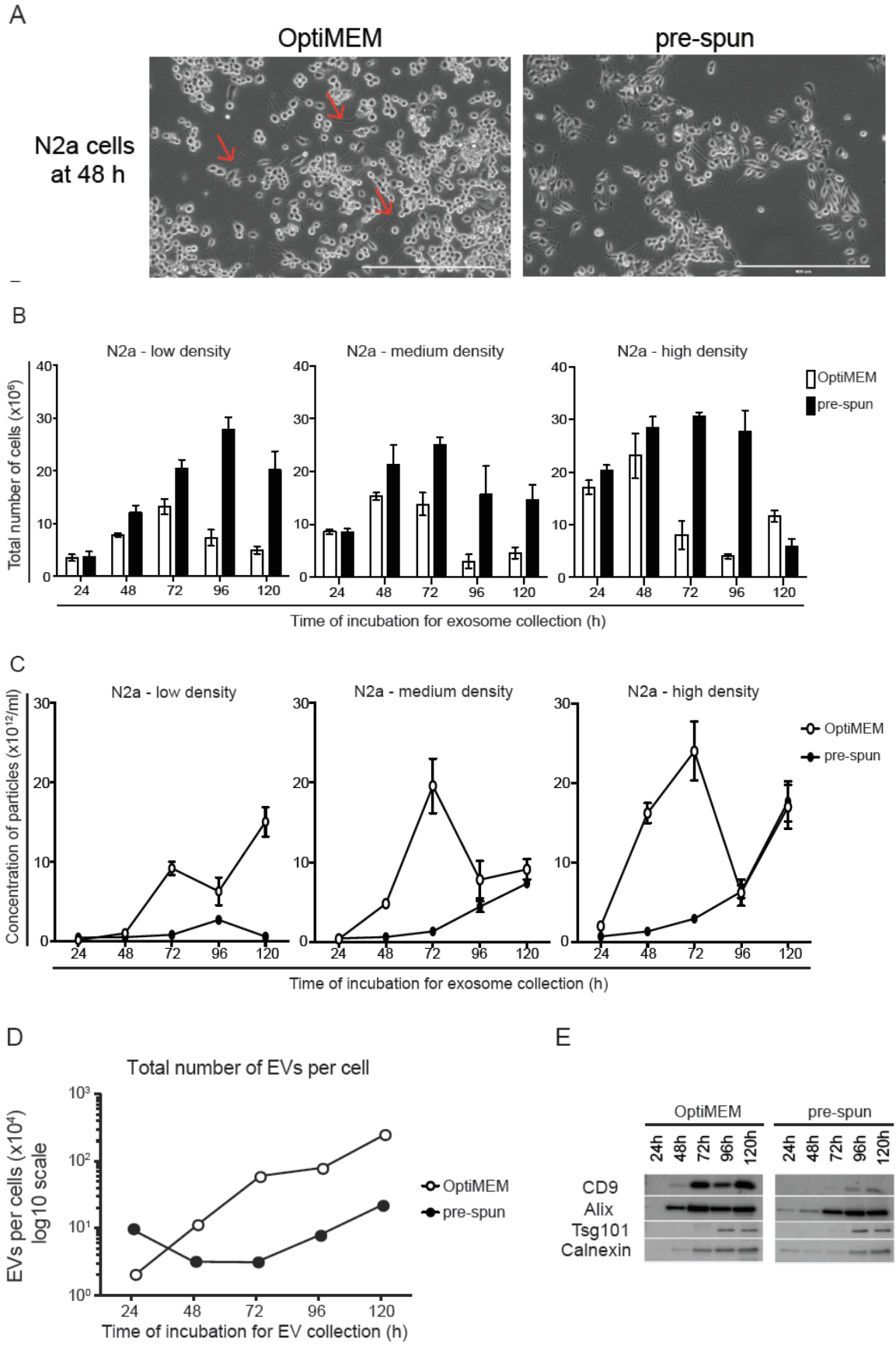
A
OptiMEM
pre-spun
N2a cells at 48 h
B
N2a - low density
N2a - medium density
N2a - high density
Total number of cells (x10⁶)
OptiMEM
pre-spun
Time of incubation for exosome collection (h)
C
N2a - low density
N2a - medium density
N2a - high density
Concentration of particles (x10¹²/ml)
OptiMEM
pre-spun
Time of incubation for exosome collection (h)
D
Total number of EVs per cell
EVs per cells (x10⁴) log10 scale
OptiMEM
pre-spun
Time of incubation for EV collection (h)
E
OptiMEM
pre-spun
24h 48h 72h 96h 120h
CD9
Alix
Tsg101
Calnexin

Figure 3.3.1. Analysis of N2a cells and EVs cultured in and collected from OptiMEM and pre-spun media

(A) Representative bright-field images of N2a cells cultured in OptiMEM or pre-spun media for 48 h. Red arrows in the OptiMEM image indicate the appearance of dendrite-like extrusions from the cells. Scale bar represents 400 μm. (B) Graphs showing the total number of cells at point of CM collection across the 5-day period for both OptiMEM (white bar) and pre-spun (black bar) cultures. (C) Graphs showing the concentration of particles ($x10^8$/ml) collected at each time point for both OptiMEM (white circle) and pre-spun (black circle) cultures across the same 5-day period. The same experiment was repeated across cultures with three varying cell densities as indicated. For data points shown in (B) and (C), n=1, bars represent mean measurements from 3 technical replicates ±SD. (D) Graph showing the kinetics of release of particles from N2a cells cultured at low density in OptiMEM (white circle) and pre-spun (black circle). (E) Representative WB pictures of EV markers (CD9, Alix and Tsg101) and Calnexin for EVs collected daily over 5 days from N2a cells cultured in OptiMEM or pre-spun media.

To confirm this trend of EV secretion from serum-free cultures, we conducted parallel experiments with another mouse neuroblastoma cell line, NSC-34. Similar to the findings in N2a cells, cell proliferation numbers were consistently lower in OptiMEM cultures than in pre-spun cultures. Again, we observed a much higher concentration of particles in OptiMEM as compared to pre-spun cultures across all time points (**Figure 3.3.2A-C**).

Figure 3.3.2

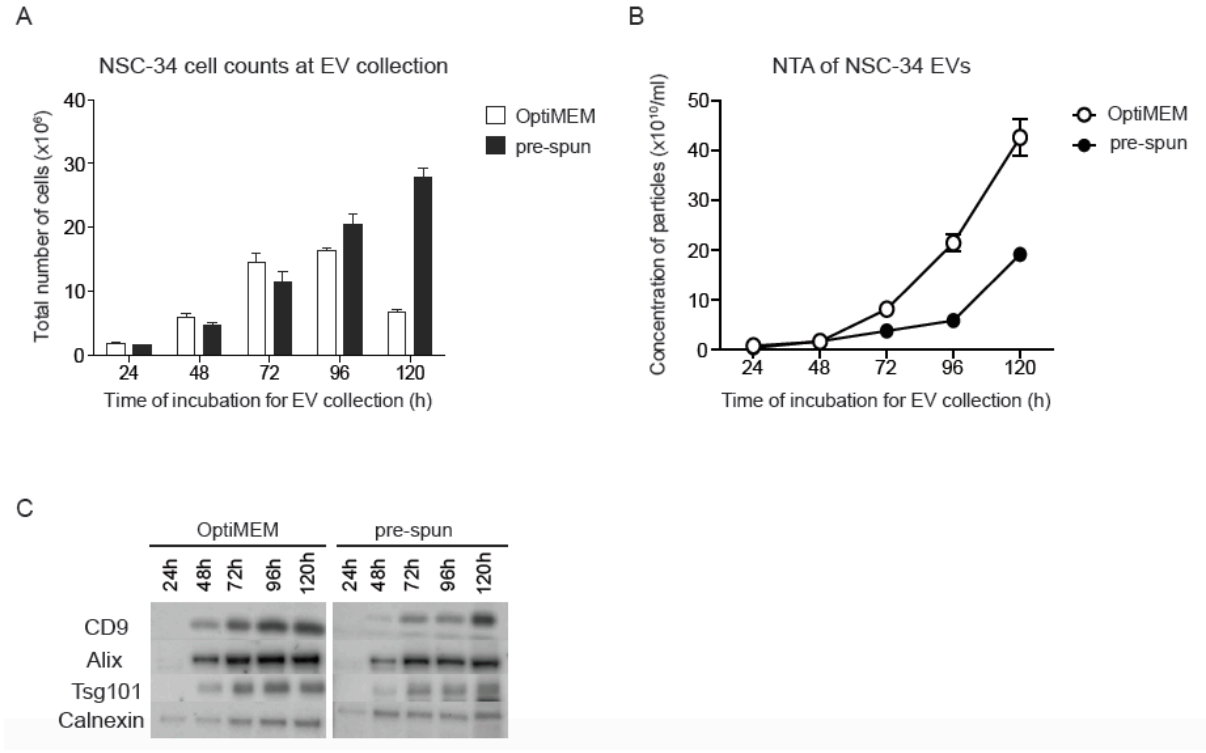

Figure 3.3.2 Analysis of NSC-34 cells and EVs cultured in and collected from OptiMEM and pre-spun media

(A) Graph showing the total number of NSC-34 cells at point of CM collected across a 5-day period for both OptiMEM (white bar) and pre-spun (black bar) cultures. (B) Graph showing the concentration of particles (x10^8/ml) collected at each time point for both OptiMEM (white circle) and pre-spun (black circle) cultures. For data points shown in (A) and (B), n=1, bars represent mean measurements for 3 technical replicates ±SD. (C) Representative WB picture of EV markers (CD9, Alix and Tsg101) and Calnexin for EVs collected daily over 5 days from NSC-34 cells cultured in OptiMEM or pre-spun media.

3.3.3 Serum-free conditions lead to secretion of EVs with an altered proteome

The appearance of calnexin in EV samples collected at prolonged incubation periods (more than 48h for OptiMEM and more than 72h for pre-spun media) clearly indicated that these preparations contained both EVs and other contaminating vesicles, most probably due to the higher levels of cell death in these cultures. In order to minimize the contamination of other proteins or vesicles, we chose to focus on comparing EVs purified from post-48h CM. Consistently across both mouse cell lines (N2a and NSC-34), the total number was higher in OptiMEM than in pre-spun cultures, albeit this difference was more pronounced in N2a EVs. Interestingly, the same trend was also detected when checking for EVs from the human neuroblastoma cell line (SH-SY5Y) (**Figure 3.3.3A**). Although the mode size of EVs between OptiMEM and pre-spun derived EVs in all three cell lines differed slightly, these differences were not significant.

In order to elucidate how serum-free culturing conditions may affect EV content, we proceeded to perform nano LC-MS/MS proteomic analysis on the N2a EVs collected from post-48h cultures. A total of 1742 proteins were identified (1% FDR) in EVs derived from both conditions. Of all the identified proteins, 1058 were common in both conditions, with 607 and 77 proteins exclusively found in OptiMEM and pre-spun EVs respectively. From these 1058 commonly identified proteins, 655 were expressed at similar levels, while 358 and 45 proteins were considered up regulated in OptiMEM and pre-spun EVs respectively (**Figure 3.3.3B&C**). For further gene ontology (GO) enrichment analysis, we sorted proteins in the following three groups:

1) 655 proteins with similar levels in both conditions, 2) 964 proteins considered up regulated in OptiMEM as compared to pre-spun and 3) 122 proteins considered up regulated in pre-spun as compared to OptiMEM. Using the Panther software, we then identified the overall GO terms of proteins in each of these three groups and listed a selected number of GO annotations, which was found to be significantly different in one as compared to the other two groups.

Generally, proteins detected at similar levels in OptiMEM and pre-spun conditions consisted of reported EV markers such as Alix, CD9 and heat-shock protein-90 (108) and some cytoskeletal proteins. Based on GO annotations, ribosomal proteins and other proteins involved in translation were also similar in EVs derived from either condition. Interestingly, EVs from OptiMEM conditions were more enriched for G-proteins, small GTPases and kinases. Moreover, proteins involved in oxygen and reactive species metabolic processes were higher in OptiMEM derived EVs over that of pre-spun derived EVs. On the other hand, pre-spun EVs were more enriched for ribonucleoproteins and microtubule family of cytoskeletal proteins. There was also an enrichment of proteins involved in mRNA processing and splicing factors for EVs derived from pre-spun cultures (**Figure 3.3.3D**).

To validate our proteomics results, we selected proteins belonging to the three groups (similar in both levels, up-regulated in pre-spun and up-regulated in OptiMEM) and compared the expression levels of these proteins by WB, in both the EVs and their source cells (**Figure 3.3.3E**). Expression levels of EV markers (Alix and CD9) were similar in EVs and cells from both conditions. Although the expression levels of other validation targets were below the detection limit in cell

lysates, we observed a slightly higher expression of melanocyte proliferating gene (MYG1) and ADP ribosylation factor 6 (ARF6) in OptiMEM EVs as opposed to pre-spun EVs and the reverse trend for serpin F1 (SERPINF1) (**Figure 3.3.3F**). These data corresponded well with the findings from the original mass spectrometry data.

Figure 3.3.3

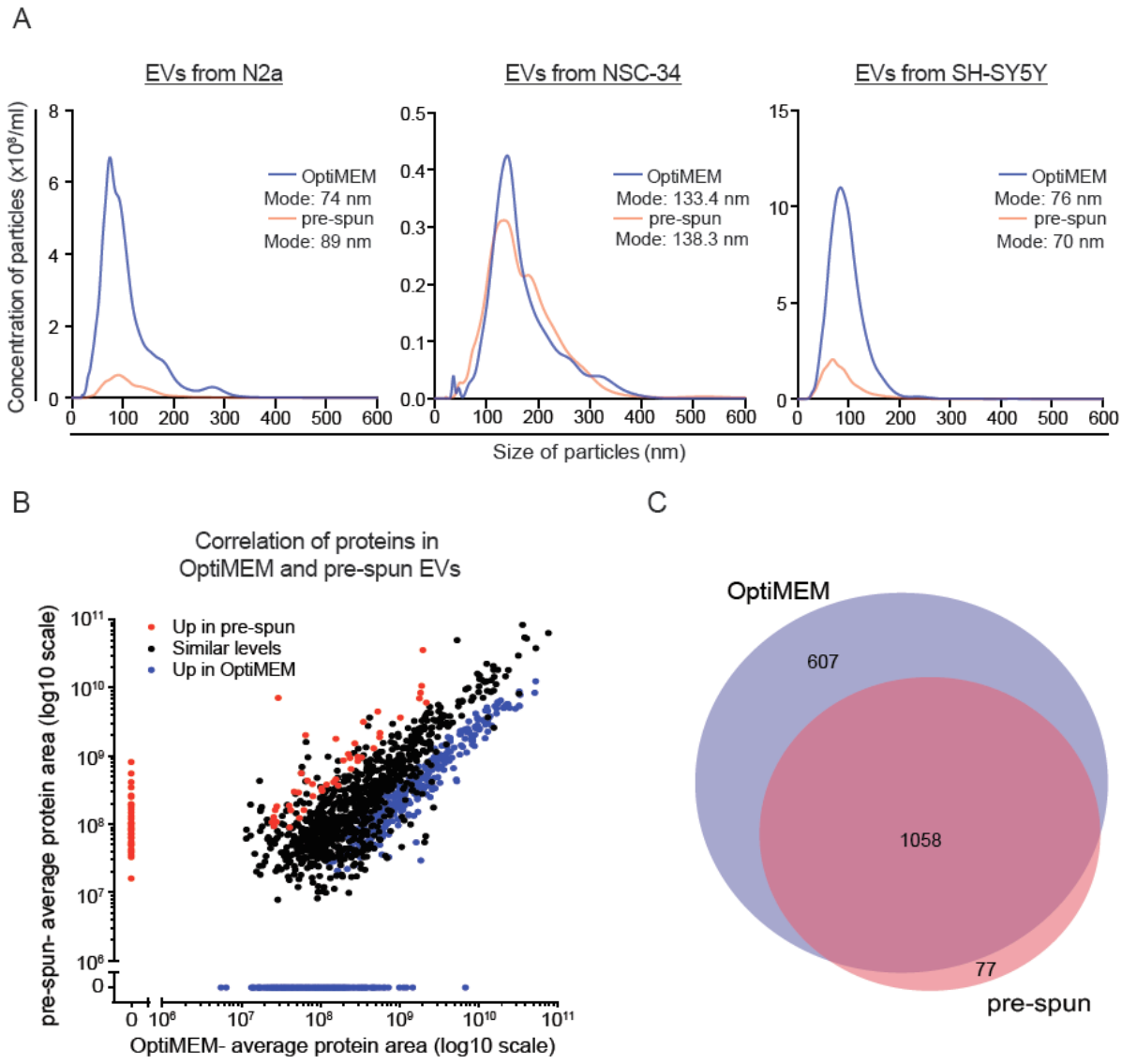

Figure 3.3.3 (cont'd)

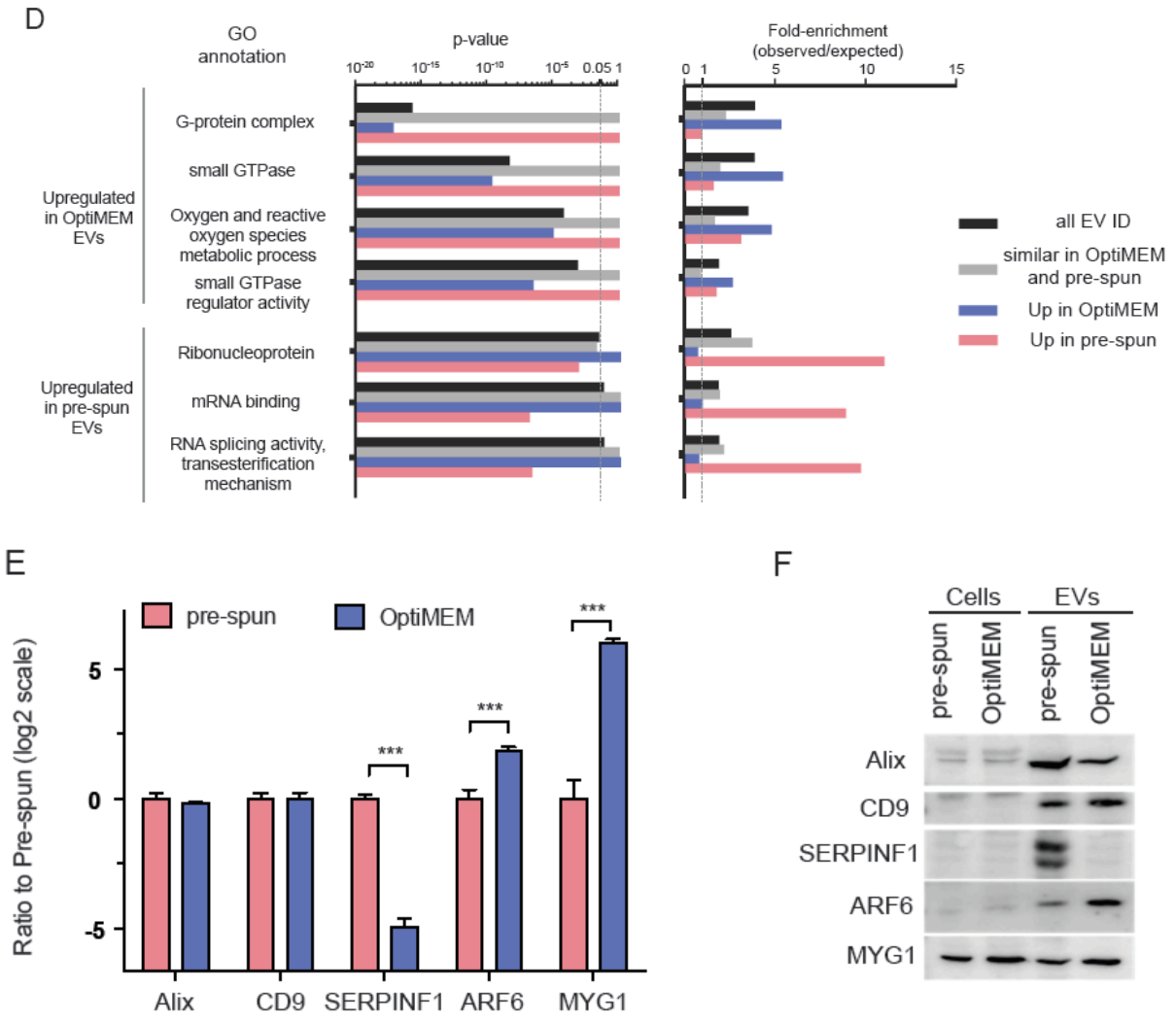

Figure 3.3.3 NTA and proteomic comparison of EVs collected from cells post-48 h incubation in OptiMEM and pre-spun media

(A) Graphs showing the size distribution profiles of EVs collected at post-48 h OptiMEM (blue) and pre-spun (red) cultures of N2a (left), NSC-34 (middle) and SH-SY5Y (right) cells. (B) Scatter plot showing the correlation of proteins identified in N2a EVs isolated from either OptiMEM or pre-spun conditions. Proteins are further classified into three groups; similar levels in both conditions (black dots), higher expression in pre-spun (red dots) and higher expression in OptiMEM (blue dots). (C) Venn diagram showing a 60% overlap of total proteins identified in EVs from both OptiMEM and pre-spun cultures. (D) A selected subset of significantly enriched GOs found to be upregulated in either OptiMEM or pre-spun media derived EVs. All proteins are grouped under the four categories: all EV IDs (black bar), proteins of similar levels in both OptiMEM and pre-spun (grey bar), higher in OptiMEM (blue bar) and higher in pre-spun (red bar). (E) Mass spectrometry data showing the ratio of OptiMEM/pre-spun (log2) on selected proteomic validation targets (Alix, CD9, SERPINF1, ARF6 and MYG1) (*** indicates $p<0.001$, 1% FDR). (F) Representative WB validation of these selected targets in both N2a cells and EVs cultured and collected under either OptiMEM or pre-spun conditions.

3.3.4 Limitations of the UC protocol for purification of EVs

Similar to many others in the EV field, we initially performed purification of EVs from *in vitro* cell sources with the most established protocol -UC. However, we found that this methodology was both laborious and resulted in relatively low yields. In the literature, there were several descriptions of other UC protocols with slight variations from the original form as reported by Théry et al (67). Hence, we wanted to evaluate how these slight variations might impact on the resultant EV product in order to devise a more optimized method for EV purification from our samples. For all optimization experiments discussed in this chapter, we chose to purify EVs from post-48 h CM collected from serum-free cultures based on the following reasons. Firstly, as shown in **section 3.3.2**, serum-free culturing conditions consistently resulted in a significantly higher release of EVs from different cell types. Hence, this would enable us to perform multiple downstream analyses on the EVs more readily. Secondly, as indicated before, serum vesicles might not be effectively removed completely from pre-spun media prior to use. Furthermore, other abundant proteins in serum (e.g. albumin) might co-pellet with the EVs and interfere with the NTA analysis. Using serum-free media for EV collection would allow us to omit these confounding factors that could further affect our comparisons on the purified EV product.

After collecting post-48h CM from serum-free N2a cultures, EVs were purified by the four UC protocol variants described in literature and listed in **figure 3.3.4A**. Based on total particle counts with NTA and WB data for EV markers and calnexin in the isolated pellets, we made the following observations regarding the UC protocol

(**Figure 3.3.4B-D**); firstly, initial low speed spins, especially the 10,000*g* step, was necessary for the removal of large apoptotic vesicles and debris that could otherwise affect EV purity. Secondly, the 10,000*g* spin might be substituted with a 0.22μm syringe filtration step, as the quantity and of EVs purified with either strategy was comparable. Thirdly, the additional PBS wash step was crucial for derivation of pure EV preparations as indicated by the disappearance of calnexin on the WB. However, this additional process compromised the overall EV yield as shown by the low recovery rates in overall particle counts when purifying EVs from N2a EVs (50.0±13.9%) and HEK EVs (61.7±8.9%) (**Figure 3.3.4E**).

Figure 3.3.4

A

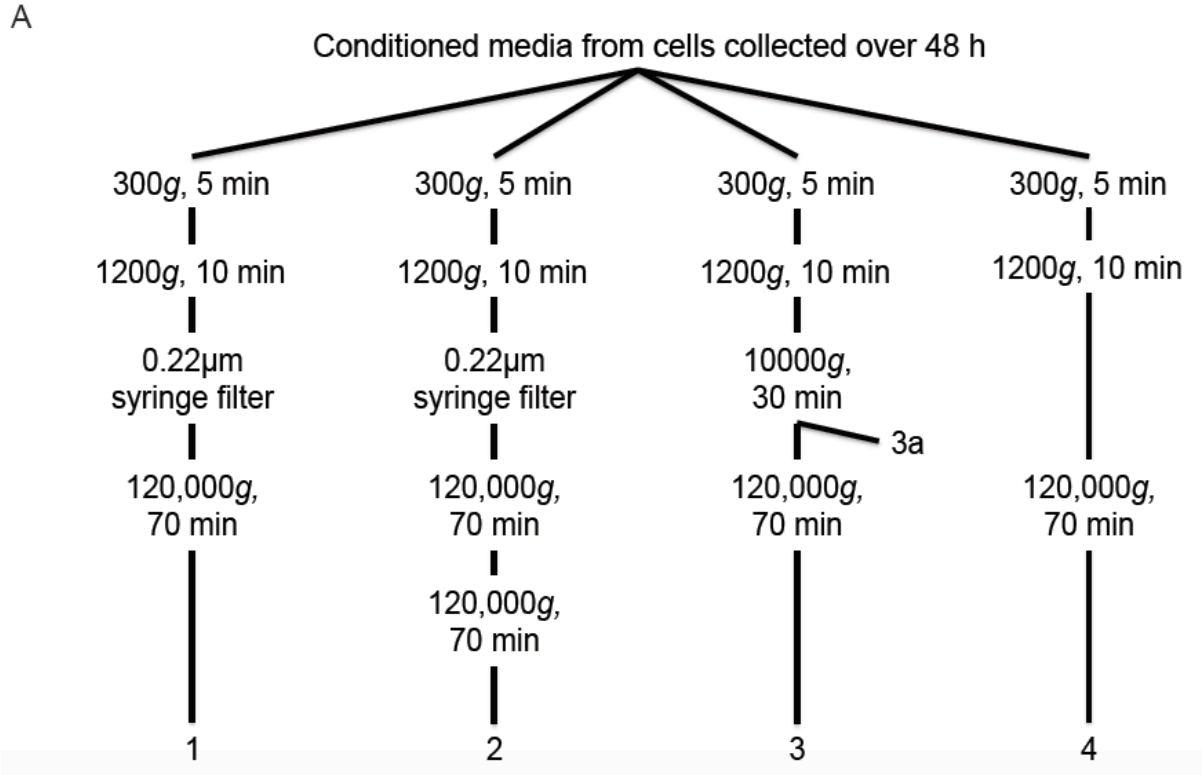

Figure 3.3.4 (cont'd)

B

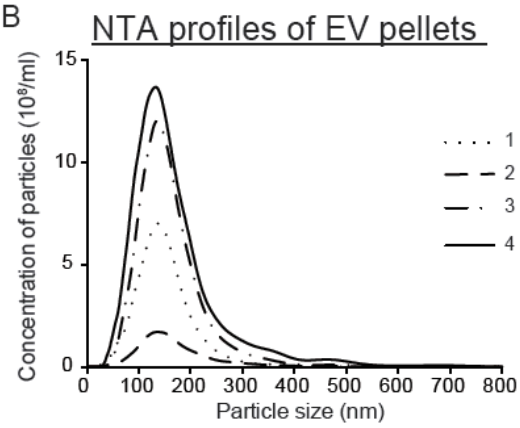

C

Sample	Mode (nm)	Mean (nm)	Conc of particles ($x10^{10}$/mL)
1	135.2	151.6	38.5
2	141.8	175.8	10.8
3	138.0	160.9	68.6
4	128.4	168.8	90.4

D

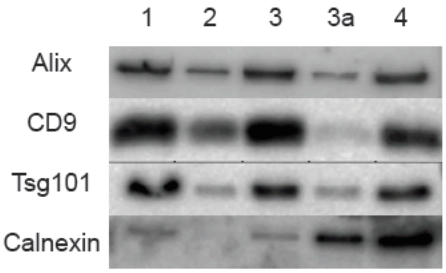

E

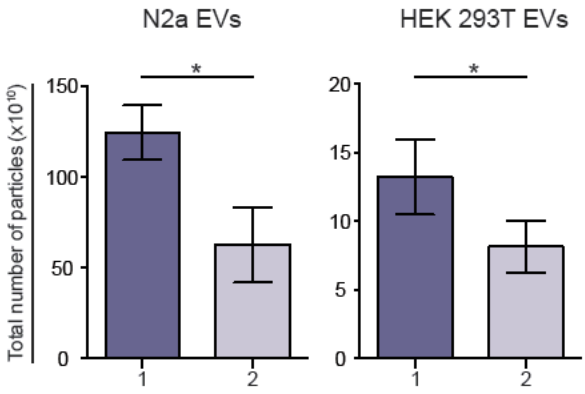

Figure 3.3.4 Analysis on EVs purified using four different UC protocols

(A) Graphical outline of the four different variations of UC tested. 3a represents the 10,000*g* pellet. (B) NTA size distribution profiles of EVs from the four UC protocols. (C) Table showing the exact mode size, mean size and concentration of particles in each of these four samples. (D) Representative WB pictures of EV markers (Alix, CD9 and Tsg101) and Calnexin in the four UC pellets and 3a pellet. (E) Graphs showing the decrease in total number of particles of UC pellet 2 as compared to pellet 1, in both N2a and HEK 293T cultures (n=3 for each cell line, bars represent mean ±SD, *indicates $p<0.05$).

3.3.5 Ultrafiltration (UF) of CM allows for purification of higher yields of intact EVs than with the UC protocol

Another issue with using the UC protocol for purification of EVs was the low percentage recovery of EVs as compared to the original starting material. From our data, we observed that the overall number of particles remaining in the supernatant after the first high-speed centrifugation is surprisingly higher than in the derivative pellet (UC-1); 3-fold for N2a and 2-fold for HEK 293T samples (**Figure 3.3.5A**). Moreover, the overall percentage of particles recovered in the final UC product (with the additional wash step) was a mere 14.0% as compared to the original CM, for both N2a and HEK samples (**Figure 3.3.5B**).

To improve on EVs yields, we tested out an alternative protocol - Ultrafiltration (UF). Similar to the UC protocol, the CM was subjected to low speed spins and 0.22um filtration to get rid of any cellular debris and larger particles. Instead of applying two high-speed centrifugation steps, the filtrate was applied on a 100-kDa molecular weight cut-off (MWCO) spin filter to concentrate the EVs and filter out smaller non-vesicular molecules (**Figure 3.3.5C**). With N2a samples, we observed that 6-fold more particles with similar size distribution were collected using the UF method as compared to the UC method (**Figure 3.3.5D**). This observation was consistent across other cell lines (HEK 293T and mouse melanoma cells-B16F10) and also for CD63-eGFP labeled HEK 293T EVs (**Figure 3.3.5E-G**). Importantly, there were very few particles in the flow-through (FT) of these spin filters, suggesting that most, if not all, of the EVs were successfully trapped in the filters (**Figure 3.3.5H**). To verify that the particles we analysed were truly EVs, we performed WB on equal volumes of the

UC and UF purified samples. The expression levels of EV markers (Alix and CD9) were much higher in UF than in UC samples (**Figure 3.3.5I**), corroborating our NTA data.

Besides improving the overall quantities of vesicles, we were also interested in understanding if the type of purification method could impact on the biophysical properties of vesicles. Hence, we visualized these EVs using TEM. The TEM pictures showed that EVs with rounded and cup-shaped morphology were present in both sample types. In some instances, EVs purified by UC appeared disrupted or fused, which was not the case with UF-purified EVs (**Figure 3.3.5J**). Moreover, fluorescence microscopy of GFP-positive EVs in suspension revealed the presence of GFP-positive aggregates only in UC samples and not for the UF sample (**Figure 3.3.5K**).

On hindsight though, these microscopy techniques were more subjective and merely semi-quantitative. Therefore, we collaborated with Dr Wolf Heusermann and Dr Nicole Meisner-Kober (Novartis Institutes) to employ fluorescence correlation spectroscopy (FCS) for more quantitative analysis of EV integrity. Using FCS, the EV hydrodynamic radius, concentration and changes in biophysical properties (e.g. fusion or fragmentation) of EVs were determined by measuring diffusion and intensity of CD63-eGFP positive EVs. The brightness of individual particles (number of CD63-eGFP molecules per vesicle) was found to be higher in UC than UF samples and this suggested the possibility of vesicle fusion within the UC sample. Moreover, we found that only 10% of total vesicles were recovered in the pellet after UC. On the other hand, in the post-UC supernatant, only 38% of the vesicles were

found to be intact while the remaining 62% of the eGFP-positive material was measured to be 2 nm, which was reported to be the putative size of free CD63-eGFP (328). Hence, our FCS findings corroborate with our previous data that there was very low pelleting efficiency of EVs with the UC method. Furthermore, we were able to prove that the UC process led to both fusion of vesicles and vesicle disruption, since free CD63-eGFP from these disrupted vesicles could be freely detected in the post-UC supernatant (**Figure 3.3.5 L&M**).

Figure 3.3.5

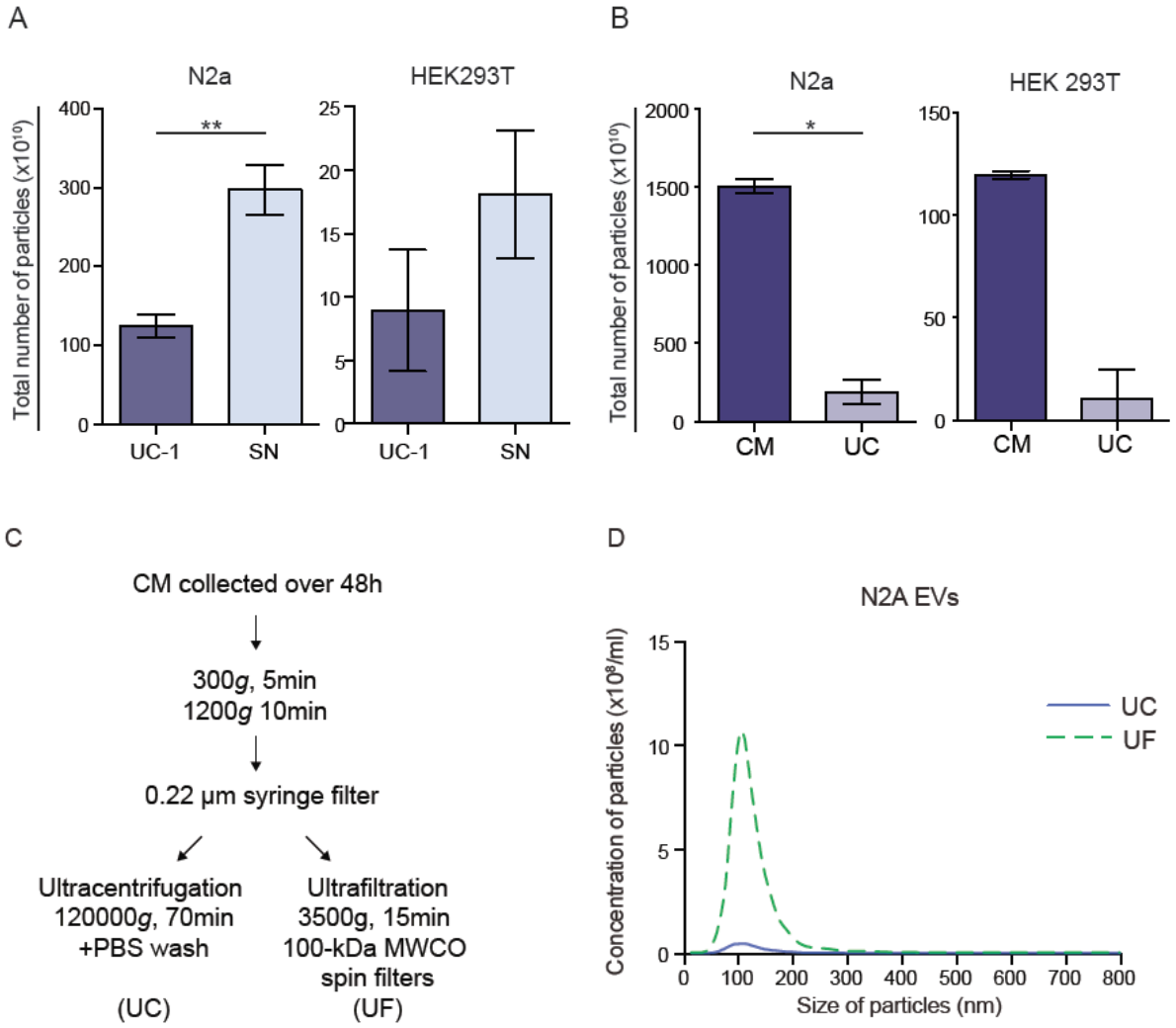

Figure 3.3.5 (cont'd)

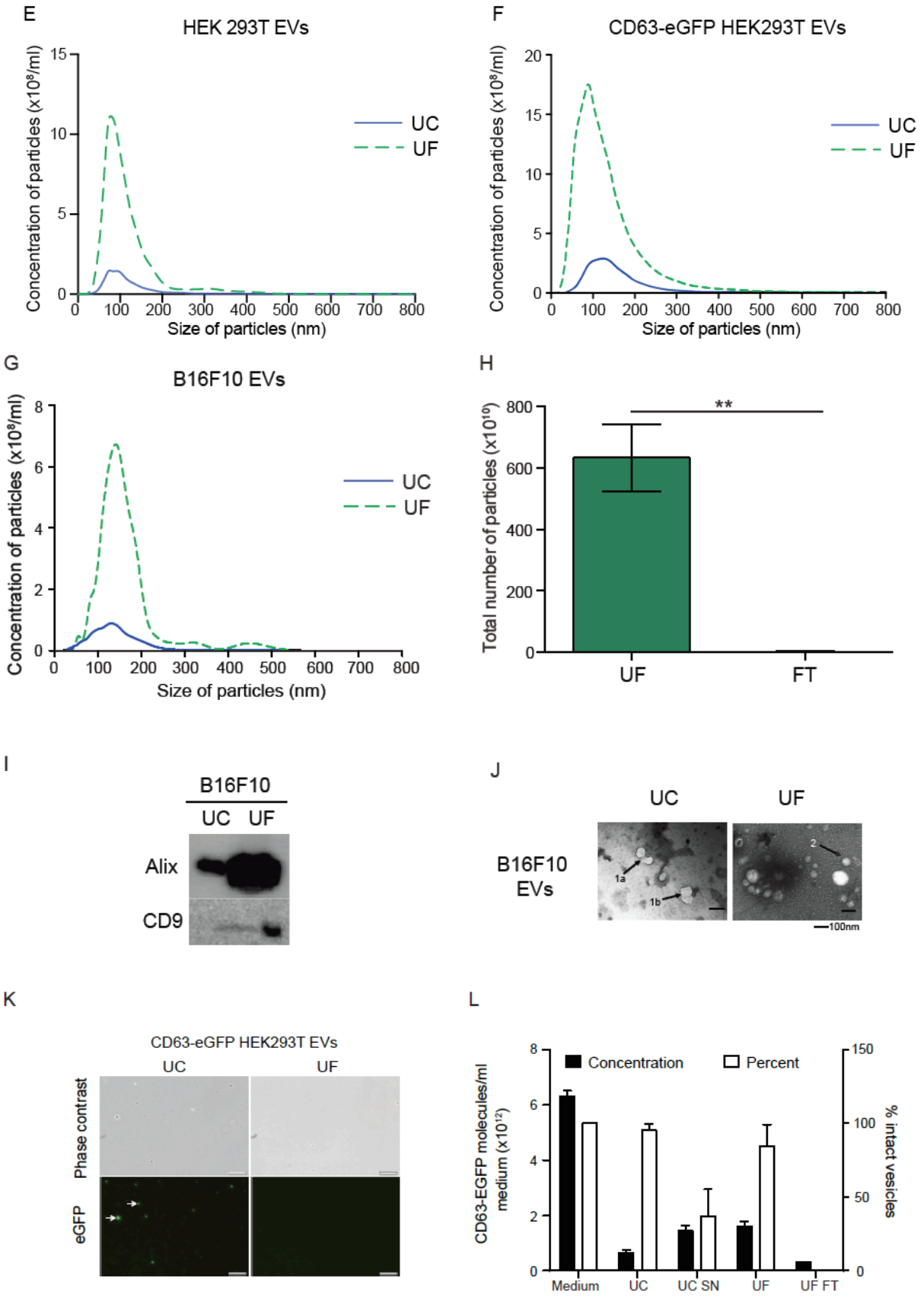

Figure 3.3.5 (cont'd)

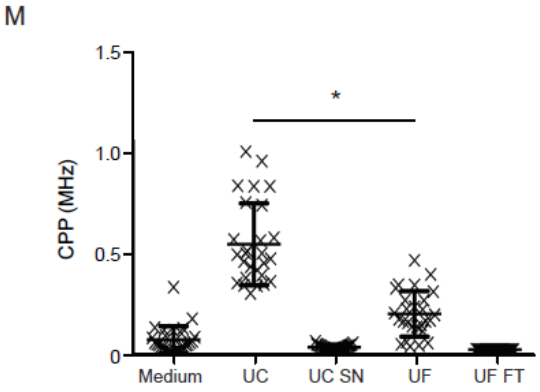

Figure 3.3.5 UF protocol enabled the purification of more EVs with intact biophysical properties as compared to UC

(A) Graphs showing a greater number of particles in the supernatant (SN) versus the pellet (UC-1) after the first high-speed centrifugation, for both N2a and HEK 293T cultures (n=3 for each cell line, bars represent mean ±SD, ** indicates $p<0.01$). (B) Graphs showing the total number of particles in the original starting CM as compared to the final UC product (UC), for both N2a and HEK 293T cultures (n=3 for each cell line, bars represent mean ±SD, *indicates $p<0.05$). (C) Graphical outline of the UC and UF protocol. Graphs showing the NTA size distribution profiles of EVs purified by the UC or UF method from N2a (D), HEK 293T (E), CD63-eGFP HEK293T (F) and B16F10 (G) cultures. (H) Graph showing the total number of particles in the UF product versus the flow-through (FT) after the UF spin from N2a cultures (n=3, bars represent mean ±SD, ** indicates $p<0.01$). (I) Representative WB pictures of EV markers (Alix and CD9) in B16F10 EVs purified by the UC or UF method. (J) Representative TEM images of B16F10 EVs purified by UC or UF. Arrows indicate phenotype of vesicles detected; 1a: broken vesicle, 1b: fusion of vesicles and 2: intact vesicle. (K) Fluorescence microscopy images of CD63-eGFP HEK293T EVs in suspension. Arrows indicate presence of GFP aggregates in UC samples only. (L) Absolute concentrations of CD63-eGFP molecules (left y-axis) and percentage of intact vesicles (right y-axis) according to FCS (SN=supernatant, FT= flow-through). (M) Molecular brightness for each particle (counts per particle)(CPP) (n=3, bars represent mean ±SD, * indicates $p< 0.05$).

3.3.6 UF co-purifies non-vesicular proteins along with EVs

Apart from NTA, we also performed protein and RNA quantification of the EVs purified by either method. Interestingly, we noticed that the overall fold change in total protein was much higher than that of the NTA and RNA quantifications (**Figure 3.3.6A**). As we assumed that the same type of EVs was purified by both methods, we speculated that this discrepancy in particle and protein fold changes might be indicative of the presence of contaminating proteins in our UF samples.

As shown in **Figure 3.3.6B**, the same amount of particles (as determined by NTA, left panel) or the same amount of proteins (as determined by microBCA assay, right panel) were loaded on a gel and blotted for Alix and CD9. When the same number of particles was loaded on the gel, the levels of Alix and CD9 appeared similar for both samples. In contrast, when equal amounts of proteins were loaded, Alix and CD9 were only detected in the UC as compared to the UF samples. To work out the extent of non-EV associated protein contamination, we used equal number of particles from UC and UF samples and back-calculated the exact protein quantities in these samples. Based on expression levels of EV markers, 3 µg of the UC product corresponded to 35 µg of the UF sample (**Figure 3.3.6C**). Hence, assuming that the same types of particles are isolated by both the UC and UF technique, we postulate that the actual protein quantity of the UF sample might have been overestimated by around 10-fold.

Figure 3.3.6

A

B16F10	Mode size (nm)	Concentration		
		Particle conc. ($x10^{10}$/ml)	Protein conc. (µg/µl)	RNA conc. (ng/µl)
UC	134.8	41.6	0.3	6.5
UF	140.7	258.1	5.9	31.5
Fold diff (vs UC)		6.2	19.7	4.7

B

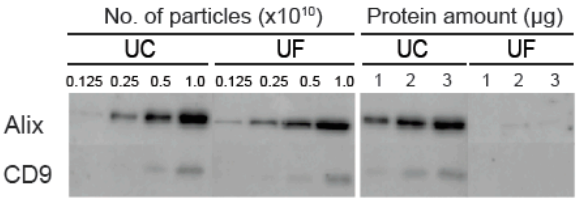

C

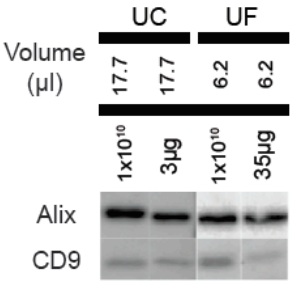

Figure 3.3.6 UF led to co-purification of non-vesicular proteins with EVs

(A) Table comparing total particle, protein and RNA concentration of B16F10 EVs purified by either the UC or UF protocol. The bottom row indicates the fold difference as compared to UC. (B) Representative WB pictures on EV markers (Alix and CD9) in N2a EVs purified by UC or UF, based on equal loading of particles (left) or protein amounts (right). (C) Representative WB pictures on EV markers (Alix and CD9) in UC and UF EVs based on equal loading of volume equivalent to $1x10^{10}$ particles. The total protein amounts indicated are calculated based on the volumes loaded.

3.3.7 LC separates EVs from non-vesicular proteins

The UF protocol used here was conducted using a 100-kDa MWCO filter, hence both EVs and other non-vesicular protein aggregates larger than this cut-off limit might remain in the filters, leading to the detection of higher protein amounts as discussed in **section 3.3.6**. To scope out the possible identities of these non-vesicular proteins, we conducted total protein staining on samples run on a SDS-PAGE gel. As compared to the UC samples, additional protein bands, particularly around the 50-70kDa ranges, were detected exclusively in the UF samples (**Figure 3.3.7A**). Preliminary mass spectrometry analysis on proteins within this size range revealed one of these proteins to be a short isoform of albumin (data not shown). As the OptiMEM used was devoid of any albumin, we speculated that these non-vesicular protein contaminations might have originated from the original growth media prior to the media change, as opposed to being true EV-associated proteins.

As EVs were much larger than these protein contaminants, we chose to fractionate the UF product on a Sephacryl S-400 size-exclusion liquid chromatography (LC) column and collected fixed 2 ml fractions eluted from the column for the entire run. The UV flow cell absorbance at 280 nm showed the presence of two distinct peaks across the entire run. After the run, we further checked each individual 2 ml fraction for total particle numbers (NTA) and protein amounts (microBCA assay) and plotted these values across the elution volume (**Figure 3.3.7B**). Based on the NTA and protein trend, we then pooled selected fractions to generate two distinct sets: fraction 1 (F1) that spans the particle and first protein peak as well as fraction 2 (F2) which spanned the second protein peak. NTA showed that the majority of particles were

recovered in F1 (98%) where the mode particle size is 97nm (**Figure 3.3.7C-D**). When we performed total protein staining on the SDS-PAGE gel, we found that many of the contaminating proteins previously seen in UF were now detected solely in F2 (**Figure 3.3.7E**).

With WB, we detected EV markers including Alix and CD9 exclusively in F1 and not F2 (**Figure 3.3.7F**). Moreover, the levels of these markers appeared to be slightly higher in F1 as compared to the UC sample and this correlated with higher particle counts in F1 than in UC sample (**Figure 3.3.7G**). Furthermore, the particle per protein ratio, which was suggested to be a good indicator of preparation purity (329), was much lower for F1 compared to UC samples (**Table 3.1& 3.2**). To ensure that the EVs purified by the LC technique were similar to that of the UC protocol, we further performed LC-MS/MS on both EV samples. Generally, the proteome of EVs from either protocol was congruent as there was a good correlation of overall protein expression and gene ontology annotations (**Figure 3.3.7H-I**). Therefore, we concluded that the addition of an LC step allowed for the purification of the same EVs with minimal protein contamination as compared to the UC protocol. Furthermore, the higher recovery percentage of particles observed with the UF protocol was maintained after this additional LC step.

Figure 3.3.7

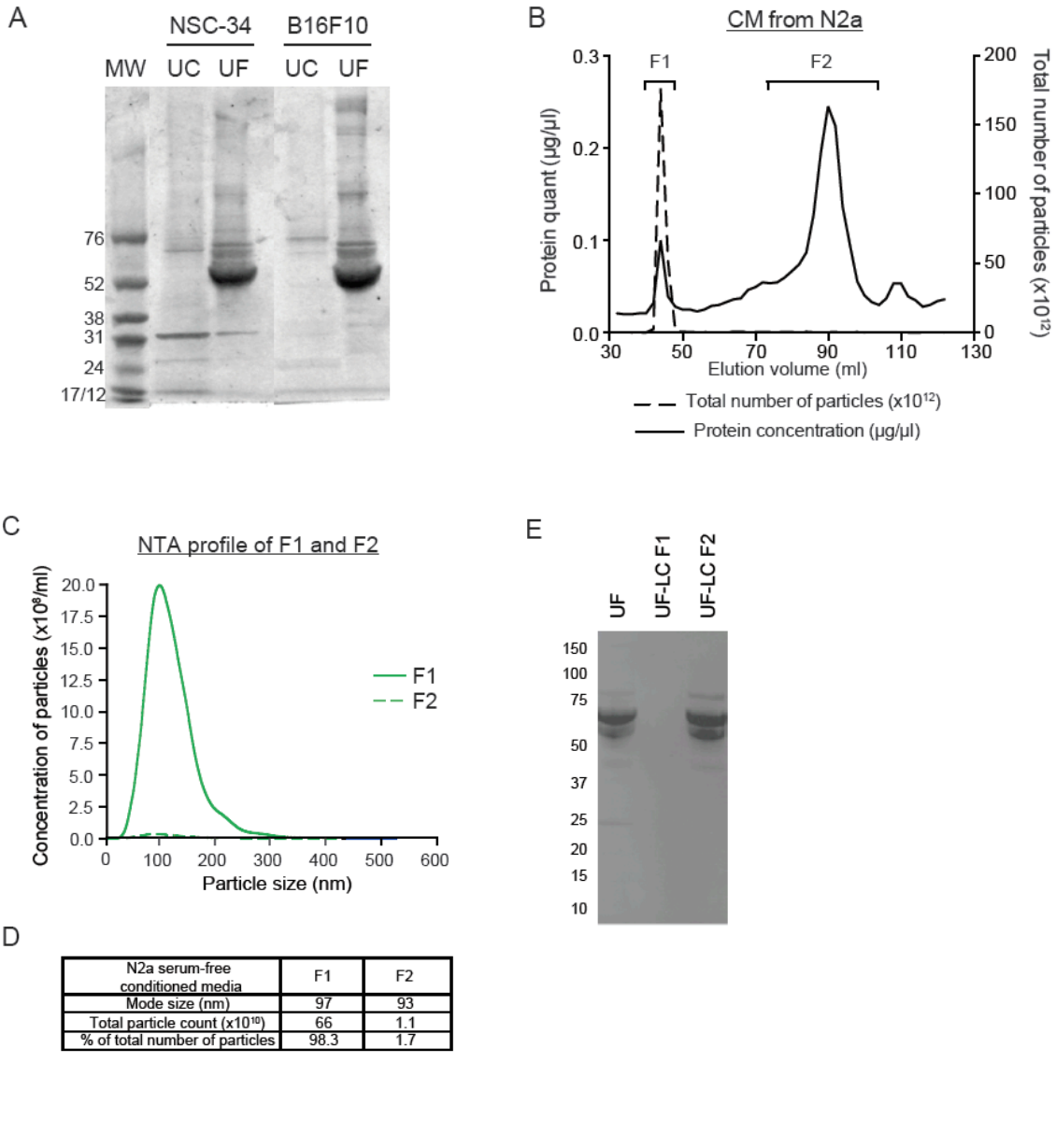

D

N2a serum-free conditioned media	F1	F2
Mode size (nm)	97	93
Total particle count (x10¹⁰)	66	1.1
% of total number of particles	98.3	1.7

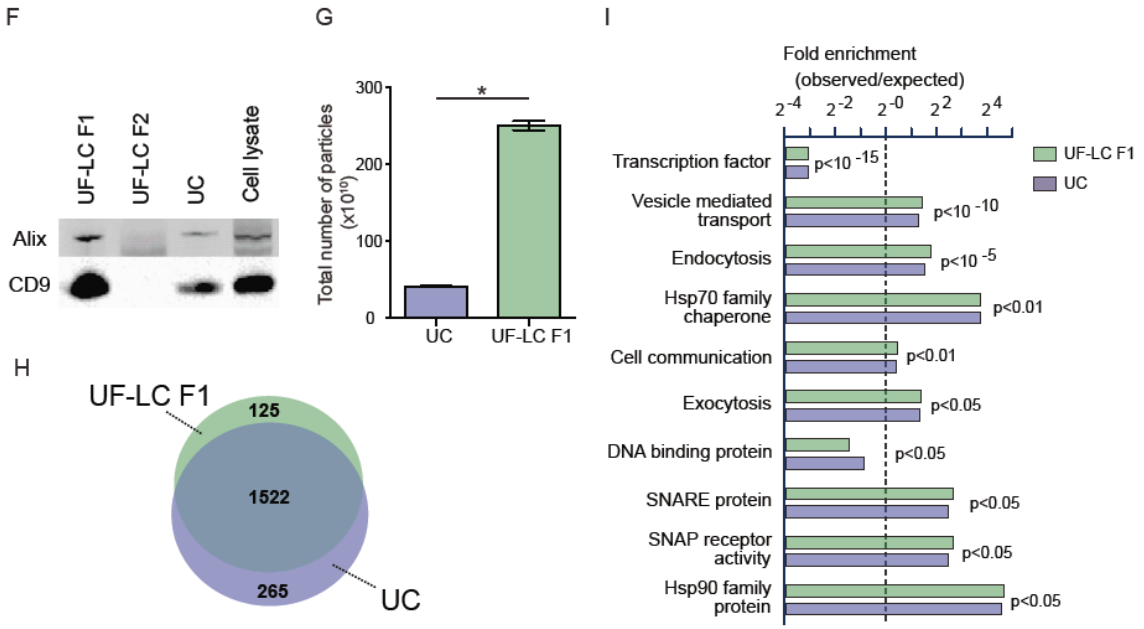

Figure 3.3.7 LC fractionation of UF product allowed for removal of protein contaminants without significantly affecting EV yields

(A) Total protein staining of SDS-PAGE gel loaded with EVs derived from NSC-34 or B16F10 cells purified by UC or UF. (B) Graph showing the protein concentration (µg/µl) (left y-axis) and total particle numbers ($x10^{10}$) (right y-axis) across the elution volume (ml) from the column (x-axis) of CM from N2a cells. Selected fractions are pooled and grouped as F1 and F2, as indicated on the graph. (C) NTA size distribution profile of F1 and F2 samples. (D) Table comparing the mode size, total particle counts and percentage of particles between F1 and F2. (E) Total protein staining of membrane with N2a EVs purified by UF, UF-LC F1 and UF-LC F2. (F) Representative WB pictures of EV markers (Alix and CD9) in N2a UF-LC F1, UF-LC F2, UC and the cell lysate. (G) Graph comparing the total number of particles purified by UC (blue) and in the UF-LC F1 sample (green) (n=3, bars represent mean ±SD, *indicates $p<0.05$). (H) Venn diagram showing good over-lap of proteins (79.6%) identified in N2a EVs purified by UF-LC F1 (green) and UC (blue). (I) Graphs showing a selected number of GO annotations of proteins identified in N2a EVs purified by UF-LC F1 (green) and UC (blue).

Table 3.1

Purity index	P/μg
High vesicular purity	$>3x10^{10}$
Low vesicular purity	$2x10^{9}$ - $2x10^{10}$
Unpure vesicles	$1.5x10^{9}$

Table 3.2

P/μg	N2a OM	N2a PS
UC pellet	$4.0x10^{9}$	$4.0x10^{9}$
LC sample	$1.4x10^{10}$	$1.7x10^{10}$

Table 3.1
Table showing the suggested purity index by Webber and Clayton (329)

Table 3.2
Table showing the purity ratios of UC and LC samples from both N2a serum-free EVs.

3.3.8 EVs purified by UF-LC maintain their biophysical properties in contrast to EVs purified by UC

As described previously in section 3.3.5, the biophysical properties (e.g. intactness and aggregation) of EVs might be affected depending on the purification method. Hence, we checked if the additional LC step could affect EV integrity. TEM analysis showed that intact cup-shaped vesicles detected in F1 were similar to that in UF samples, while F2 contained mainly “chains” of protein aggregates (**Figure 3.3.8A**). To assess the state of aggregation of vesicles, we collaborated with Dr. Mattias Hällbrink (Stockholm University) to perform total internal reflection fluorescence (TIRF) imaging on HEK 293T GFP-labeled EVs purified by either UC or the LC method. Based on TIRF, a greater fraction of EVs purified by the UC method was larger than the average size of all vesicles within the image (**Figure 3.3.8B&C**),

indicating that EVs purified by the UC method tend to aggregate more than those from the UF-LC method. To understand the *in vivo* biological implications of this aggregation phenomenon, we injected the same number of DiR-labeled EVs in mice and visualised the biodistribution of these labeled EVs 24 h after injection. Generally, the biodistribution profile was similar for both UC and LC-purified EVs across all organs, with most of the overall signal detected in the liver. Interestingly though, UC-purified EVs showed a 4.6 times stronger signal in the lungs as compared to the LC group. Correspondingly, we saw a significantly higher signal in the liver with the LC over the UC group of EVs (**Figure 3.3.8D-E**). Hence, we here demonstrated that the change in biophysical properties of the resultant EVs could have a profound impact on the bio-distribution of EVs.

Figure 3.3.8

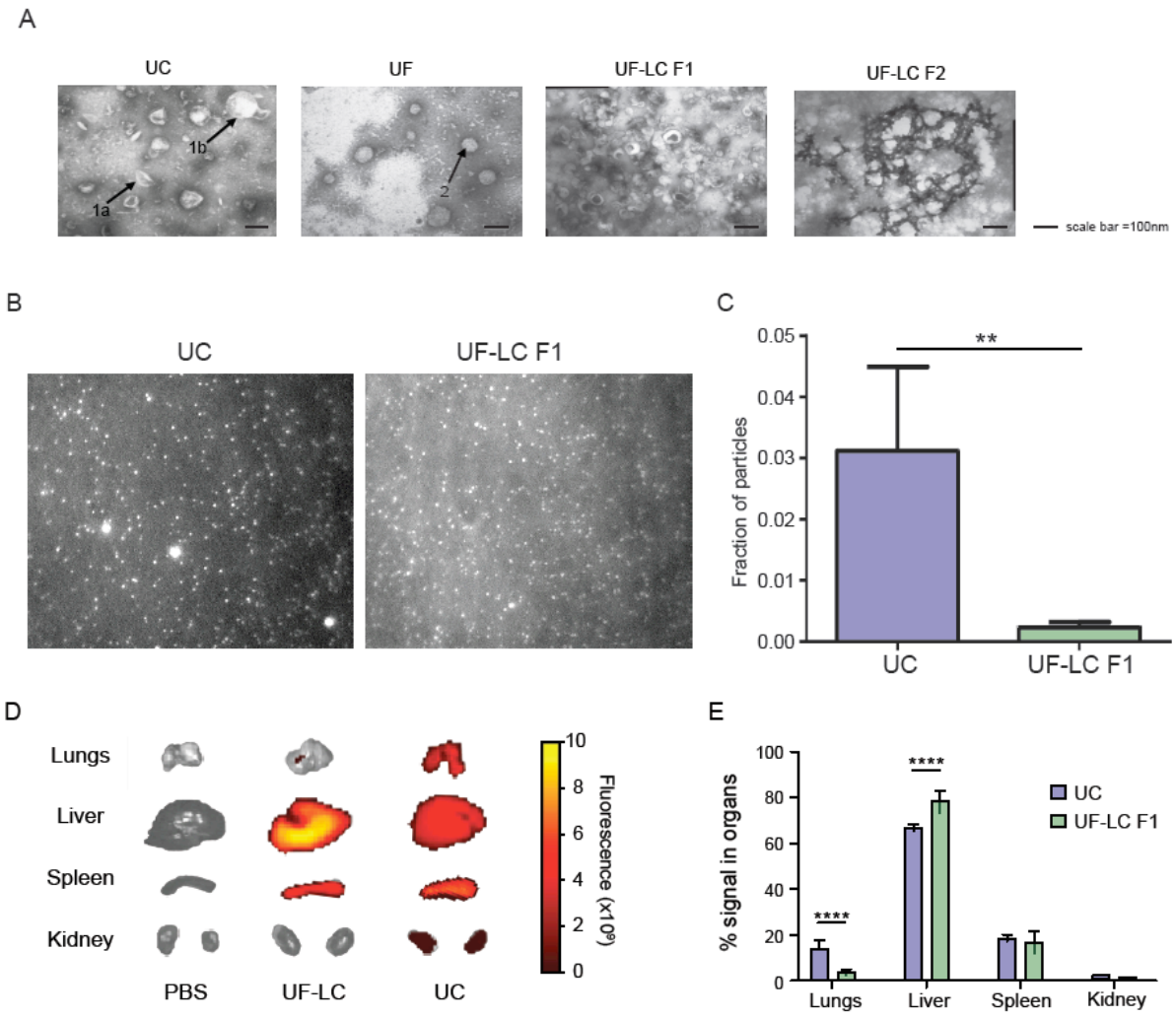

Figure 3.3.8 LC step did not compromise the EV integrity

(A) Representative TEM pictures showing N2a EVs purified by UC, UF, UF-LC F1 and UF-LC F2. Scale bar indicates 100nm. (B) TIRF imaging of CD63-eGFP labeled HEK 293T EVs by UC and UF-LC F1. (C) Graph comparing the fraction of particles measured to be larger than the average size of vesicles within the pool for UC (blue) and UF-LC F1 (green) samples (n=3) (D) IVIS imaging of selected organs 24 h post injection of EVs purified by UF-LC or UC. (E) Graphs comparing the percentage of overall fluorescence signal detected in the lungs, liver, spleen and kidneys of mice injected with UC (blue) or UF-LC F1 (green) EVs (n=5, bars represent mean ±SD, ****indicates p< 0.0001)

3.3.9 LC methodology is applicable for purification of EVs from serum-containing media

With the understanding that the LC methodology was suitable for purification of EVs, we decided to further test if this protocol could be extended to serum-containing media. Using the same protocol as described previously, pre-spun CM was collected post 48 h from N2a cells and subjected to the same pre-filtration step (UF), followed by fractionation on the LC column. Interestingly we noticed that the protein and total particle profiles from the eluted volume were less distinct as compared to serum-free CM. Using the same parameters as before, we pooled the individual fractions into four general groups (F1-F4) (**Figure 3.3.9A**). Based on NTA and protein quantities, F1 and F2 contained the majority of all the particles eluted, F3 represented the intermediate region between the protein and particle peaks and F4 contained the bulk of the proteins detected. The latter two fractions contained only few particles (**Figure 3.3.9B-C**). As expected, and in accordance with the previous results on serum-free conditioned media, WB for EV markers showed that Alix and CD9 could only be detected in F1 (**Figure 3.3.9D**). All of these results were consistently found when testing on pre-spun CM from another cell source- HEK 293T (**Figure 3.3.9E-F**).

Figure 3.3.9

A

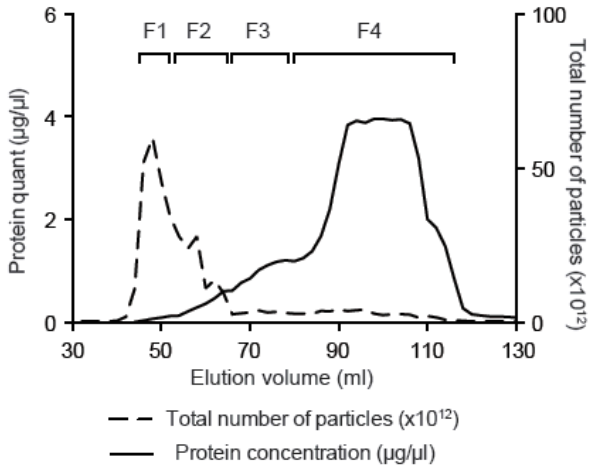

B

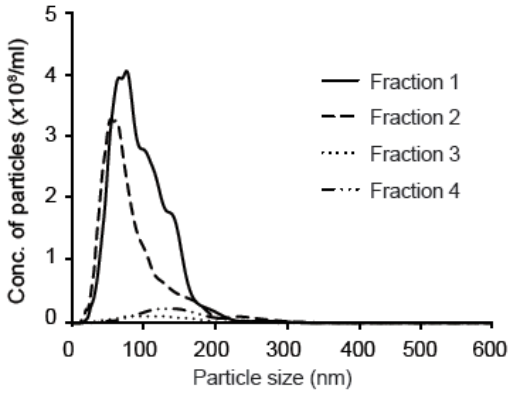

C

N2a pre-spun CM	F1	F2	F3	F4
Mode (nm)	99	89	127	151
Total no. of particles (x10^{10})	275	183	13	56
% of total no. of particles	52	35	2	11

D

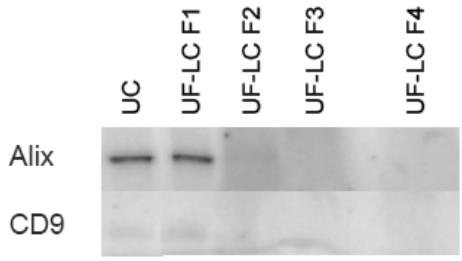

E

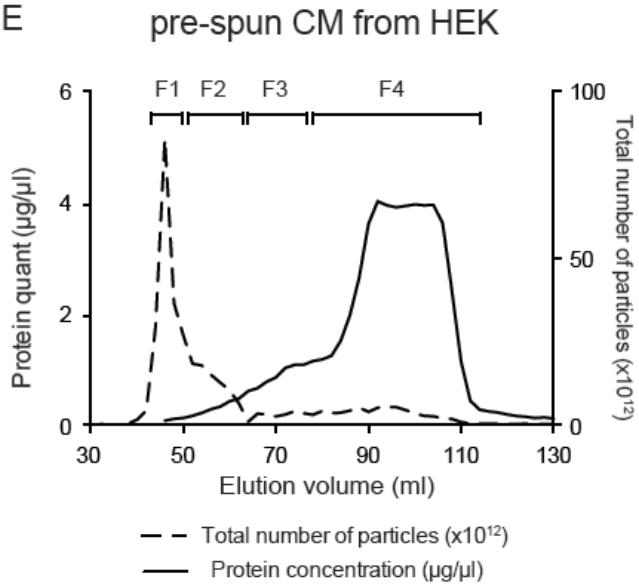

F

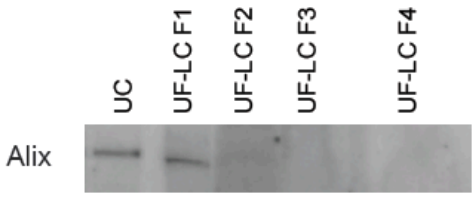

Figure 3.3.9 UF-LC protocol can be applied to serum-containing media

(A) Graph showing the protein concentration (µg/µl) (left y-axis) and total particle numbers ($x10^{10}$) (right y-axis) across the elution volume (ml) from the column (x-axis) after running pre-spun CM from N2a cells. Selected fractions are pooled and grouped as F1, F2, F3 and F4, as indicated on the graph. (B) NTA size distribution profiles of F1-F4 samples. (C) Table indicating the mode size, total number of particles and % of total number of particles across F1-F4. (D) Representative WB pictures showing that EV markers (Alix and CD9) were exclusively detected in UC and UF-LC F1 samples. (E) Graph showing the protein concentration (µg/µl) (left y-axis) and total particle numbers ($x10^{10}$) (right y-axis) across the elution volume (ml) from the column (x-axis) after running pre-spun CM from HEK 293T cells. Selected fractions are pooled and grouped as F1, F2, F3 and F4, as indicated on the graph. (F) Representative WB pictures showing that the EV marker (Alix) was exclusively detected in UC and UF-LC F1 samples.

3.4 Discussion

3.4.1 Serum-free conditions lead to increased production of EVs with different proteome

In this chapter, we first investigated the relationship between different external culturing factors (cell density, incubation period and type of conditioned media) with EV quantity and protein content. Generally, we found an inverse relationship between the starting cell density and incubation periods for total EV yields. At lower cell density cultures, longer incubation periods for CM collection derive similar EV yield as shorter incubation periods of higher cell density cultures. This was perhaps unsurprising, as all cells could constitutively secrete vesicles into the external environment, hence, more cells would lead to a greater release of vesicles. However, at longer incubation periods (>48 h for OptiMEM and >72 h for pre-spun media), we reported that the use of NTA as a sole indicator of EV yield was inaccurate due to the increasing presence of calnexin seen with WB. Generally, we noticed that these cultures mostly comprise of unhealthy and dying cells, which were capable of releasing apoptotic bodies. Subsequently, some of these smaller apoptotic bodies would be pelleted with EVs and attribute partially to the total particles counts detected by NTA. Hence, we believed that it is crucially important to collect EVs from healthy cells over a suitable shorter incubation period (≤48 h), to minimize any cross-contamination in EV analysis.

More interestingly, we found that the absence of serum in the conditioned media greatly affected the overall EV yield and content. Across different mouse and human

neuroblastoma cell lines, cells cultured in serum-free conditions displayed very different EV release kinetics, with more EVs detected, as compared to serum-containing conditions. This is despite the fact that additional serum EVs, which were inefficiently removed from pre-spun media could have contributed to overall total EV counts. Importantly, we here showed that this trend was consistent, regardless of total cell numbers or conditioning time. Furthermore, nano LC-MS/MS analysis revealed that the general proteome of EVs collected from the two conditions were slightly different; with only 62% of commonly identified proteins expressed at similar levels in EVs isolated from both conditions.

In OptiMEM-derived EVs, we saw an up-regulation of several G-proteins and GTPase/Ras-related proteins. Some studies have reported that ARF6 and its effector phospholipase D2 (PLD2) could regulate the formation of ILVs in MVBs (330). Furthermore, small GTPases such as Rab 27a and Rab 27b, have been shown to be directly involved in both MVB re-localization and docking at the plasma membrane prior to EV release (331,332). Coincidentally, ARF6 was one of the most significantly up regulated protein in OptiMEM-derived EVs highlighted from our proteomics data. Apart from G-proteins, proteins involved in oxygen and reactive species metabolic process were also significantly higher in OptiMEM-derived EVs as compared to pre-spun EVs. Importantly, we know that the absence of serum in OptiMEM media can induce a type of cellular stress. Some reports have shown that other forms of cellular stresses (e.g. hypoxia, exposure to TNF- α or high glucose) have no effect in the physical aspects of EVs but rather altered the intra-EV protein and RNA content drastically (333). Similarly, we did not detect any differences in the mode size of EVs from the two conditions, but rather found an enrichment of stress-

related proteins such as macrophage migration inhibitory factor (MIF), epoxide hydrolase 1 (EPHX1) and MYG1 (334–336). Hence, we speculated that under stressful OptiMEM conditions, some of these stress-related proteins in the cells are re-packaged into MVBs. Furthermore; higher levels of ARF6 and other small GTPases in cells could have promoted increased MVB docking at the plasma membrane and as a result, lead to an increased secretion of EVs containing these proteins. Interestingly for pre-spun-derived EVs, proteins involved in mRNA binding, splicing and processing activity were enriched as compared to OptiMEM-derived EVs. We selected and validated SERPINF1, which was identified as one of the most differently expressed proteins in pre-spun as compared to OptiMEM EVs. SERPINF1, also known as pigment epithelium derived factor (PEDF), is a serine protease inhibitor (337) involved in anti-angiogenic activity and cell proliferation in neuroblastoma tumour cells (338,339). Previously, PEDF was found in EVs from pleural effusions (340), however, its role in EVs remained unclear.

Our data here clearly indicated that the absence or presence of serum in culture could affect both the quantity and composition of EV released from cells. Based on the proteomics data, we hypothesize that under OptiMEM serum-free conditions, N2a cells responded to this switch in media by activating specific signaling cascades, including those involved in EVs biogenesis and release. Moreover, these results could offer some insights into how the extracellular environment can interact with intracellular signaling pathways, and subsequently affect EV production and content.

3.4.2 The UC protocol is not ideal for EV purification

Although EVs have received increasing attention due to the role in intercellular communication, one significant bottleneck in EV research was the lack of consensus on a purification method that permitted isolation of pure and intact vesicles from both *in vitro* and *in vivo* samples.

The current most common method used across the field for EV research was the UC method. This protocol is easy-to-follow and requires little use of specialized equipment, apart an ultracentrifugation unit that could be commonly found in most laboratories. With the availability of better EV characterization tools, such as NTA and WB for reported EV markers and contaminating markers, it was becoming more evident that the UC protocol has several drawbacks. Initially, we compared four different UC protocol variations as reported in literature, aiming to evaluate and derive an optimal UC protocol. Our preliminary data on the UC protocol showed that an additional PBS wash step was crucial for obtaining a pure EV product with minimal contamination. Unfortunately though, this extra step resulted in reduced EV yields as compared to the pellet after the first high-speed spin. Furthermore, based on NTA quantification, the final amount of EVs was found to be only a small fraction of the original starting amount in CM. To address this issue, we checked the supernatants after the first high-speed spin and to our surprise, there was much more particles in the supernatants as compared to the EV pellet, strongly suggesting most of the EVs were not pelleted initially. Indeed, there have been some recent reports commenting and suggesting solutions to curb the low EV recovery rates with the UC protocol. Momen-Heravi et al found that the viscosity of the sample type

inversely correlated with EV recovery yields. Hence, they suggest that samples should be pre-diluted prior to the UC protocol (69). Alternatively, there were some debates that the suggested centrifugation time (70 min) might not be sufficient for complete pelleting of EVs. One study demonstrated that an 18 h centrifugation period allows for clearance of 95% of RNA-containing FBS EVs (341). On the other hand, Cvjetkovic et al report that excessively long spin times (more than 4 h) could lead to co-pelleting of non-vesicular proteins (68). Overall, there is still a lack of understanding regarding the overall EV yields with respect to the duration of UC spin. Furthermore, there has yet to be any detailed study regarding the impact of UC spins on EV integrity; one might be tempted to speculate that the high gravitational (*g)* forces applied in the UC protocol might introduce extensive shear forces and contribute to potential vesicle rupture, aggregation or even fusion.

Nonetheless, our data here corroborated with previous reports on how the UC protocol leads to low and operator-dependent yields (342,343). More importantly, as the UC protocol could not be translated easily for large-scale isolation of vesicles, which is imperative for large clinical studies, we aimed to seek an alternative method for our purification of EVs.

3.4.3 Ultrafiltration (UF) of sample leads to higher EV yields but with co-purification of proteins

To improve our EV yields during purification, we tested the possibility of using an ultrafiltration device that would concentrate CM and filter out smaller non-vesicular

proteins. Previously, the use of similar filtration-based strategies for purification of EVs had only been described for urine (344) and plasma (345) samples.

Here, our side-by-side comparisons between the UC and the UF protocol on cell culture CM showed that UF allows for the purification of 6-fold more vesicles than UC. This trend was consistently seen across both human and mouse cell types, and also when purifying a specific pool of GFP-labeled EVs. Importantly, we demonstrated that the biophysical aspects of EVs are well preserved with the UF method and not with UC, based on TEM imaging and with the more quantitative FCS methodology. We believe that this phenomenon was simply due to the lack of high *g* force spins in the UF protocol, and this in turn allowed for the purification of EVs in a less harsh process.

On hindsight though, we found a huge discrepancy in the fold changes with respect to NTA and protein quantifications. Based on mass spectrometry and total protein staining, we deduced that certain proteins, such as albumin that was originally present in the growth media prior to media change, were not removed even with repeated PBS washes of the cells. Instead, these proteins can get trapped in the filters (346) and co-purify with the EVs. As a result, the purity of EVs is severely compromised and the actual protein quantity and content of the EVs in the UF product are grossly overestimated.

3.4.4 Subsequent LC allows for separation of EVs from contaminating proteins without affect EV yield and integrity

Besides causing problems in EV quantification, the presence of these contaminating proteins could also impact negatively on the application of more in-depth analysis of the EVs such as proteomics and RNA sequencing. Hence, we devised a second part downstream to the UF protocol- size exclusion-based LC, which aimed at separating non-vesicular protein aggregates from EVs. Indeed, our LC chromatographs showed that we were able to obtain two distinct peaks; the first fraction containing majority of the total number of particles that stained positively for EV markers while the second fraction consisted of mainly proteins that we had previously identified as contaminating proteins from the UF purification. Importantly, we showed that the superior yield obtained from the initial UF over the UC purification was not significantly compromised even with the addition of this LC step.

To further verify that we had indeed purified EVs by the UF-LC protocol, we performed mass spectrometry-based proteomics comparison on EVs purified by UF-LC to those purified by UC. Overall, the proteins identified in the two groups were very similar where the protein abundance of reported EV proteins (108) such as Alix, Hsp-90 family of proteins and UBC as well as GO annotations of a variety of different molecular pathways matched well between the two groups of EVs. In addition to the molecular characterization of EVs, we also checked the biophysical properties of EVs after the LC step. Generally, the EVs appeared to be similar as EVs prior to the LC process. On the other hand, the formation of aggregates exclusively in EVs purified by the UC protocol was again confirmed with TIRF imaging. To assess the possible effect of vesicle integrity with the functionality of EVs, we performed in vivo bio-distribution studies in mice injected with either group of EVs. Similar to earlier reports of large aggregates of different nanoparticle formulations (347,348), we saw

a similar trend of UC-purified EVs accumulating in the lungs, which could potentially affect the respiratory tract of animals treated with EVs. Besides the therapeutic aspects of EVs, we strongly believed that the UF-LC methodology for EV purification would also be suitable for studies relating to the biological roles of EVs as hampered vesicle integrity and aggregation might have profound impact on their natural activity.

Most of the comparison data reported here have been carried out on EVs purified from serum-free CM. There were reports that EVs are constitutively secreted from all cell types in normal growing conditions and also into different bodily fluids. Hence, we further tested if the UF-LC protocol was equally useful for other sample types, such as serum-containing conditioned media. Our data here demonstrated that the UF-LC protocol was similarly able to purify EVs from serum-containing media, which express similar EV markers as that of UC purified EVs. We strongly believed that our finding here was especially useful for others in the field who are investigating EVs from different biological fluids, as these samples often contain complex compositions of contaminating proteins that could pose as a significant problem when using the standard UC protocol for vesicle purification.

3.5 Conclusion

In this chapter, we initially showed data on how external factors could affect EV secretion and content. From this study though, we realized that there were many difficulties associated with the traditional ultracentrifugation protocol. Hence, we designed a two-step strategy- UF-LC for EV purification, based on several protocols developed by others (84,193). This was the first ever study providing a comprehensive comparison on both molecular and biophysical aspects of EVs purified by the UC versus the UF-LC protocol, showing that the UF-LC was more beneficial in terms of EV purity and yields. More importantly, we demonstrated that the harsh conditions employed in the UC protocol had a negative impact on the integrity of EVs, and how this had implications for downstream *in vivo* applications of these EVs. We strongly believed that the UF-LC protocol as described here would aid in the purification of EVs across the field, such that these EVs could now be applied to different biological assays to unravel their biological functions and unleash their potential in therapeutic applications.

Chapter 4

Optimisation of method for collection and purification of EVs from pluripotent stem cell sources

4.1 Introduction

One of the main aims of this thesis was to investigate the roles of EVs released from pluripotent stem cell sources, namely iPSCs. Previously, there have only been a handful of studies describing EVs released from embryonic stem cell (ESCs) sources and their functional roles in the delivery of pluripotency associated molecules (120,349,350). However, research on ESCs has been tempered with numerous ethical debates regarding the origin of these ESCs and their subsequent scientific and medical uses. With the discovery of iPSCs and new understanding on how these alternative forms of stem cell could be used to study differentiation status and re-modeling of diseases, there has been a gradual shift of interest towards this group of pluripotent stem cells. Currently, there has yet to be any published data about EVs released from iPSCs in their undifferentiated state.

In collaboration with Dr Paul Fairchild's lab (Dunn School of Pathology, University of Oxford), we initially attempted to purify EVs from both iPSCs and ESCs using the established UC method. However, as shown in our preliminary analysis in **figure 1.7**, we found a number of problems in characterizing EVs from these cells using this

method. Firstly, there was a huge discrepancy in the protein and NTA quantifications of total EV yield. Furthermore, these quantities did not correlate with the expression of EV markers as detected by western blotting. Based on these results, we hypothesized that the UC protocol resulted in pelleting of many non-vesicular proteins, which would interfere with subsequent downstream analysis of the pure EV content.

From our earlier findings in chapter 3, we learned that the derivation of pure EVs could be influenced by the following two factors; the type of CM used for EV collection and the method used for EV purification. As discussed by others in the field (341) and in this thesis, there is still some ambiguity in the use of pre-spun media due to the inefficient removal of all serum microvesicles prior to use, which in turn can affect subsequent quantification and molecular analysis of EVs. On the other hand, complete removal of serum EVs has been recently shown to result in reduced growth rate in a number of different immortalized cell types (351). In stem cell cultures, an absence of serum has been reported to induce spontaneous differentiation of the stem cells (352). Hence, in this chapter, we first described our efforts in testing alternative media types for the collection of EVs from stem cells. Following a 48 h incubation period in these different media types, we monitored for any changes in stem cell viability and the corresponding EV yields to deduce the most suitable type of media for EV collection from stem cells.

Previously, we showed that the UF-LC method for EV purification was more advantageous than the original UC protocol in terms of EV yield, purity and vesicle integrity; all of which are crucial for unraveling the biological functions of EVs. On

hindsight though, all of our earlier work on UF-LC were conducted on either serum-free or pre-spun CM. Stem cell media, however, is more complex and protein-rich than the regular pre-spun media used for immortalized cell lines. As there has yet to be any data showing if the use of different purification methods can impact on EVs purified from stem cell media, we carried out a detailed comparative study of stem cell EVs purified by either the UC or the UF-LC method to elucidate which method was most suited for purification of EVs from stem cells. All of the data described in this chapter was based on CM derived from mouse iPSCs and ESCs.

4.2 Material and methodologies

4.2.1 Evaluation of stem cells in different media types

All mouse ESCs (ESF121 line), mouse iPSCs (imef14 line) and mouse embryonic fibroblasts (MEFs) described in this chapter, were derived from Prof. Paul Fairchild's lab (Dunn School of Pathology, University of Oxford). All conditions for culturing MEFs and the mouse embryonic stem cells are as described in **section 2.1.2**.

To evaluate the possibility of using alternative media types for collection of EVs from stem cells, we analysed the stem cells and their derivative EVs at 48 h. Generally, when the stem cells grown on gelatin approached 70% confluence, growth media was removed; cells were washed with phosphate buffer saline (PBS) and replaced with fresh stem cell media, pre-spun stem cell media or serum-free media/OptiMEM supplemented with 50 μg/ml of P/S and 10^6 units of mLIF. Pre-spun stem cell media

described here is complete stem cell media that had been pre-spun at 120,000*g* for 16 h prior to use. 48 h later after the media change, stem cells were imaged under the light microscope to investigate their morphology and CM was collected for EV collection. The CM collected from all three culturing conditions was initially processed for EV purification using the UC protocol (**section 2.3.1**). Following collection of CM, cells were trypsinised, stained with tryphan blue and counted with a haemocytometer. Each EV sample was subsequently subjected to NTA (**section 2.4.1**) for quantification and determination of the size distribution of particles and western blotting (**section 2.4.2**) for reported EV markers (Alix, Tsg101 and CD9) and stem cell marker (POU5F1/OCT-4).

4.2.2 Comparison study of stem cell EVs purified by UC or UF-LC method

A similar comparison study to that described in Chapter 3 was conducted on mouse stem cell (ESCs and iPSCs) CM to evaluate the usefulness of UF-LC as a purification tool for EVs from complex media sources. For EV collection, CM was collected post-48 h after media change and equally divided into two halves, one for purification with the UC protocol (**section 2.3.1**) and the other for UF with subsequent LC protocol (**section 2.3.2**). For more thorough analysis of the UC pellet and the initial LC sample, these samples were subjected to an additional LC step as described in **section 2.3.2** in order to improve on the purity of the EVs.

4.2.3 Sucrose gradient density centrifugation of EVs

The sucrose gradient density centrifugation protocol used here was based from the protocol described by Théry et al in 2006. Briefly, hydroxyethylpiperazine-*N*'-2-ethanesulfonic acid (HEPES)/sucrose stock solution was prepared by mixing 428 g of protease-free sucrose (Sigma) in 500 ml of 20 mM of HEPES buffer. The pH was adjusted to 7.4 with 1M sodium hydroxide (NaOH) and stored at 4°C. Prior to construction of the sucrose gradient, the HEPES/sucrose stock solution was diluted with 20mM HEPES buffer to generate 10 concentrations of sucrose solutions (0.25-2.5M with 0.25 increments). The EV sample collected after UC and LC was pre-mixed with either 0.25M or 2.5M of HEPES/sucrose stock to 1 ml total volume and loaded at either at the top or bottom of the linear sucrose gradient respectively. The sucrose gradient was then centrifuged at 200,000*g* for 16 h or 72 h at 4°C in a SW 40 swing rotor (Beckman Coulter). 1 ml fractions were carefully collected from the top and each fraction was weighed to obtain an estimated density of each fraction. Each 1ml sucrose fraction was subsequently diluted in 25 ml of PBS and centrifuged at 120,000*g* for 70 min at 4°C to wash and pellet the particles. The resultant UC pellet of each fraction was re-suspended in 50 µl of PBS and subjected to molecular analysis.

4.2.4 Molecular and biophysical characterisation of stem cell EVs

EVs purified by either the UC, LC method or with sucrose gradient centrifugation was first analysed by NTA (**section 2.4.1**), quantified for protein and RNA quantification (**section 2.4.2**) and western blotting for reported EV markers (**section 2.4.3**). RNA extracted from the different EV samples was also subjected to RNA profiling using the Agilent Bioanalyzer small RNA and Pico chip (**section 2.4.6**). For better

understanding of the biophysical properties of EVs, samples were negatively stained and visualised with TEM (**section 2.4.4**).

4.2.5 Statistics

The student's t-test was used when comparing EVs derived by the UC versus LC purification (**Figure 4.3.4B&C** and **Figure 4.3.5B&C**).

4.3 Results

4.3.1 Use of alternative types of serum-depleted media is not a viable option for EV collection from stem cells

The inclusion of serum in stem cell media culture was deduced as one of the contributing factors for the maintenance of stem cells in their undifferentiated state. With the potential use of stem cells for cell transplantations, a number of researchers have started to use alternatives to serum (e.g. serum-replacement media) to avoid potential transmission of animal pathogens. Similarly, the inclusion of serum in stem cell media would pose a problem as serum contains microvesicles could be co-purified and interfere with downstream analysis of stem cell EVs. Hence, we chose to adopt the same strategy, by substituting the serum component of our stem cell media with knockout serum replacement media (KOSR). From the ingredient list of KOSR (353), it is reported that KOSR would not contain any serum microvesicles. However, there was less information related to the exact concentrations of the different proteins in this replacement media such as albumin.

To evaluate if the KOSR media might display similar problems in NTA quantification as that of pre-spun media, we subjected the media alone to the UC purification method and analysed the resultant UC pellet by NTA. In addition to the standard stem cell media supplemented with KOSR (SR), we further prepared two other media types for comparison; pre-spun SR-media (PS) and the serum-free media/OptiMEM (OM). Interestingly, the NTA size distribution profiles of all three

types of media pellets indicated that some particles could be detected in all three media pellets, with the highest concentration of particles detected in the SR-media UC pellet (**Figure 4.3.1A&B**). Importantly, the mode sizes of particles in the SR-media UC pellet were similar to EVs.

To assess the viability of stem cells grown in these media types for EV collection, we changed mouse iPSCs and ESCs cultures to fresh SR-media, pre-spun or OptiMEM media. After 48 h, we imaged the cells in culture and purified EVs from the CM using the established UC method. Interestingly, both iPSCs (**Figure 4.3.1C&D**) and ESCs (**Figure 4.3.1F&G**) performed differently in the three media types. Generally in PS media, both cell types did not seem to be as healthy based on cell morphology and had much lower total cell counts as compared to the normal SR-media condition. On the other hand, stem cells appeared to have proliferated at a higher rate and in some instances, displayed altered morphology when cultured under OptiMEM media. By NTA, we found that the highest amount of particles was consistently recovered from SR-CM, followed by OptiMEM and lastly pre-spun SR-media (**Figure 4.3.1E&H**).

From these preliminary studies, we deduced that using pre-spun SR-media was not a viable option for culturing of these cells. On the other hand, although stem cells appeared to be more viable in OptiMEM conditions, it appeared that most of the stem cells had undergone spontaneous differentiation due to the lack of serum and this effect would result in the release of EVs from both stem cells and the differentiated cells. Hence, we decided that the most suitable media type for collection of EVs from stem cells would be the original stem cell media supplemented with KOSR.

Figure 4.3.1

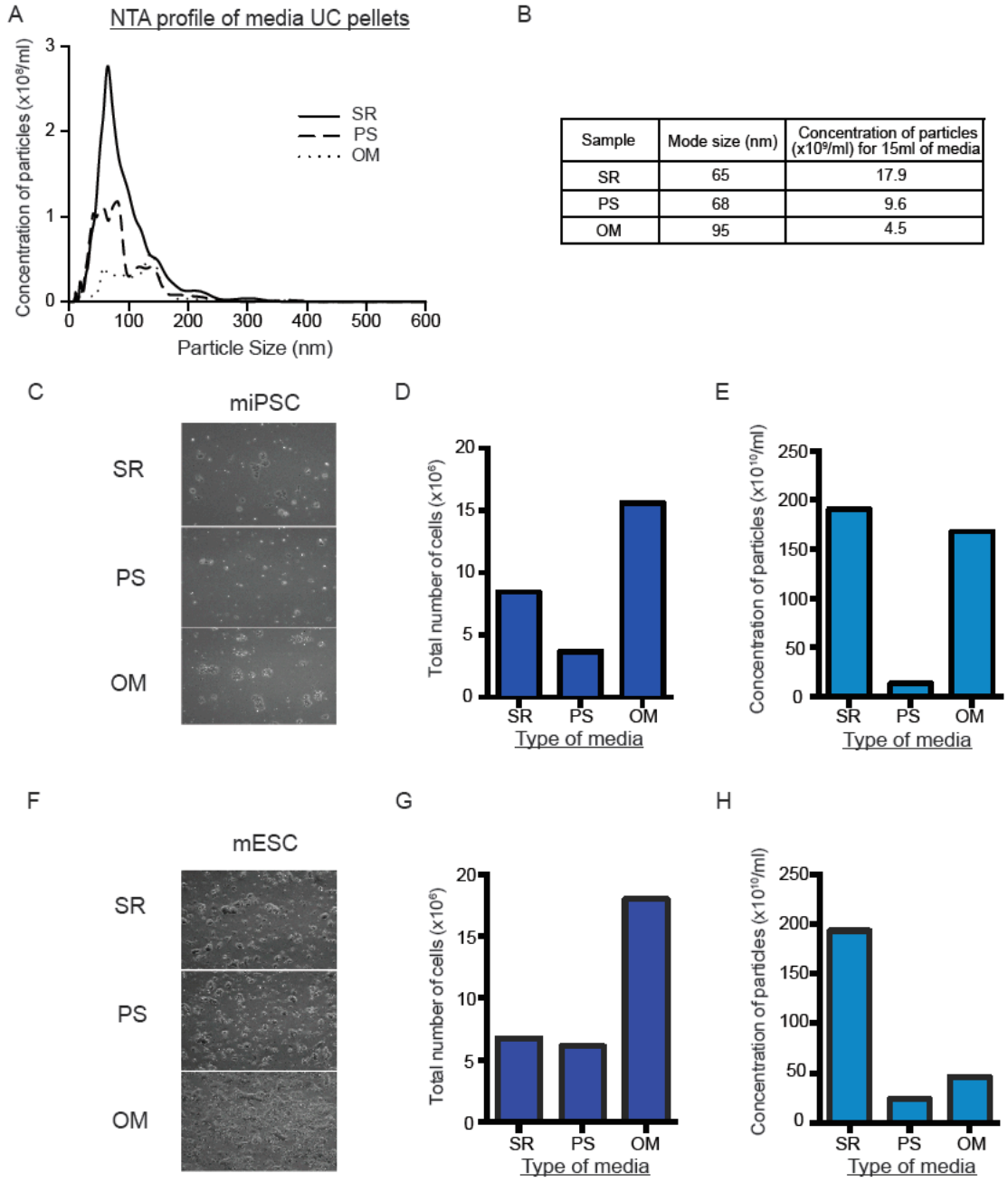

Sample	Mode size (nm)	Concentration of particles (x10⁹/ml) for 15ml of media
SR	65	17.9
PS	68	9.6
OM	95	4.5

Figure 4.3.1 Testing the feasibility of using of alternative types of serum-depleted media for EV collection from stem cells

(A) NTA size distribution profiles of UC pellets after centrifugation of the three types of media: KOSR-supplemented stem cell media (SR), Pre-spun stem cell media (PS) and serum-free media/OptiMEM (OM). (B) Table showing the mode size (nm) and concentration of particles (x10^9/ml) detected in the UC pellet of the each media type. Representative bright-field images of mouse iPSCs (C) and mouse ESCs (F) after 48h culture in SR, PS or OM. Graph comparing the total number of viable cells in the miPSCs (D) and mESCs (E) cultures at point of CM collection. Graphs comparing the total concentration of particles (x10^{10}/ml) detected by NTA in the UC pellet of miPSCs (G) and mESCs (H) in the three different media types. For figures (C-H), data was collected from one preliminary experiment (n=1).

4.3.2 UF-LC fractionation of stem cell CM allows for the purification of EVs

As described in chapter 3, the UC methodology for purification of EVs was not be ideal due to the low EV yields and additional damage of EV integrity due to the high gravitational forces applied in the repeated UC spins. Furthermore, we noticed that UC pelleting of the SR-media alone resulted in detection of particles by NTA (**Figure 4.3.1A&B**), which in turn would affect accurate quantification of particles in the actual EV sample itself. Reassured that serum microvesicles were not present in the original stem cell media, we speculated that these “particles” were instead free proteins that aggregated into nano-sized structures during the pelleting process.

The UF-LC protocol, as described in the previous chapter, omitted the use of any high-speed spins. Hence, we first tested how the LC profile of the stem cell media alone looked upon fractionation in the size-exclusion column. Generally, the total protein and particle number profiles were overlapping, where the fractions with the highest amounts of protein corresponded to the fractions with the highest number of particles (**Figure 4.3.2A**). Unlike the LC profiles of serum-free CM, the LC profiles of stem cell media were less distinct. Based on parameters used for pre-spun media in **chapter 3**, we portioned the entire LC eluted volume into four general fractions: F1-F4. Interestingly, NTA profiles of these fractions indicated that F2 appeared to have the greatest number of particles, while F1 and F3 had similar particle size distribution profiles. F4, on the other hand, had the least number of particles detected (**Figure 4.3.2B**). Next, we subjected CM collected from mouse iPSCs and ESCs to the same UF-LC protocol. Generally, the LC profiles were similar in both cell types, and

contrary to the results on media alone, NTA profiles of these stem cell samples displayed the greatest number of particles in F1 followed by F2, while F3 and F4 contained very few particles overall (**Figure 4.3.2C-F**) When we overlapped the total number of particles of all three LC profiles, we noticed that the particle peak (F1) was significantly higher in cell-derived samples than that of media alone. Hence, we were certain that the LC purification method for EVs allowed for reliable EV quantification by NTA, which was not possible with the original UC method (**Figure 4.3.2G**).

In addition to checking the NTA profiles, we further confirmed the presence of EVs through the detection of EV markers (Alix and CD9) exclusively in F1 (**Figure 4.3.2H&I**). Although we had previously detected particles in the other three fractions, none of these were positive for either EV marker. Besides protein markers, we also extracted and investigated the general RNA profiles for the media only sample and CM from mouse iPSCs and ESCs. Based on the small RNA bioanalyzer data, we showed that the RNA profiles of the F1 fractions were highly similar across both cell types with the appearance of a distinctive peak at the 60-nucleotide range. Expectedly for the media only F1 sample, there were very little amounts of small RNA detected (**Figure 4.3.2J**).

Figure 4.3.2

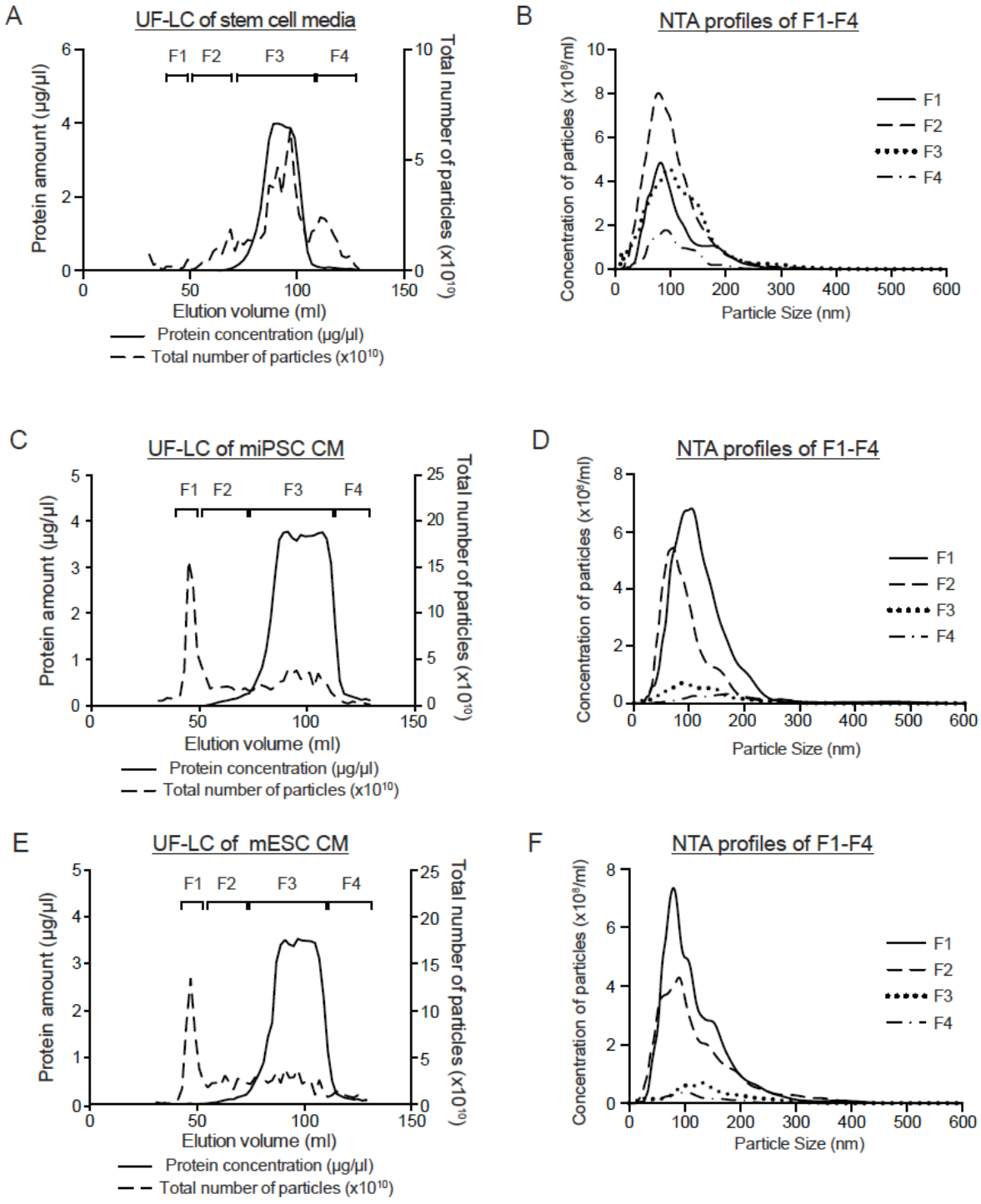
A
UF-LC of stem cell media
F1 F2 F3 F4
Protein amount (µg/µl)
Total number of particles (x10¹⁰)
Elution volume (ml)
Protein concentration (µg/µl)
Total number of particles (x10¹⁰)
B
NTA profiles of F1-F4
Concentration of particles (x10⁹/ml)
Particle Size (nm)
F1
F2
F3
F4
C
UF-LC of miPSC CM
F1 F2 F3 F4
Protein amount (µg/µl)
Total number of particles (x10¹⁰)
Elution volume (ml)
Protein concentration (µg/µl)
Total number of particles (x10¹⁰)
D
NTA profiles of F1-F4
Concentration of particles (x10⁹/ml)
Particle Size (nm)
F1
F2
F3
F4
E
UF-LC of mESC CM
F1 F2 F3 F4
Protein amount (µg/µl)
Total number of particles (x10¹⁰)
Elution volume (ml)
Protein concentration (µg/µl)
Total number of particles (x10¹⁰)
F
NTA profiles of F1-F4
Concentration of particles (x10⁹/ml)
Particle Size (nm)
F1
F2
F3
F4

Figure 4.3.2 (cont'd)

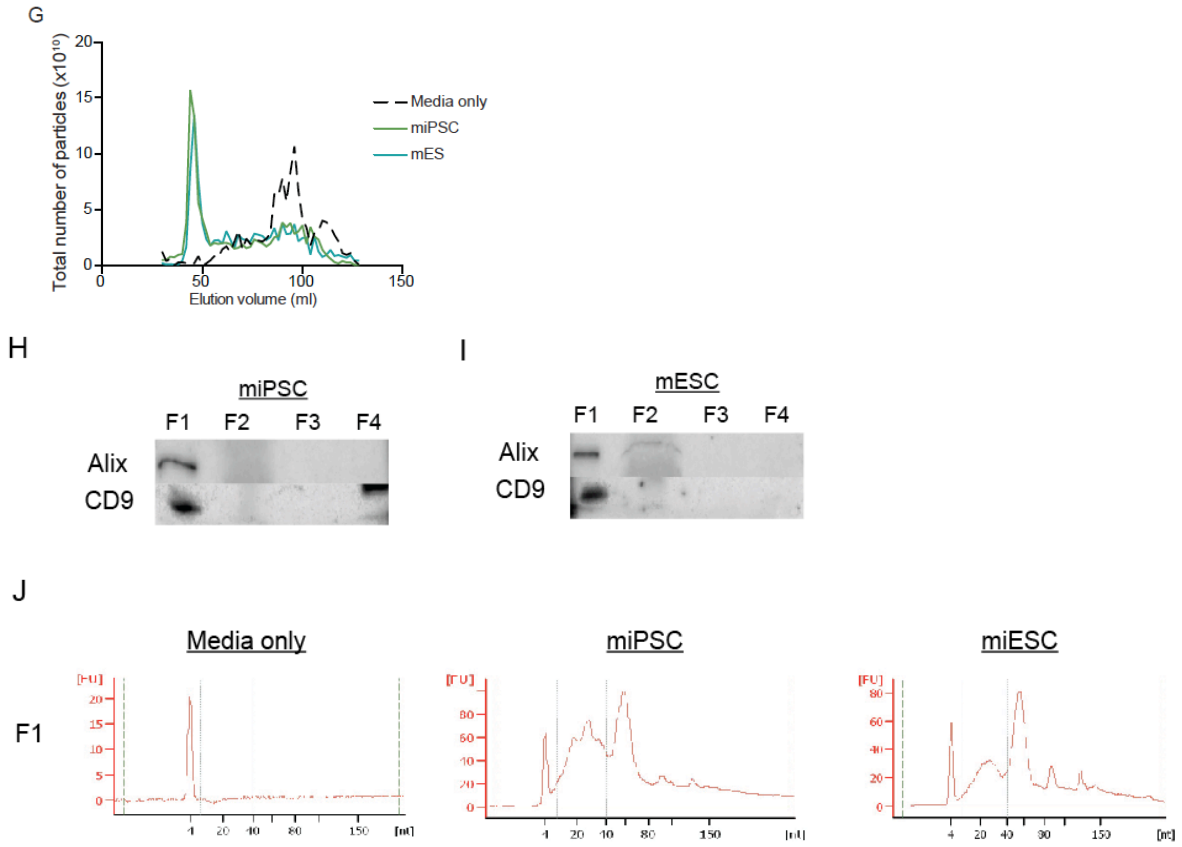

Figure 4.3.2 UF-LC fractionation of stem cell CM allows for purification of EVs

Graph showing the protein concentration (µg/µl) and the total number of particles ($x10^{10}$) across the LC run of stem cell media only (A), miPSCs CM (C) and mESCs CM (E). The entire elute sample was partitioned into four general fractions as indicated: F1-F4. NTA size distribution graphs of the four fractions from stem cell media only (B), miPSCs (D) and mESCs (F). (G) Graphs comparing the total number of particles ($x10^{10}$) from the media only versus the CM from miPSCs and mESCs. Representative western blotting pictures for EV markers (Alix and CD9) in miPSCs (H) and mESCs (I) samples where equal volume of fractions were loaded in each well. (J) Small RNA bioanalyzer profiles of the F1 from stem cell media only, miPSCs and mESCs.

4.3.3 LC protocol is highly reproducible for EV purification from stem cells

In our preliminary study (**Figure 1.7**), we noticed that there was a huge mismatch in the quantification and detection of EV markers on different batches of EVs purified from stem cells. Based on data in section 4.3.2, we speculated that the pelleting of additional protein aggregates during the UC process could have contributed to the overestimation of the actual protein and particle amounts in our earlier samples. Additionally, we noticed that there was low reproducibility in the total EV yields with the UC method; previously in serum-free cultures (**Chapter 3**) and here in our stem cell replicate samples (**Figure 1.7**).

To assess if the LC method of EV purification presented with a similar drawback, we cross-compared replicate runs of both the mouse iPSCs and ESCs CM. Generally, the LC chromatograph of the fractionated stem cell CM was consistent across all three replicates in both cell types (**Figure 4.3.3A&D**) and more importantly, the peak was consistent in the void volume range where EVs eluted (**Figure 4.3.3B&E**). Moreover, we verified that the size distribution profiles of the pooled F1 were overlapping and the total number of particles was comparable across all three replicates (**Figure 4.3.3C&F**). With western blotting, we showed that the expression level of EV markers (Alix and CD9) was comparable across EV replicates in both cell types (**Figure 4.3.3G**). Furthermore, the small RNA profiles showed very similar trends across the replicates and between cell types (**Figure 4.3.3H**).

Figure 4.3.3

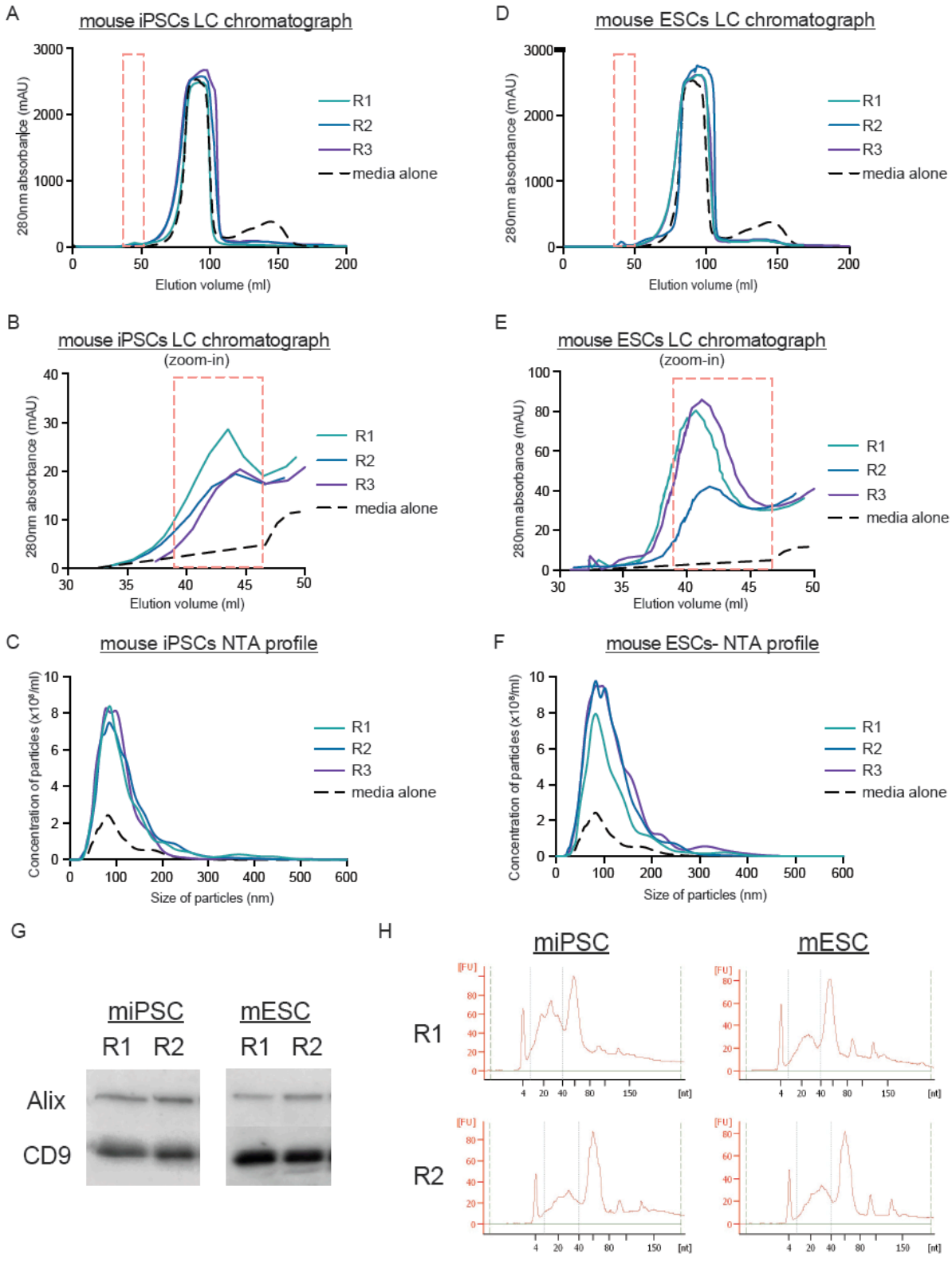
A
mouse iPSCs LC chromatograph
280nm absorbance (mAU)
Elution volume (ml)
R1
R2
R3
media alone
D
mouse ESCs LC chromatograph
B
mouse iPSCs LC chromatograph
(zoom-in)
E
mouse ESCs LC chromatograph
(zoom-in)
C
mouse iPSCs NTA profile
Concentration of particles (x10⁸/ml)
Size of particles (nm)
F
mouse ESCs- NTA profile
G
miPSC
mESC
R1 R2 R1 R2
Alix
CD9
H
miPSC
mESC
R1
R2
[FU]
[nt]

Figure 4.3.3 LC protocol is highly reproducible for EV purification from stem cells

LC chromatographs showing the detection of 280nm absorbance across the eluted volume after fractionation of replicate samples (R1-R3) from miPSCs CM (A) and mESCs CM (D). The region where EVs eluted is indicated with the red dashed rectangle. A zoomed-in of the LC chromatographs at the region where EVs were eluted for miPSCs (B) and mESCs (E). NTA size distribution profiles of the EVs collected from three replicates (R1-R3) of miPSCs (C) and mESCs (F). (G) Representative western blotting pictures for EV markers (Alix and CD9) in duplicate EVs samples (R1-R2) from miPSCs and mESCs. The same number of particles ($4x10^{10}$), as determined by NTA, was loaded in each well. (H) Small RNA bioanalyzer profiles of duplicate EV samples (R1-R2) from miPSCs and mESCs.

4.3.4 UC purified samples contain more particles, protein and RNA than LC-derived samples

Although we had shown that the LC protocol was more reproducible than the original UC protocol, it was still unknown if the LC protocol was more efficient in terms of EV yields, better purity and maintenance of EV integrity as demonstrated for serum-free conditions in the **chapter 3**. Hence, we performed a systematic comparison of stem cell EVs purified by either the UC or the LC method.

Generally, the size distribution profile of particles in the F1 fraction of iPSCs CM was found to be similar to the UC sample; where the mode size of particles were overlapping in both groups. Contrary to our expectations, we detected a significantly higher number of particles in the UC group as opposed to the LC group (**Figure 4.3.4A&B**). This trend was also observed in our total protein and RNA quantification of the EV samples (**Figure 4.3.4C**). To verify our findings, we repeated the same experimental setup on mouse ESC CM. Interestingly; we observed the same trends of higher particle numbers, protein and RNA detected in the mouse ESC UC-purified EV (**Figure 4.3.5A-C**). Previously in serum-free conditions (**Chapter 3**), we had consistently observed higher particle yields in the LC sample over the UC sample.

Hence, we decided to perform more in-depth analysis on the stem cell EV samples to unravel the basis of this opposite trend.

4.3.5 UC pellet displays different molecular characteristics as compared to the LC product

To better understand the molecular characteristics of the EVs prepared by either method, we subjected the purified samples to further RNA, protein and TEM analysis. Firstly, with small RNA bioanalyzer profiling, we observed that the UC and LC samples of mouse iPSCs displayed slightly different small RNA size distribution patterns. When comparing the same amount of RNA, a greater proportion of small RNAs were detected around the size range for miRNAs (15-40nt) in the UC pellet than RNAs in the LC sample. Furthermore, the LC sample had a distinctive peak of RNAs detected at the 60-nucleotide size range, a feature that was not observed in the UC sample (**Figure 4.3.4D**). Interestingly, these findings were consistent in both mouse iPSC and ESC samples (**Figure 4.3.5D**). As there had not been any reports stating the actual small RNA profiles of EVs, we were unable to discern which one of these RNA profiles was the more accurate representation of RNAs in stem cell EVs.

Assuming that the same EVs were purified with either method, we hypothesised that the expression levels of reported EV markers would be similar when loading the same number of particles of the UC and LC samples on a gel. Interestingly, we detected a stronger expression of both Alix and CD9 in the LC sample as compared to the UC sample. In addition, we also probed for the expression of a pluripotency marker, OCT-4, in both samples. Interestingly, we observed the opposite trend;

where the expression of OCT-4 was higher in UC than in LC samples (**Figure 4.3.4E**). All of these observations were again similarly found in EVs purified from mouse ESCs (**Figure 4.3.5E**). In literature, it has been suggested that EV markers are highly enriched in EVs as compared their parental cells (108,354). When we cross-compared the expression levels using same amount of total protein of mouse iPSC cells and their EVs, we noticed that the expression levels of EV markers (Alix, Tsg101 and CD9) were similar between the cell lysates and the LC-purified samples. However, there was negligible detection of any of these proteins in the UC sample. On the other hand, there was a higher detection of OCT-4 in the UC pellet than in the LC sample (**Figure 4.3.4E**). Next, from the total protein staining of gels loaded with equal number of particles, we found that there was a slightly stronger protein-staining pattern in the UC sample than in the LC sample, particularly at two different size ranges (51-76kDa and 17-20kDa) (**Figure 4.3.4F**). This difference was more pronounced when considering EVs samples from mouse ESCs (**Figure 4.3.5F**).

Besides RNA and protein analysis, we were also interested in assessing whether the biophysical properties of EVs were altered by the different purification method used, as demonstrated in **chapter 3**. Moreover, we wanted to verify our NTA results on the size and quantity of stem cell EVs with TEM. Interestingly, the TEM pictures of UC and LC-purified EVs were drastically different from each other (**Figure 4.3.4G**). In the UC sample, there was a general observation of high ‘cloudy’ background, which made it more difficult to visualize the EVs. In contrast, the LC sample had a clearer background where particles could be easily detected. Again, the exact same observation was made for EVs purified by UC or LC from mouse ESCs (**Figure 4.3.5G**).

Figure 4.3.4

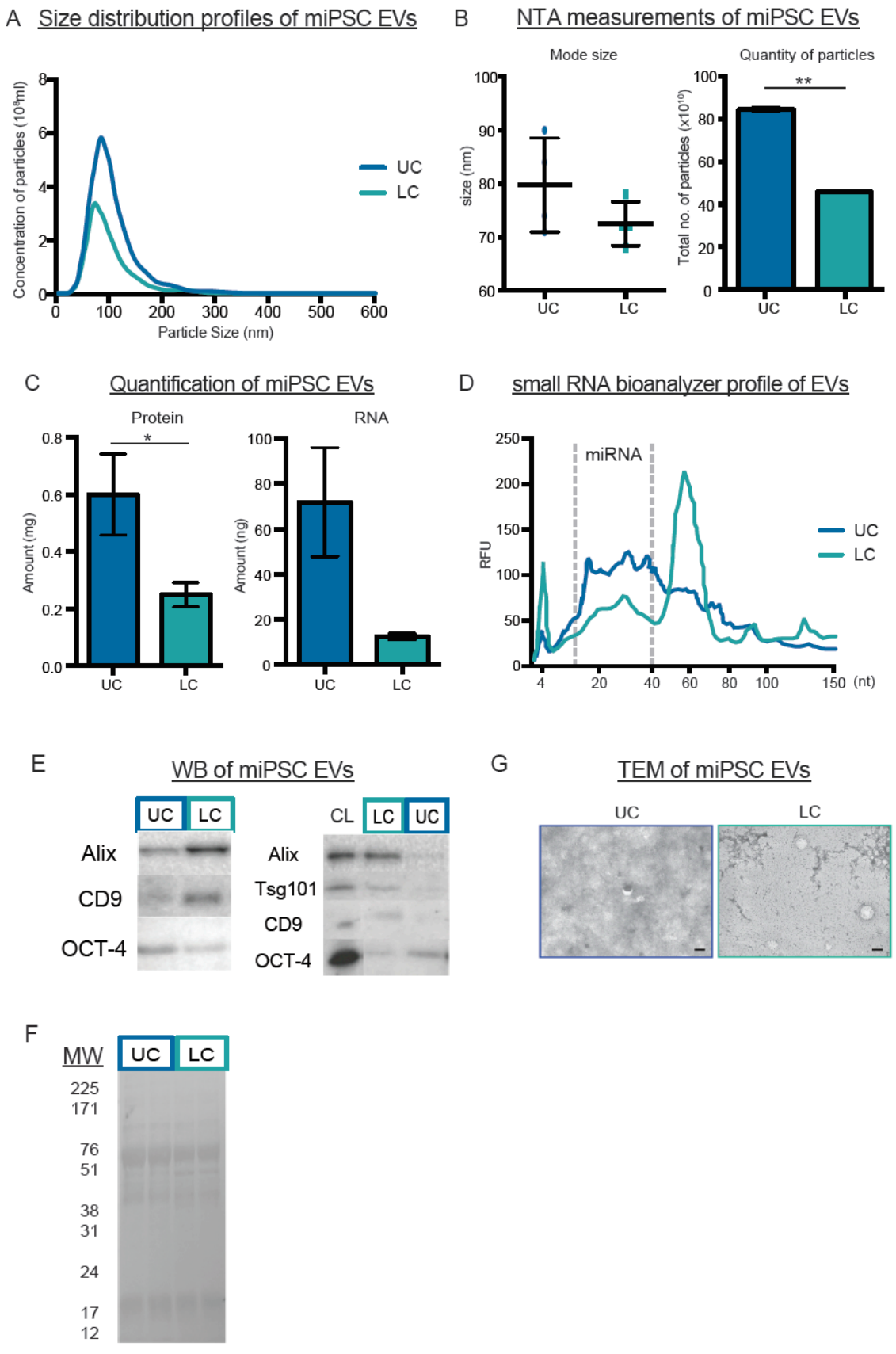
A Size distribution profiles of miPSC EVs
Concentration of particles (10⁹/ml)
Particle Size (nm)
UC
LC
B NTA measurements of miPSC EVs
Mode size
size (nm)
Quantity of particles
Total no. of particles (x10¹⁰)
**
C Quantification of miPSC EVs
Protein
*
Amount (mg)
RNA
Amount (ng)
D small RNA bioanalyzer profile of EVs
miRNA
RFU
(nt)
E WB of miPSC EVs
Alix
CD9
OCT-4
CL
Tsg101
F
MW
225
171
76
51
38
31
24
17
12
G TEM of miPSC EVs

Figure 4.3.4 Comparison study on the miPSCs EVs purified by either UC or LC

(A) NTA size distribution profiles of EVs purified by UC or LC. (B) The mode size (nm) and total number of particles ($x10^{10}$) detected by NTA in UC or LC samples (n=4, bar represented mean ±SD, **p<0.01). (C) Protein and RNA quantification of EVs in the UC and LC samples (n=4, bar represented mean ±SD, *p<0.05). (D) Small RNA bioanalyzer profiles of the UC and LC samples (E) Representative western blotting pictures of UC and LC sample; left panel comparing equal amount of particles ($4x10^{10}$), right panel comparing equal amount of protein (10μg) of cell lysate (CL) and the EV samples. (F) Total protein staining of the UC and LC samples (G) Representative TEM images of the EVs purified by UC or LC. The scale bar represents 100nm.

Figure 4.3.5

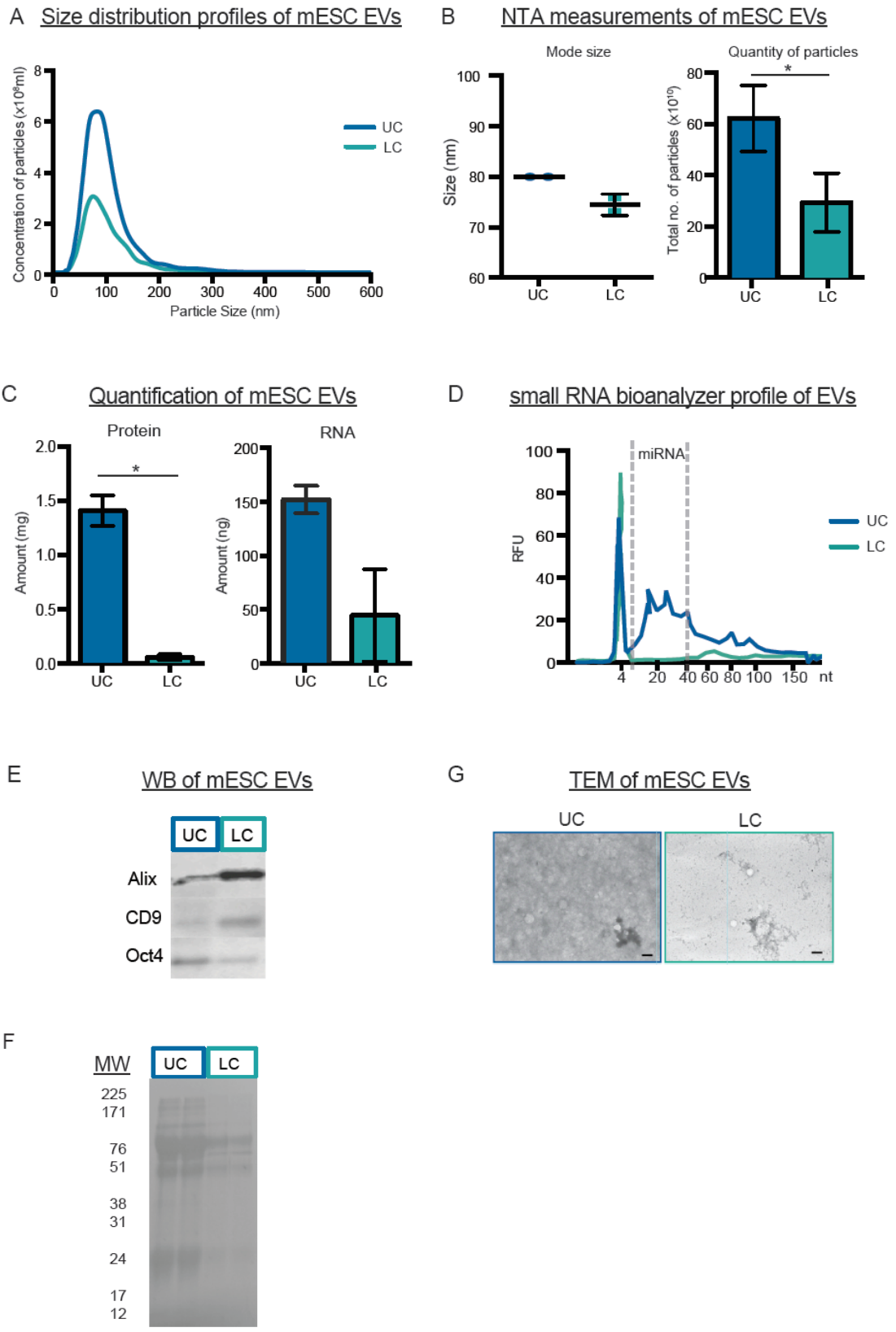
A Size distribution profiles of mESC EVs
Concentration of particles (x10⁸/ml)
Particle Size (nm)
UC
LC
B NTA measurements of mESC EVs
Mode size
Size (nm)
Quantity of particles
Total no. of particles (x10¹⁰)
C Quantification of mESC EVs
Protein
Amount (mg)
RNA
Amount (ng)
D small RNA bioanalyzer profile of EVs
miRNA
RFU
nt
E WB of mESC EVs
Alix
CD9
Oct4
G TEM of mESC EVs
F
MW
225
171
76
51
38
31
24
17
12

Figure 4.3.5 Comparison study on the mESCs EVs purified by either UC or LC

(A) NTA size distribution profiles of EVs purified by UC or LC. (B) The mode size (nm) and total number of particles ($x10^{10}$) detected by NTA in UC or LC samples (n=4, bar represent mean ±SD, *p<0.05). (C) Protein and RNA quantification of EVs in the UC and LC samples (n=4, bar represent mean ±SD, *p<0.05). (D) Small RNA bioanalyzer profiles of the UC and LC samples (E) Representative western blotting pictures of UC and LC sample; comparing equal amount of particles. (F) Total protein staining of the UC and LC samples (G) Representative TEM images of the EVs purified by UC or LC. The scale bar represents 100nm.

From all of these datasets, we postulate that the 'cloudy' background in the UC sample was due to the huge amount of protein aggregates that were pelleted together with the EVs during the UC process. As a result, this led to the detection of more proteins in the UC sample. Furthermore, when we calculated the particle per protein ratio (P/µg) and compare them to benchmark values suggested for EV purity (**Table 4.1.1**) (329), we found that the P/µg ratio for UC sample matched with the values defined for impure vesicles. In contrast, the LC samples had slightly higher P/µg ratios and were considered to be of low vesicular purity (**Table 4.1.2**).

Table 4.1.1

Purity index	P/µg
High vesicular purity	$>3x10^{10}$
Low vesicular purity	$2x10^{9}$ - $2x10^{10}$
Unpure vesicles	$<1.5x10^{9}$

Table 4.1.1
Table showing the suggested purity index Webber and Clayton (329)

Table 4.1.2

P/µg	miPSC	mESC
UC pellet	$1.6±0.5\ x10^{9}$	$0.4±0.1x10^{9}$
LC sample	$3.6±1.6x10^{9}$	$6.2±1.1x10^{9}$

Table 4.1.2
Table showing the purity ratios of UC and LC samples from both stem cell types.

4.3.6 Sucrose gradient flotation of UC pellet shows discrepancy in EV density determination

One of the proposed methods for deriving pure, clinically-grade EVs was by floating EVs on a discontinuous sucrose gradient overnight (343). Furthermore, EVs have been shown to float at a unique density range (1.15-1.19g/ml), differing to vesicles derived from other organelles and free proteins aggregates (355). In order to confirm our earlier hypothesis that there was a huge amount of free protein aggregates in the UC pellet, we floated the mouse ESC UC pellet on the top of a discontinuous sucrose gradient. Generally, the overall particle counts peaked across fractions 5-9 (**Figure 4.3.6A**). Interestingly though, the expression of EV markers (Alix and CD9) was exclusively detected in fractions 5 and 6 and these fractions corresponded to the reported EV density range of 1.15-1.18 g/ml (**Figure 4.3.6B**). However, there have been some reports suggesting that the top-loading method of EVs on a sucrose gradient might be inaccurate. Hence, we used the alternative protocol where the pre-made gradient was loaded on our impure EV samples. Interestingly in the bottom-loaded fractions, we noticed a rather different trend in particle counts across the fractions where the particle counts peaked at fraction 8 instead (**Figure 4.3.6A**). Furthermore, the detection of the same EV markers was more prominent in fractions 7 and 8, which corresponded to a higher density range of 1.21-1.22 g/ml (**Figure 4.3.6B**). Importantly, these fractions were the exact same fractions where there was the greatest detection of proteins, which we hypothesized to be non-vesicular contaminants (**Figure 4.3.6C**).

From these data, we speculated that the presence of non-vesicular proteins in the UC pellet might have stalled the migration of EVs to their true densities. Hence, we tested if the use of a longer sucrose gradient fractionation centrifugation time would allow for vesicles to reach their true density equilibrium. Interestingly, the trend in total number of particles was similar in both the overnight (16 h) and 72 h sets, where the bulk of particles were consistently detected in fractions 8-10 (**Figure 4.3.6D**). Furthermore, this pattern was similarly observed when considering the total amount of proteins across the gradient fractions (**Figure 4.3.6E**). To verify the location of EVs or non-vesicular proteins, we probed for the expression levels of another EV marker (CD81) and OCT-4. For the 16 h sample, the detection of CD81 was positive in two different regions: fractions 8-9 (1.25-1.28g/ml) and fractions 10-11 (1.30g/ml). On the other hand, OCT-4 was mainly detected in fractions 8-10 only (**Figure 4.3.6F**). Interestingly, the detection of CD81 in the 72 h sample was more widespread, with the appearance of faint bands in fractions 5-9 (1.14-1.25g/ml) and much stronger bands at fractions 10-11 (1.28g/ml). On the other hand, the expression of OCT-4 in the 72 h sample was identical to that observed in the 16 h samples, where it was exclusively detected in fractions 8-10 (**Figure 4.3.6G**). Based on total protein staining, the expression of CD81 was present in the same fractions as those positive for the appearance of background proteins in the 16 h samples (**Figure 4.3.6H**), this corroborated our earlier findings in **Figure 4.3.6C**. Similar to the 16 h sample, the 72 h sample showed the appearance of background protein staining bands in fractions 8-11. Interestingly though, there was minimal background protein staining in fractions 5-7, which had also stained positively for CD81 (**Figure 4.3.6I**). Overall, based on the expression of CD81, we deduced that prolonged

periods of fractionation on the sucrose gradient only allowed for a partial separation of stem cell EVs from protein contaminants within the UC pellet.

Figure 4.3.6

A

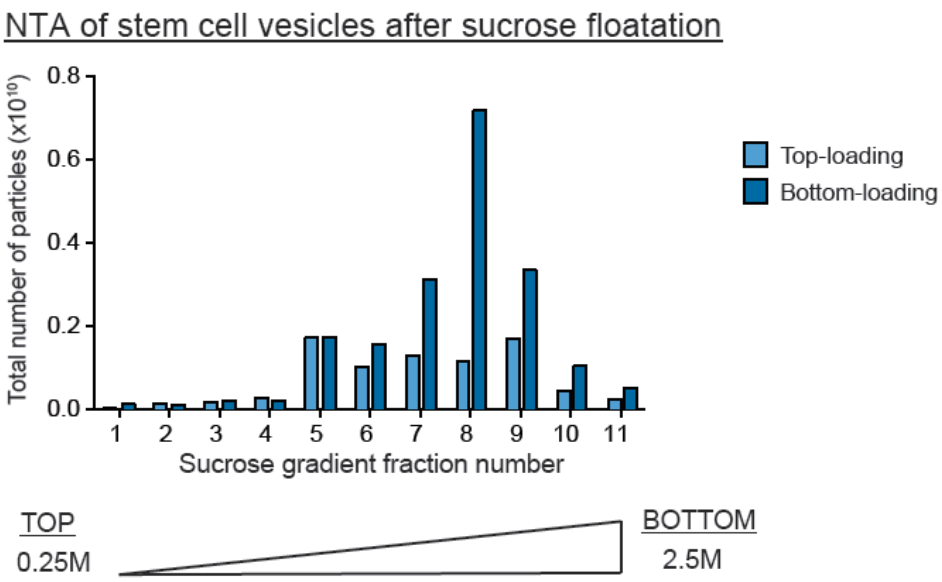

B

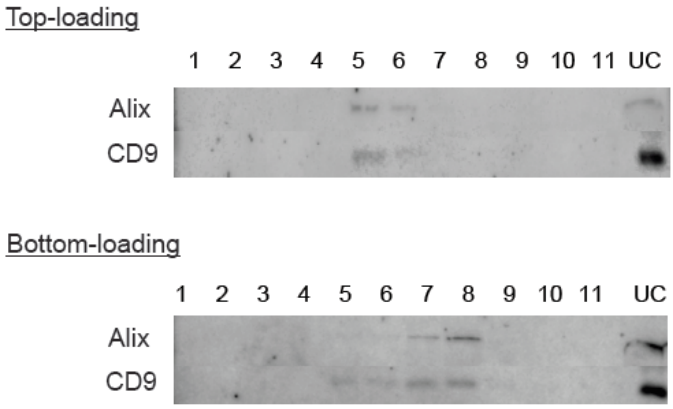

C

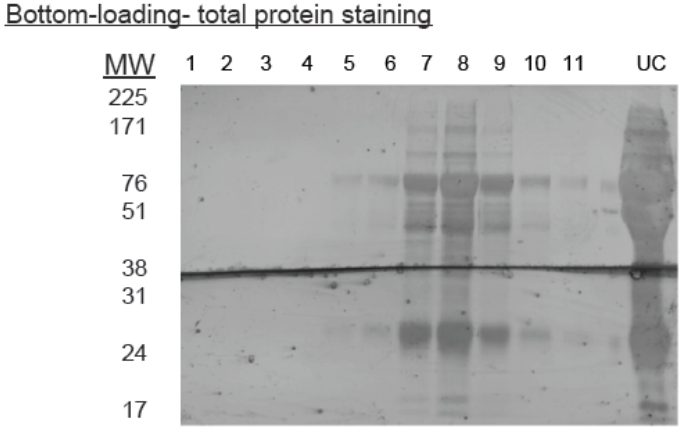

Figure 4.3.6 (cont'd)

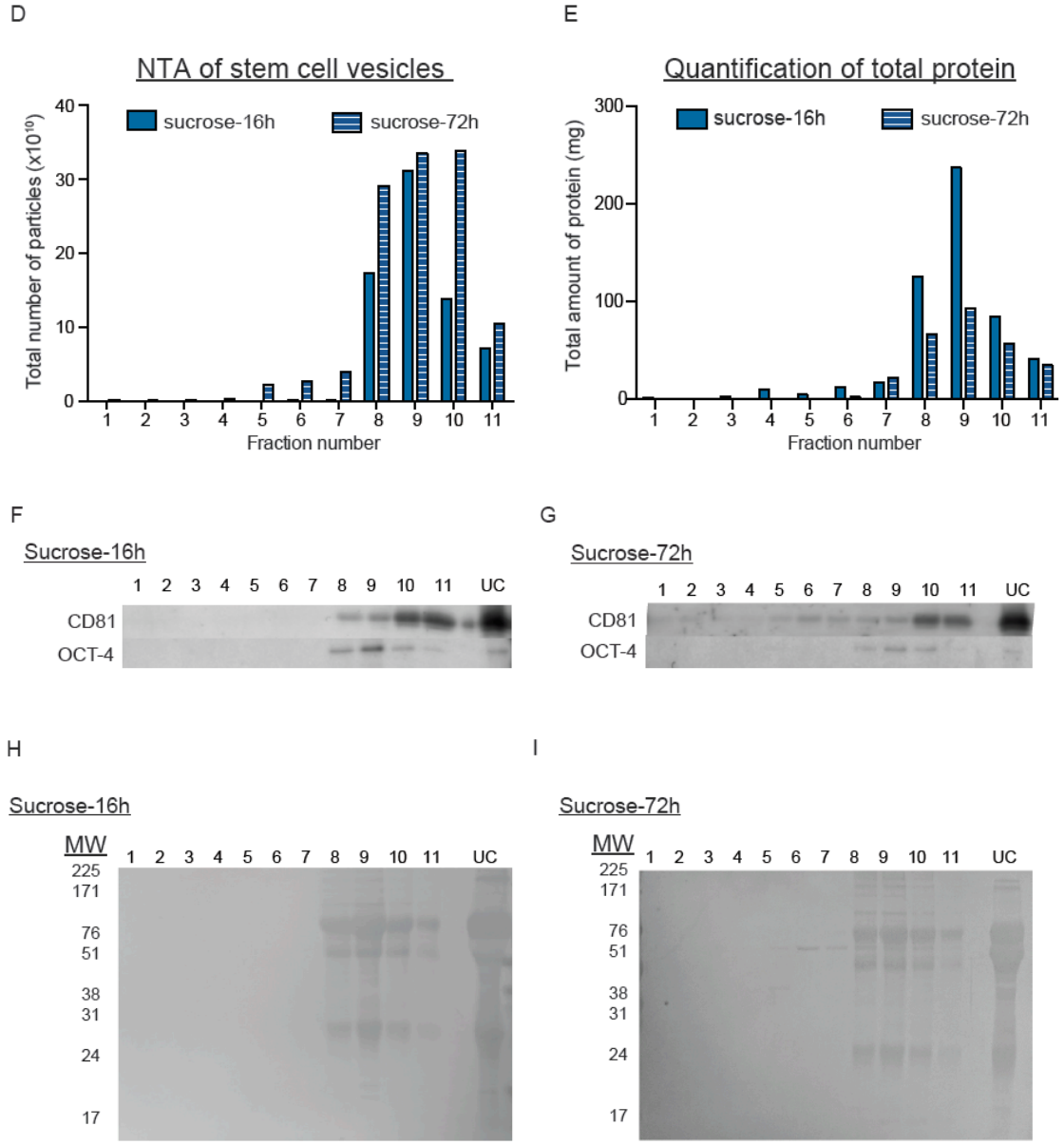

Figure 4.3.6 Sucrose gradient fractionation of UC pellet shows the co-existence of EVs with non-vesicular proteins

(A) Graph showing the total number of particles detected in each sucrose gradient fraction with either top loading (light blue) or bottom loading (dark blue) of the sample. The samples are numbered accordingly from the top to the bottom of the gradient. (B) Representative western blotting pictures of EV markers for the top-loading and bottom-loading gradients. UC represents the original UC pellet. (C) Total protein staining of the membrane with gradient fractions from the bottom-loading sample. Graphs showing the total number of particles (D) or protein (E) detected in each fraction when UC samples was bottom-loaded and floated for 16 h (dark blue bar) or 72 h (striped blue bar). Representative western blotting pictures of UC samples floated in the sucrose gradient for either 16 h (F) or 72 h (G). Total protein staining of the membrane of UC samples floated in the sucrose gradient for either 16 h (H) or 72 h (I)

4.3.7 LC fractionation of UC pellet reveals co-precipitation of proteins

Our sucrose gradient data showed that we were unable to ascertain the absolute distinction of EVs from non-vesicular proteins in the UC pellet. Hence, we tested the possibility of subjecting the mouse iPSC UC pellet for fractionation on the LC column (**Figure 4.3.7A**). Interestingly, the LC chromatograph of the UC pellet indicated the presence of several peaks: the first peak corresponding to the region where EVs elute from the column and a second peak appearing just after the first peak (**Figure 4.3.7B**). We next proceeded to pool the individual fractions spanning these two peaks (UC-LC1 and UC-LC2) and analysed them by NTA. Generally, the size distribution profiles and mode size of particles detected in UC-LC1 and UC-LC2 samples were very similar (**Figure 4.3.7C**). Based on total particle counts by NTA, we observed a low 20% recovery rate of particles in UC-LC1 sample as compared to the original UC pellet (**Figure 4.3.7D**).

To certify the presence of EVs in UC-LC1, we proceeded with western blotting for EV markers. Generally, the expression levels of Alix and CD9 were slightly less in the UC-LC1 than in the original UC sample. Interestingly, we observed a much fainter band of OCT-4 in the UC-LC1 as compared to that of the UC pellet (**Figure 4.3.7E**). With total protein staining, we observed that most of the extensive protein bands detected in the original UC pellet were now detected in UC-LC2. Importantly, UC-LC1 appeared much cleaner than UC and UC-LC2, with some remnant protein bands at around the 51-76kDa-size range (**Figure 4.3.7F**). To understand if this fractionation had any additional effect on the biophysical properties of the vesicles, we proceeded with TEM analysis. In the UC sample, we visualized the same

“cloudy” image as reported in **section 4.3.5**. However, the UC-LC1 had a much lighter background with clear appearance of nano-sized structures (**Figure 4.3.7G**). Interestingly, this image of the UC-LC1 sample resembled that of the LC sample previously shown in **figure 4.3.4G**. Furthermore, when we calculated the P/µg ratio for vesicle purity, we found that the UC-LC1 sample had a slightly higher ratio than the original UC pellet and were now classified under low vesicular purity (**Table 4.1.3**). From all of these data, we concluded that the original UC pellet contained non-vesicular protein contamination and by performing sequential fractionation on a size-exclusion column, we were able to improve the overall EV purity of the UC pellet.

Figure 4.3.7

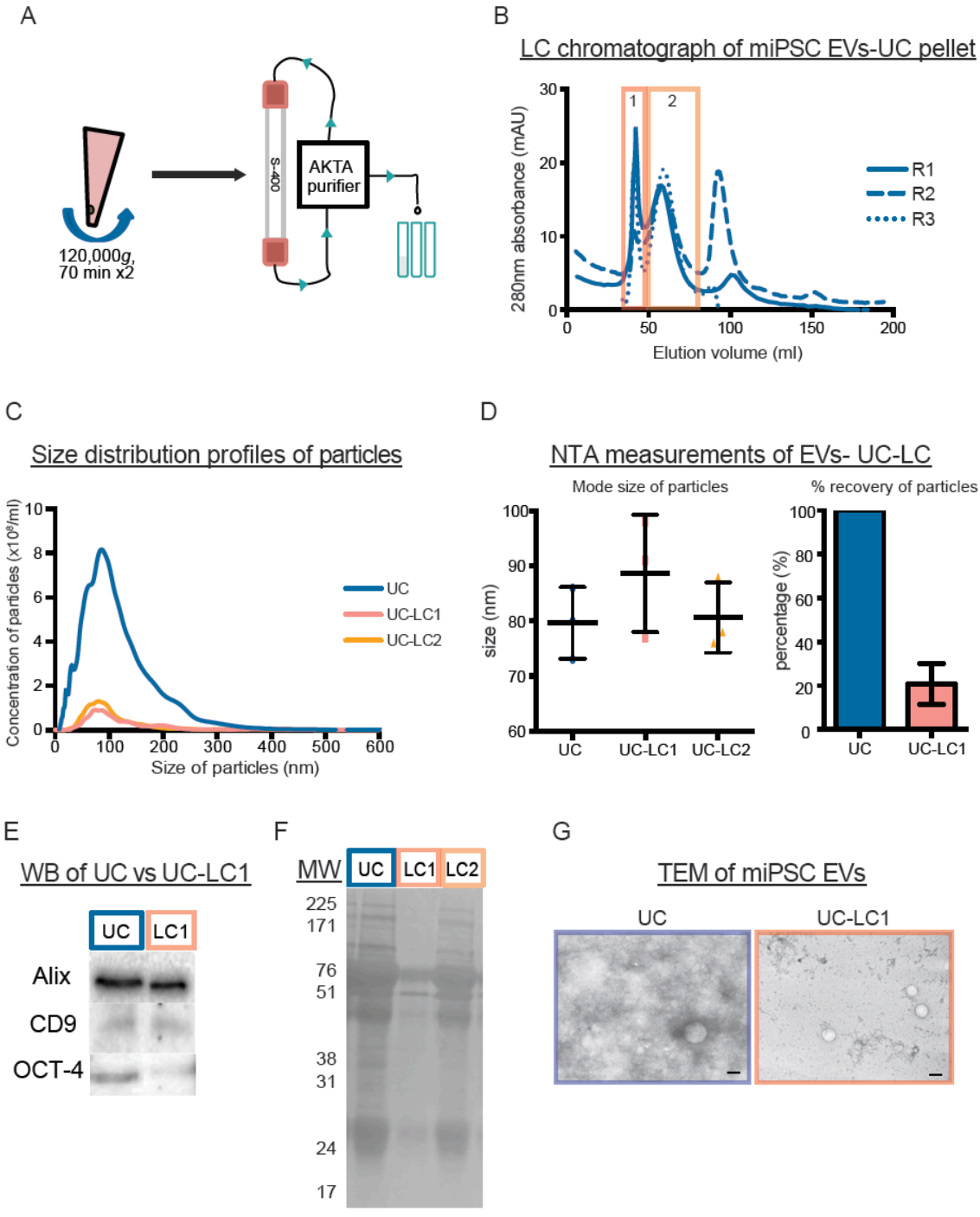
A
120,000g,
70 min x2
S-400
AKTA
purifier
B
LC chromatograph of miPSC EVs-UC pellet
280nm absorbance (mAU)
Elution volume (ml)
1
2
R1
R2
R3
C
Size distribution profiles of particles
Concentration of particles (x10⁸/ml)
Size of particles (nm)
UC
UC-LC1
UC-LC2
D
NTA measurements of EVs- UC-LC
Mode size of particles
% recovery of particles
size (nm)
percentage (%)
UC
UC-LC1
UC-LC2
E
WB of UC vs UC-LC1
UC
LC1
Alix
CD9
OCT-4
F
MW
UC
LC1
LC2
225
171
76
51
38
31
24
17
G
TEM of miPSC EVs
UC
UC-LC1

Figure 4.3.7 LC fractionation of UC pellet reveals co-precipitation of proteins with EVs in UC pellet

(A) Schematic outline of LC fractionation of UC pellet. (B) LC chromatograph showing the 280nm absorbance across the elution volume from the LC column for three replicate samples (R1-R3). The first peak (pink box) corresponds to the region where EVs elute. The second peak (orange box) shows the appearance of another peak after EVs. (C) NTA size distribution profiles of particles in the original UC sample (blue) and in the pooled fractions of the first peak (UC-LC1) and second peak (UC-LC2). (D) The mode size (nm) of particles in original UC sample, UC-LC1 and UC-LC2 (n=3, bar represent mean ±SD). Graph showing the overall percentage of particles detected in the UC versus UC-LC1 sample (n=3, bar represent mean ±SD). (E) Representative western blotting pictures when loading the sample amount of particles for UC and UC-LC1. (F) Total protein staining of the membrane with UC, UC-LC1 and UC-LC2 samples. (G) Representative TEM images of UC and UC-LC1 sample. The scale bar represents 100nm.

Table 4.1.3

P/μg	miPSC
UC pellet	$1.6\pm0.5 \times 10^9$
UC-LC1 sample	$2.8\pm1.1 \times 10^9$

Table 4.1.3
Table showing the purity ratios of UC and UC-LC1 samples from miPSCs.

4.3.8 LC samples float at lower densities than UC samples

Although the LC sample was found to be cleaner than the UC pellet (**Table 4.1.2**), total protein staining of the LC sample on a gel still indicated the presence of excessive protein bands similar to those detected in the UC samples (**Figure 4.3.4F& 4.3.5F**). Importantly, we found that these bands corresponded exactly to the bands seen in the F1 fraction of the media only sample (**Figure 4.3.8A**) Hence, we speculated that even within the cleaner LC sample, there might still be inclusion of some non-vesicular proteins from the media.

In order to separate these proteins from our EVs, we first attempted to float the LC samples through a discontinuous sucrose gradient and analysed each individual fraction for particle counts and total protein amounts. After a 16 h centrifugation period, we found that the estimated density of each individual fraction was generally similar, regardless of the type of sample loaded in the gradient (**Figure 4.3.8B**). Generally, we noticed that the peak of particles appeared in fraction 7 in both LC samples, with fewer particles detected in fractions 8 to 10. Interestingly, the peak of particles for LC samples consistently appeared to be two fractions earlier than that of the UC pellet (fraction 9) (**Figure 4.3.8C&D**). To evaluate if particle counts corresponded to the presence of actual EVs, we performed western blotting on the purified fractions. For mouse ESC samples, EV markers (Alix, Tsg101 and CD81) were detected at two regions, around fractions 4-5 (1.12-1.16g/ml) and at fractions 7-9 (1.21-1.25g/ml) (**Figure 4.3.8E**). As for mouse iPSC samples, the detection of these EV markers were mainly in fractions 7-9 (1.22-1.27g/ml), which corresponded directly with the fractions that had the most number of particles overall (**Figure**

4.3.8F). Next, to check if this sucrose centrifugation step was able to weed out the contaminating protein bands detected previously, we performed total protein staining and absolute protein quantifications of each individual fraction. From these data though, we noticed that the fractions that had the most number of particles and the expression of EV markers, also displayed high protein concentrations (**Figure 4.3.8G-H**). Overall, it seemed as if the sucrose gradient centrifugation process was not able to completely separate EVs-purified by LC from these other proteins.

Figure 4.3.8

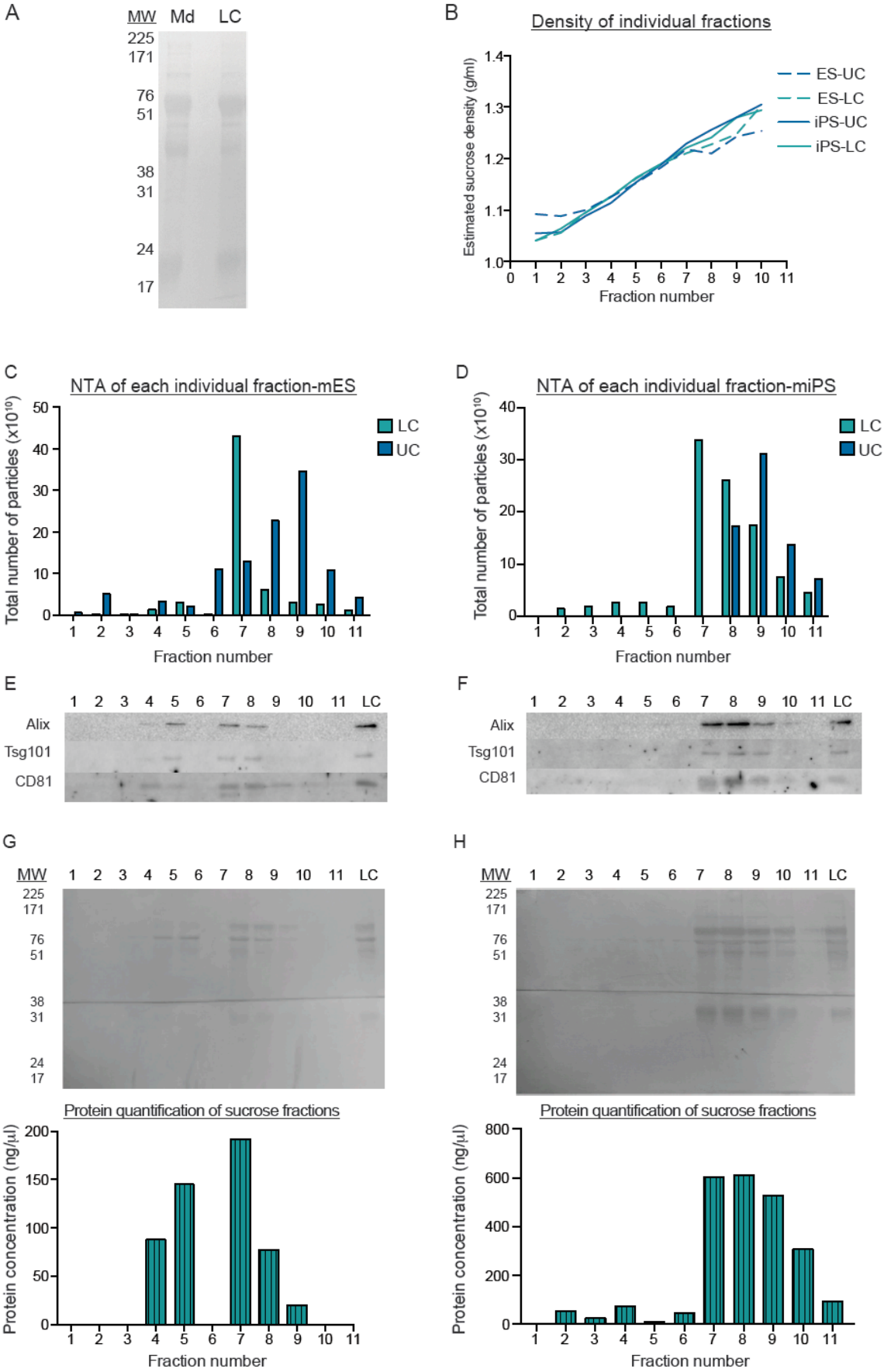
A
MW
Md
LC
225
171
76
51
38
31
24
17
B
Density of individual fractions
Estimated sucrose density (g/ml)
1.4
1.3
1.2
1.1
1.0
0 1 2 3 4 5 6 7 8 9 10 11
Fraction number
ES-UC
ES-LC
iPS-UC
iPS-LC
C
NTA of each individual fraction-mES
Total number of particles (x10¹⁰)
50
40
30
20
10
0
1 2 3 4 5 6 7 8 9 10 11
Fraction number
LC
UC
D
NTA of each individual fraction-miPS
Total number of particles (x10¹⁰)
40
30
20
10
0
1 2 3 4 5 6 7 8 9 10 11
Fraction number
LC
UC
E
1 2 3 4 5 6 7 8 9 10 11 LC
Alix
Tsg101
CD81
F
1 2 3 4 5 6 7 8 9 10 11 LC
Alix
Tsg101
CD81
G
MW
1 2 3 4 5 6 7 8 9 10 11 LC
225
171
76
51
38
31
24
17
Protein quantification of sucrose fractions
Protein concentration (ng/µl)
200
150
100
50
0
1 2 3 4 5 6 7 8 9 10 11
Fraction number
H
MW
1 2 3 4 5 6 7 8 9 10 11 LC
225
171
76
51
38
31
24
17
Protein quantification of sucrose fractions
Protein concentration (ng/µl)
800
600
400
200
0
1 2 3 4 5 6 7 8 9 10 11
Fraction number

Figure 4.3.8 Sucrose gradient fractionation of LC samples reveals the presence of some non-vesicular proteins with EVs

(A) Total protein staining of membrane with the media only F1 sample (Md) and a LC sample. (B) Graph showing the overlaps in estimated densities of individual fractions from four different gradients. Graphs comparing the total number of particles detected in each gradient fraction of UC versus LC samples, for both mESCs (C) and miPSCs (D) samples. Representative western blotting pictures of EV markers (Alix, Tsg101 and CD81) in each gradient fraction derived from the LC samples of mESCs (E) and miPSCs (F). LC represents the original sample prior to sucrose gradient fractionation. Total protein staining of the membranes and protein quantification of each gradient fraction derived from mESCs (G) and miPSCs (H) samples.

4.3.9 Additional LC fractionation improves the EV purity marginally

From **section 4.3.6 and 4.3.7**, we found that LC fractionation was more efficient than the sucrose gradient centrifugation process in the separation of non-vesicular proteins from EVs. Hence, we subjected the LC sample to an additional LC fractionation step to check if we could further improve on the purity of the LC-derived EV sample (**Figure 4.3.9A**).

From the LC chromatograph of the fractionated LC sample, we observed the presence of two distinct peaks, the first peak corresponding to the region where EVs elute and a second peak much later at around 90 ml of the eluted volume (**Figure 4.3.9B**). As we were only interested in comparing the EVs before and after this additional LC fractionation step, we pooled the fractions spanning the first peak (LC'1). From NTA, it appeared that the size distribution profiles of the LC and LC'1 were generally similar and they both have similar mode sizes. However, in terms of overall quantities, only 22.8% of particles were from the original LC product (**Figure 4.3.9C&D**). With western blotting, we observed that the expression levels of Tsg101 was slightly greater in the LC'1 fraction while the opposite trend was noticed for the

CD9 protein (**Figure 4.3.9E**). Moreover, we deduced that the additional LC step had improved the vesicle purity marginally as shown by the detection of fainter bands with total protein staining on the gel (**Figure 4.3.9F**) and a small increase in the P/µg ratio in the LC'1 versus LC sample (**Table 4.1.4**).

As we were unsure if the remaining unidentified protein bands on the LC'1 profile were true EV proteins or the result of protein-EV association due to the initial concentration step (UF) prior to LC fractionation, we concentrated stem cell CM using the tangential flow filtration (TFF) device instead. The LC chromatograph showed that both the UF and TFF samples had rather similar 280nm absorbance profiles. The only slight difference detected was a higher 280nm absorbance in the UF sample, most evidently in the regions spanning F3 and F4 (**Figure 4.3.9G**). NTA analysis of each individual fraction across the eluted samples indicated that there was a similar sharp peak for both sample types and this corresponded to the F1 fraction of EVs. In the latter fractions, there was a slightly different trend; where there were more particles detected in the UF sample than in the TFF sample. Interestingly, this pattern overlapped with the fractions where higher 280nm absorbance was detected in the UF sample (**Figure 4.3.9H**).

When comparing the EVs from both preparations, we observed that the particles were of similar mode size and overall quantities (**Figure 4.3.9I**). Western blotting of equal amounts of particles quantified in each sample type showed that the expression of EV markers (Alix and Tsg101) was generally comparable **(Figure 4.3.9J**). Furthermore, the small RNA bioanalyzer analysis showed that the RNA profiles were overlapping across both types (**Figure 4.3.9K**). Lastly, the total protein

staining of the gel and the P/μg ratio for vesicle purity was very similar between the UF and TFF sample (**Figure 4.3.9L** and **Table 4.1.5**).

Figure 4.3.9

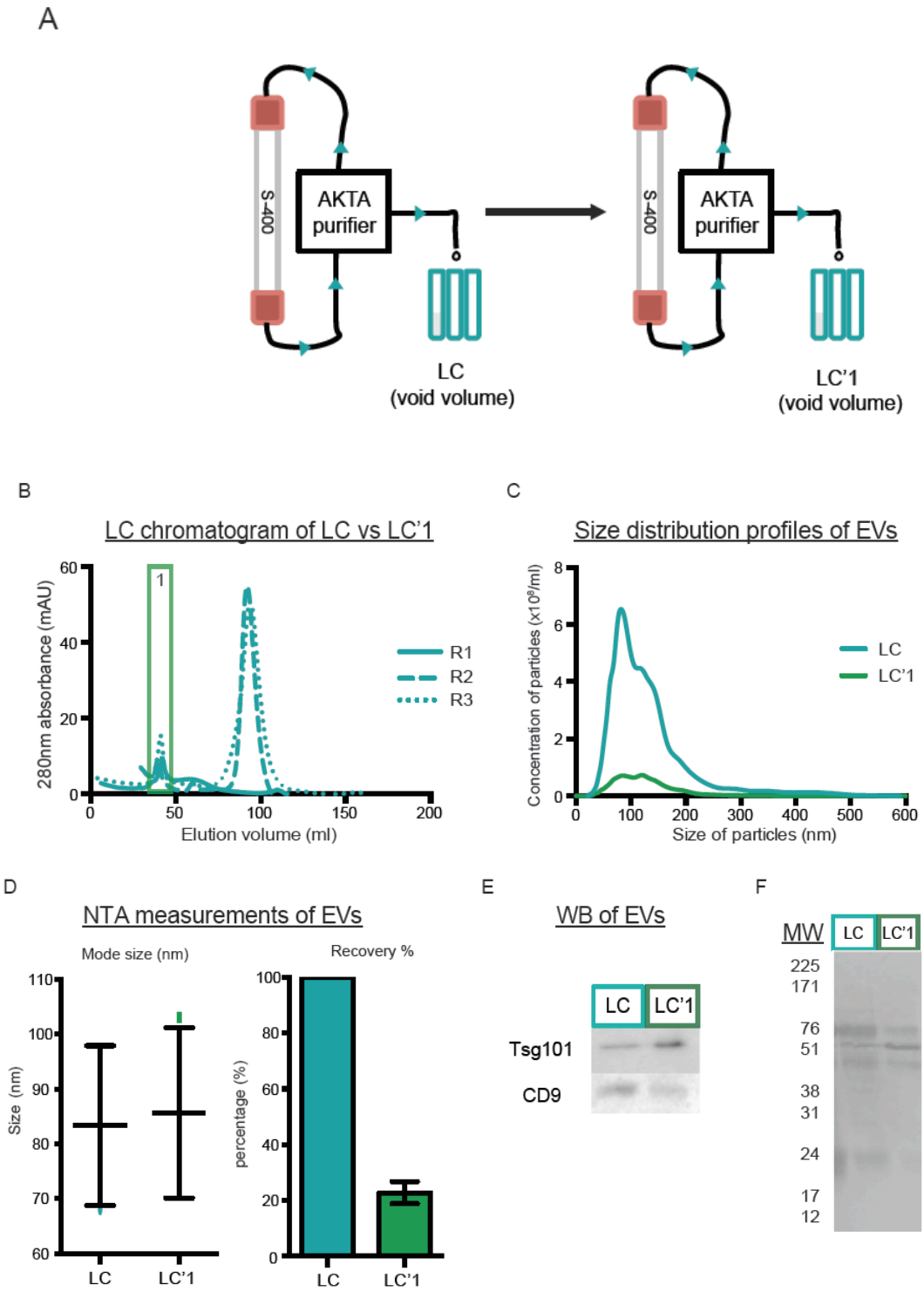
A
S-400
AKTA purifier
LC
(void volume)
S-400
AKTA purifier
LC'1
(void volume)
B
LC chromatogram of LC vs LC'1
280nm absorbance (mAU)
Elution volume (ml)
R1
R2
R3
C
Size distribution profiles of EVs
Concentration of particles (x10⁸/ml)
Size of particles (nm)
LC
LC'1
D
NTA measurements of EVs
Mode size (nm)
Size (nm)
Recovery %
percentage (%)
LC
LC'1
E
WB of EVs
LC
LC'1
Tsg101
CD9
F
MW
LC
LC'1
225
171
76
51
38
31
24
17
12

Figure 4.3.9 (cont'd)

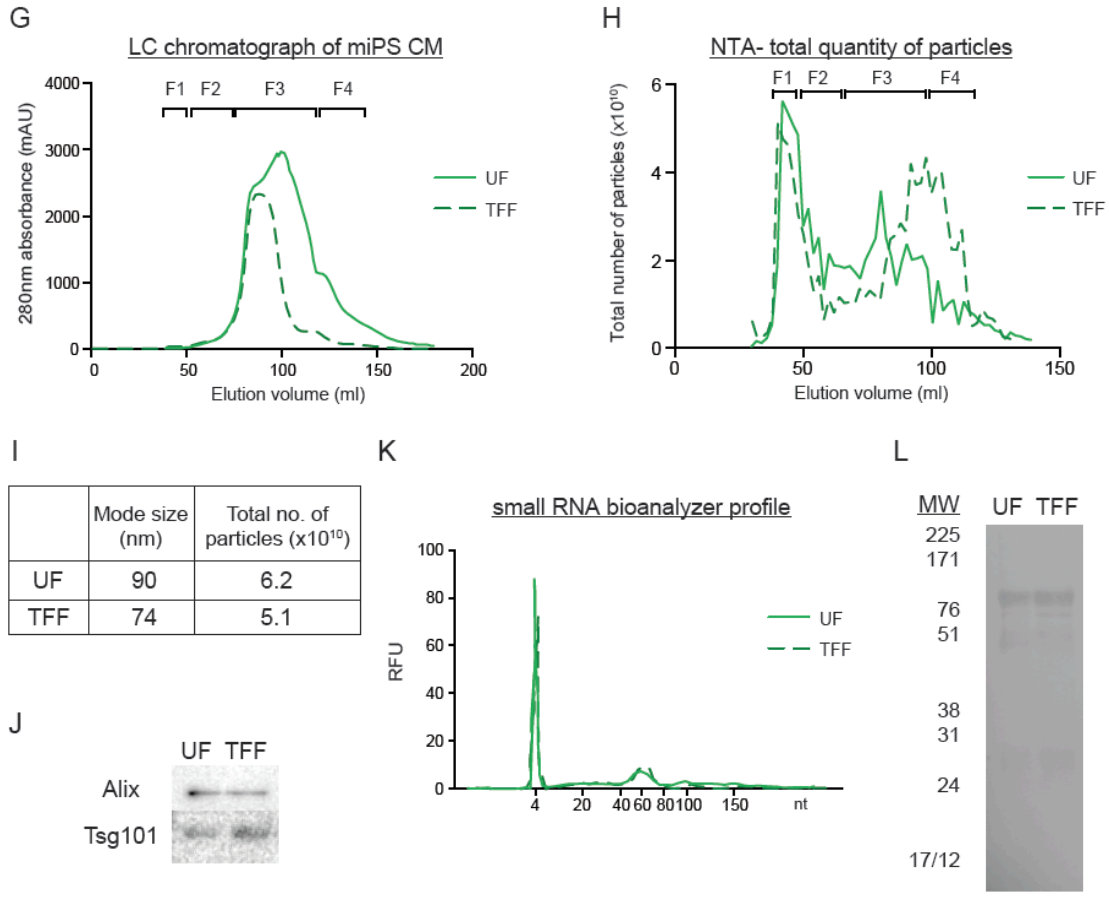

Figure 4.3.9 Additional LC fractionation of the LC sample improves the EV purity marginally

(A) Schematic outline of the additional LC fractionation set-up. (B) LC chromatograph showing the 280nm absorbance across the elution volume from the LC column for three replicate samples (R1-R3). The first peak (green box) corresponds to the region where EVs elute. (C) NTA size distribution profiles of particles in the original LC sample and the pooled fractions of the first peak (LC'1). (D) The node size of particles in the original LC sample and the LC'1 sample (n=3). Graphs showing the overall percentage of particles detected in the LC versus LC'1 sample. (E) Representative western blotting pictures when loading the same amount of particles for LC and LC'1. (F) Total protein staining of the membrane with LC and LC'1 samples. (G) LC chromatograph showing the 280nm absorbance across the elution volume from the LC column for UF (line) or TFF (dashed line) concentrated samples. (H) Graph showing the total number of particles detected across the elution volume for UF (line) or TFF (dashed line) samples. (I) Table showing the mode size (nm) and total number of particles ($x10^{10}$) of UF and TFF samples. (J) Representative western blotting pictures of the when loading the sample number of particles for UF and TFF samples. (K) Small RNA bioanalyzer profiles of the UF (line) and TFF (dashed line) samples. (L) Total protein staining of the membrane for UF and TFF samples.

Table 4.1.4

P/μg	miPSC
LC sample	$3.6\pm1.6x10^9$
LC'1 sample	$5.3\pm2.0x10^9$

Table 4.1.4
Table showing the purity ratios of LC and LC'1 samples from miPSCs.

Table 4.1.5

P/μg	miPSC
UF-LC sample	$3.6\pm1.6x10^9$
TFF-LC sample	$4.1\pm0.5x10^9$

Table 4.1.5
Table showing the purity ratios of UF-LC and TFF-LC sample from miPSCs

4.4 Discussion

In **chapter 3**, we discussed how two different factors; the type of media used for EV collection and the purification strategy, could impact on the subsequent molecular and biophysical characterization of EVs from cell lines. Drawing from the lessons learnt in these earlier studies, we attempted to translate these findings into the purification of EVs from pluripotent stem cells. As the type of cell culture for stem cells was relatively more complex than for immortalized cell lines, we first sought to evaluate an optimal type of media and purification method for derivation of pure EVs from mouse pluripotent stem cells.

4.4.1 The use of serum-replacement media is ideal for collection of stem cell EVs

In stem cell culture, inclusion of serum has been reported to be of major importance for maintenance of the stem cells in their undifferentiated state. However in early stem cell transplantation studies, there were some concerns raised about the risks in pathogen transmission in relation to the use of animal derived components (e.g. cow serum) in the culturing media (356). Consequently, extensive efforts were made in the development of serum alternatives (e.g. KOSR) to substitute the serum component without affecting the viability and differentiation state of stem cells.

Although KOSR did not contain any serum microvesicles, we detected particles that were similar to EVs in terms of size in the UC pellet of the KOSR stem cell media

alone, which could affect downstream EV quantification by NTA. Hence, we prepared a separate set of ‘pre-spun’ stem cell media, by overnight centrifugation and OptiMEM as two alternative media types for EV collection.

Our preliminary studies on alternative media types for stem cell cultures clearly demonstrated that a short-term incubation (48 h) of stem cells in different media types had a profound impact on the viability of cells and subsequent EV release. We hypothesised that during the overnight preparation step of pre-spun media, many growth factors, proteins and RNAs may have been pelleted. Hence, the stem cells did not appear viable in pre-spun media. The low cell counts in pre-spun cultures would also account for the low amount of EVs pelleted. On the other hand, cells cultured in OptiMEM had the highest cell counts after 48 h. Although the expression of the pluripotency marker OCT-4 could still be detected in the cells (data not shown), we believed that this culture contained a mixture of stem cells and differentiated cells as judged by the visible change in cellular morphology. As we were doubtful if the EVs collected from OptiMEM cultures were still representative of undifferentiated stem cells, we chose to continue our EV studies on stem cells using the original KOSR stem cell media.

4.4.2 LC method highlights the various problems associated with UC purification of EVs from stem cell sources

As the KOSR was reported not to contain any serum, we were surprised to detect particles in the UC pellet of the stem cell media alone. This led us to speculate that the high-speed spins in the UC process might have promoted the pelleting of protein

aggregates, which appeared as nano-sized particles that could be quantified by NTA. Furthermore, this would explain the discrepancy in the overall particle quantifications and detection of EV markers in our preliminary EV samples from stem cells as shown in **Figure 1.7**. We thus concluded that UC was not a suitable purification method for EVs from stem cells.

The alternative purification method- UF-LC that we demonstrated in **Chapter 3** would not comprise of any high-speed spins. Hence, we speculated that this protocol would allow us to bypass the problems identified with using the UC technique. Indeed, fractionation of the stem cell media alone showed that very few particles were detected in the region where EVs were expected to elute. Surprisingly, majority of particles were detected overall were found in the latter two fractions that correspond directly with higher protein amounts. For stem cell CM, we observed that the LC fractionation pattern was reproducible across replicates and consistent across different cell types. On hindsight though, we noticed that there was a lack of distinct cut-off points between the particle and protein peaks in the LC profile of stem cell CM as compared to serum-free conditions. As a similar trend was observed for pre-spun media (**chapter 3**), we hypothesized that this could be a common LC profile when fractionating complex media types. With western blotting, we verified the presence of EV markers exclusively in F1. Hence, we strongly believe that this data supports our earlier hypothesis that the ‘particles’ detected in the stem cell media only UC pellet were protein aggregates.

Previously, we found that the LC protocol allowed for high EV recovery rates. Unexpectedly, however, for the stem cell media, we observed that the purified EVs

by LC only accounted for approximately 10% of the total number of particles in the original CM. We were unsure if this finding meant that the LC protocol was inefficient in purifying EVs from stem cell media and hence, we performed a systematic comparison study to investigate stem cell EVs purified by the original UC method or this new LC protocol.

Surprisingly, our side-by-side UC and LC comparison indicated that the UC pellet contained more particles, total protein and RNA amounts than the LC sample. This result, observed across both stem cell types, was rather unexpected, as we had observed the opposite trend previously in serum-free CM. However, as we were aware that protein aggregates in the UC pellet would appear as ‘particles’ on the NTA, the actual reliability of these NTA and protein quantifications of UC-purified EVs could be questioned. Hence, we performed more detailed comparison characterisation studies on the EVs from either purification strategy.

From the previous chapter, our proteomics analysis of EVs derived from serum-free conditions demonstrated that the overall proteome was congruent across both purification strategies; including that of reported EV markers. Unexpectedly, we found that the expression levels of these EV markers were generally higher when comparing equal number of particles of the LC sample to the UC pellet. On the other hand, the expression level of OCT-4 followed the opposite trend to that of the EV markers. Although OCT-4 was previously reported to be present in ESC-EVs (349), recent reports have shown that OCT-4 could also be secreted from cells directly into the extracellular environment (357). Hence, we speculated that the a portion of these secreted OCT-4 proteins in the CM might have pelleted together with the stem cell

EVs during the UC process and explain for the higher levels of OCT-4 detected by western blotting of UC-purified EVs.

Besides the differences in protein expression, we also observed significant differences in other aspects such as small RNA profiles and TEM imaging of vesicles. In the latter study, we hypothesized that the excessive presence of free proteins in the UC pellet contributed to the ‘cloudy’ background and interfered with the proper visualization of the EVs. Furthermore, the P/µg ratio was slightly lower in the UC as compared to the LC samples; which corroborate with our earlier data that the UC pellet was of lower vesicle purity.

Hence, all these lines of evidence led us to further conclude that the UC methodology was not suitable for purification of EVs from stem cell media as this process involved the pelleting of non-vesicular proteins that could not be easily removed with additional PBS washes. At the same time though, we were unsure what percentage of these UC-purified particles were truly EVs and if an additional clean up step would allow the removal of these contaminations.

The first clean up strategy we attempted was sucrose gradient centrifugation. Previously, it has been reported that EVs float uniquely at 1.15-1.19 g/ml, which is slightly different to other vesicles originating from other cellular organelles such as the endoplasmic reticulum (1.18-1.25 g/ml) or the Golgi (1.05-1.12 g/ml). These flotation interval have been verified by several other on different cellular sources of EVs and found to be regardless of the actual method of loading the EV sample on the top or bottom of the sucrose gradient (22,358,359). However, others have

debated that overnight centrifugation was insufficient for vesicles to efficiently penetrate in the denser fractions and reach density equilibrium within 16 h centrifugation period (59).

We first tested floating the UC pellet on a sucrose gradient with both loading strategies and at two different lengths of centrifugation period. Unexpectedly, we noticed an inconsistency in the total particle counts and presence of EV markers when cross comparing the two loading strategies. Importantly, we noted that for the bottom-loaded sample, the gradient fractions positive for EV markers were overlapping with those containing non-vesicular protein bands. Hence, we hypothesised that the EVs in UC pellet might be trapped by the protein aggregates at higher densities and thereby are unable to freely migrate to their actual density within the overnight time frame.

When we bottom-loaded and floated EVs for a longer time frame (72 h), we did not observed any difference in the general trend for particle counts in total protein quantification across the gradient fractions as compared to the shorter time frame. Interestingly though, the expression of the EV marker, CD81 was more diverse at 72 h than in the 16 h sample. Hence, we hypothesized that indeed at this longer incubation period, a portion of EVs were able to escape from the protein aggregates and float at their true densities. On hindsight though, the detection of CD81 was consistently higher in the higher density fractions. Based on these data alone, it was very difficult to ascertain if the particles appearing at higher densities and stained positively for CD81 were truly EVs remaining trapped with non-vesicular proteins.

In an attempt to better clean up the UC product, we next chose to fractionate the UC pellet on an LC column. Here, we detected another protein peak immediately after the initial EV peak, which signified the presence smaller proteins within the UC pellet with our EVs. Importantly though, the particles in this second peak did not express any of the tested EV markers and this further supports our previous deduction that proteins could appear as particles on the NTA. Overall, it appeared that the additional LC fractionation of the UC pellet could eliminate some of these contaminating proteins and this result greatly contributed to the better visualization of vesicles under TEM, the decrease in the overall expression of non-vesicular proteins (OCT-4) as well as the increase in the P/μg vesicle purity ratio. However, there was a relative low percentage recovery of EVs from the starting UC pellet. Hence, we deduced that the UC method was not suitable for purification of EVs from stem cell media as the derivation of pure EVs required additional cleanup processes that was time consuming and would further compromise on the overall EV yields.

4.4.3 EVs may function as ‘sponges’ for free proteins in the extracellular environment

Although the LC product was an improvement in the derivation of purer EVs from stem cells as compared to the traditional UC method, residual proteins matching those found in the media only sample were also present in the LC sample. In order to re-evaluate if these were non-vesicular associated proteins, we adopted the same clean up strategies as before, first by floating the LC product through a sucrose gradient. Compared to the UC pellet, the peak in particle counts and expression of EV markers and OCT-4 appeared to be consistently one fraction earlier in the LC

sample. Since the LC product had much lower protein contamination than the UC pellet, we hypothesized that the lack of these contaminating proteins allowed for EVs to migrate more quickly to their actual densities. Despite that, these LC-purified EVs still floated at a slightly higher density range than reported of EVs previously. Furthermore, total protein staining indicated that these fractions still contained some protein bands that were similar to those detected in the media only sample. Hence, we proposed two possibilities; first, the sucrose gradient centrifugation methodology was unable to accurately separate EVs from these proteins or second, stem cells EVs functioned as a sponge and sequestered free proteins from the media, hence they truly floated at a higher density as compared to other EVs.

Similar to the approach on the UC pellet, we subjected the LC product to a sequential LC step. Interestingly, after the initial EV peak, a second protein peak appeared much later in the eluate, which could be due to the presence of some free small proteins that possibly did not get separated properly in the first LC run or was part of the proteins which fractionated at the end boundaries selected for F1. Interestingly, when comparing EVs from the second LC run to the original LC product, we noticed that there was a slightly lower expression of the transmembrane protein (CD9), while the opposite trend was noticed for the intraluminal protein (Tsg101). With this data, it was tempting to speculate if one might need to take caution in the choice of EV markers to use for identification of EVs. Overall, we demonstrated that an additional LC step allowed for marginal improvement in vesicle purity as evident by the slight increase in P/μg ratio as well as the decrease in background bands on the total protein gel staining.

Albeit subjecting the purified EVs to a second LC run, the protein bands were not completely removed. Previously, we demonstrated that concentration of serum-free CM lead to the accumulation of non-vesicular proteins such as albumin in the filters. From literature, we knew that KOSR also contained high amounts of albumin and other proteins to replace the serum component; hence we postulated that the concentration step of the stem cell CM with spin filters might have contributed to the capture of albumin aggregates in the filters. Unlike the conventional spin filters, the tangential flow filtration (TFF) device bypassed the potential problem of clogging the filters through diafiltration-based processing of the CM. As expected, the sample concentrated by spin filters contained more proteins of smaller sizes than the sample concentrated by TFF, despite using the same molecular cut-off size (100-kDa). Interestingly though, there was not a major difference in the overall quantities and molecular characteristics of EVs concentrated and purified by either method. Hence, we speculated that some free proteins in the media could have bond onto EVs by non-covalent means and be ferried to other cells as a means of cell-cell communication.

4.5 Conclusion

In conclusion, we first learnt that the use of serum-free media or pre-spun media was not compatible with stem cell culturing and subsequent EV collection, as these conditions impact greatly the phenotype of the stem cells. Additionally, we learnt that KOSR was a good alternative to serum as it kept the stem cells viable and undifferentiated. In **chapter 3**, we found that the UC methodology presents with several drawbacks in terms of EV yields and integrity as compared to the newer LC strategy for serum-free cultures. As for stem cell cultures, we initially noticed the opposite trend for the overall EV yields. Here, we have shown that non-vesicular proteins could be pelleted during the UC process and appear as particles on the NTA. This additionally led to the detection of higher overall amounts of proteins (such as OCT-4) and RNAs, which are not normally associated with the EVs in the UC pellet. Furthermore, additional strategies that were needed to improve the purity of UC-derived EVs turned out to be inefficient and time-consuming. Hence, we concluded that UC was not an appropriate method for purification of EVs from stem cell media or other protein-rich biological fluids. In contrast, the LC sample appeared significantly cleaner. Although we could improve on the vesicle purity of LC samples with an additional LC step, there remained some protein background bands in these samples. Hence, we speculate that free proteins in the extracellular environment bound naturally onto EVs and get co-purified during the LC step. Overall, we have demonstrated that the LC method was a more suitable for purification of EVs. As stem cell media used here is highly complex and rich in proteins, we strongly believe that this technique could be extended to the derivation of EVs from other complex culture conditions or biological fluids such as plasma and serum.

Besides the derivation of a more suitable purification method for stem cell EVs, our data here have highlighted the need to be cautious when using current tools for the interpretation of EVs purified from more complex media or biological fluids. In this chapter, we have many lines of evidences, which clearly demonstrated that contaminants such as protein aggregates could be readily detected and quantified as particles on NTA, or detected as additional proteins and RNAs by quantification kits. Hence, it would not be advisable to rely solely on the overall particle, protein and RNA quantifications for the evaluation of EV yields. Next, one would need to be careful in the interpretation of the vesicle purity ratio. This ratio was calculated by dividing the total particle numbers by the overall protein amounts. As discussed before, since our protein aggregates were detected as ‘particles’ in NTA, purified samples with higher amounts of protein aggregates might similarly appear to have a relatively high vesicle purity ratio than expected. From these data, we learnt that one should perform both quantification and molecular characterization studies of EVs in parallel in order to accurately discern and evaluate the molecular and physical characteristics of EVs.

Chapter 5

Characterisation of EVs from pluripotent stem cells

5.1 Introduction

As mentioned in **section 1.1.4.1**, there has only been two studies characterising and showing the horizontal transfer of ESC-EV cargoes across cell lines. Firstly, Ratajczak et al. showed that the EVs purified from mouse and human ESCs express Wnt-3 proteins and are selectively enriched in mRNAs coding for pluripotent transcription regulatory factors such as OCT-4, Rex-1, Nanog, Scl and GATA-2 as compared to parent cells. Subsequently, when these EVs were added onto HPCs, the HPCs had prolonged survival and increased expansion. Interestingly, the authors found that these treated HPCs carried mRNAs for pluripotency markers (e.g. OCT-4, Nanog and Rex-1), expression of some early haematopoietic stem cell markers such as Scl, HoxB4 and GATA-2. Furthermore, these cells were found to have increased phosphorylation of MAPK and AKT post-treatment with EVs (118). In the other study, Yuan et al. published a similar study on ESC-EVs, with more focus on the types of miRNAs in ESC-EVs. Based on RT-PCR analysis, they found that ESC-EVs contain less polyA-containing RNA than the cells. Subsequently, they looked at a number of different ESC-specific miRNAs (miR-290, miR-291-3P, miR-292-3p, miR-294 and miR295) as well as two miRNAs (miR-21 and miR-22), which were normally up regulated in differentiated ESCs. Generally, all of these miRNAs were less abundant

in EVs as compared to their parent cells when normalizing to the same amount of RNA. Interestingly, there were some significant differences in the relative abundance levels when cross comparing each individual miRNAs within this selected group. Further, the authors reported on the kinetics of EV uptake when treating MEFs; the increase in levels of all of these ESC-specific miRNAs was as early as 1 h after treatment. The peak in miRNA detection was observed at between 12-36 h. After 54 h, the levels of these miRNAs in treated MEFs were found to be back to basal levels. Interestingly, it was observed that miRNAs, which were more abundant in ESCs over MEFs, had the highest transfer efficiency (120). All in all, both of these studies showed that ESC-EVs contain mRNAs and miRNAs, which encode for pluripotency factors. Furthermore, these EVs could transfer their cargoes onto other non-related cells and induced functional changes in these recipient cells.

The idea of a stem cell niche was first brought up by Schofield in 1978, where he described the presence of a specialised environment containing functional attributes of stem cells to maintain their self-renewal capacity (360). Similarly, the continuum model of stem cell biology proposed by Quesenberry and Aliotta (**section 1.1.4.4**) showed that stem cells could undergo cellular changes through the introduction of mRNAs and proteins via EVs from differentiated or injured cells. Hence, based on all of these evidences, we postulate that stem cell secrete EVs that contain mRNA coding for pluripotency factors (e.g. OCT-4, Nanog and Rex1). Subsequently, these release EVs can be taken up by other surrounding stem cells and as a result ensure the maintenance of stem cells in their undifferentiated state.

Apart from stem cell maintenance, a certain group of stem cell EVs (MSC-EVs) has

recently been described for use in regenerative medicine. Due to their natural low tendency to induce immune responses and their natural ability to home on disease cells, MSCs has been the primary type of cell used for the cell-based therapies in a number of different disease states such as graft versus host disease, bone regeneration and acute kidney diseases (see **section 1.1.4.4**). Interestingly, it has been shown that the CM or EVs alone can often induce beneficial effects, which are comparable to that of using MSCs alone. Studies have indicated that the EVs from MSCs are enriched in specific miRNAs and ribonucleoproteins that are involved in the regulation of intracellular RNA trafficking. Furthermore, it was deduced that these MSC-EVs could regulate the expression of anti-apoptotic genes at the site of injury and stimulate the proliferation of remaining surviving cells to replace injured cells.

Recently, Katsman and colleagues demonstrated that EVs from ESCs transferred specific mRNAs (e.g. OCT-4 and Sox2) and the miRNAs of the 290 cluster, which are all involved in the maintenance of pluripotency, when they were incubated with Müller cells. Furthermore, there was an up-regulation of genes and miRNAs involved in the induction of pluripotency, cellular proliferation, early ocular genes and genes important for retinal protection and remodeling. On the other hand, there was down-regulation of inhibitory and scar-related genes and miRNAs involved in differentiation and cell cycle arrest (350). Hence, based on these data, it is becoming increasingly evident that stem cell EVs could play important roles in both the maintenance of stem cell biology and in the promotion of regeneration in injured cells.

As ESCs are able to differentiate into any cell type, there was a great interest in the use of these cells for transplantation or tissue engineering applications in

regenerative medicine (361–363). Furthermore, ESCs were found to be invaluable for studying diseases lacking appropriate modeling systems, such as Fragile-X syndrome and cystic fibrosis (364,365). With hindsight though, ESCs are normally derived from the inner cell mass (ICM) of the embryos. Hence, the process of obtaining ESCs would subsequently lead to the destruction of the blastocyst (366). With this knowledge, the use of ESCs for medical research has been rather controversial, with numerous ethical debates on whether the use of these embryos is morally justified (367). As a result, access to such cell lines is highly restricted in the United Kingdom and other countries.

More recently, Yamanaka and his colleagues demonstrated the derivation of another type of pluripotent stem cells- iPSCs, through the introduction of four pluripotency markers (OCT-4, NANOG, cMYC and KLF4) in fibroblast cells via transfection. This reprogramming technique was first demonstrated in mouse and a year later, in human cells (321,322). Unlike ESCs, it has now been shown that iPSCs can be easily generated from a variety of adult somatic cell types and reprogrammed using a number of different methodologies (368–373). For example, the original strategy was based on the use of viral vectors such as retroviruses and lentiviruses, to introduce the reprogramming factors into host genomes. However, concerns were raised that such strategies may increase the risk of tumour formation in the cells. Hence, there have been reports discussing non-integration methods, which could overcome these safety concerns. For example, one could use adenovirus vectors or plasmid to transiently express the reprogramming factors. On the other hand, others have directly delivery these reprogramming proteins or synthetic mRNAs to induce pluripotency. Subsequently, such iPSCs can be used for a wide variety of biological

applications such as modeling of both monogenic and polygenic diseases (374) or even to replace the use of animals testing for toxicology studies, similar to that of ESCs.

Based on different gene expression studies, there have been two different schools of thought about the overall similarity of DNA methylation patterns, differentiation ability and rate of teratoma formation between iPSCs and ESCs. On one hand, it has been shown that iPSCs closely resemble ESCs in both of these aspects (375–377). On the other hand, there are several others studies which contradict these findings (378–385). Interestingly, Yamanaka recently commented that the different observations in these comparison studies may simply be due to other physical or technical factors such as dissimilar culturing conditions between laboratories or even on the total number of cell lines used in the comparison study (386).

Currently, there has yet not been any published data regarding the release of EVs from undifferentiated iPSCs and their role in stem cell biology or in regenerative medicine. As both iPSCs and ESCs are types of PSCs, we hypothesise that stem cell derived EVs from iPSCs could play a similar role in the maintenance of the stem cell state. Next, we, and others, have previously discussed that there are several common factors across all EVs, regardless of their parent cell. For example, all EVs are enriched in a set of EV RNAs and proteins.

In collaboration with Mr Tim Davies and Dr Paul Fairchild, we first tried to purify EVs from mouse iPSCs reprogrammed in their laboratory (387). Unfortunately, as shown in our preliminary study (**Chapter 1- Figure 1.7**), we faced several problems in the

initial quantification and derivation of pure EVs due to the lack of an optimal methodology for EV purification. With the positive data from the systematic comparison studies described in **Chapter 3 and Chapter 4**, we successfully showed that the LC methodology was significantly better for the purification of EVs from mouse iPSCs cultures.

In this chapter, one of the main aims is to perform novel characterization studies on EVs from iPSCs. Here, we started with the LC purification of EVs from two different mouse iPSC lines. As both iPSCs and ESCs have been described to be highly similar, where both are self-renewing and multipotent, we chose to perform an in-depth comparison study between EVs from mouse iPSCs to that from mouse ESCs with LC/MS-MS. Similar to the previous studies done by Ratajczak et al. and Yuan et al, we then compared the overall proteome of EVs with that of the parent cells, to find out the similarities of EVs as compared to cells. Lastly, we share some preliminary data on EVs released from human stem cell sources.

5.2 Material and methodologies

5.2.1 Comparison of EVs from mouse iPSCs and mouse ESCs

All mouse ESCs (ESF121 line and ESF166 line), mouse iPSCs (imef14 and imef9) and MEFs described in this chapter were provided by Dr Paul Fairchild's lab (Dunn School of Pathology, University of Oxford). All conditions for culturing MEFs and the mouse stem cells are described in **section 2.1.2**. For the derivation of EVs from ESCs and iPSCs, CM was collected from the cell cultures (**section 2.2.2**) and processed by the LC protocol (**section 2.3.2**).

5.2.2 Molecular quantification and characterisation of mouse EVs and cell lysates for stem cell comparison study

Each purified EV sample was subjected to NTA for quantification and determination of the size distribution of particles (**section 2.4.1**), western blotting for reported EV markers (Alix, Tsg101 and CD9) (**section 2.4.3**) and TEM (**section 2.4.4**). Subsequently, EVs and cell pellets were subjected to LC-MS/MS for proteomics analysis (**section 2.4.7**). For this set of LC-MS/MS, the reference list used was generated based on all proteins identified within this stem cell set. In order to classify the commonly identified proteins when comparing two sample types, we calculated the ratio of area of proteins of one sample over the other. Proteins that had a 2-fold change in ratio were designated to be "up-regulated". These groups were then analysed in Panther to evaluate enrichment of GO terms.

5.2.3 Characterisation of EVs from human pluripotent stem cell lines

5.2.3.1 Culturing conditions of Human iPSCs

Dr Alison Leishman and Miss Patty Sachmitr (from Dr Paul Fairchild's lab) cultured all the human iPSCs described in this chapter. Human iPSC lines (C15 derived from Lee Carpenter's lab (388) and NHDF1 derived from Dr Sally Cowley's lab, University of Oxford) were cultured on matrigel-coated plates in mTeSR™1 (Stem Cell Technologies, UK) with a daily change of fresh media. For the comparison across different stem cell media, TeSR™-E8™ media (Stem Cell Technologies, UK) was used in place of mTeSR™1. All cells were cultured at 37°C with 5% CO_2. For derivation of EVs from human iPSCs, CM was collected every 24 h and processed by the UC (**section 2.3.1**) or LC protocol (**section 2.3.2**) as indicated.

5.2.3.2 Culturing conditions of Human ESCs

Dr Sarita Panula (from Dr Outi Hovatta's lab, Department of Clinical Science, Karolinska Institutet) cultured all the human ESCs described in this chapter. Human ESCs (HS401 cell line) were cultured on matrigel-coated plates in mTeSR™1 (Stem Cell Technologies, UK) with a daily change of fresh media. All cells were cultured at 37°C with 5% CO_2. For derivation of EVs from human iPSCs, CM was collected every 24 h from these cells and were processed by the UC (**section 2.3.1**) or LC protocol (**section 2.3.2**) as indicated.

5.2.3.3 Molecular quantification and characterisation of human EVs for human stem cell comparison study

Each purified EV sample was subjected to NTA for quantification and determination of the size distribution of particles (**section 2.4.1**), western blotting for reported EV markers (Alix, Tsg101 and CD9) (**section 2.4.3**) and TEM (**section 2.4.4**).

5.2.4 Characterisation of EVs from DCs differentiated from human iPSCs

5.2.4.1 Directed differentiation of Human iPSCs into DCs

Dr Alison Leishman and Miss Patty Sachmitr performed differentiation of human iPSCs to DCs based on the differentiation protocol developed in Dr Paul Fairchild's lab (389–391). Briefly, human iPSCs were seeded at a density of $3x10^6$ cells/well on ultra low attachment (ULA) 6-well plates in differentiation media (X-VIVO-15, Lonza, UK) supplemented with growth factors (50ng/ml of recombinant human bone morphogenetic protein-4 (BMP-4), 50ng/ml of recombinant human vascular endothelial growth factor (VEGF), 20ng/ml of recombinant human stem cell factor (SCF) and 50ng/ml of recombinant human granulocyte macrophage-colony stimulating factor (GM-CSF)) in a 37°C incubator with 5% CO_2. Over the differentiation process, cultures were fed every other day and growth factors were successively removed from the differentiation culture until only GM-CSF remained. When macrophages were observed in the cultures at around days 13-17, 25ng/ml or recombinant human interleukin-4 (IL-4) was added to the cultures in increasing

concentration to 100ng/ml. IL-4 was added to skew monocyte-like cells or DC precursors towards a DC phenotype. Generally, the generation of DCs from human iPSCs took 24-28 days, although there might have been some variation between wells within the same differentiation batch of cells.

5.2.4.2 Maturation of DCs differentiated from human iPSCs

At the final day of the differentiation experiment, immature DCs were harvested by gentle pipetting, leaving behind the embryoid bodies and macrophages. The harvested DCs were re-plated at $1x10^6$ cells/well into 6-well plates. After 2-4 days, DCs were matured using X-VIVO-15 media containing 50ng/ml of GM-CSF, 100ng/ml of IL-4 and a cocktail of cytokines (50ng/ml of recombinant human tumour necrosis factor-α (TNF-α), 20ng/ml of recombinant human interferon-γ (IFN-γ) and 1μg/ml of prostaglandin-2) for 48 h.

5.2.4.3 Collection of EVs and molecular characterisation of EVs from DCs

To investigate the release of EVs across the entire differentiation process, CM was collected at various different stages of the differentiation process (as indicated by the asterisks in Figure 5.3.8A) and from the subsequent cultures of immature and mature DCs. The different CM samples were processed by the LC protocol (**section 2.3.2**) and each individual 2ml fractions eluted from the column was subjected to NTA for quantification and determination of the size distribution of particles (**section 2.4.1**) and protein quantification (**section 2.4.2**). The F1 fractions containing the EVs released from immature and mature DCs were concentrated and characterized by

NTA (**section 2.4.1**) and western blotting for reported EV markers (Alix and Tsg101) and the DC marker (CD11c) (**section 2.4.3**). RNA was subsequently extracted from both immature and mature DC EV samples and subjected to RNA profiling using the small RNA and Pico chip (**section 2.4.6**).

5.2.5 Statistics

All bars in graphs represent mean ±SD.

5.3 Results

5.3.1 EVs from mouse iPSCs and ESCs have similar size distribution profiles and expression of EV markers

Previously in **chapter 4**, the LC method was demonstrated to be a better method for purification of EVs from stem cell sources as compared to the original UC protocol as the presence of non-vesicular protein contamination was high in the UC pellet. In order to accurately unravel the molecular characteristics of EVs, we chose to employ the use of the LC protocol for all EV purification from mouse stem cells.

First, we collected CM from two different mouse iPSC lines (imef14 and imef19) and subjected them to fractionation on the LC column. Generally, both sample types showed a similar 280nm absorbance pattern across the eluted volume (**Figure 5.3.1A**), with a peak at the F3 region. As we were only interested in the EVs, we pooled fractions across the region where EVs elute (F1) and analyzed the particles with NTA. As shown in **figure 5.3.1B**, the size distribution profiles of both mouse iPSC-derived EVs were overlapping. Next, we performed the same purification for two different mouse ESC lines (ESF121 and ESF166). The LC chromatograph of these ESC samples were generally similar to each other (**Figure 5.3.1C**) and with that of the iPSC-derived CM. Further, NTA showed that the size distribution across both ESC sample types were highly similar (**Figure 5.3.1D**). Overall, EVs derived across these four cell lines were found to be similar in both their mean and mode sizes (**Figure 5.3.1E**). Moreover, TEM on EVs from both mouse ESCs and iPSCs

verified the NTA measurements and showed that the particles from both cell types appeared to be relatively similar (**Figure 5.3.1F**). Furthermore, we detected similar expression levels of EV markers (Alix and CD9) across both mouse iPSC and ESC-derived EVs (**Figure 5.3.1G**). Lastly, we found that the P/μg ratio of the EVs across all four sample types were similar to each other (**Figure 5.3.1H**).

Figure 5.3.1

A

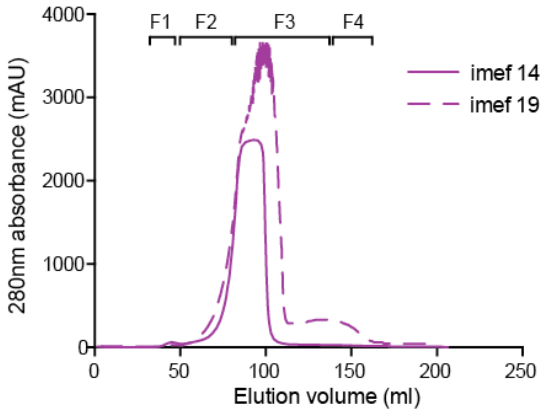

B

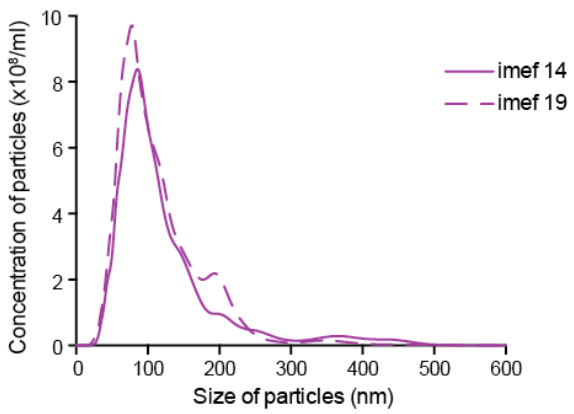

C

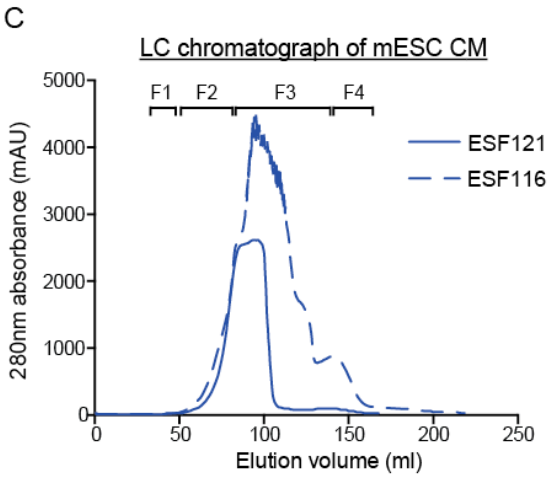

D

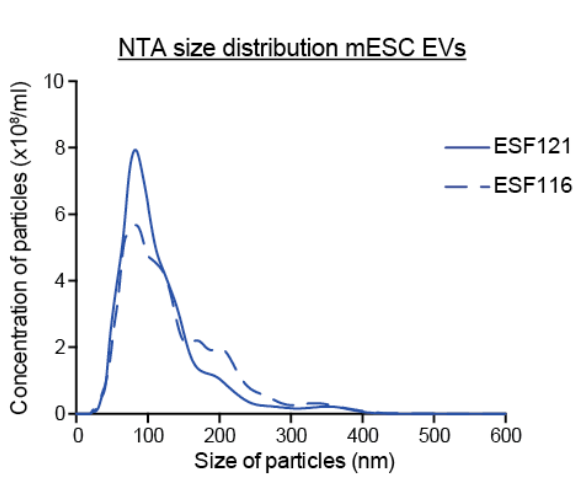

E

		Mean size (nm)	Mode size (nm)
Mouse iPSC	imef 14	124.7	84
	imef 19	115.9	72
Mouse ESC	ESF121	116.7	84
	ESF166	135.8	81

F

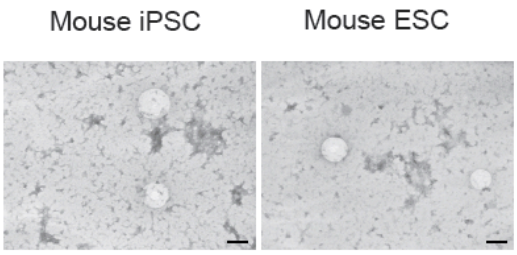

G

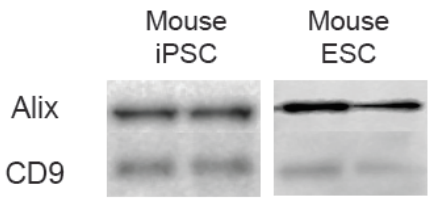

H

P/μg	1	2
miPSC	3.6×10^9	6.5×10^9
mESC	6.2×10^9	6.8×10^9

Figure 5.3.1 Characterisation of EVs from mouse iPSCs and ESCs with NTA, TEM and western blotting

Representative LC chromatographs of two different mouse iPSC cell lines (imef14 and imef19) (A) and mouse ESC cell line (ESF121 and ESF166) (C). NTA size distribution profiles of EVs from mouse iPSCs (B) and mouse ESCs (D). (E) Table showing the mean and mode size of EVs from both mouse iPSCs and ESCs. (F) Representative TEM images of EVs from mouse iPSCs and mouse ESCs. (G) Representative western blotting of EV markers (Alix and CD9) when loading the same amount of EVs from mouse iPSCs and mouse ESCs in each well. (H) Table showing the P/μg ratio of EVs purified from two mouse iPSCs and ESCs experiments.

5.3.2 EVs display different protein and RNA profiles as compared to their parental cells

Besides comparing the EVs across mouse iPSCs and ESCs, we were interested in understanding how EVs compared to their parental cells. First, we performed western blotting analysis for EV markers (Alix and CD9) as well as a stem cell marker (Pou5f1/Oct4) when loading equal protein amounts. Interestingly, we noticed that there was a slight enrichment of Alix and CD9 in the EVs as compared to the cell lysates (**Figure 5.3.2A**). On the other hand, the opposite trend was noticed for OCT-4. Next, we investigated the RNA profile of EVs versus their cells. Using the small RNA chip, we noticed that the small RNA profiles of EVs were highly similar, where EVs from both cell types showed a peak around the 60-nucleotide region. On the other hand, the small RNA profiles of both cell types were distinctly different to that of the EVs (**Figure 5.3.2B**). Next, with the Pico chip, we checked for a broader size range of RNA. Again, we found that the RNA profiles were more similar between EV samples than between EVs and their parental cells. For example, one obvious difference between EVs and cells was the absence of the 18S and 28S ribosomal peaks in the EV samples (**Figure 5.3.2C**).

Figure 5.3.2

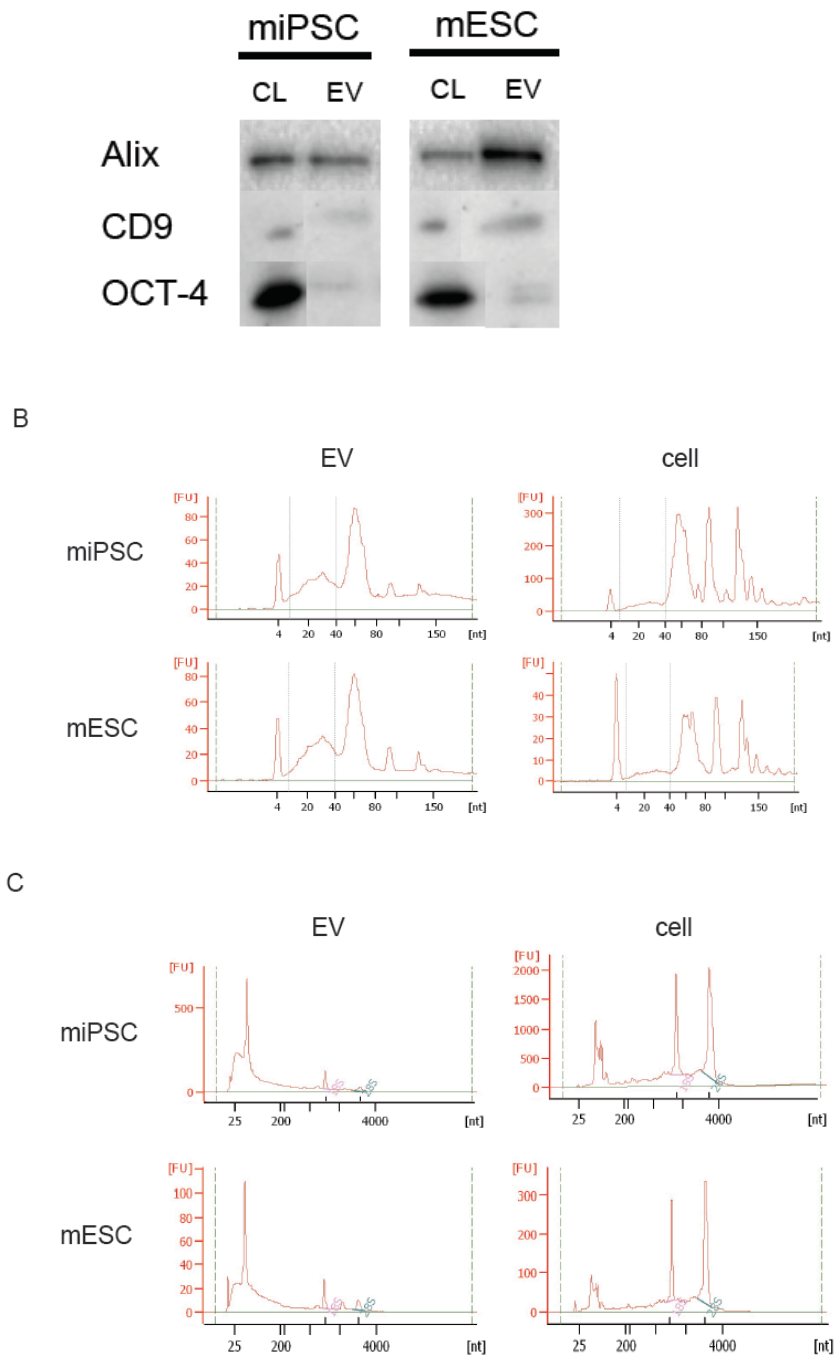

Figure 5.3.2 Comparison of EVs and their parental cells by western blotting and RNA bioanalzyer

(A) Western blotting comparing the expression of EV markers and Oct4 in cell lysates (CL) and EVs. The same amount of protein (10 μg) was loaded in each well. Small RNA chip (B) and pico chip (C) bioanalyzer data of RNA in EVs and cells.

5.3.3 Preliminary proteomics on stem cell media reveal the presence of contaminating proteins

In order to characterise our EVs more thoroughly, we decided to run EVs derived from mouse iPSCs and ESCs for LC-MS/MS proteomics analysis. As mentioned previously, the P/µg ratios for all our EV samples (**section 5.3.1**) was considered to be of low purity, possibly suggesting that the remnants of some contamination present in our EV samples. To scope out the amount of contaminants from the stem cell media only, we fractionated 15 ml of the stem cell media on the LC column. Subsequently, we pooled individual fractions corresponding region where EVs elute and termed this pool as Md. With total protein staining on the gel, we detected the presence of unknown protein bands in this Md fraction of stem cell media (**Figure 5.3.3A&B**). Hence, to evaluate the degree of non-vesicular protein contamination in our EV samples, we first performed LC-MS/MS on the Md fraction from stem cell media and the gelatin used for coating the cell culture plates.

Based on absolute protein identities, we detected 35 cow and 29 mouse proteins in the Md fraction (**Table 5.1A**), with many of mouse proteins mapping to specific proteins such as fibronectin, heat shock protein and keratins (**Table 5.1B**). In the gelatin sample, majority of the proteins detected was collagen (**Table 5.2**). In both the Md fraction and gelatin, we detected both cow albumin protein and mouse keratin proteins (**Table 5.3**). Unfortunately, many of these proteins were detected at high abundance within our EV samples as shown by the correlation graph of protein areas (**Figure 5.3.3C**). In order to analyse true EV proteins, we decided to subtract

the identities of all of these contaminating proteins prior to performing bioinformatics on the EV proteomic data.

Figure 5.3.3

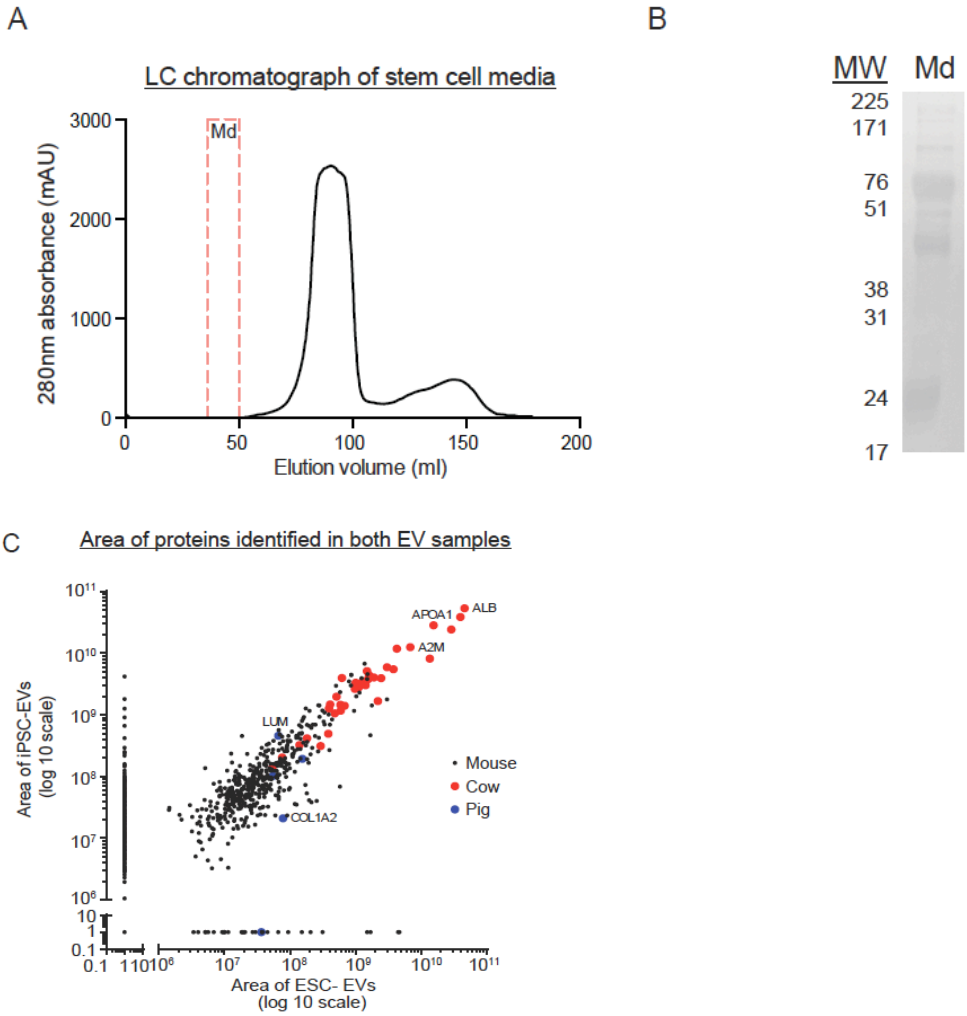

Figure 5.3.3 Preliminary proteomics on media and gelatin sample

(A) LC chromatograph of unconditioned stem cell media. Md indicated the region where EVs normally elute from the LC column. (B) Total protein staining of the Md sample indicates presence of unknown protein bands. (C) Scatter plot showing the correlation between the areas of proteins identified in the preliminary run on both iPSC and ESC EV samples. Proteins detected from different species are as labeled: mouse (black dots), cow (red dots) and pig (blue dots)

Table 5.1A

Species of protein	Name of protein	Accession number
Bos taurus	Alpha-1-acid glycoprotein	Q3SZR3
	Alpha-1-antiproteinase	P34955
	Alpha-1B-glycoprotein	Q2KJF1
	Alpha-2-antiplasmin	P28800
	Alpha-2-HS-glycoprotein	P12763
	Alpha-2-macroglobulin	Q7SIH1
	Antithrombin-III	F1MSZ6
	Apolipoprotein A-I	P15497
	Apolipoprotein A-IV	F1N3Q7
	C1QC protein (Fragment)	Q1RMH5
	Complement C3	G3X7A5
	Complement component C9	Q3MHN2
	FGG protein	Q3SZZ9
	Fibrinogen alpha chain	A5PJE3
	Fibrinogen beta chain	F1MAV0
	Gelsolin	F1MJH1
	Haptoglobin	G3X6K8
	Hemoglobin subunit beta	P02070
	Inter-alpha-trypsin inhibitor heavy chain H1	F1MMP5
	Inter-alpha-trypsin inhibitor heavy chain H4	F1MMD7
	Leucine-rich alpha-2-glycoprotein 1	Q2KIF2
	Protein AMBP	F1MMK9
	Prothrombin	P00735
	Serotransferrin	Q29443
	Serpin A3-5	A2I7N1
	Serpin A3-7	A2I7N3
	Uncharacterized protein (Fragment)	G3N0V0
	Uncharacterized protein (Fragment)	G5E513
	Uncharacterized protein	F1N514
	Uncharacterized protein	F1N076
	Uncharacterized protein	E1BH06
	Uncharacterized protein	F1MLW8
	Uncharacterized protein	F1MCF8
	Vitamin D-binding protein	F1N5M2

Table 5.1B

Species of protein	Class of protein	Name of protein	Accession number
Mus musculus	Fibronectin	Fibronectin	A0A087WS56
		Fibronectin	B7ZNJ1
	Heat shock protein	Heat shock protein 75 kDa, mitochondrial	Q9CQN1
		Heat shock protein HSP 90-alpha	P07901
		Heat shock protein HSP 90-beta	P11499
	Keratin	Keratin, type I cytoskeletal 16	Q9Z2K1
		Keratin, type I cytoskeletal 17	Q9QWL7
		Keratin, type I cytoskeletal 18	P05784
		Keratin, type I cytoskeletal 19	P19001
		Keratin, type II cytoskeletal 2 epidermal	Q3TTY5
		Keratin, type II cytoskeletal 8	P11679
	L-lactate dehydrogenase	L-lactate dehydrogenase A chain	P06151
		L-lactate dehydrogenase B chain	P16125
	Others	Actin, cytoplasmic 1	P60710
		Annexin (Fragment)	B0V2N7
		Apolipoprotein B-100 (Fragment)	E9Q1Y3
		Apoptosis facilitator Bcl-2-like protein 14	Q9CPT0
		Beta-actin-like protein 2	Q8BFZ3
		Complement component C8 beta chain	Q8BH35
		E3 ubiquitin-protein ligase TRIP12	A0A087WNZ7
		Filamin-C	D3YW87
		Fructose-bisphosphate aldolase A	P05064
		Gelsolin	P13020
		Hemoglobin subunit alpha	P01942
		Histone H4	P62806
		Junction plakoglobin	Q02257
		Rho guanine nucleotide exchange factor 9 (Fragment)	S4R1J2
		Ubiquitin-associated domain-containing protein 2	Q8R1K1

Table 5.1

Table showing the list of cow (A) and mouse (B) proteins exclusively identified in the media sample.

Table 5.2

Species of protein	Class of protein	Name of protein	Accession number
Mus musculus	Collagen	Collagen alpha-1(I) chain	P11087
		Collagen alpha-1(II) chain	P28481
		Collagen alpha-1(III) chain	P08121
		Collagen alpha-1(V) chain	O88207
		Collagen alpha-2(I) chain	Q01149
	Others	Ig gamma-2A chain C region secreted form	P01864
		Ig heavy chain V region MOPC 47A	P01786
		Protein Ahnak	E9Q616
		Protein BC067074 (Fragment)	F6Z6Y0

List excludes the detection of 8 uncharacterised sus scrofa proteins

Table 5.2

Table showing the list of mouse proteins exclusively identified in the gelatin sample.

Table 5.3

Species of protein	Class of protein	Name of protein	Accession number
Bos taurus	Albumin	Serum albumin	P02769
Mus musculus	Keratin	Keratin, type II cytoskeletal 79	Q8VED5
		Keratin, type II cytoskeletal 75	Q8BGZ7
		Keratin, type II cytoskeletal 5	Q922U2
		Keratin, type II cytoskeletal 1	P04104
		Keratin, type I cytoskeletal 10	A2A513

List excludes 2 uncharacterised sus scrofa proteins

Table 5.3

Table showing the list of proteins commonly identified in both the media and gelatin sample.

5.3.4 EVs from iPSCs and ESCs contain proteins mapping to similar GO annotations

After filtering out these contaminating proteins, we found that a total of 1387 proteins were detected across both EV populations from iPSCs and ESCs, where 33.1% of them over-lapped across both groups (**Figure 5.3.4A**). Interestingly, more proteins were detected in the iPSC-EVs than that in ESC-EVs (593 versus 35). However, upon more in-depth analysis, many of these exclusively detected proteins in either iPSCs or ESCs-derived EVs, were found to classify under similar GO annotations such as protein binding and cytosol. Next, we considered the 459 proteins, which were common in both types of EVs and divided them into three groups: proteins with similar expression, proteins up regulated in iPSC-EVs and proteins up-regulated in ESC-EVs. Generally, majority of these common proteins were of similar protein levels to each other (**Figure 5.3.4B**). To cross-compare this dataset to our previous western blotting for EV markers, we checked for the fold enrichment of vesicle-associated GO terms. As expected, we found that the EVs were of similar levels and enrichments in GO terms for extracellular vesicle, extracellular exosome, membrane-bound exosome and vesicle, in both stem cell sample types (**Figure 5.3.4C**). Upon deeper analysis of the individual identities of proteins, we noticed the appearance of EV markers that we had earlier used for characterisation (e.g. CD9, CD81 and Alix) as well as other reported EV-associated proteins as shown in **Figure 5.3.4D**. On the other hand, there were a handful of GO terms, which were significantly different between the two types of EVs. For example, GO terms for translation initiation factor activity, translation factor activity, RNA binding and protein heterooligomerisation

was up-regulated in EVs from iPSCs, while proteins in the plasma membrane part GO term was up-regulated in EVs from ESCs (**Figure 5.3.4E**).

Figure 5.3.4

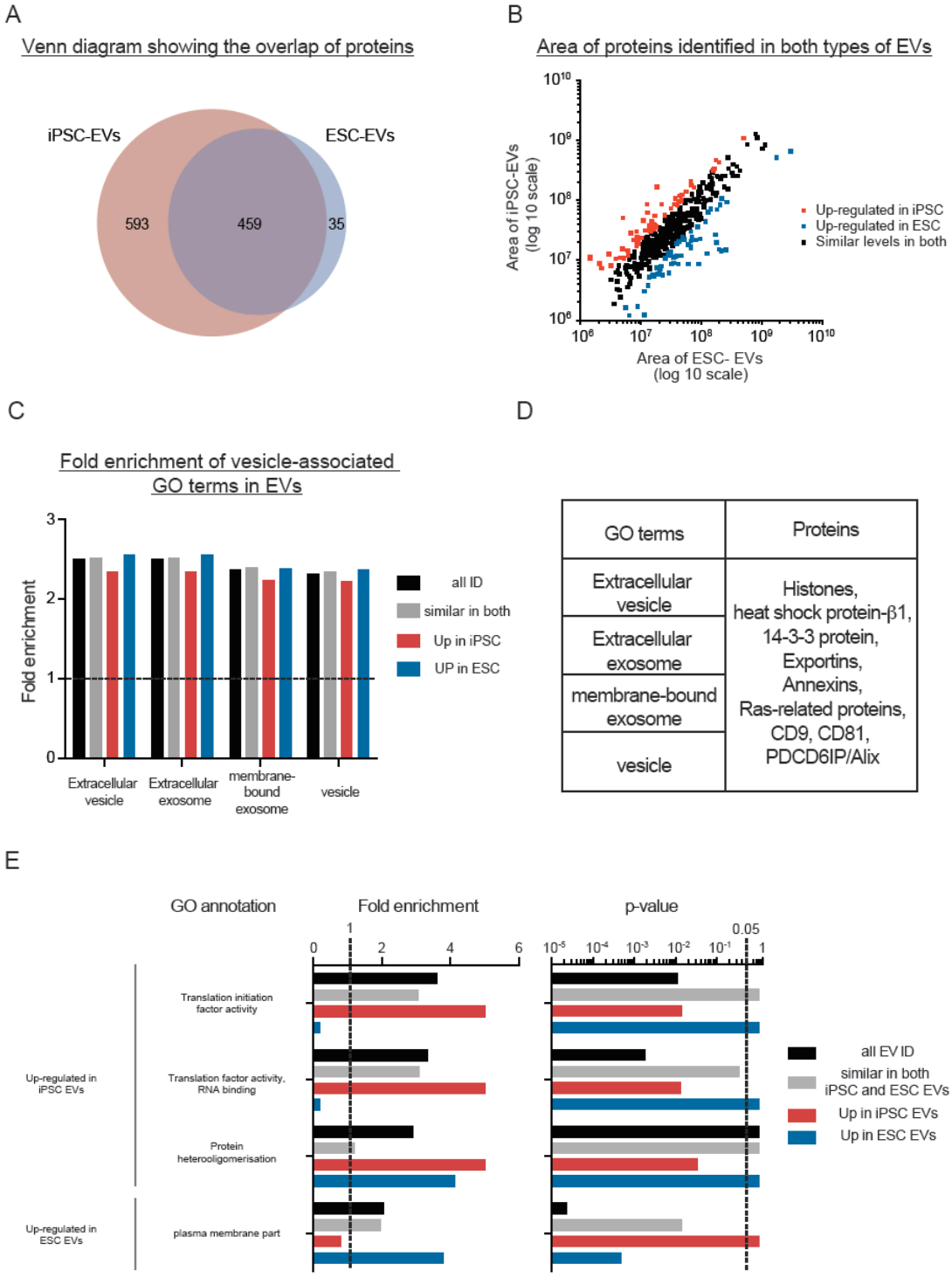

Figure 5.3.4 Preliminary proteomics on EVs from mouse iPSCs and ESCs

(A) Venn diagram showing the overlap of proteins identified from the two pools of stem cell EVs. (B) Scatter plot showing the correlation between the areas of commonly identified proteins in both iPSC-EVs and ESC-EVs. All proteins were classified into three distinct groups: up regulated in iPSC-EVs (red dots), up regulated in ESC-EVs (blue dots) and of similar levels in both iPSC and ESC-derived EVs (black dots). (C) Graph showing the fold enrichments of both iPSC-EVs and ESC-EVs over the reference list, in four vesicle-related GO terms: extracellular vesicle, extracellular exosome, membrane-bound exosome and vesicle. (D) List of individual proteins identified in these four GO terms. (E) A subset of significantly enriched GOs from proteins considered to be up regulated in either iPSC or ESC-derived EVs. All proteins are grouped under the four categories: all EV IDs (black bar), proteins of similar levels in both iPSC-EVs and ESC-EVs (grey bar), up regulated in iPSC-EVs (red bar) and up-regulated in ESC-EVs (blue bar).

5.3.5 EVs from mouse iPSCs have distinct proteomic features as compared to their parental cells

To analyse if the lack of differences in the EVs was related to the proteome of their parental cells, we further analysed the cellular proteome from the exact batch of iPSCs and ESCs from which the EVs were derived. Overall, there were more proteins detected in cells than in EVs (3565 versus 1387). Of these proteins, there was an overlap of 71.6% of them in both cell types (**Figure 5.3.5A**). Although there were some proteins, which were exclusively detected in either group, most of these proteins mapped to similar GO terms (e.g. nucleotide and RNA binding, organelle and membrane part). Similar as before, we segregated the commonly identified proteins into three broad groups; similar in both, up-regulated in iPSCs and up-regulated in ESCs. Although there appeared to be some differences in GO enrichments, none of these differences were found to be significant. Interestingly, the correlation plot of individual protein areas showed the exception of two outliers: mitochondrial ribosomal protein S25 (MRPS25) and activating signal cointegrator 1

complex subunit 3 (ASCC3), both of which were found to be more abundant in ESCs than in iPSCs (**Figure 5.3.5B**).

Our initial proteomics data here indicate that the enrichment of GO terms was similar across EVs and cells from two cell types. However, in our previous western blotting cross-comparing EV and cell samples, we noticed a difference in the expression levels of EV markers (**Figure 5.3.2A**). Hence, we proceeded to compare the individual EV samples back to their parental cells. Interestingly, we found that there was much less overlap across EVs and cells; 28.5% for the iPSC set and 15.5% for the ESC set (**Figure 5.3.5C&E**). From the correlation graphs of commonly identified proteins in EVs versus cells, we observed that many protein identities were differentially detected in one group than the other (**Figure 5.3.5D&F**). As a result, these differences contributed to the enrichment of certain GO terms in each group. For example, in the iPSC set, the GO terms for translation initiation factor activity, translation factor activity, RNA binding, extracellular matrix and extracellular space were all found to be up regulated in EVs. On the other hand, GO terms for structural constituent of ribosome, mRNA binding, cytosolic part and intracellular non-membrane-bounded organelle was up regulated in cells (**Figure 5.3.5G**). As for the ESC set, we observed enrichment of GO terms for glycolipid binding, G-protein beta/gamma-subunit complex binding, external side of plasma membrane and extracellular matrix component in the EVs. As for the ESCs, there was an up-regulation of GO terms for the structural constituent of cytoskeleton, histone binding, protein-DNA complex assembly and chromatin assembly or disassembly, as compared to EVs (**Figure 5.3.5H**). Interestingly, there were some GO terms, which were similarly enriched in EVs as compared to cells, across both stem cell types. For

example, the GO term for basal lamina was enriched in EVs from both iPSCs and ESCs as compared to their parent cells. On the other hand, GO terms for protein-DNA complex subunit organisation, DNA replication-dependent nucleosome organisation, nuclear chromosome and nuclear nucleosome were more enriched in both cell samples as compared to their EVs (**Figure 5.3.5l**).

Figure 5.3.5

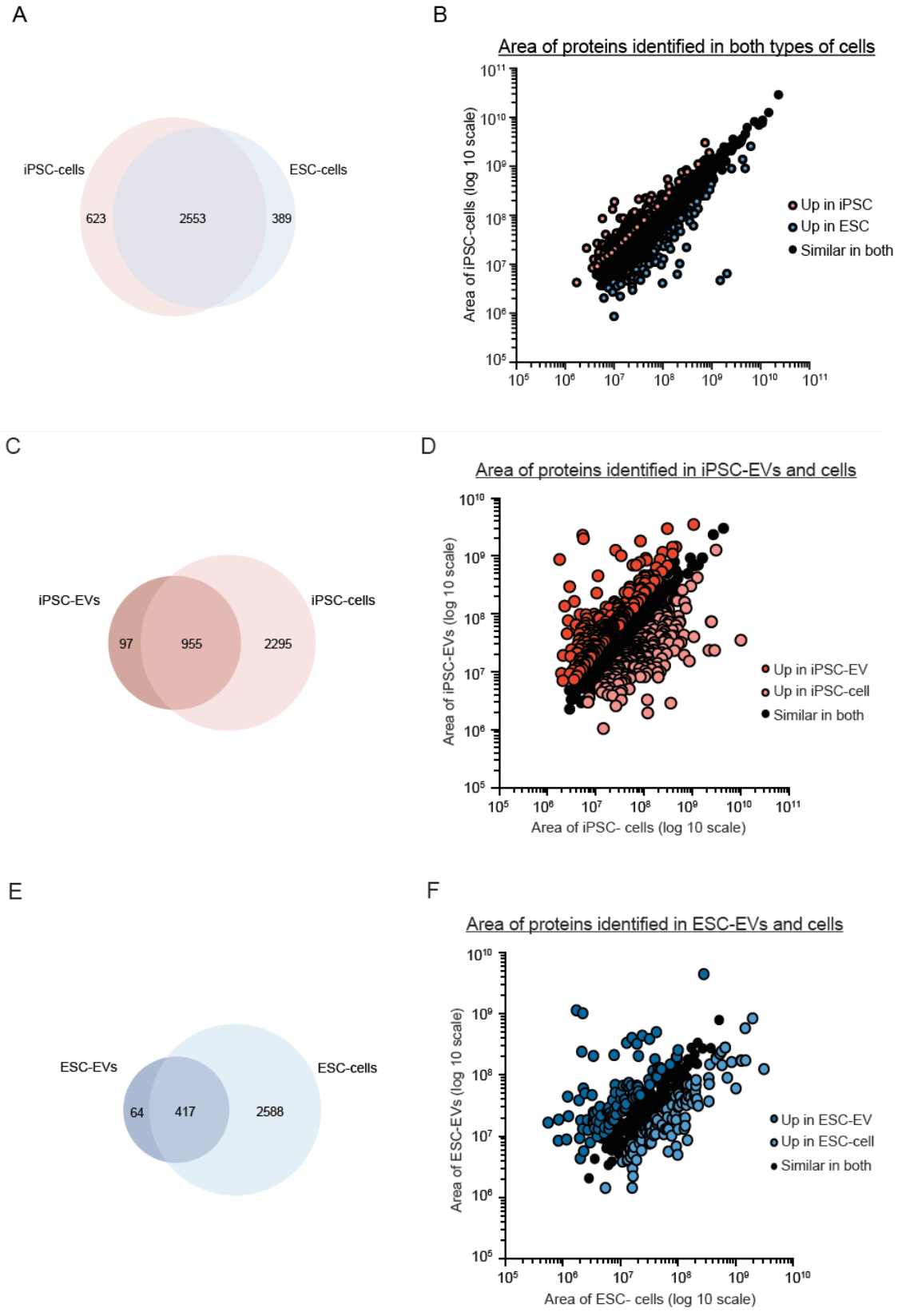
A
iPSC-cells
ESC-cells
623
2553
389
B
Area of proteins identified in both types of cells
Area of iPSC-cells (log 10 scale)
Up in iPSC
Up in ESC
Similar in both
C
iPSC-EVs
iPSC-cells
97
955
2295
D
Area of proteins identified in iPSC-EVs and cells
Area of iPSC-EVs (log 10 scale)
Area of iPSC- cells (log 10 scale)
Up in iPSC-EV
Up in iPSC-cell
Similar in both
E
ESC-EVs
ESC-cells
64
417
2588
F
Area of proteins identified in ESC-EVs and cells
Area of ESC-EVs (log 10 scale)
Area of ESC- cells (log 10 scale)
Up in ESC-EV
Up in ESC-cell
Similar in both

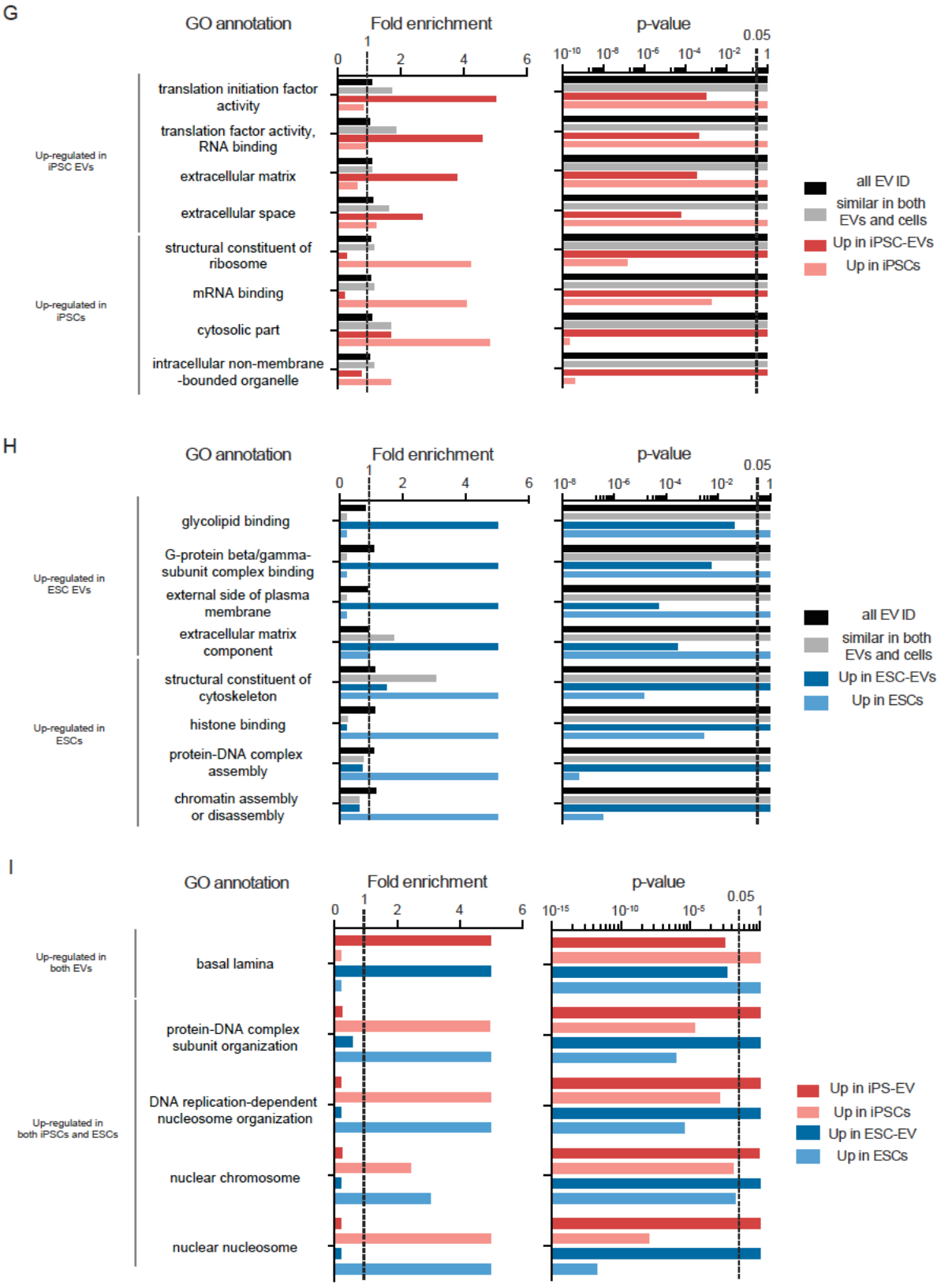
G
GO annotation
Fold enrichment
p-value
translation initiation factor activity
translation factor activity, RNA binding
extracellular matrix
extracellular space
structural constituent of ribosome
mRNA binding
cytosolic part
intracellular non-membrane -bounded organelle
Up-regulated in iPSC EVs
Up-regulated in iPSCs
all EV ID
similar in both EVs and cells
Up in iPSC-EVs
Up in iPSCs
H
GO annotation
Fold enrichment
p-value
glycolipid binding
G-protein beta/gamma-subunit complex binding
external side of plasma membrane
extracellular matrix component
structural constituent of cytoskeleton
histone binding
protein-DNA complex assembly
chromatin assembly or disassembly
Up-regulated in ESC EVs
Up-regulated in ESCs
all EV ID
similar in both EVs and cells
Up in ESC-EVs
Up in ESCs
I
GO annotation
Fold enrichment
p-value
basal lamina
protein-DNA complex subunit organization
DNA replication-dependent nucleosome organization
nuclear chromosome
nuclear nucleosome
Up-regulated in both EVs
Up-regulated in both iPSCs and ESCs
Up in iPS-EV
Up in iPSCs
Up in ESC-EV
Up in ESCs

Figure 5.3.5 Preliminary proteomics comparing GO terms in EVs and cells from mouse iPSCs and ESCs
Venn diagram showing the high overlap of proteins identified from the two stem cells (A), between mouse iPSC-EVs and iPSCs (C) and mouse ESC-EVs and ESCs (E). Scatter plots showing the correlation between the areas of commonly identified proteins in each of these three pairing: iPSCs versus ESCs (B), iPSC-EVs versus iPSCs (D) and ESC-EVs versus ESCs (F). All proteins were classified into three distinct groups as indicated in the graphs. (G) A subset of significantly enriched GOs from proteins considered to be up regulated in either iPSC or ESCs (G), in either iPSC-EVs or iPSCs (H) and in either ESC-EVs or ESCs (I).

5.3.6 LC purification of EVs from CM of human iPSCs show very low levels of secreted EVs

As discussed in **section 5.1**, human iPSCs are becoming useful tools in medical sciences in terms of re-modeling of different disease phenotypes and potentially for personalised medicine. Hence, we felt that it would be interesting to investigate the release of EVs from human iPSCs. In collaboration with Dr Alison Leishman and Miss Patty Sachmitr (Dr Paul Fairchild's lab, University of Oxford), we collected and purified EVs from human iPSCs.

One major difference between human and mouse stem cells are the type of media used for culture and the exact culturing conditions. Unlike that for mouse cultures, all human iPSCs and ESCs discussed in this thesis were cultured on matrigel-coated plates and stem cell media (mTeSR^{TM}) was replaced daily on the cells. As a result of this different culturing methodology, we initially started with daily collections of CM to check the trend of vesicle release in relation to the different time points within the same passage of cells. Furthermore, our initial studies showed that the human stem cell media was similarly complex and protein-rich as mouse stem cell media (data not shown). Hence, all human stem cell EVs described here were purified by the LC method.

Generally, the LC chromatograph of CM from different time point of collection of the human iPSC cultures showed the same trend as that of complex media types: a huge broad peak around the 75-110ml elution volume (**Figure 5.3.6A**). This peak generally corresponded with the F3 region of mouse stem cell media. As we

expected the EVs to be of the same size range as those discussed earlier, the same limits for the F1 fraction of mouse stem cell lines was used here. Interestingly, the three replicate sets of human iPSC-EVs displayed different trends with respect to the total number of particles across cell confluence. In particular, the total number of particles for sets 2 and 3 peaked on the first time point of collection, before dropping down to low levels for the rest of the time points. At the final collection time point (when cells were around 90-100% confluence, the total number of particles across all three sets were comparable (**Figure 5.3.6B**). At the first 24 h time point, we postulate that there may have different levels of apoptosis and necrosis of freshly trypsinised cells across different batches of cultures. Hence, we chose to focus on the EVs purified from the last 24 h where cells were at their highest confluence state. NTA showed that the overall size distribution profiles of EVs at this stage was variable across replicate sets of EVs, although the mode size of EVs was still around 100nm (**Figure 5.3.6C&D**). Furthermore, we found that the total number of particles detected per well was around $7x10^8$ (**Figure 5.3.6D**), which is substantially lower than the levels seen for mouse stem cells or other immortalized cell lines tested (e.g. HEK293T). To verify this finding was accurate, we further tested culturing the iPSCs in an alternative, more defined media type – TeSR™-E8™ (E8). As compared to mTeSR™, E8 media only contains 8 ingredients with the total absence of albumin. As a result, these differences in media composition were clearly reflected in the LC chromatograph of CM; where the E8 sample did not show the huge protein peak around the 75-110ml elution volume (**Figure 5.3.6E**). When we simply considered the F1 fraction of EVs derived from both media types, we found that both the overall particle counts and the size distribution profiles were largely similar (**Figure 5.3.6F**). Unfortunately, we were unable to detect any expression of EV markers (Alix and

CD9) via western blotting from any of these human iPSC-derived EVs (data not shown).

Figure 5.3.6

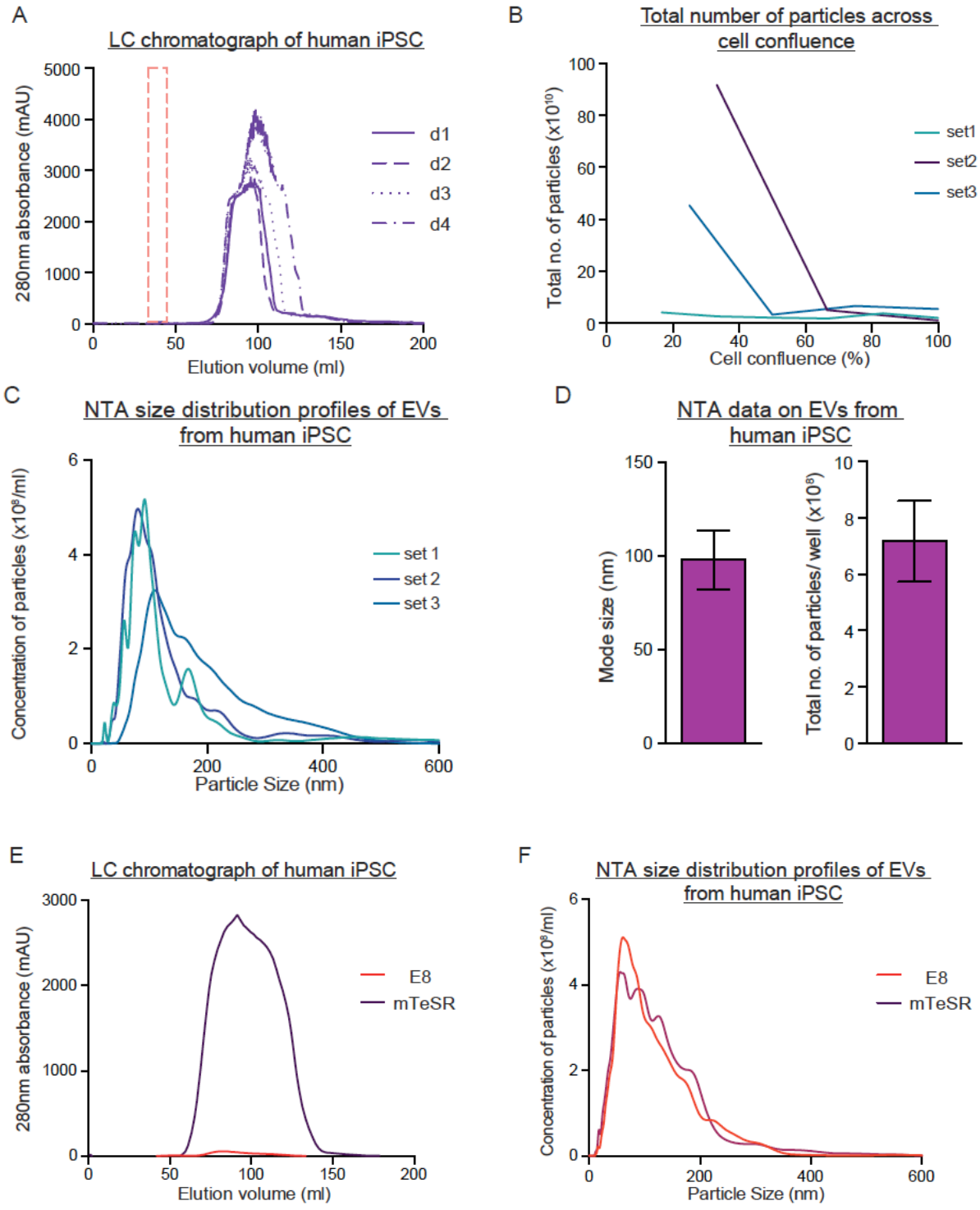

Figure 5.3.6 LC purification and characterisation of EVs from human iPSCs.

(A) LC chromatograph showing the profiles of CM samples collected every 24 h, over a total of four days (d1-d4). (B) Graph showing the total number of particles pelleted from the 24 h samples across cell confluence, in three replicate sets. (C) NTA size distribution profiles of EVs purified on the final 24 h (d4) time point. (D) Graphs showing the mode size of particles and the total number of particles per well from the final 24 h time point. (E) LC chromatograph showing the profiles of CM samples collected from two different media conditions (E8 and mTeSR) of human iPSCs. (F) NTA size distribution profiles of EVs purified from these two media conditions.

5.3.7 Human ESCs display higher secretion of EVs than human iPSCs

From **section 5.3.6**, we noticed low particle counts from the human iPSCs, as compared to the mouse samples. As we were unsure if this phenomenon was a species or cell type dependent effect, we collaborated with Dr Sarita Panula (Karolinska Institutet) to investigate whether human ESCs could be similar to human iPSCs in displaying low levels of EV secretion, under the same culturing conditions.

After fractionation of the human ESC sample on the LC column, there was the similar detection of a peak at the region corresponding to the F3 protein peaks (**Figure 5.3.7A**). As with the human iPSC samples, we pooled the same region of fractions where EVs were expected to elute and performed NTA on this F1 fraction. Interestingly, the size distribution of EVs was relatively broader and with multiple peaks (**Figure 5.3.7B**) and this trend was rather different as compared to the human iPSC sample (**Figure 5.3.6C**). In particular, particles from the human ESCs were much larger (average mode size was around 150nm) and around 5-fold more particles per well ($35x10^8$) (**Figure 5.3.7C**). Furthermore, we were able to detect the presence of Alix and Tsg101 in these human ESC-derived EVs through western blotting (**Figure 5.3.7D**).

Figure 5.3.7

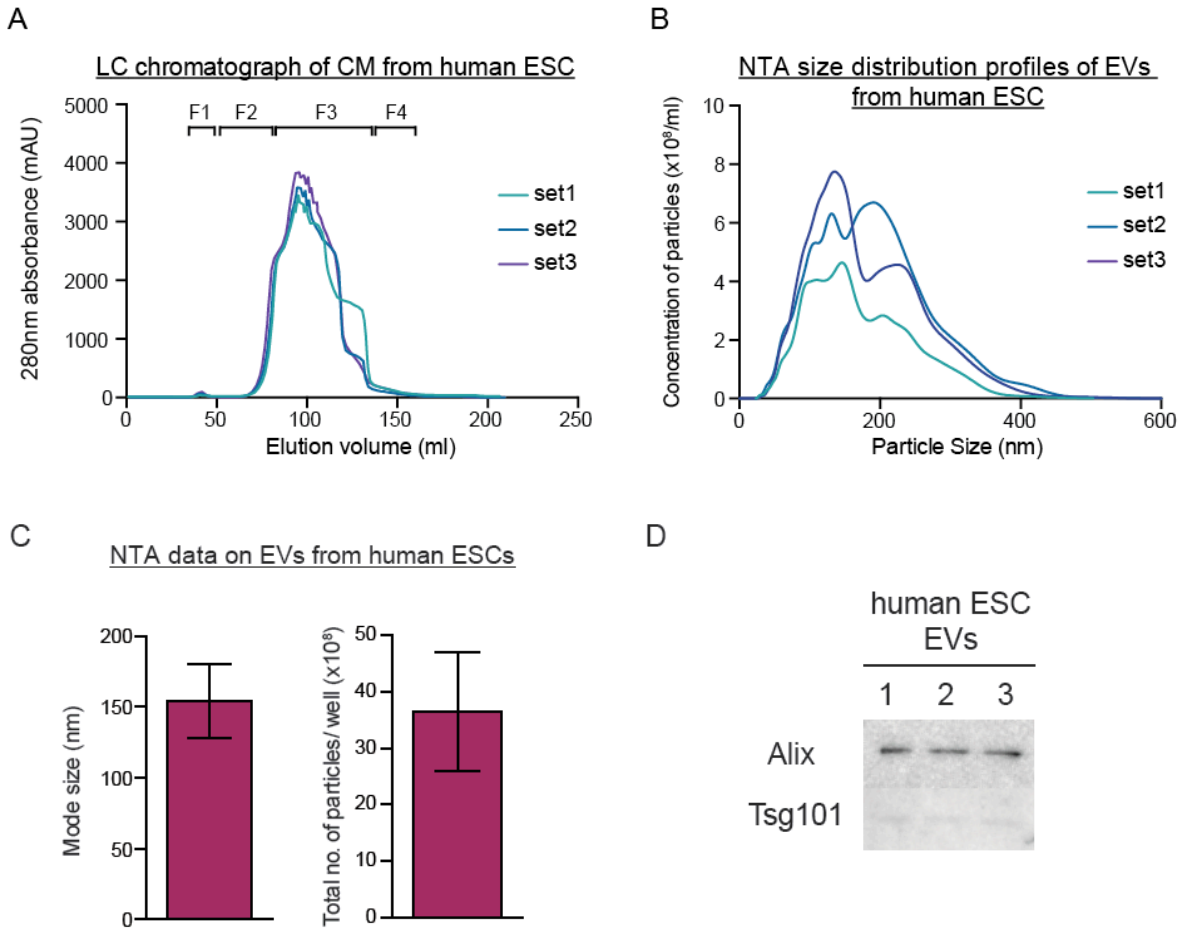

Figure 5.3.7 LC purification and characterisation of EVs from human ESCs.
(A) LC chromatograph showing the profiles of replicate CM samples from human ESC cultures. (B) NTA size distribution profiles of EVs purified from human ESCs. (C) Graphs showing the mode size of particles and the total number of particles per well from human ESC cultures. (D) Representative western blotting pictures for EV markers (Alix and Tsg101) in EVs purified from three replicate sets of human ESCs.

5.3.8 DCs differentiated from iPSCs release high amounts of EVs

From **section 5.3.7**, we observed that there were some differences in the particles purified from human iPSCs and human ESCs in terms of the size, the overall amounts and the presence of EV markers. To investigate further if this phenomenon was specifically due to our iPSC line, we tested collecting EVs derived from DCs differentiated from these human iPSCs in collaboration with Dr Alison Leishman and Miss Patty Sachmitr (Dr Paul Fairchild's lab, University of Oxford).

The protocol used for directed differentiation from human iPSCs to DCs was developed in Dr Paul Fairchild's lab. As illustrated on **figure 5.3.8A**, there is the inclusion and subsequent removal of different factors during the entire differentiation process, with a change of the media every 48 h. Initially, we collected CM from the different stages of the differentiation process (as indicated by the asterisks) and purified the EVs using the LC protocol. Across the eluted volume, we saw that all of the samples had the same huge protein peak corresponding to the region where the F3 protein peaks were found for previous stem cell samples (**Figure 5.3.8B**). Interestingly, when quantified the total number of particles across the eluted volume, there was an increase in the peak height at the F1 region, corresponding to the progress of the differentiation process (**Figure 5.3.8B**).

At the end of the differentiation process, the DCs were harvested and half of pool was matured. We then collected the CM from these two populations of DCs (immature and mature) and fractionated them on the LC column. From the NTA data on the F1 fractions, we observed that both the immature and mature DC-derived EVs

were had very similar size distribution profiles (**Figure 5.3.8C**). Overall, the mode sizes and total amount of particles were quite similar in both groups of DCs (**Figure 5.3.8D**). To further verify these particles as EVs, we extracted RNA and subjected them to the small RNA bioanalyzer chip. Interestingly, we saw a similar RNA profile in both samples where there was a significant peak at the 60nucleotide range (**Figure 5.3.8E**). Lastly, western blotting of the EVs from both immature and mature DCs showed the presence of both EV markers (Alix and Tsg101) and a DC marker (CD11c). Interestingly, there appeared to be slightly higher amounts of CD11c in the mature than in the immature sample (**Figure 5.3.8F**).

Figure 5.3.8

A

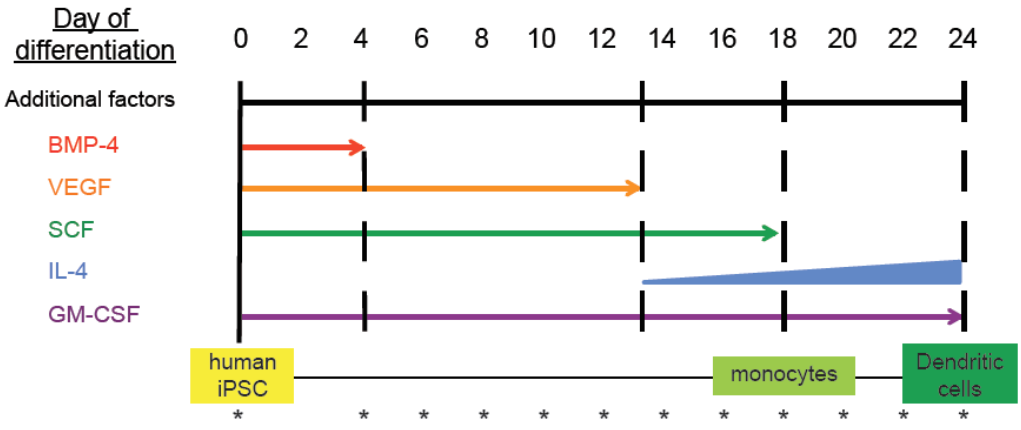

B

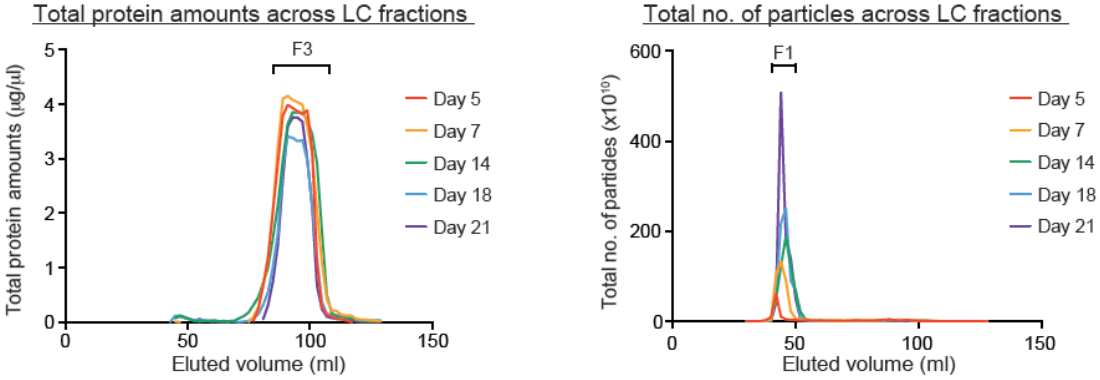

C

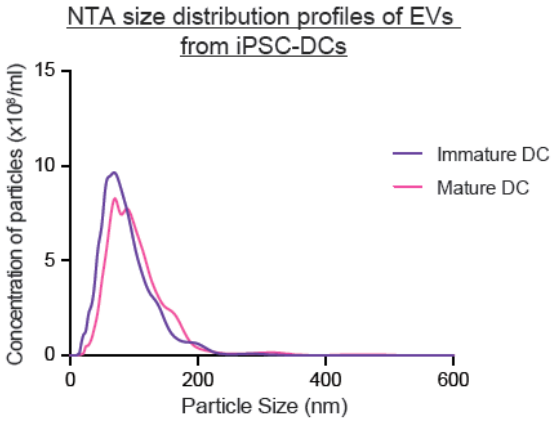

E

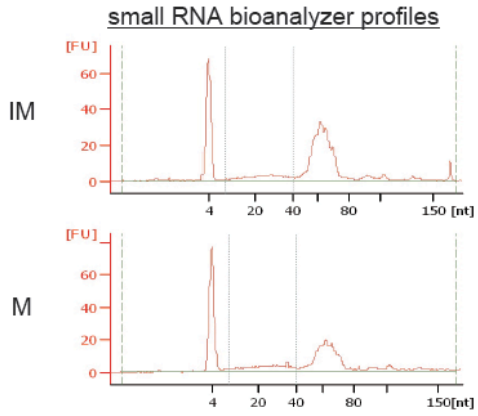

D

EV Sample	Mode size (nm)	Total no. of particles (x10^{11})
Immature DC	70	7.6
Mature DC	77	7.1

F

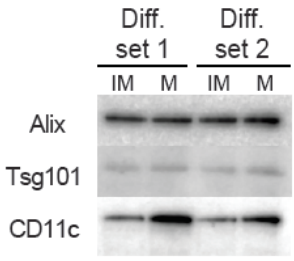

Figure 5.3.8 LC purification and characterisation of EVs from DCs differentiated from human iPSCs

(A) Schematic outline of the directed differentiation of human iPSCs into DCs. (B) Graphs showing the total protein amounts (µg/µl) (left panel) and total number of particles (right panel) across the fractions eluted from the LC column. Samples from the different days of differentiation (day 5, 7, 14, 18 and 21) are overlayed on each other. (C) NTA size distribution profiles of EVs purified from immature and mature DCs. (D) Table showing the mode size and overall yields of EVs from immature and mature DCs. (E) small RNA bioanalyzer profiles of EVs purified from immature and mature DCs. (F) Representative western blotting pictures for EV markers (Alix and Tsg101) as well as a reported DC marker (CD11c) when loading the same number of EVs purified from immature and mature DCs.

5.4 Discussion

Based on the data from **chapter 3** and **chapter 4**, we deduced that the LC protocol was an optimal method for purification of EVs from stem cell. Hence, we first used this methodology to purify and characterise EVs from mouse iPSCs and ESCs, in order to unravel their biological functions in stem cell biology.

To verify that our data on EVs from stem cell sources, we purified EVs from two different mouse iPSC and ESC lines and quantified these EVs by NTA. Moreover, to minimise any differences due to gender or the strain of the mice, we specifically selected cell lines, which were derived from female mice of the same mouse strain-CBA. Generally, the physical aspects (size distribution, mode size) and the purity of EVs from the different iPSCs and ESC lines appeared to be similar with each other. Furthermore, the appearance of Alix and CD9 was similar in the EVs and across both iPSCs and ESCs. To improve our understanding regarding the exact molecular features of these EVs and as compared to their parental cell sources, we performed some preliminary proteomics studies on all of these samples.

5.4.1 Proteomics of EVs reveal the presence of contaminating proteins derived from the media and gelatin

Unlike previous studies on stem cell derived-EVs which were collected from serum-free conditions (120,349,350), we chose to use the addition of the serum-replacement media component to all our cultures as we had observed spontaneously differentiation of our stem cells in the absence of serum (**chapter 4**). However, the exact composition of the different ingredients in the serum-replacement component was not clearly reported. Furthermore, we observed the presence of a huge unknown protein bands in the F1 fraction of media alone. Hence, prior to proteomic analysis on the stem cell-derived EVs, we first analyzed the identities of proteins in the Md media fraction and in the gelatin used for coating the plates.

Most of the proteins in the Md fraction of the media alone were mapped to a variety of different cow and mouse proteins. Expectedly for the porcine derived gelatin, we detected some pig and mouse proteins. Importantly in both samples, there were relatively high amounts of cow albumin and a number of mouse keratin proteins. As the serum-replacement media contained AlbuMax^{TM} (Life Technologies, UK), we hypothesised that this is the main source of the cow albumin in our samples. Importantly, as it was rather difficult to be certain if these other mouse proteins were purely contaminants or possibly EV-associated proteins, we chose to pre-filter and eliminate the identities of these proteins before analysing the EV samples.

5.4.2 EVs across both stem cell types show high similarity in the overall proteome

Generally, we show that the EVs from iPSCs and ESCs have rather similar proteome. Although, there was a disparity in the total number of proteins detected in the iPSC-EVs as compared to ESC-EVs, most of these exclusively expressed proteins did not have any significant difference in enrichments of GO terms. Furthermore, we observed a similar enrichment of EV-related GO terms in both iPSC-EVs and ESC-EVs over the reference data, which corroborated with our western blotting data of EV markers in EVs. Furthermore, from the proteomics data, we uncovered the identities of other reported EV markers, which could serve as useful indicators for future studies on stem cell EVs.

Next, to understand if these similarities between EVs were specific to EVs or related to their parental cells, we analysed the proteome of the cells from which the EVs were derived. Generally, the cell proteome of both stem cells were found to be highly similar. However, when we cross-compared the EVs individually with their cellular source, we noticed very little overlap between the overall total protein identities, due to the large difference in overall proteins identified in the cells versus that in the EVs. Of the commonly identified proteins, we observed enrichment of specific GO terms in EVs over cells, which was unique to iPSC or ESC individually and common regardless of cell types. Interestingly, based on the GO terms listed, there is some preliminary indication that GO terms enriched in EVs are associated to extracellular processes while GO terms enriched in cells are involved in cytoplasmic or nuclear processes. Furthermore, we did not detect significant amounts of pluripotent stem

cell markers in the EVs as compared to their parental cells. Hence, we speculate that the little difference in proteome of EVs from both iPSCs and ESCs could be due to both the huge similarities in their parental cell source and the encapsulation of specific proteins common to all EVs.

On hindsight though, the proteomics data we described here are general trends noticed from our preliminary runs on individual EV and cell samples. Furthermore, it is uncertain how the contamination from the media and gelatin might have affected the overall mass spectrometry data. To date, there has only been a handful of published proteomics studies on mouse ESCs (392) and human iPSCs and ESCs (393,394), all of which have been performed on different ESC and iPSC lines. On the other hand, there has yet to be any published proteomic data about EVs from pluripotent sources. Hence, we believe that by performing more proteomic analysis across more EVs samples and across EVs from different stem cell lines, we would be more able to ascertain the relevance and applicability of stem cell EVs in stem cell biology and regenerative medicine.

5.4.3 Reduced EV secretion from human iPSCs may be cell type specific

From our mouse data, we thought it would be interesting to see if the same phenomenon was happening in human iPSCs too. Hence, we performed some preliminary studies purifying EVs from human iPSCs. The culturing conditions for human cells were different from that of mice, where a daily change of media was required to maintain the human stem cells in an undifferentiated state. Hence, we

decided to capitalise on this set-up and investigate the trend of EV release across increasing cell confluence.

Generally, we found that the total number of particles detected peaked at the first collection time point. We hypothesise that the release of apoptotic or necrotic vesicles from freshly trypsinised cells as they were plated could have skewed the particle counts. Hence, we focused on last collection time point instead. Unexpectedly, at the final collection time point where the cell confluence was the highest, the CM was shown to contain the least number of particles. Furthermore, this trend was consistent across two different types of stem cell media for human PSCs. Interestingly, these results contradicted with our findings in **chapter 3** where we found that the total number of particles was proportional to the overall cell confluence from both mouse and human immmortalised cell lines. Moreover, the overall absolute counts of particles as measured by NTA from human iPSCs was significantly lower than that of the mouse iPSCs, when considering similar overall cell counts at point of CM collection.

From literature, there have been discussions concerning the species differences in stem cells (395). For example, mouse and human pluripotent stem cells (PSCs) have been suggested to have contrasting signaling pathways (396). Moreover, studies have shown that core developmentally regulated epigenetic factors such as myeloid/lymphoid or mixed-lineage leukemia 4 (MLL4), histone deacetylase 2 (HDAC2) and Kruppel-like factors (KLF) are differentially expressed in the two species. Furthermore, the specific targets of both pluripotency markers, such as OCT-4, SOX2 and NANOG, and these epigenetic regulators differ significantly

between species. Moreover, as shown here, mouse and human PSCs were cultured differently with respect to the media used and the method of culture. Hence, we believe that these differences may have contributed to fundamental differences between mouse and human PSCs, and account partially for the differences in our EV data. Furthermore, it was not possible to cross compare our earlier mouse EV data to these data derivative from the human stem cells. Hence, we sought to investigate the trend of EVs from other human cells.

To understand if this phenomenon of low EV secretion from iPSCs was cell type specific, we analyzed the release of EVs from human ESCs. Using the same experimental set-up as that for iPSCs, we observed that 5-fold more particles were purified from ESCs. Furthermore, these particles stained positively for EV markers such as Alix and Tsg101. Although iPSCs and ESCs are both PSCs, there have been reports about contradictory results from comparison studies conducted between these two cell types (386,397,398). On one hand, some have reported on the lack of significant differences between ESCs and iPSCs (399–401), rather it was commented that variations within individual clones of ESC and iPSC appeared greater (402–404). However, there have also been a wealth of papers showing differences between iPSCs and ESCs in various aspects such as their differentiation potential, DNA methylation status and expression levels of core genes in iPSCs as compared to ESCs (376,378,380,381,385). Moreover, some of these differences could be linked to the presence of residual transgene expression and epigenetic memories of the donor cell in iPSCs (382–384). Interestingly, it was reported that other non-described genes responsible for other biological process such as cell-cell communication was also found to be expressed at lower levels in iPSCs (405).

Hence, we speculate that these differences could possibly explain the lower levels of EVs from iPSCs than that from ESCs.

To further ensure that our findings were not due to an unknown abnormality specific to our iPSC cell line, we differentiated these iPSCs to DCs and investigated the release of EVs from these differentiated cells. Interestingly, we observed an increase in particle numbers as the differentiation process to DCs progressed. At the end of the differentiation process, both immature and mature iPSC-DCs were found to secrete relatively higher numbers of EVs with the expression of both EV markers and a DC-specific marker (CD11c) (406). From this data, we believe that the phenomenon we observed with human iPSCs may be a specific feature of iPSCs.

5.5 Conclusion

Following the development of an optimal method for purification of EVs from complex media sources, as described in **chapters 3 and 4**, we here performed some characterisation studies on the EVs from pluripotent stem cells. First, we demonstrate that EVs from both mouse iPSCs and ESCs display similar size distributions, appearance under the TEM and purity levels. With our preliminary proteomics, we initially demonstrated that there was extensive contamination from both the media alone and the gelatin used for coating the culture plates. After eliminating the identities of these proteins, we observed that the proteome was generally similar in across EVs and cells in these two types of pluripotent stem cells. On the other hand, the expression levels of certain proteins in EVs were found to be rather different as compared to their parental cells. Next, we performed some preliminary experiments to determine if these results were similar in human pluripotent stem cells. Unexpectedly, we found that human iPSCs secrete lower levels of EVs as compared to human ESCs and DCs derived from these iPSCs. Based on these data, we hypothesise that the lower secretion rates of EVs from human iPSCs is a cell type specific phenomenon.

Chapter 6

General discussion

6.1 Summary of findings from the current study

There have been several lines of evidence showing the roles of different stem cell EVs in both stem cell biology and regenerative medicine. However, there has yet to be any data published regarding the release and possible roles of EVs derived from iPSCs. At the start of this study, we attempted to purify and characterize EVs from mouse iPSCs. However, as illustrated in our preliminary test (**Chapter 1- Figure 1.7**), we observed a significant discrepancy in the quantities of particles (as measured by NTA) with respect to the detection of EV markers. Although EVs are known to play an important role in cell-cell communication in both normal physiology and in some pathophysiological situations, there was still a lack of consensus on the optimal methods to be used for collection and purification of EVs for subsequent in-depth molecular analysis. Hence, we decided to first re-evaluate the methods for collection and purification of EVs, in order to derive a suitable workflow for characterization of EVs from iPSCs, which would be of use to the rest of the EV field.

6.1.1 LC is a better method for purification of EVs than UC

In **chapter 3**, we first demonstrated that different physical factors, such as the cell density, length of time for CM collection and the type of media used for CM collection, had profound effects on the overall quantities and content of EVs released *in vitro*. Generally, the overall quantity of EVs collected was proportional to the cell density at the time point of CM collection. However, if the collection period was extended to more than 48 h, the pelleted EV samples would typically contain some contaminating apoptotic bodies, most probably released from dying cells in the culture. This result is of particular importance as we found that these contaminating proteins could not be efficiently separated from EVs, even after the use of a sucrose gradient centrifugation protocol (**Appendix 8.2.1**). Moreover, one interesting observation from this study was that serum-free culture led to an increase in overall EV amounts. However, these EVs derived from serum-free conditions had a noticeable difference in overall proteome as compared to EVs derived from cells grown under serum-containing conditions[1].

For these initial experiments, we employed the use of the most established method for EV purification- UC. However, we began to realize that the UC protocol was associated with several drawbacks such as operator-dependent yields, low purity and implications for vesicle integrity. Hence, we designed an alternative strategy - LC and evaluated the resultant LC-purified EVs compared to those pelleted by the UC technique. For practical reasons, we first conducted this systematic comparison study on EVs derived from serum-free cultures. Here, we demonstrated that the LC

[1] This data described here is now published in the Journal of Extracellular Vesicles (**Appendix 8.2**).

methodology was clearly superior to the UC protocol in terms of overall EV yield, EV purity and biophysical properties[2].

6.1.2 LC allows for the purification EVs of stem cell sources

With these positive findings on using the LC protocol, we next applied the protocol for purifying EVs from stem cell media sources. As described in **chapter 4**, we found that stem cells required media supplemented with serum-replacement components, for both their normal growth and to maintain pluripotency. Unlike serum-free media, stem cell media was found to be relatively more complex, as they contain much higher amounts of proteins than regular media types. Hence, we chose to perform a similar comparative study, as shown in **chapter 3**, between the UC versus LC protocol for purification of EVs from stem cell sources. Unexpectedly, we observed the opposite trend for stem cells; where there were higher particle counts by NTA, protein and RNA in the UC pellet than in the LC fraction. Through more thorough molecular and physical analysis of the UC pellet, we found that the initial comparisons of EV yields based on NTA, protein and RNA measurements were misleading. Using LC fractionation, we proved that the UC pellet contained a mixture of EVs with non-vesicular proteins and RNAs that had co-precipitated in the UC process. Comparatively, the LC protocol was able to purify EVs more efficiently and of higher purity.

6.1.3 EVs from mouse iPSCs and ESCs are similar in both molecular and physical aspects

[2] The data described here is now published in Nanomedicine (NBM) (**Appendix 8.2**).

Using the LC protocol, we initially started with characterisation of EVs from mouse iPSCs and ESCs, as described in **chapter 5**. Generally, EVs from both pluripotent stem cells had similar size distribution profiles, appearance under TEM and similar levels of purity. Based on preliminary proteomics studies, the proteome of these EVs was generally similar across both iPSCs and ESCs, with the exception of a handful of GO terms such as translation processing that was found to be more enriched in EVs from iPSCs than those from ESCs. To investigate if these similarities were due to the source cells, we investigated and found the proteome of both cells to be rather congruent. On the other hand, the comparison between EVs and their respective parental cells showed much lower overlap in commonly identified proteins and enrichment of several GO annotations of one group over the other.. Interestingly, there was a number of GO terms which was commonly identified to be enriched in EVs over cells, across both iPSCs and ESCs.

Next, we attempted to extend these findings on EVs to human PSCs. Hence, we tried purifying EVs from both human iPSCs and ESCs. Unexpectedly, we found that human iPSCs secrete significantly lower levels of EVs as compared to human ESCs. On the other hand, once iPSCs are differentiated into DCs, there was a corresponding increase in the release of EVs from the differentiating cells. Based on these preliminary data, we hypothesised that the lower secretion rates of EVs from human iPSCs is cell type specific phenomenon.

6.2 Limitations and future directions from the current study

6.2.1 LC method for purification of EVs

Although we have clearly demonstrated that the LC method is optimal for purification of EVs in different sample types, there are a number of aspects with respect to the current LC protocol, which could be further addressed to supplement our data here on the use of LC as a purification method for EVs.

One of the main reasons we advocated the use of LC for purification of EVs was based on the ability to maintain vesicle integrity and prevent EV aggregation during the purification process. As shown by our biodistribution study (**chapter 3**), vesicle aggregation led to a higher accumulation of UC-purified EVs in the lungs, which ultimately could have detrimental effects for the use of EVs for therapeutic uses. However, we have yet to demonstrate if maintaining the intactness of vesicles could have a similar positive impact on their functionality. Currently, there is an increasing number of groups who are keen to use EVs as a form of gene delivery agent for different diseases. Hence, it would be particularly relevant to evaluate if the LC method of EV purification method could positively influence on both the integrity and functionality of EVs.

Next, all of the LC-based purification experiments conducted in this thesis was using the same type of gel-filtration column (Sephacryl S-400). On hindsight though, we noticed that the LC chromatograph profiles differed slightly, depending on the

sample type. Generally in serum-free samples, the vesicular fractions were clearly separated from the protein peak (**chapter 3**). However, in the more protein-rich samples such as pre-spun or stem cell CM, the distinction between peaks was less obvious. As a result of this poor resolution between the EVs and non-vesicular proteins, some of these larger protein contaminants may be included in the stem cell EV samples and as a result, were detected in in our proteomics data (**chapters 4 and 5**). Apart from the Sephacryl S-400 column we have used here, there are several other column types with gel beads of variable pore sizes. Furthermore, some studies have recently demonstrated the purification of EVs from plasma using a different type of gel material (Sepharose) (83,85). Unfortunately, there is very little understanding if the purification of EVs might differ with different gel filtration materials. Moreover, depending on the sample type or the downstream applications of EVs, one might have to factor in the length of column used. For example, for health screening purposes, one might prefer the use of shorter columns for quick purification of EVs. On the other hand, when analyzing more complex, protein-rich sample types like stem cell media or serum, one might want to utilise longer columns for better separation of EVs from the non-vesicular proteins. Hence, there are still several aspects of the LC protocol that require more refinement before it could be considered as an optimal method for purification of EVs.

In this thesis, we consistently showed that the LC protocol is better than the most established protocol for EV isolation- UC. Furthermore, LC is a useful methodology for the purification of EVs from a novel cell type- iPSCs. Although we managed to improve on the purity of EVs from stem cells significantly with LC, our proteomics data showed that these samples were still plagued with contaminants from the media

and require further downstream strategies to clean up the sample. Here we tested the usefulness of a sucrose gradient centrifugation subsequent to LC, which has been reported to be an optimal strategy for purification of EVs (343). Unfortunately, we here demonstrated that this extra step did not significantly eliminate the contaminants from EVs. Furthermore, we postulate that we were only able to recover a low percentage of particles after the gradient centrifugation as most of the vesicles may have been fragmented during the centrifugation step or damaged due to the differences in osmotic pressure when the starting EV samples were mixed in 2.5 M of sucrose. In recent years, there has been the emergence of alternative purification methods to replace UC such as precipitation-based capture and immuno-based capture (as discussed in **chapter 1**). Hence, it would be particularly interesting to cross compare the LC protocol with these alternative purification protocols and test whether some of these purification strategies could be used in combination to improve on the purity of EVs.

All in all, we here demonstrated that the molecular and biophysical phenotype of EVs could change depending on the type of purification method used. As a result of different studies employing the use of different purification strategies, the molecular data on EVs from the same cell type present fairly varied results. We feel that these additional comparison studies would contribute to the search for an optimal method for EV purification across different sample types and in turn, ensure more coherent EV data from the various labs across the world.

On a side note, we here focused solely on EVs purified by the LC column. However, one could also collect fractions after the initial EV peak to investigate the overall cell

secretome. As discussed in **chapter 1**, MSCs were found to secrete EVs and free cytokines, which contributed to a regenerative effect when applied to injury models such as myocardial infarction and acute renal injury. Hence, apart from purifying EVs, we feel that the LC protocol would serve as a useful tool for the evaluation of the entire secretome from cells. In particular, the LC column could be used to evaluate how vesicular RNAs and circulating extracellular RNAs from the non-vesicular fractions could contribute to various physiological and pathological conditions.

6.2.2 Characterisation studies on stem cell vesicles

In **chapter 5**, we performed more in-depth characterisation studies on EVs derived from mouse iPSC and ESCs to elucidate their roles in stem cell biology. On hindsight though, there were some aspects of the current study set-up that could be improved on and followed up with future investigations.

Firstly, our proteomics analysis showed presence of high levels of cow albumin, which could have interfered with both the protein quantification and mask the detection of other less abundant EV proteins. As discussed in **section 6.2.1**, one solution would be to find alternative strategies to further improve on the purity of the LC product. Alternatively, one could switch to more chemically-defined media and control the inclusion of 'contaminating' proteins such as albumin. For human pluripotent stem cells, there has already been several papers reporting on the availability of serum-free and albumin-free media for human stem cells such as the TeSR^{TM}-E8 media (407–409). Importantly, the total protein content in this media is

433 times less than mTeSR™-1 media. Furthermore, when we tested this media on the LC, we found that the second extensive protein peak in LC chromatograph of stem cell media was notably absent. Hence, it would be very useful to develop similar defined media formulations for future studies on EVs from mouse stem cells.

Next, we here show that the overall small RNA profiles of EVs across different cell types: mouse stem cells (**chapters 3 and 4**) and human DCs differentiated from iPSCs (**chapter 5**) are largely similar. Notably, there was a distinct peak at the 60 nucleotide size range consistently across all EVs types, regardless of their parent cells. Furthermore, the small RNA pattern of EVs was rather different from cell samples (**chapter 5**). This unique small RNA profile in EVs was previously similar to that in EVs collected from B-lymphoblasts (410). Furthermore, several deep-sequencing studies on EVs suggest the enrichment of several small non-coding RNA species such as tRNAs, snoRNAs and Y-RNAs (411). Also, the two early studies on ESC-EVs demonstrated the selective enrichment of RNAs associated with pluripotency factors into EVs. Hence, it would be interesting to further analyse the exact identities of RNAs across our EVs samples derived from the different cell types and evaluate the presence of common and cell-specific RNA markers. Subsequently, these common RNA markers could be useful for identification of purified EVs, similar to how EV protein markers are currently being applied.

Lastly, all of our EV data here were merely descriptions of the molecular phenotypes of stem cell EVs. In order to link these data to their biological functions, it would be crucial to perform more functional studies such as the transfer of stem cell EVs to recipient cells or via the use of co-culture systems. On the side, we attempted to

transfer our mouse iPSC-EVs and ESC-EVs onto mouse fibroblasts. Unfortunately, we failed to detect any transfer of any stem cell markers (data not shown). Apart from our data here, there has only been two other reports about EVs from iPSCs to date. The first is a poster presentation which described the transfer of bioactive content following the incubation EVs from mouse iPSCs on human cells. The second presentation described the transfer of active content in EVs derived from human iPSC onto primary mature cardiac cells. In both of these studies, the authors suggest that these iPSC-EVs may be carriers of pro-angiogenic, cardiomyogenic factors for use in future heart regeneration strategies (304). With hindsight though, the authors had employed the use of the UC methodology for purification of their EVs. **In chapters 3 and 4**, we demonstrated that purification using UC led to the co-pelleting of other proteins from the protein rich media. Hence, it would be interesting to cross-compare if our LC-purified EVs from iPSCs could have a similar therapeutic effect as shown by these authors.

Beside EVs from stem cells, another interesting finding from this study was the increasing amounts of EVs released as the differentiation of stem cells progressed into DCs. In a recent report, Nair et al. demonstrated that EVs from preosteoblasts were able to direct ESC differentiation to a neuroectodermal state (412). Similarly, we hypothesis that the EVs released through the differentiation process may encourage the differentiation state of stem cells through the exchange of DC-specific factors. Furthermore, we here proved that EVs are released from DCs differentiated from human iPSCs. In line with the idea of using DC-EVs as immunotherapeutic agents, we postulate that these iPSC-DCs could potentially serve as one alternative source of such EVs. Interestingly, one recent report has shown that EVs released

from MSCs differentiated from iPSCs were beneficial in cutaneous wound healing and tissue repair through the promotion of collagen synthesis and angiogenesis (413).

6.3 Concluding remarks

From the studies described in this thesis, we have discovered that the type of purification method could have a profound impact on both the molecular and physical aspects of EVs. Subsequently, these results could have huge implications on downstream characterisation or application of EVs in therapeutic settings. Here, we demonstrated that the LC protocol is clearly superior to the original UC method in terms of vesicle yield, purity and integrity. This phenomenon was consistently observed for the derivation of EVs from both serum-free and complex stem cell media. Stem cell EVs (e.g. MSC-EVs) have been postulated to influence the stem cell maintenance and used as potential therapeutic agents in regenerative diseases. Here, we show novel characterisation data on EVs purified from both mouse and human iPSCs. Our preliminary proteomics data indicated that EVs from mouse iPSCs closely resembled that of EVs from mouse ESCs. However, the general proteome of EVs differed greatly from that of their parental cells; GO terms enriched in EVs were observed to be associated to extracellular processes while GO terms enriched in cells were found to be involved in cytoplasmic or nuclear processes. On the other hand, we observed that human iPSCs release relatively fewer EVs as compared to human ESCs and DCs differentiated from the same iPSCs. We believe that this phenomenon may be a cell-specific feature due to the different molecular state of iPSCs. Nonetheless, our data here clearly indicate that both iPSCs and ESCs do release EVs. Hence, it would be interesting to further investigate how these EVs could be used for studying stem cell biology or as potential tools for regenerative medicine.

Chapter 7

List of references:

1. Wolf P. The Nature and Significance of Platelet Products in Human Plasma. Br J Haematol. 1967 May;13(3):269–88.

2. Raz A, Barzilai R, Spira G, Inbar M. Oncogenicity and immunogenicity associated with membranes isolated from cell-free ascites fluid of lymphoma-bearing mice. Cancer Res. 1978 Aug;38(8):2480–5.

3. Trams EG, Lauter CJ, Salem N, Heine U. Exfoliation of membrane ecto-enzymes in the form of micro-vesicles. Biochim Biophys Acta. 1981 Jul 6;645(1):63–70.

4. Mitchell P, Petfalski E, Shevchenko A, Mann M, Tollervey D. The exosome: a conserved eukaryotic RNA processing complex containing multiple 3'-->5' exoribonucleases. Cell. 1997 Nov 14;91(4):457–66.

5. Harding C, Heuser J, Stahl P. Receptor-mediated endocytosis of transferrin and recycling of the transferrin receptor in rat reticulocytes. J Cell Biol. 1983 Aug;97(2):329–39.

6. Pan BT, Johnstone RM. Fate of the transferrin receptor during maturation of sheep reticulocytes in vitro: selective externalization of the receptor. Cell. 1983 Jul;33(3):967–78.

7. Harding C, Heuser J, Stahl P. Endocytosis and intracellular processing of transferrin and colloidal gold-transferrin in rat reticulocytes: demonstration of a pathway for receptor shedding. Eur J Cell Biol. 1984 Nov;35(2):256–63.

8. Pan BT, Teng K, Wu C, Adam M, Johnstone RM. Electron microscopic evidence for externalization of the transferrin receptor in vesicular form in sheep reticulocytes. J Cell Biol. 1985 Sep;101(3):942–8.

9. Raposo G, Nijman HW, Stoorvogel W, Liejendekker R, Harding CV, Melief CJ, et al. B lymphocytes secrete antigen-presenting vesicles. J Exp Med. 1996 Mar 1;183(3):1161–72.

10. Zitvogel L, Regnault A, Lozier A, Wolfers J, Flament C, Tenza D, et al. Eradication of established murine tumors using a novel cell-free vaccine: dendritic cell-derived exosomes. Nat Med. 1998 May;4(5):594–600.

11. Lee Y, El Andaloussi S, Wood MJA. Exosomes and microvesicles: extracellular vesicles for genetic information transfer and gene therapy. Hum Mol Genet. 2012 Oct 15;21(R1):R125–34.

12. Colombo M, Moita C, van Niel G, Kowal J, Vigneron J, Benaroch P, et al. Analysis of ESCRT functions in exosome biogenesis, composition and secretion highlights the heterogeneity of extracellular vesicles. J Cell Sci. 2013 Dec 15;126(Pt 24):5553–65.

13. King HW, Michael MZ, Gleadle JM. Hypoxic enhancement of exosome release by breast cancer cells. BMC Cancer. 2012;12:421.

14. Koles K, Nunnari J, Korkut C, Barria R, Brewer C, Li Y, et al. Mechanism of evenness interrupted (Evi)-exosome release at synaptic boutons. J Biol Chem. 2012 May 11;287(20):16820–34.

15. Phuyal S, Hessvik NP, Skotland T, Sandvig K, Llorente A. Regulation of exosome release by glycosphingolipids and flotillins. FEBS J. 2014 May;281(9):2214–27.

16. Tamai K, Tanaka N, Nakano T, Kakazu E, Kondo Y, Inoue J, et al. Exosome secretion of dendritic cells is regulated by Hrs, an ESCRT-0 protein. Biochem Biophys Res Commun. 2010 Aug 27;399(3):384–90.

17. Baietti MF, Zhang Z, Mortier E, Melchior A, Degeest G, Geeraerts A, et al. Syndecan-syntenin-ALIX regulates the biogenesis of exosomes. Nat Cell Biol. 2012;14(7):677–85.

18. Hurley JH, Odorizzi G. Get on the exosome bus with ALIX. Nat Cell Biol. 2012;14(7):654–5.

19. Nabhan JF, Hu R, Oh RS, Cohen SN, Lu Q. Formation and release of arrestin domain-containing protein 1-mediated microvesicles (ARMMs) at plasma membrane by recruitment of TSG101 protein. Proc Natl Acad Sci U S A. 2012 Mar 13;109(11):4146–51.

20. Kajimoto T, Okada T, Miya S, Zhang L, Nakamura S. Ongoing activation of sphingosine 1-phosphate receptors mediates maturation of exosomal multivesicular endosomes. Nat Commun. 2013;4:2712.

21. Kosaka N, Iguchi H, Yoshioka Y, Takeshita F, Matsuki Y, Ochiya T. Secretory mechanisms and intercellular transfer of microRNAs in living cells. J Biol Chem. 2010 Jun 4;285(23):17442–52.

22. Trajkovic K, Hsu C, Chiantia S, Rajendran L, Wenzel D, Wieland F, et al. Ceramide triggers budding of exosome vesicles into multivesicular endosomes. Science. 2008 Feb 29;319(5867):1244–7.

23. Subra C, Grand D, Laulagnier K, Stella A, Lambeau G, Paillasse M, et al. Exosomes account for vesicle-mediated transcellular transport of activatable phospholipases and prostaglandins. J Lipid Res. 2010 Aug;51(8):2105–20.

24. Subra C, Laulagnier K, Perret B, Record M. Exosome lipidomics unravels lipid sorting at the level of multivesicular bodies. Biochimie. 2007 Feb;89(2):205–12.

25. D'Souza-Schorey C, Clancy JW. Tumor-derived microvesicles: shedding light on novel microenvironment modulators and prospective cancer biomarkers. Genes Dev. 2012 Jun 15;26(12):1287–99.

26. Budagian V, Bulanova E, Brovko L, Orinska Z, Fayad R, Paus R, et al. Signaling through P2X7 receptor in human T cells involves p56lck, MAP kinases, and transcription factors AP-1 and NF-kappa B. J Biol Chem. 2003 Jan 17;278(3):1549–60.

27. Duan S, Neary JT. P2X7 receptors: Properties and relevance to CNS function. Glia. 2006 Nov 15;54(7):738–46.

28. Turola E, Furlan R, Bianco F, Matteoli M, Verderio C. Microglial microvesicle secretion and intercellular signaling. Front Physiol. 2012;3:149.

29. Muralidharan-Chari V, Clancy J, Plou C, Romao M, Chavrier P, Raposo G, et al. ARF6-regulated shedding of tumor cell-derived plasma membrane microvesicles. Curr Biol CB. 2009 Dec 1;19(22):1875–85.

30. Di Vizio D, Kim J, Hager MH, Morello M, Yang W, Lafargue CJ, et al. Oncosome formation in prostate cancer: association with a region of frequent chromosomal deletion in metastatic disease. Cancer Res. 2009 Jul 1;69(13):5601–9.

31. Peng J, Wallar BJ, Flanders A, Swiatek PJ, Alberts AS. Disruption of the Diaphanous-related formin Drf1 gene encoding mDia1 reveals a role for Drf3 as an effector for Cdc42. Curr Biol CB. 2003 Apr 1;13(7):534–45.

32. Del Conde I, Shrimpton CN, Thiagarajan P, López JA. Tissue-factor-bearing microvesicles arise from lipid rafts and fuse with activated platelets to initiate coagulation. Blood. 2005 Sep 1;106(5):1604–11.

33. Pilzer D, Gasser O, Moskovich O, Schifferli JA, Fishelson Z. Emission of membrane vesicles: roles in complement resistance, immunity and cancer. Springer Semin Immunopathol. 2005 Nov;27(3):375–87.

34. Booth AM. Exosomes and HIV Gag bud from endosome-like domains of the T cell plasma membrane. J Cell Biol. 2006 Mar 6;172(6):923–35.

35. Votteler J, Sundquist WI. Virus Budding and the ESCRT Pathway. Cell Host Microbe. 2013 Sep;14(3):232–41.

36. Kesimer M, Scull M, Brighton B, DeMaria G, Burns K, O'Neal W, et al. Characterization of exosome-like vesicles released from human tracheobronchial ciliated epithelium: a possible role in innate defense. FASEB J. 2009 Jun 1;23(6):1858–68.

37. Van Niel G, Raposo G, Candalh C, Boussac M, Hershberg R, Cerf-Bensussan N, et al. Intestinal epithelial cells secrete exosome-like vesicles. Gastroenterology. 2001 Aug;121(2):337–49.

38. Waldenström A, Gennebäck N, Hellman U, Ronquist G. Cardiomyocyte Microvesicles Contain DNA/RNA and Convey Biological Messages to Target Cells. PLoS ONE. 2012 Apr 10;7(4):e34653.

39. Caby M-P. Exosomal-like vesicles are present in human blood plasma. Int Immunol. 2005 May 20;17(7):879–87.

40. Asea A, Jean-Pierre C, Kaur P, Rao P, Linhares IM, Skupski D, et al. Heat shock protein-containing exosomes in mid-trimester amniotic fluids. J Reprod Immunol. 2008 Oct;79(1):12–7.

41. Street JM, Barran PE, Mackay CL, Weidt S, Balmforth C, Walsh TS, et al. Identification and proteomic profiling of exosomes in human cerebrospinal fluid. J Transl Med. 2012;10(1):5.

42. Greco V, Hannus M, Eaton S. Argosomes: a potential vehicle for the spread of morphogens through epithelia. Cell. 2001 Sep 7;106(5):633–45.

43. Vincent JP, Magee T. Argosomes: membrane fragments on the run. Trends Cell Biol. 2002 Feb;12(2):57–60.

44. Christian JL. Argosomes: Intracellular Transport Vehicles for Intercellular Signals? Sci Signal. 2002 Mar 19;2002(124):pe13–pe13.

45. Sadallah S, Eken C, Schifferli JA. Ectosomes as modulators of inflammation and immunity: Immunomodulation by ectosomes. Clin Exp Immunol. 2011 Jan;163(1):26–32.

46. Eken C, Gasser O, Zenhaeusern G, Oehri I, Hess C, Schifferli JA. Polymorphonuclear neutrophil-derived ectosomes interfere with the maturation of monocyte-derived dendritic cells. J Immunol Baltim Md 1950. 2008 Jan 15;180(2):817–24.

47. Davizon P, López JA. Microparticles and thrombotic disease. Curr Opin Hematol. 2009 Sep;16(5):334–41.

48. Boulanger CM. Microparticles, vascular function and hypertension. Curr Opin Nephrol Hypertens. 2010 Mar;19(2):177–80.

49. Ling L, Huang H, Zhu L, Mao T, Shen Q, Zhang H. Evaluation of plasma endothelial microparticles in pre-eclampsia. J Int Med Res. 2014 Feb;42(1):42–51.

50. Italiano JE, Mairuhu ATA, Flaumenhaft R. Clinical relevance of microparticles from platelets and megakaryocytes. Curr Opin Hematol. 2010 Nov;17(6):578–84.

51. Burger D, Schock S, Thompson CS, Montezano AC, Hakim AM, Touyz RM. Microparticles: biomarkers and beyond. Clin Sci Lond Engl 1979. 2013 Apr;124(7):423–41.

52. Boilard E, Nigrovic PA, Larabee K, Watts GFM, Coblyn JS, Weinblatt ME, et al. Platelets amplify inflammation in arthritis via collagen-dependent microparticle production. Science. 2010 Jan 29;327(5965):580–3.

53. Ronquist G. Prostasomes are mediators of intercellular communication: from basic research to clinical implications. J Intern Med. 2012 Apr;271(4):400–13.

54. Ronquist KG, Carlsson L, Ronquist G, Nilsson S, Larsson A. Prostasome-derived proteins capable of eliciting an immune response in prostate cancer patients. Int J Cancer J Int Cancer. 2006 Aug 15;119(4):847–53.

55. Ronquist KG, Ronquist G, Larsson A, Carlsson L. Proteomic analysis of prostate cancer metastasis-derived prostasomes. Anticancer Res. 2010 Feb;30(2):285–90.

56. Arienti G, Carlini E, Saccardi C, Palmerini CA. Role of human prostasomes in the activation of spermatozoa. J Cell Mol Med. 2004 Mar;8(1):77–84.

57. Sahlén G, Ahlander A, Frost A, Ronquist G, Norlén BJ, Nilsson BO. Prostasomes are secreted from poorly differentiated cells of prostate cancer metastases. The Prostate. 2004 Nov 1;61(3):291–7.

58. Burden HP, Holmes CH, Persad R, Whittington K. Prostasomes--their effects on human male reproduction and fertility. Hum Reprod Update. 2006 Jun;12(3):283–92.

59. Aalberts M, Sostaric E, Wubbolts R, Wauben MWM, Nolte-'t Hoen ENM, Gadella BM, et al. Spermatozoa recruit prostasomes in response to capacitation induction. Biochim Biophys Acta. 2013 Nov;1834(11):2326–35.

60. Carlsson L, Påhlson C, Bergquist M, Ronquist G, Stridsberg M. Antibacterial activity of human prostasomes. The Prostate. 2000 Sep 1;44(4):279–86.

61. Wang J, Lundqvist M, Carlsson L, Nilsson O, Lundkvist O, Ronquist G. Prostasome-like granules from the PC-3 prostate cancer cell line increase the motility of washed human spermatozoa and adhere to the sperm. Eur J Obstet Gynecol Reprod Biol. 2001 May;96(1):88–97.

62. Maguire CA, Balaj L, Sivaraman S, Crommentuijn MHW, Ericsson M, Mincheva-Nilsson L, et al. Microvesicle-associated AAV vector as a novel gene delivery system. Mol Ther J Am Soc Gene Ther. 2012 May;20(5):960–71.

63. Hristov M, Erl W, Linder S, Weber PC. Apoptotic bodies from endothelial cells enhance the number and initiate the differentiation of human endothelial progenitor cells in vitro. Blood. 2004 Nov 1;104(9):2761–6.

64. Huber J, Vales A, Mitulovic G, Blumer M, Schmid R, Witztum JL, et al. Oxidized membrane vesicles and blebs from apoptotic cells contain biologically active oxidized phospholipids that induce monocyte-endothelial interactions. Arterioscler Thromb Vasc Biol. 2002 Jan;22(1):101–7.

65. Bobrie A, Colombo M, Krumeich S, Raposo G, Théry C. Diverse subpopulations of vesicles secreted by different intracellular mechanisms are present in exosome preparations obtained by differential ultracentrifugation. J Extracell Vesicles. 2012;1.

66. Gould SJ, Raposo G. As we wait: coping with an imperfect nomenclature for extracellular vesicles. J Extracell Vesicles [Internet]. 2013 Feb 15 [cited 2014 Dec 2];2(0). Available from: http://www.journalofextracellularvesicles.net/index.php/jev/article/view/20389

67. Théry C, Amigorena S, Raposo G, Clayton A. Isolation and characterization of exosomes from cell culture supernatants and biological fluids. Curr Protoc Cell Biol Editor Board Juan Bonifacino Al. 2006 Apr;Chapter 3:Unit 3.22.

68. Cvjetkovic A, Lötvall J, Lässer C. The influence of rotor type and centrifugation time on the yield and purity of extracellular vesicles. J Extracell Vesicles [Internet]. 2014 Mar 25 [cited 2015 Feb 7];3(0). Available from: http://www.journalofextracellularvesicles.net/index.php/jev/article/view/23111

69. Momen-Heravi F, Balaj L, Alian S, Trachtenberg AJ, Hochberg FH, Skog J, et al. Impact of Biofluid Viscosity on Size and Sedimentation Efficiency of the Isolated Microvesicles. Front Physiol [Internet]. 2012 [cited 2015 Feb 7];3. Available from: http://journal.frontiersin.org/Journal/10.3389/fphys.2012.00162/full

70. Alvarez ML, Khosroheidari M, Kanchi Ravi R, DiStefano JK. Comparison of protein, microRNA, and mRNA yields using different methods of urinary exosome isolation for the discovery of kidney disease biomarkers. Kidney Int. 2012 Nov;82(9):1024–32.

71. Kordelas L, Rebmann V, Ludwig A-K, Radtke S, Ruesing J, Doeppner TR, et al. MSC-derived exosomes: a novel tool to treat therapy-refractory graft-versus-host disease. Leukemia [Internet]. 2014 Jan 21 [cited 2015 Mar 31]; Available from: http://www.nature.com/doifinder/10.1038/leu.2014.41

72. Ghosh A, Davey M, Chute IC, Griffiths SG, Lewis S, Chacko S, et al. Rapid Isolation of Extracellular Vesicles from Cell Culture and Biological Fluids Using a Synthetic Peptide with Specific Affinity for Heat Shock Proteins. Fan G-C, editor. PLoS ONE. 2014 Oct 17;9(10):e110443.

73. Brownlee Z, Lynn KD, Thorpe PE, Schroit AJ. A novel "salting-out" procedure for the isolation of tumor-derived exosomes. J Immunol Methods. 2014 May;407:120–6.

74. Yamada T, Inoshima Y, Matsuda T, Ishiguro N. Comparison of methods for isolating exosomes from bovine milk. J Vet Med Sci Jpn Soc Vet Sci. 2012 Nov;74(11):1523–5.

75. Oksvold MP, Neurauter A, Pedersen KW. Magnetic bead-based isolation of exosomes. Methods Mol Biol Clifton NJ. 2015;1218:465–81.

76. Chen C, Skog J, Hsu C-H, Lessard RT, Balaj L, Wurdinger T, et al. Microfluidic isolation and transcriptome analysis of serum microvesicles. Lab Chip. 2010 Feb 21;10(4):505–11.

77. Shao H, Chung J, Balaj L, Charest A, Bigner DD, Carter BS, et al. Protein typing of circulating microvesicles allows real-time monitoring of glioblastoma therapy. Nat Med. 2012 Dec;18(12):1835–40.

78. Kanwar SS, Dunlay CJ, Simeone DM, Nagrath S. Microfluidic device (ExoChip) for on-chip isolation, quantification and characterization of circulating exosomes. Lab Chip. 2014 Jun 7;14(11):1891–900.

79. He M, Crow J, Roth M, Zeng Y, Godwin AK. Integrated immunoisolation and protein analysis of circulating exosomes using microfluidic technology. Lab Chip. 2014 Jul 18;14(19):3773.

80. Santana SM, Antonyak MA, Cerione RA, Kirby BJ. Microfluidic isolation of cancer-cell-derived microvesicles from hetergeneous extracellular shed vesicle populations. Biomed Microdevices. 2014 Dec;16(6):869–77.

81. Taylor DD, Akyol S, Gercel-Taylor C. Pregnancy-associated exosomes and their modulation of T cell signaling. J Immunol Baltim Md 1950. 2006 Feb 1;176(3):1534–42.

82. Chen TS, Arslan F, Yin Y, Tan SS, Lai RC, Choo ABH, et al. Enabling a robust scalable manufacturing process for therapeutic exosomes through oncogenic immortalization of human ESC-derived MSCs. J Transl Med. 2011;9:47.

83. Welton JL, Webber JP, Botos L-A, Jones M, Clayton A. Ready-made chromatography columns for extracellular vesicle isolation from plasma. J Extracell Vesicles. 2015;4:27269.

84. Arslan F, Lai RC, Smeets MB, Akeroyd L, Choo A, Aguor ENE, et al. Mesenchymal stem cell-derived exosomes increase ATP levels, decrease oxidative stress and activate PI3K/Akt pathway to enhance myocardial viability and prevent adverse remodeling after myocardial ischemia/reperfusion injury. Stem Cell Res. 2013 May;10(3):301–12.

85. Böing AN, van der Pol E, Grootemaat AE, Coumans FAW, Sturk A, Nieuwland R. Single-step isolation of extracellular vesicles by size-exclusion chromatography. J Extracell Vesicles [Internet]. 2014 Sep 8 [cited 2015 Mar 31];3(0). Available from: http://www.journalofextracellularvesicles.net/index.php/jev/article/view/23430

86. Rekker K, Saare M, Roost AM, Kubo A-L, Zarovni N, Chiesi A, et al. Comparison of serum exosome isolation methods for microRNA profiling. Clin Biochem. 2014 Jan;47(1-2):135–8.

87. Rood IM, Deegens JKJ, Merchant ML, Tamboer WPM, Wilkey DW, Wetzels JFM, et al. Comparison of three methods for isolation of urinary microvesicles to identify biomarkers of nephrotic syndrome. Kidney Int. 2010 Oct;78(8):810–6.

88. Tauro BJ, Greening DW, Mathias RA, Ji H, Mathivanan S, Scott AM, et al. Comparison of ultracentrifugation, density gradient separation, and immunoaffinity capture methods for isolating human colon cancer cell line LIM1863-derived exosomes. Methods San Diego Calif. 2012 Feb;56(2):293–304.

89. Zhang Z, Wang C, Li T, Liu Z, Li L. Comparison of ultracentrifugation and densityï¿½gradient separation methods for isolating Tca8113 human tongue cancer cell line-derived exosomes. Oncol Lett [Internet]. 2014 Jul 23 [cited 2015

Mar 31]; Available from: http://www.spandidos-publications.com/10.3892/ol.2014.2373

90. Van Deun J, Mestdagh P, Sormunen R, Cocquyt V, Vermaelen K, Vandesompele J, et al. The impact of disparate isolation methods for extracellular vesicles on downstream RNA profiling. J Extracell Vesicles [Internet]. 2014 Sep 18 [cited 2015 Mar 31];3(0). Available from: http://www.journalofextracellularvesicles.net/index.php/jev/article/view/24858

91. Lane RE, Korbie D, Anderson W, Vaidyanathan R, Trau M. Analysis of exosome purification methods using a model liposome system and tunable-resistive pulse sensing. Sci Rep. 2015 Jan 6;5:7639.

92. Tatischeff I, Larquet E, Falcón-Pérez JM, Turpin P-Y, Kruglik SG. Fast characterisation of cell-derived extracellular vesicles by nanoparticles tracking analysis, cryo-electron microscopy, and Raman tweezers microspectroscopy. J Extracell Vesicles [Internet]. 2012 Nov 21 [cited 2015 Mar 31];1(0). Available from: http://journalofextracellularvesicles.net/index.php/jev/article/view/19179

93. Arraud N, Linares R, Tan S, Gounou C, Pasquet J-M, Mornet S, et al. Extracellular vesicles from blood plasma: determination of their morphology, size, phenotype and concentration. J Thromb Haemost. 2014 May;12(5):614–27.

94. Yuana Y, Koning RI, Kuil ME, Rensen PCN, Koster AJ, Bertina RM, et al. Cryo-electron microscopy of extracellular vesicles in fresh plasma. J Extracell Vesicles [Internet]. 2013 Dec 31 [cited 2015 Mar 31];2(0). Available from: http://www.journalofextracellularvesicles.net/index.php/jev/article/view/21494

95. Van der Meel R, Fens MHAM, Vader P, van Solinge WW, Eniola-Adefeso O, Schiffelers RM. Extracellular vesicles as drug delivery systems: lessons from the liposome field. J Control Release Off J Control Release Soc. 2014 Dec 10;195:72–85.

96. Lawrie AS, Albanyan A, Cardigan RA, Mackie IJ, Harrison P. Microparticle sizing by dynamic light scattering in fresh-frozen plasma. Vox Sang. 2009 Apr;96(3):206–12.

97. Maas SLN, De Vrij J, Broekman MLD. Quantification and size-profiling of extracellular vesicles using tunable resistive pulse sensing. J Vis Exp JoVE. 2014;(92):e51623.

98. Filipe V, Hawe A, Jiskoot W. Critical evaluation of Nanoparticle Tracking Analysis (NTA) by NanoSight for the measurement of nanoparticles and protein aggregates. Pharm Res. 2010 May;27(5):796–810.

99. Soo CY, Song Y, Zheng Y, Campbell EC, Riches AC, Gunn-Moore F, et al. Nanoparticle tracking analysis monitors microvesicle and exosome secretion from immune cells. Immunology. 2012 Jun;136(2):192–7.

100. Gardiner C, Ferreira YJ, Dragovic RA, Redman CWG, Sargent IL. Extracellular vesicle sizing and enumeration by nanoparticle tracking analysis. J Extracell Vesicles [Internet]. 2013 Feb 14 [cited 2015 Mar 31];2(1). Available from: http://www.journalofextracellularvesicles.net/index.php/jev/article/view/19671

101. Dragovic RA, Gardiner C, Brooks AS, Tannetta DS, Ferguson DJP, Hole P, et al. Sizing and phenotyping of cellular vesicles using Nanoparticle Tracking Analysis. Nanomedicine Nanotechnol Biol Med. 2011 Dec;7(6):780–8.

102. Sharma S, Rasool HI, Palanisamy V, Mathisen C, Schmidt M, Wong DT, et al. Structural-Mechanical Characterization of Nanoparticle Exosomes in Human Saliva, Using Correlative AFM, FESEM, and Force Spectroscopy. ACS Nano. 2010 Apr 27;4(4):1921–6.

103. Yuana Y, Oosterkamp TH, Bahatyrova S, Ashcroft B, Garcia Rodriguez P, Bertina RM, et al. Atomic force microscopy: a novel approach to the detection of nanosized blood microparticles. J Thromb Haemost JTH. 2010 Feb;8(2):315–23.

104. Palanisamy V, Sharma S, Deshpande A, Zhou H, Gimzewski J, Wong DT. Nanostructural and Transcriptomic Analyses of Human Saliva Derived Exosomes. Hansen IA, editor. PLoS ONE. 2010 Jan 5;5(1):e8577.

105. Sverdlov ED. Amedeo Avogadro's cry: what is 1 μg of exosomes? BioEssays News Rev Mol Cell Dev Biol. 2012 Oct;34(10):873–5.

106. Chevillet JR, Kang Q, Ruf IK, Briggs HA, Vojtech LN, Hughes SM, et al. Quantitative and stoichiometric analysis of the microRNA content of exosomes. Proc Natl Acad Sci U S A. 2014 Oct 14;111(41):14888–93.

107. Kim D-K, Lee J, Kim SR, Choi D-S, Yoon YJ, Kim JH, et al. EVpedia: a community web portal for extracellular vesicles research. Bioinforma Oxf Engl. 2015 Mar 15;31(6):933–9.

108. Mathivanan S, Fahner CJ, Reid GE, Simpson RJ. ExoCarta 2012: database of exosomal proteins, RNA and lipids. Nucleic Acids Res. 2012 Jan;40(Database issue):D1241–4.

109. Pisitkun T, Shen R-F, Knepper MA. Identification and proteomic profiling of exosomes in human urine. Proc Natl Acad Sci. 2004 Sep 7;101(36):13368–73.

110. Camussi G, Deregibus MC, Bruno S, Cantaluppi V, Biancone L. Exosomes/microvesicles as a mechanism of cell-to-cell communication. Kidney Int. 2010 Nov;78(9):838–48.

111. Polgar J, Matuskova J, Wagner DD. The P-selectin, tissue factor, coagulation triad. J Thromb Haemost JTH. 2005 Aug;3(8):1590–6.

112. Feng D, Zhao W-L, Ye Y-Y, Bai X-C, Liu R-Q, Chang L-F, et al. Cellular internalization of exosomes occurs through phagocytosis. Traffic Cph Den. 2010 May;11(5):675–87.

113. Mulcahy LA, Pink RC, Carter DRF. Routes and mechanisms of extracellular vesicle uptake. J Extracell Vesicles. 2014;3.

114. Tian T, Wang Y, Wang H, Zhu Z, Xiao Z. Visualizing of the cellular uptake and intracellular trafficking of exosomes by live-cell microscopy. J Cell Biochem. 2010 Oct 1;111(2):488–96.

115. Keller S, Ridinger J, Rupp A-K, Janssen JW, Altevogt P. Body fluid derived exosomes as a novel template for clinical diagnostics. J Transl Med. 2011;9(1):86.

116. Mittelbrunn M, Gutiérrez-Vázquez C, Villarroya-Beltri C, González S, Sánchez-Cabo F, González MÁ, et al. Unidirectional transfer of microRNA-loaded exosomes from T cells to antigen-presenting cells. Nat Commun. 2011;2:282.

117. Montecalvo A, Larregina AT, Shufesky WJ, Stolz DB, Sullivan MLG, Karlsson JM, et al. Mechanism of transfer of functional microRNAs between mouse dendritic cells via exosomes. Blood. 2012 Jan 19;119(3):756–66.

118. Ratajczak J, Miekus K, Kucia M, Zhang J, Reca R, Dvorak P, et al. Embryonic stem cell-derived microvesicles reprogram hematopoietic progenitors: evidence for horizontal transfer of mRNA and protein delivery. Leuk Off J Leuk Soc Am Leuk Res Fund UK. 2006 May;20(5):847–56.

119. Valadi H, Ekström K, Bossios A, Sjöstrand M, Lee JJ, Lötvall JO. Exosome-mediated transfer of mRNAs and microRNAs is a novel mechanism of genetic exchange between cells. Nat Cell Biol. 2007 Jun;9(6):654–9.

120. Yuan A, Farber EL, Rapoport AL, Tejada D, Deniskin R, Akhmedov NB, et al. Transfer of microRNAs by embryonic stem cell microvesicles. PloS One. 2009;4(3):e4722.

121. Deregibus MC, Cantaluppi V, Calogero R, Lo Iacono M, Tetta C, Biancone L, et al. Endothelial progenitor cell derived microvesicles activate an angiogenic program in endothelial cells by a horizontal transfer of mRNA. Blood. 2007 Oct 1;110(7):2440–8.

122. Dempsey PW, Vaidya SA, Cheng G. The art of war: Innate and adaptive immune responses. Cell Mol Life Sci CMLS. 2003 Dec;60(12):2604–21.

123. Anand PK, Anand E, Bleck CKE, Anes E, Griffiths G. Exosomal Hsp70 induces a pro-inflammatory response to foreign particles including mycobacteria. PloS One. 2010;5(4):e10136.

124. Bhatnagar S, Schorey JS. Exosomes released from infected macrophages contain Mycobacterium avium glycopeptidolipids and are proinflammatory. J Biol Chem. 2007 Aug 31;282(35):25779–89.

125. Bhatnagar S, Shinagawa K, Castellino FJ, Schorey JS. Exosomes released from macrophages infected with intracellular pathogens stimulate a proinflammatory response in vitro and in vivo. Blood. 2007 Nov 1;110(9):3234–44.

126. Pletinckx K, Döhler A, Pavlovic V, Lutz MB. Role of dendritic cell maturity/costimulation for generation, homeostasis, and suppressive activity of regulatory T cells. Front Immunol. 2011;2:39.

127. Théry C, Regnault A, Garin J, Wolfers J, Zitvogel L, Ricciardi-Castagnoli P, et al. Molecular characterization of dendritic cell-derived exosomes. Selective accumulation of the heat shock protein hsc73. J Cell Biol. 1999 Nov 1;147(3):599–610.

128. Segura E, Amigorena S, Théry C. Mature dendritic cells secrete exosomes with strong ability to induce antigen-specific effector immune responses. Blood Cells Mol Dis. 2005 Oct;35(2):89–93.

129. Segura E, Nicco C, Lombard B, Véron P, Raposo G, Batteux F, et al. ICAM-1 on exosomes from mature dendritic cells is critical for efficient naive T-cell priming. Blood. 2005 Jul 1;106(1):216–23.

130. Théry C, Boussac M, Véron P, Ricciardi-Castagnoli P, Raposo G, Garin J, et al. Proteomic analysis of dendritic cell-derived exosomes: a secreted subcellular compartment distinct from apoptotic vesicles. J Immunol Baltim Md 1950. 2001 Jun 15;166(12):7309–18.

131. Utsugi-Kobukai S, Fujimaki H, Hotta C, Nakazawa M, Minami M. MHC class I-mediated exogenous antigen presentation by exosomes secreted from immature and mature bone marrow derived dendritic cells. Immunol Lett. 2003 Oct 31;89(2-3):125–31.

132. Hanayama R, Tanaka M, Miwa K, Shinohara A, Iwamatsu A, Nagata S. Identification of a factor that links apoptotic cells to phagocytes. Nature. 2002 May 9;417(6885):182–7.

133. Cai Z, Zhang W, Yang F, Yu L, Yu Z, Pan J, et al. Immunosuppressive exosomes from TGF-β1 gene-modified dendritic cells attenuate Th17-mediated inflammatory autoimmune disease by inducing regulatory T cells. Cell Res. 2012 Mar;22(3):607–10.

134. Heekim S, Bianco N, Menon R, Lechman E, Shufesky W, Morelli A, et al. Exosomes Derived from Genetically Modified DC Expressing FasL Are Anti-inflammatory and Immunosuppressive. Mol Ther. 2006 Feb;13(2):289–300.

135. Kim S-H, Lechman ER, Bianco N, Menon R, Keravala A, Nash J, et al. Exosomes Derived from IL-10-Treated Dendritic Cells Can Suppress Inflammation and Collagen-Induced Arthritis. J Immunol. 2005 May 15;174(10):6440–8.

136. Kim SH, Bianco NR, Shufesky WJ, Morelli AE, Robbins PD. Effective Treatment of Inflammatory Disease Models with Exosomes Derived from Dendritic Cells Genetically Modified to Express IL-4. J Immunol. 2007 Aug 15;179(4):2242–9.

137. Quah BJC, O'Neill HC. The immunogenicity of dendritic cell-derived exosomes. Blood Cells Mol Dis. 2005 Oct;35(2):94–110.

138. Ruffner MA, Kim SH, Bianco NR, Francisco LM, Sharpe AH, Robbins PD. B7-1/2, but not PD-L1/2 molecules, are required on IL-10-treated tolerogenic DC and DC-derived exosomes for *in vivo* function. Eur J Immunol. 2009 Nov;39(11):3084–90.

139. Aline F, Bout D, Amigorena S, Roingeard P, Dimier-Poisson I. Toxoplasma gondii Antigen-Pulsed-Dendritic Cell-Derived Exosomes Induce a Protective Immune Response against T. gondii Infection. Infect Immun. 2004 Jul 1;72(7):4127–37.

140. Beauvillain C, Juste MO, Dion S, Pierre J, Dimier-Poisson I. Exosomes are an effective vaccine against congenital toxoplasmosis in mice. Vaccine. 2009 Mar 10;27(11):1750–7.

141. Del Cacho E, Gallego M, Lee SH, Lillehoj HS, Quilez J, Lillehoj EP, et al. Induction of Protective Immunity against Eimeria tenella, Eimeria maxima, and Eimeria acervulina Infections Using Dendritic Cell-Derived Exosomes. Infect Immun. 2012 May 1;80(5):1909–16.

142. Pegtel DM, van de Garde MDB, Middeldorp JM. Viral miRNAs exploiting the endosomal-exosomal pathway for intercellular cross-talk and immune evasion. Biochim Biophys Acta. 2011 Dec;1809(11-12):715–21.

143. Izquierdo-Useros N, Naranjo-Gómez M, Erkizia I, Puertas MC, Borràs FE, Blanco J, et al. HIV and mature dendritic cells: Trojan exosomes riding the Trojan horse? PLoS Pathog. 2010 Mar;6(3):e1000740.

144. Beckett K, Monier S, Palmer L, Alexandre C, Green H, Bonneil E, et al. Drosophila S2 cells secrete wingless on exosome-like vesicles but the wingless gradient forms independently of exosomes. Traffic Cph Den. 2013 Jan;14(1):82–96.

145. Bischoff M, Gradilla A-C, Seijo I, Andrés G, Rodríguez-Navas C, González-Méndez L, et al. Cytonemes are required for the establishment of a normal Hedgehog morphogen gradient in Drosophila epithelia. Nat Cell Biol. 2013 Oct 13;15(11):1269–81.

146. Callejo A, Bilioni A, Mollica E, Gorfinkiel N, Andrés G, Ibáñez C, et al. Dispatched mediates Hedgehog basolateral release to form the long-range morphogenetic gradient in the Drosophila wing disk epithelium. Proc Natl Acad Sci U S A. 2011 Aug 2;108(31):12591–8.

147. Gradilla A-C, González E, Seijo I, Andrés G, Bischoff M, González-Mendez L, et al. Exosomes as Hedgehog carriers in cytoneme-mediated transport and secretion. Nat Commun. 2014 Dec 4;5:5649.

148. Gross JC, Chaudhary V, Bartscherer K, Boutros M. Active Wnt proteins are secreted on exosomes. Nat Cell Biol. 2012 Oct;14(10):1036–45.

149. Liegeois S. The V0-ATPase mediates apical secretion of exosomes containing Hedgehog-related proteins in Caenorhabditis elegans. J Cell Biol. 2006 Jun 19;173(6):949–61.

150. Vyas N, Walvekar A, Tate D, Lakshmanan V, Bansal D, Lo Cicero A, et al. Vertebrate Hedgehog is secreted on two types of extracellular vesicles with different signaling properties. Sci Rep. 2014;4:7357.

151. Antonucci F, Turola E, Riganti L, Caleo M, Gabrielli M, Perrotta C, et al. Microvesicles released from microglia stimulate synaptic activity via enhanced sphingolipid metabolism. EMBO J. 2012 Mar 7;31(5):1231–40.

152. Fauré J, Lachenal G, Court M, Hirrlinger J, Chatellard-Causse C, Blot B, et al. Exosomes are released by cultured cortical neurones. Mol Cell Neurosci. 2006 Apr;31(4):642–8.

153. Krämer-Albers E-M, Bretz N, Tenzer S, Winterstein C, Möbius W, Berger H, et al. Oligodendrocytes secrete exosomes containing major myelin and stress-protective proteins: Trophic support for axons? Proteomics Clin Appl. 2007 Nov;1(11):1446–61.

154. Wang G, Dinkins M, He Q, Zhu G, Poirier C, Campbell A, et al. Astrocytes Secrete Exosomes Enriched with Proapoptotic Ceramide and Prostate Apoptosis Response 4 (PAR-4): POTENTIAL MECHANISM OF APOPTOSIS INDUCTION IN ALZHEIMER DISEASE (AD). J Biol Chem. 2012 Jun 15;287(25):21384–95.

155. Lachenal G, Pernet-Gallay K, Chivet M, Hemming FJ, Belly A, Bodon G, et al. Release of exosomes from differentiated neurons and its regulation by synaptic glutamatergic activity. Mol Cell Neurosci. 2011 Feb;46(2):409–18.

156. Bahi A, Dreyer J-L. Cocaine-induced expression changes of axon guidance molecules in the adult rat brain. Mol Cell Neurosci. 2005 Feb;28(2):275–91.

157. Hienola A, Tumova S, Kulesskiy E, Rauvala H. N-syndecan deficiency impairs neural migration in brain. J Cell Biol. 2006 Aug 14;174(4):569–80.

158. Frühbeis C, Fröhlich D, Kuo WP, Amphornrat J, Thilemann S, Saab AS, et al. Neurotransmitter-triggered transfer of exosomes mediates oligodendrocyte-neuron communication. PLoS Biol. 2013 Jul;11(7):e1001604.

159. Hendrix A, Westbroek W, Bracke M, De Wever O. An Ex(o)citing Machinery for Invasive Tumor Growth. Cancer Res. 2010 Dec 1;70(23):9533–7.

160. Park JE, Tan HS, Datta A, Lai RC, Zhang H, Meng W, et al. Hypoxic tumor cell modulates its microenvironment to enhance angiogenic and metastatic potential by secretion of proteins and exosomes. Mol Cell Proteomics MCP. 2010 Jun;9(6):1085–99.

161. Khan S, Jutzy JMS, Aspe JR, McGregor DW, Neidigh JW, Wall NR. Survivin is released from cancer cells via exosomes. Apoptosis Int J Program Cell Death. 2011 Jan;16(1):1–12.

162. Skog J, Würdinger T, van Rijn S, Meijer DH, Gainche L, Sena-Esteves M, et al. Glioblastoma microvesicles transport RNA and proteins that promote tumour growth and provide diagnostic biomarkers. Nat Cell Biol. 2008 Dec;10(12):1470–6.

163. Huber V, Fais S, Iero M, Lugini L, Canese P, Squarcina P, et al. Human Colorectal Cancer Cells Induce T-Cell Death Through Release of Proapoptotic Microvesicles: Role in Immune Escape. Gastroenterology. 2005 Jun;128(7):1796–804.

164. Whiteside TL. Immune modulation of T-cell and NK (natural killer) cell activities by TEXs (tumour-derived exosomes). Biochem Soc Trans. 2013 Feb 1;41(1):245–51.

165. Lundholm M, Schröder M, Nagaeva O, Baranov V, Widmark A, Mincheva-Nilsson L, et al. Prostate tumor-derived exosomes down-regulate NKG2D expression on natural killer cells and CD8+ T cells: mechanism of immune evasion. PloS One. 2014;9(9):e108925.

166. Szajnik M, Czystowska M, Szczepanski MJ, Mandapathil M, Whiteside TL. Tumor-derived microvesicles induce, expand and up-regulate biological activities of human regulatory T cells (Treg). PloS One. 2010;5(7):e11469.

167. Whiteside TL, Mandapathil M, Szczepanski M, Szajnik M. Mechanisms of tumor escape from the immune system: adenosine-producing Treg, exosomes and tumor-associated TLRs. Bull Cancer (Paris). 2011 Feb;98(2):E25–31.

168. Yu S, Liu C, Su K, Wang J, Liu Y, Zhang L, et al. Tumor exosomes inhibit differentiation of bone marrow dendritic cells. J Immunol Baltim Md 1950. 2007 Jun 1;178(11):6867–75.

169. Khazaie K, Blatner NR, Khan MW, Gounari F, Gounaris E, Dennis K, et al. The significant role of mast cells in cancer. Cancer Metastasis Rev. 2011 Mar;30(1):45–60.

170. Al-Nedawi K, Meehan B, Kerbel RS, Allison AC, Rak J. Endothelial expression of autocrine VEGF upon the uptake of tumor-derived microvesicles containing oncogenic EGFR. Proc Natl Acad Sci U S A. 2009 Mar 10;106(10):3794–9.

171. Hegmans JPJJ, Bard MPL, Hemmes A, Luider TM, Kleijmeer MJ, Prins J-B, et al. Proteomic analysis of exosomes secreted by human mesothelioma cells. Am J Pathol. 2004 May;164(5):1807–15.

172. Sheldon H, Heikamp E, Turley H, Dragovic R, Thomas P, Oon CE, et al. New mechanism for Notch signaling to endothelium at a distance by Delta-like 4 incorporation into exosomes. Blood. 2010 Sep 30;116(13):2385–94.

173. Hood JL, Pan H, Lanza GM, Wickline SA, Consortium for Translational Research in Advanced Imaging and Nanomedicine (C-TRAIN). Paracrine induction of endothelium by tumor exosomes. Lab Investig J Tech Methods Pathol. 2009 Nov;89(11):1317–28.

174. Peinado H, Alečković M, Lavotshkin S, Matei I, Costa-Silva B, Moreno-Bueno G, et al. Melanoma exosomes educate bone marrow progenitor cells toward a pro-metastatic phenotype through MET. Nat Med [Internet]. 2012 May 27 [cited 2012 Jun 24]; Available from: http://www.ncbi.nlm.nih.gov/pubmed/22635005

175. Janowska-Wieczorek A, Wysoczynski M, Kijowski J, Marquez-Curtis L, Machalinski B, Ratajczak J, et al. Microvesicles derived from activated platelets induce metastasis and angiogenesis in lung cancer. Int J Cancer J Int Cancer. 2005 Feb 20;113(5):752–60.

176. Shedden K, Xie XT, Chandaroy P, Chang YT, Rosania GR. Expulsion of small molecules in vesicles shed by cancer cells: association with gene expression and chemosensitivity profiles. Cancer Res. 2003 Aug 1;63(15):4331–7.

177. Safaei R, Larson BJ, Cheng TC, Gibson MA, Otani S, Naerdemann W, et al. Abnormal lysosomal trafficking and enhanced exosomal export of cisplatin in drug-resistant human ovarian carcinoma cells. Mol Cancer Ther. 2005 Oct;4(10):1595–604.

178. Ciravolo V, Huber V, Ghedini GC, Venturelli E, Bianchi F, Campiglio M, et al. Potential role of HER2-overexpressing exosomes in countering trastuzumab-based therapy. J Cell Physiol. 2012 Feb;227(2):658–67.

179. Chen W, Liu X, Lv M, Chen L, Zhao J, Zhong S, et al. Exosomes from drug-resistant breast cancer cells transmit chemoresistance by a horizontal transfer of microRNAs. PloS One. 2014;9(4):e95240.

180. Bellingham SA, Guo BB, Coleman BM, Hill AF. Exosomes: Vehicles for the Transfer of Toxic Proteins Associated with Neurodegenerative Diseases? Front Physiol [Internet]. 2012 May 3 [cited 2012 Jul 9];3. Available from: http://www.ncbi.nlm.nih.gov/pmc/articles/PMC3342525/

181. Alvarez-Erviti L, Seow Y, Schapira AH, Gardiner C, Sargent IL, Wood MJA, et al. Lysosomal dysfunction increases exosome-mediated alpha-synuclein release and transmission. Neurobiol Dis. 2011 Jun;42(3):360–7.

182. Emmanouilidou E, Melachroinou K, Roumeliotis T, Garbis SD, Ntzouni M, Margaritis LH, et al. Cell-produced alpha-synuclein is secreted in a calcium-dependent manner by exosomes and impacts neuronal survival. J Neurosci Off J Soc Neurosci. 2010 May 19;30(20):6838–51.

183. Hansen C, Angot E, Bergström A-L, Steiner JA, Pieri L, Paul G, et al. α-Synuclein propagates from mouse brain to grafted dopaminergic neurons and seeds aggregation in cultured human cells. J Clin Invest. 2011 Feb;121(2):715–25.

184. Desplats P, Lee H-J, Bae E-J, Patrick C, Rockenstein E, Crews L, et al. Inclusion formation and neuronal cell death through neuron-to-neuron transmission of alpha-synuclein. Proc Natl Acad Sci U S A. 2009 Aug 4;106(31):13010–5.

185. Russo I, Bubacco L, Greggio E. Exosomes-associated neurodegeneration and progression of Parkinson's disease. Am J Neurodegener Dis. 2012;1(3):217–25.

186. Rajendran L, Honsho M, Zahn TR, Keller P, Geiger KD, Verkade P, et al. Alzheimer's disease beta-amyloid peptides are released in association with exosomes. Proc Natl Acad Sci U S A. 2006 Jul 25;103(30):11172–7.

187. Vingtdeux V, Hamdane M, Loyens A, Gelé P, Drobeck H, Bégard S, et al. Alkalizing drugs induce accumulation of amyloid precursor protein by-products in luminal vesicles of multivesicular bodies. J Biol Chem. 2007 Jun 22;282(25):18197–205.

188. Sharples RA, Vella LJ, Nisbet RM, Naylor R, Perez K, Barnham KJ, et al. Inhibition of gamma-secretase causes increased secretion of amyloid precursor protein C-

terminal fragments in association with exosomes. FASEB J Off Publ Fed Am Soc Exp Biol. 2008 May;22(5):1469–78.

189. Ghidoni R, Paterlini A, Albertini V, Glionna M, Monti E, Schiaffonati L, et al. Cystatin C is released in association with exosomes: a new tool of neuronal communication which is unbalanced in Alzheimer's disease. Neurobiol Aging. 2011 Aug;32(8):1435–42.

190. Basso M, Pozzi S, Tortarolo M, Fiordaliso F, Bisighini C, Pasetto L, et al. Mutant Copper-Zinc Superoxide Dismutase (SOD1) Induces Protein Secretion Pathway Alterations and Exosome Release in Astrocytes: IMPLICATIONS FOR DISEASE SPREADING AND MOTOR NEURON PATHOLOGY IN AMYOTROPHIC LATERAL SCLEROSIS. J Biol Chem. 2013 May 31;288(22):15699–711.

191. Gomes C, Keller S, Altevogt P, Costa J. Evidence for secretion of Cu,Zn superoxide dismutase via exosomes from a cell model of amyotrophic lateral sclerosis. Neurosci Lett. 2007 Nov 20;428(1):43–6.

192. Li J, Sherman-Baust CA, Tsai-Turton M, Bristow RE, Roden RB, Morin PJ. Claudin-containing exosomes in the peripheral circulation of women with ovarian cancer. BMC Cancer. 2009;9(1):244.

193. Taylor DD, Gercel-Taylor C. MicroRNA signatures of tumor-derived exosomes as diagnostic biomarkers of ovarian cancer. Gynecol Oncol. 2008 Jul;110(1):13–21.

194. Szajnik M, Derbis M, Lach M, Patalas P, Michalak M, Drzewiecka H, et al. Exosomes in Plasma of Patients with Ovarian Carcinoma: Potential Biomarkers of Tumor Progression and Response to Therapy. Gynecol Obstet Sunnyvale Calif. 2013 Apr 29;Suppl 4:3.

195. Kobayashi M, Salomon C, Tapia J, Illanes SE, Mitchell MD, Rice GE. Ovarian cancer cell invasiveness is associated with discordant exosomal sequestration of Let-7 miRNA and miR-200. J Transl Med. 2014;12(1):4.

196. Smalley DM, Sheman NE, Nelson K, Theodorescu D. Isolation and Identification of Potential Urinary Microparticle Biomarkers of Bladder Cancer. J Proteome Res. 2008 May 2;7(5):2088–96.

197. Perez A, Loizaga A, Arceo R, Lacasa I, Rabade A, Zorroza K, et al. A Pilot Study on the Potential of RNA-Associated to Urinary Vesicles as a Suitable Non-Invasive Source for Diagnostic Purposes in Bladder Cancer. Cancers. 2014;6(1):179–92.

198. Welton JL, Khanna S, Giles PJ, Brennan P, Brewis IA, Staffurth J, et al. Proteomics analysis of bladder cancer exosomes. Mol Cell Proteomics MCP. 2010 Jun;9(6):1324–38.

199. Beckham CJ, Olsen J, Yin P-N, Wu C-H, Ting H-J, Hagen FK, et al. Bladder cancer exosomes contain EDIL-3/Del1 and facilitate cancer progression. J Urol. 2014 Aug;192(2):583–92.

200. Akers JC, Ramakrishnan V, Kim R, Skog J, Nakano I, Pingle S, et al. miR-21 in the Extracellular Vesicles (EVs) of Cerebrospinal Fluid (CSF): A Platform for Glioblastoma Biomarker Development. Chen M, editor. PLoS ONE. 2013 Oct 21;8(10):e78115.

201. Graner MW, Epple LM, Dusto NL, Lencioni AM, Nega M, Herring M, et al. Circulating exosomes as new biomarkers for brain disease and injury. In: Southern ŠO, editor. 2013 [cited 2015 Apr 1]. p. 87230R. Available from: http://proceedings.spiedigitallibrary.org/proceeding.aspx?doi=10.1117/12.2027435

202. Noerholm M, Balaj L, Limperg T, Salehi A, Zhu LD, Hochberg FH, et al. RNA expression patterns in serum microvesicles from patients with glioblastoma multiforme and controls. BMC Cancer. 2012;12:22.

203. Manterola L, Guruceaga E, Gállego Pérez-Larraya J, González-Huarriz M, Jauregui P, Tejada S, et al. A small noncoding RNA signature found in exosomes of GBM patient serum as a diagnostic tool. Neuro-Oncol. 2014 Apr;16(4):520–7.

204. Chen WW, Balaj L, Liau LM, Samuels ML, Kotsopoulos SK, Maguire CA, et al. BEAMing and Droplet Digital PCR Analysis of Mutant IDH1 mRNA in Glioma Patient Serum and Cerebrospinal Fluid Extracellular Vesicles. Mol Ther Acids. 2013 Jul;2(7):e109.

205. Nilsson J, Skog J, Nordstrand A, Baranov V, Mincheva-Nilsson L, Breakefield XO, et al. Prostate cancer-derived urine exosomes: a novel approach to biomarkers for prostate cancer. Br J Cancer. 2009 May 19;100(10):1603–7.

206. Mitchell PJ, Welton J, Staffurth J, Court J, Mason MD, Tabi Z, et al. Can urinary exosomes act as treatment response markers in prostate cancer? J Transl Med. 2009;7(1):4.

207. Bryant RJ, Pawlowski T, Catto JWF, Marsden G, Vessella RL, Rhees B, et al. Changes in circulating microRNA levels associated with prostate cancer. Br J Cancer. 2012 Feb 14;106(4):768–74.

208. Khan S, Jutzy JMS, Valenzuela MMA, Turay D, Aspe JR, Ashok A, et al. Plasma-derived exosomal survivin, a plausible biomarker for early detection of prostate cancer. PloS One. 2012;7(10):e46737.

209. Gabriel K, Ingram A, Austin R, Kapoor A, Tang D, Majeed F, et al. Regulation of the Tumor Suppressor PTEN through Exosomes: A Diagnostic Potential for Prostate Cancer. Batra SK, editor. PLoS ONE. 2013 Jul 25;8(7):e70047.

210. Cheng L, Sharples RA, Scicluna BJ, Hill AF. Exosomes provide a protective and enriched source of miRNA for biomarker profiling compared to intracellular and cell-free blood. J Extracell Vesicles [Internet]. 2014 Mar 26 [cited 2015 Apr 3];3(0). Available from: http://www.journalofextracellularvesicles.net/index.php/jev/article/view/23743

211. Tan KH, Tan SS, Sze SK, Lee WKR, Ng MJ, Lim SK. Plasma biomarker discovery in preeclampsia using a novel differential isolation technology for circulating extracellular vesicles. Am J Obstet Gynecol. 2014 Oct;211(4):380.e1–13.

212. Michaelis M, Gralla O, Behrends T, Scharpf M, Endermann T, Rijntjes E, et al. Selenoprotein P in seminal fluid is a novel biomarker of sperm quality. Biochem Biophys Res Commun. 2014 Jan 17;443(3):905–10.

213. Bala S, Petrasek J, Mundkur S, Catalano D, Levin I, Ward J, et al. Circulating microRNAs in exosomes indicate hepatocyte injury and inflammation in alcoholic, drug-induced, and inflammatory liver diseases. Hepatol Baltim Md. 2012 Nov;56(5):1946–57.

214. Sonoda H, Yokota-Ikeda N, Oshikawa S, Kanno Y, Yoshinaga K, Uchida K, et al. Decreased abundance of urinary exosomal aquaporin-1 in renal ischemia-reperfusion injury. Am J Physiol Renal Physiol. 2009 Oct;297(4):F1006–16.

215. Zhou H, Pisitkun T, Aponte A, Yuen PST, Hoffert JD, Yasuda H, et al. Exosomal Fetuin-A identified by proteomics: a novel urinary biomarker for detecting acute kidney injury. Kidney Int. 2006 Nov;70(10):1847–57.

216. Raimondo F, Corbetta S, Morosi L, Chinello C, Gianazza E, Castoldi G, et al. Urinary exosomes and diabetic nephropathy: a proteomic approach. Mol Biosyst. 2013 Jun;9(6):1139–46.

217. Ristorcelli E, Beraud E, Verrando P, Villard C, Lafitte D, Sbarra V, et al. Human tumor nanoparticles induce apoptosis of pancreatic cancer cells. FASEB J Off Publ Fed Am Soc Exp Biol. 2008 Sep;22(9):3358–69.

218. Wolfers J, Lozier A, Raposo G, Regnault A, Théry C, Masurier C, et al. Tumor-derived exosomes are a source of shared tumor rejection antigens for CTL cross-priming. Nat Med. 2001 Mar;7(3):297–303.

219. Napoletano C, Rughetti A, Landi R, Pinto D, Bellati F, Rahimi H, et al. Immunogenicity of allo-vesicle carrying ERBB2 tumor antigen for dendritic cell-based anti-tumor immunotherapy. Int J Immunopathol Pharmacol. 2009 Sep;22(3):647–58.

220. Morelli AE, Larregina AT, Shufesky WJ, Sullivan MLG, Stolz DB, Papworth GD, et al. Endocytosis, intracellular sorting, and processing of exosomes by dendritic cells. Blood. 2004 Nov 15;104(10):3257–66.

221. Li J, Liu K, Liu Y, Xu Y, Zhang F, Yang H, et al. Exosomes mediate the cell-to-cell transmission of IFN-α-induced antiviral activity. Nat Immunol. 2013 Jul 7;14(8):793–803.

222. Gehrmann U, Hiltbrunner S, Georgoudaki A-M, Karlsson MC, Näslund TI, Gabrielsson S. Synergistic induction of adaptive antitumor immunity by codelivery of antigen with α-galactosylceramide on exosomes. Cancer Res. 2013 Jul 1;73(13):3865–76.

223. Escudier B, Dorval T, Chaput N, André F, Caby M-P, Novault S, et al. Vaccination of metastatic melanoma patients with autologous dendritic cell (DC) derived-exosomes: results of thefirst phase I clinical trial. J Transl Med. 2005 Mar 2;3(1):10.

224. Morse MA, Garst J, Osada T, Khan S, Hobeika A, Clay TM, et al. A phase I study of dexosome immunotherapy in patients with advanced non-small cell lung cancer. J Transl Med. 2005 Feb 21;3(1):9.

225. Dai S, Wei D, Wu Z, Zhou X, Wei X, Huang H, et al. Phase I clinical trial of autologous ascites-derived exosomes combined with GM-CSF for colorectal cancer. Mol Ther J Am Soc Gene Ther. 2008 Apr;16(4):782–90.

226. Agarwal A, Fanelli G, Letizia M, Tung SL, Boardman D, Lechler R, et al. Regulatory T Cell-Derived Exosomes: Possible Therapeutic and Diagnostic Tools in Transplantation. Front Immunol [Internet]. 2014 Nov 5 [cited 2015 Apr 1];5. Available from: http://journal.frontiersin.org/article/10.3389/fimmu.2014.00555/abstract

227. Taieb J, Chaput N, Schartz N, Roux S, Novault S, Ménard C, et al. Chemoimmunotherapy of tumors: cyclophosphamide synergizes with exosome based vaccines. J Immunol Baltim Md 1950. 2006 Mar 1;176(5):2722–9.

228. Ghiringhelli F, Menard C, Puig PE, Ladoire S, Roux S, Martin F, et al. Metronomic cyclophosphamide regimen selectively depletes CD4+CD25+ regulatory T cells and restores T and NK effector functions in end stage cancer patients. Cancer Immunol Immunother CII. 2007 May;56(5):641–8.

229. Quesenberry PJ, Dooner MS, Aliotta JM. Stem cell plasticity revisited: the continuum marrow model and phenotypic changes mediated by microvesicles. Exp Hematol. 2010 Jul;38(7):581–92.

230. Aliotta JM, Sanchez-Guijo FM, Dooner GJ, Johnson KW, Dooner MS, Greer KA, et al. Alteration of marrow cell gene expression, protein production, and engraftment into lung by lung-derived microvesicles: a novel mechanism for phenotype modulation. Stem Cells Dayt Ohio. 2007 Sep;25(9):2245–56.

231. Del Tatto M, Ng T, Aliotta JM, Colvin GA, Dooner MS, Berz D, et al. Marrow cell genetic phenotype change induced by human lung cancer cells. Exp Hematol. 2011 Nov;39(11):1072–80.

232. Aliotta JM, Pereira M, Johnson KW, de Paz N, Dooner MS, Puente N, et al. Microvesicle entry into marrow cells mediates tissue-specific changes in mRNA by direct delivery of mRNA and induction of transcription. Exp Hematol. 2010 Mar;38(3):233–45.

233. Cantaluppi V, Biancone L, Figliolini F, Beltramo S, Medica D, Deregibus MC, et al. Microvesicles derived from endothelial progenitor cells enhance neoangiogenesis of human pancreatic islets. Cell Transplant [Internet]. 2012 Mar 22 [cited 2012 Jun 24]; Available from: http://www.ncbi.nlm.nih.gov/pubmed/22455973

234. Quesenberry PJ, Dooner MS, Goldberg LR, Aliotta JM, Pereira M, Amaral A, et al. A new stem cell biology: the continuum and microvesicles. Trans Am Clin Climatol Assoc. 2012;123:152–66; discussion 166.

235. Panagopoulos K, Cross-Knorr S, Dillard C, Pantazatos D, Del Tatto M, Mills D, et al. Reversal of chemosensitivity and induction of cell malignancy of a non-malignant prostate cancer cell line upon extracellular vesicle exposure. Mol Cancer. 2013;12(1):118.

236. Cossetti C, Iraci N, Mercer TR, Leonardi T, Alpi E, Drago D, et al. Extracellular Vesicles from Neural Stem Cells Transfer IFN-γ via Ifngr1 to Activate Stat1 Signaling in Target Cells. Mol Cell. 2014 Oct;56(2):193–204.

237. Till JE, Mcculloch EA. REPAIR PROCESSES IN IRRADIATED MOUSE HEMATOPOIETIC TISSUE. Ann N Y Acad Sci. 1964 Mar 31;114:115–25.

238. Friedenstein AJ, Chailakhjan RK, Lalykina KS. The development of fibroblast colonies in monolayer cultures of guinea-pig bone marrow and spleen cells. Cell Tissue Kinet. 1970 Oct;3(4):393–403.

239. Lee OK, Kuo TK, Chen W-M, Lee K-D, Hsieh S-L, Chen T-H. Isolation of multipotent mesenchymal stem cells from umbilical cord blood. Blood. 2004 Mar 1;103(5):1669–75.

240. Bosch P, Musgrave DS, Lee JY, Cummins J, Shuler T, Ghivizzani TC, et al. Osteoprogenitor cells within skeletal muscle. J Orthop Res Off Publ Orthop Res Soc. 2000 Nov;18(6):933–44.

241. Zvaifler NJ, Marinova-Mutafchieva L, Adams G, Edwards CJ, Moss J, Burger JA, et al. Mesenchymal precursor cells in the blood of normal individuals. Arthritis Res. 2000;2(6):477–88.

242. Musina RA, Belyavski AV, Tarusova OV, Solovyova EV, Sukhikh GT. Endometrial mesenchymal stem cells isolated from the menstrual blood. Bull Exp Biol Med. 2008 Apr;145(4):539–43.

243. Katsuda T, Tsuchiya R, Kosaka N, Yoshioka Y, Takagaki K, Oki K, et al. Human adipose tissue-derived mesenchymal stem cells secrete functional neprilysin-bound exosomes. Sci Rep [Internet]. 2013 Feb 1 [cited 2015 Apr 3];3. Available from: http://www.nature.com/doifinder/10.1038/srep01197

244. Casiraghi F, Azzollini N, Cassis P, Imberti B, Morigi M, Cugini D, et al. Pretransplant infusion of mesenchymal stem cells prolongs the survival of a semiallogeneic heart transplant through the generation of regulatory T cells. J Immunol Baltim Md 1950. 2008 Sep 15;181(6):3933–46.

245. Jarvinen L, Badri L, Wettlaufer S, Ohtsuka T, Standiford TJ, Toews GB, et al. Lung resident mesenchymal stem cells isolated from human lung allografts inhibit T cell proliferation via a soluble mediator. J Immunol Baltim Md 1950. 2008 Sep 15;181(6):4389–96.

246. Sheng H, Wang Y, Jin Y, Zhang Q, Zhang Y, Wang L, et al. A critical role of IFNgamma in priming MSC-mediated suppression of T cell proliferation through up-regulation of B7-H1. Cell Res. 2008 Aug;18(8):846–57.

247. Djouad F, Charbonnier L-M, Bouffi C, Louis-Plence P, Bony C, Apparailly F, et al. Mesenchymal stem cells inhibit the differentiation of dendritic cells through an interleukin-6-dependent mechanism. Stem Cells Dayt Ohio. 2007 Aug;25(8):2025–32.

248. Beyth S, Borovsky Z, Mevorach D, Liebergall M, Gazit Z, Aslan H, et al. Human mesenchymal stem cells alter antigen-presenting cell maturation and induce T-cell unresponsiveness. Blood. 2005 Mar 1;105(5):2214–9.

249. Jiang X-X, Zhang Y, Liu B, Zhang S-X, Wu Y, Yu X-D, et al. Human mesenchymal stem cells inhibit differentiation and function of monocyte-derived dendritic cells. Blood. 2005 May 15;105(10):4120–6.

250. Corcione A, Benvenuto F, Ferretti E, Giunti D, Cappiello V, Cazzanti F, et al. Human mesenchymal stem cells modulate B-cell functions. Blood. 2006 Jan 1;107(1):367–72.

251. Selmani Z, Naji A, Zidi I, Favier B, Gaiffe E, Obert L, et al. Human leukocyte antigen-G5 secretion by human mesenchymal stem cells is required to suppress T lymphocyte and natural killer function and to induce CD4+CD25highFOXP3+ regulatory T cells. Stem Cells Dayt Ohio. 2008 Jan;26(1):212–22.

252. Aggarwal S, Pittenger MF. Human mesenchymal stem cells modulate allogeneic immune cell responses. Blood. 2005 Feb 15;105(4):1815–22.

253. Ortiz LA, Gambelli F, McBride C, Gaupp D, Baddoo M, Kaminski N, et al. Mesenchymal stem cell engraftment in lung is enhanced in response to bleomycin exposure and ameliorates its fibrotic effects. Proc Natl Acad Sci U S A. 2003 Jul 8;100(14):8407–11.

254. Rojas M, Xu J, Woods CR, Mora AL, Spears W, Roman J, et al. Bone marrow-derived mesenchymal stem cells in repair of the injured lung. Am J Respir Cell Mol Biol. 2005 Aug;33(2):145–52.

255. Kidd S, Spaeth E, Dembinski JL, Dietrich M, Watson K, Klopp A, et al. Direct evidence of mesenchymal stem cell tropism for tumor and wounding microenvironments using in vivo bioluminescent imaging. Stem Cells Dayt Ohio. 2009 Oct;27(10):2614–23.

256. Ponte AL, Marais E, Gallay N, Langonné A, Delorme B, Hérault O, et al. The in vitro migration capacity of human bone marrow mesenchymal stem cells: comparison of chemokine and growth factor chemotactic activities. Stem Cells Dayt Ohio. 2007 Jul;25(7):1737–45.

257. Birnbaum T, Roider J, Schankin CJ, Padovan CS, Schichor C, Goldbrunner R, et al. Malignant gliomas actively recruit bone marrow stromal cells by secreting angiogenic cytokines. J Neurooncol. 2007 Jul;83(3):241–7.

258. Dwyer RM, Potter-Beirne SM, Harrington KA, Lowery AJ, Hennessy E, Murphy JM, et al. Monocyte chemotactic protein-1 secreted by primary breast tumors stimulates migration of mesenchymal stem cells. Clin Cancer Res Off J Am Assoc Cancer Res. 2007 Sep 1;13(17):5020–7.

259. Menon LG, Picinich S, Koneru R, Gao H, Lin SY, Koneru M, et al. Differential gene expression associated with migration of mesenchymal stem cells to conditioned medium from tumor cells or bone marrow cells. Stem Cells Dayt Ohio. 2007 Feb;25(2):520–8.

260. Le Blanc K, Frassoni F, Ball L, Locatelli F, Roelofs H, Lewis I, et al. Mesenchymal stem cells for treatment of steroid-resistant, severe, acute graft-versus-host disease: a phase II study. Lancet. 2008 May 10;371(9624):1579–86.

261. García-Olmo D, García-Arranz M, Herreros D, Pascual I, Peiro C, Rodríguez-Montes JA. A phase I clinical trial of the treatment of Crohn's fistula by adipose mesenchymal stem cell transplantation. Dis Colon Rectum. 2005 Jul;48(7):1416–23.

262. Horwitz EM, Gordon PL, Koo WKK, Marx JC, Neel MD, McNall RY, et al. Isolated allogeneic bone marrow-derived mesenchymal cells engraft and stimulate growth in children with osteogenesis imperfecta: Implications for cell therapy of bone. Proc Natl Acad Sci U S A. 2002 Jun 25;99(13):8932–7.

263. Le Blanc K, Götherström C, Ringdén O, Hassan M, McMahon R, Horwitz E, et al. Fetal mesenchymal stem-cell engraftment in bone after in utero transplantation in a patient with severe osteogenesis imperfecta. Transplantation. 2005 Jun 15;79(11):1607–14.

264. Otsuru S, Gordon PL, Shimono K, Jethva R, Marino R, Phillips CL, et al. Transplanted bone marrow mononuclear cells and MSCs impart clinical benefit to children with osteogenesis imperfecta through different mechanisms. Blood. 2012 Aug 30;120(9):1933–41.

265. Semedo P, Palasio CG, Oliveira CD, Feitoza CQ, Gonçalves GM, Cenedeze MA, et al. Early modulation of inflammation by mesenchymal stem cell after acute kidney injury. Int Immunopharmacol. 2009 Jun;9(6):677–82.

266. Schrepfer S, Deuse T, Reichenspurner H, Fischbein MP, Robbins RC, Pelletier MP. Stem cell transplantation: the lung barrier. Transplant Proc. 2007 Mar;39(2):573–6.

267. Fischer UM, Harting MT, Jimenez F, Monzon-Posadas WO, Xue H, Savitz SI, et al. Pulmonary Passage is a Major Obstacle for Intravenous Stem Cell Delivery: The Pulmonary First-Pass Effect. Stem Cells Dev. 2009 Jun;18(5):683–92.

268. Morigi M. Mesenchymal Stem Cells Are Renotropic, Helping to Repair the Kidney and Improve Function in Acute Renal Failure. J Am Soc Nephrol. 2004 Jul 1;15(7):1794–804.

269. Herrera MB, Bussolati B, Bruno S, Morando L, Mauriello-Romanazzi G, Sanavio F, et al. Exogenous mesenchymal stem cells localize to the kidney by means of CD44 following acute tubular injury. Kidney Int. 2007 Aug;72(4):430–41.

270. Toma C, Pittenger MF, Cahill KS, Byrne BJ, Kessler PD. Human mesenchymal stem cells differentiate to a cardiomyocyte phenotype in the adult murine heart. Circulation. 2002 Jan 1;105(1):93–8.

271. Wang Z, Goh J, Das De S, Ge Z, Ouyang H, Chong JSW, et al. Efficacy of bone marrow-derived stem cells in strengthening osteoporotic bone in a rabbit model. Tissue Eng. 2006 Jul;12(7):1753–61.

272. Freyman T. A quantitative, randomized study evaluating three methods of mesenchymal stem cell delivery following myocardial infarction. Eur Heart J. 2005 Oct 17;27(9):1114–22.

273. Imberti B, Morigi M, Tomasoni S, Rota C, Corna D, Longaretti L, et al. Insulin-like growth factor-1 sustains stem cell mediated renal repair. J Am Soc Nephrol JASN. 2007 Nov;18(11):2921–8.

274. Mirotsou M, Zhang Z, Deb A, Zhang L, Gnecchi M, Noiseux N, et al. Secreted frizzled related protein 2 (Sfrp2) is the key Akt-mesenchymal stem cell-released paracrine factor mediating myocardial survival and repair. Proc Natl Acad Sci U S A. 2007 Jan 30;104(5):1643–8.

275. Gnecchi M, He H, Liang OD, Melo LG, Morello F, Mu H, et al. Paracrine action accounts for marked protection of ischemic heart by Akt-modified mesenchymal stem cells. Nat Med. 2005 Apr;11(4):367–8.

276. Timmers L, Lim SK, Hoefer IE, Arslan F, Lai RC, van Oorschot AAM, et al. Human mesenchymal stem cell-conditioned medium improves cardiac function following myocardial infarction. Stem Cell Res. 2011 May;6(3):206–14.

277. Collino F, Deregibus MC, Bruno S, Sterpone L, Aghemo G, Viltono L, et al. Microvesicles derived from adult human bone marrow and tissue specific mesenchymal stem cells shuttle selected pattern of miRNAs. PloS One. 2010;5(7):e11803.

278. Chen TS, Lai RC, Lee MM, Choo ABH, Lee CN, Lim SK. Mesenchymal stem cell secretes microparticles enriched in pre-microRNAs. Nucleic Acids Res. 2010 Jan;38(1):215–24.

279. Bruno S, Grange C, Collino F, Deregibus MC, Cantaluppi V, Biancone L, et al. Microvesicles derived from mesenchymal stem cells enhance survival in a lethal model of acute kidney injury. PloS One. 2012;7(3):e33115.

280. Kim H-S, Choi D-Y, Yun SJ, Choi S-M, Kang JW, Jung JW, et al. Proteomic analysis of microvesicles derived from human mesenchymal stem cells. J Proteome Res. 2012 Feb 3;11(2):839–49.

281. Lai RC, Arslan F, Lee MM, Sze NSK, Choo A, Chen TS, et al. Exosome secreted by MSC reduces myocardial ischemia/reperfusion injury. Stem Cell Res. 2010 May;4(3):214–22.

282. Gatti S, Bruno S, Deregibus MC, Sordi A, Cantaluppi V, Tetta C, et al. Microvesicles derived from human adult mesenchymal stem cells protect against ischaemia-reperfusion-induced acute and chronic kidney injury. Nephrol Dial Transplant Off Publ Eur Dial Transpl Assoc - Eur Ren Assoc. 2011 May;26(5):1474–83.

283. Bruno S, Grange C, Deregibus MC, Calogero RA, Saviozzi S, Collino F, et al. Mesenchymal stem cell-derived microvesicles protect against acute tubular injury. J Am Soc Nephrol JASN. 2009 May;20(5):1053–67.

284. Herrera MB, Fonsato V, Gatti S, Deregibus MC, Sordi A, Cantarella D, et al. Human liver stem cell-derived microvesicles accelerate hepatic regeneration in hepatectomized rats. J Cell Mol Med. 2010 Jun;14(6B):1605–18.

285. Xin H, Li Y, Buller B, Katakowski M, Zhang Y, Wang X, et al. Exosome-mediated transfer of miR-133b from multipotent mesenchymal stromal cells to neural cells contributes to neurite outgrowth. Stem Cells Dayt Ohio. 2012 Jul;30(7):1556–64.

286. Wei X, Yang X, Han Z, Qu F, Shao L, Shi Y. Mesenchymal stem cells: a new trend for cell therapy. Acta Pharmacol Sin. 2013 Jun;34(6):747–54.

287. Breitbach M, Bostani T, Roell W, Xia Y, Dewald O, Nygren JM, et al. Potential risks of bone marrow cell transplantation into infarcted hearts. Blood. 2007 Aug 15;110(4):1362–9.

288. Epperly MW, Guo H, Gretton JE, Greenberger JS. Bone marrow origin of myofibroblasts in irradiation pulmonary fibrosis. Am J Respir Cell Mol Biol. 2003 Aug;29(2):213–24.

289. Kunter U, Rong S, Boor P, Eitner F, Müller-Newen G, Djuric Z, et al. Mesenchymal stem cells prevent progressive experimental renal failure but maldifferentiate into glomerular adipocytes. J Am Soc Nephrol JASN. 2007 Jun;18(6):1754–64.

290. Rubio D, Garcia S, Paz MF, De la Cueva T, Lopez-Fernandez LA, Lloyd AC, et al. Molecular Characterization of Spontaneous Mesenchymal Stem Cell Transformation. Najbauer J, editor. PLoS ONE. 2008 Jan 2;3(1):e1398.

291. Kidd S, Spaeth E, Watson K, Burks J, Lu H, Klopp A, et al. Origins of the Tumor Microenvironment: Quantitative Assessment of Adipose-Derived and Bone Marrow–Derived Stroma. Rameshwar P, editor. PLoS ONE. 2012 Feb 20;7(2):e30563.

292. Biancone L, Bruno S, Deregibus MC, Tetta C, Camussi G. Therapeutic potential of mesenchymal stem cell-derived microvesicles. Nephrol Dial Transplant Off Publ Eur Dial Transpl Assoc - Eur Ren Assoc. 2012 Aug;27(8):3037–42.

293. Sanchez M, Bruno S, Grange C, Tapparo M, Cantaluppi V, Tetta C, et al. Human liver stem cells and derived extracellular vesicles improve recovery in a murine model of acute kidney injury. Stem Cell Res Ther. 2014;5(6):124.

294. Alvarez-Erviti L, Seow Y, Yin H, Betts C, Lakhal S, Wood MJA. Delivery of siRNA to the mouse brain by systemic injection of targeted exosomes. Nat Biotechnol. 2011 Apr;29(4):341–5.

295. Wahlgren J, Karlson TDL, Brisslert M, Vaziri Sani F, Telemo E, Sunnerhagen P, et al. Plasma exosomes can deliver exogenous short interfering RNA to monocytes and lymphocytes. Nucleic Acids Res [Internet]. 2012 May 22 [cited 2012 Jun 24]; Available from: http://www.ncbi.nlm.nih.gov/pubmed/22618874

296. Shtam TA, Kovalev RA, Varfolomeeva E, Makarov EM, Kil YV, Filatov MV. Exosomes are natural carriers of exogenous siRNA to human cells in vitro. Cell Commun Signal. 2013;11(1):88.

297. Kooijmans SAA, Stremersch S, Braeckmans K, de Smedt SC, Hendrix A, Wood MJA, et al. Electroporation-induced siRNA precipitation obscures the efficiency of siRNA loading into extracellular vesicles. J Control Release Off J Control Release Soc. 2013 Nov 28;172(1):229–38.

298. Mizrak A, Bolukbasi MF, Ozdener GB, Brenner GJ, Madlener S, Erkan EP, et al. Genetically Engineered Microvesicles Carrying Suicide mRNA/Protein Inhibit Schwannoma Tumor Growth. Mol Ther. 2013 Jan;21(1):101–8.

299. Ohno S, Takanashi M, Sudo K, Ueda S, Ishikawa A, Matsuyama N, et al. Systemically injected exosomes targeted to EGFR deliver antitumor microRNA to breast cancer cells. Mol Ther J Am Soc Gene Ther. 2013 Jan;21(1):185–91.

300. Bolukbasi MF, Mizrak A, Ozdener GB, Madlener S, Str|[ouml]|bel T, Erkan EP, et al. miR-1289 and |[ldquo]|Zipcode|[rdquo]|-like Sequence Enrich mRNAs in Microvesicles. Mol Ther — Nucleic Acids. 2012;1(2):e10.

301. Batagov AO, Kuznetsov VA, Kurochkin IV. Identification of nucleotide patterns enriched in secreted RNAs as putative cis-acting elements targeting them to exosome nano-vesicles. BMC Genomics. 2011 Nov 30;12 Suppl 3:S18.

302. Batagov AO, Kurochkin IV. Exosomes secreted by human cells transport largely mRNA fragments that are enriched in the 3'-untranslated regions. Biol Direct. 2013;8:12.

303. Zhuang X, Xiang X, Grizzle W, Sun D, Zhang S, Axtell RC, et al. Treatment of brain inflammatory diseases by delivering exosome encapsulated anti-inflammatory drugs from the nasal region to the brain. Mol Ther J Am Soc Gene Ther. 2011 Oct;19(10):1769–79.

304. Third International Meeting of ISEV 2014. J Extracell Vesicles [Internet]. 2014 Apr 25 [cited 2015 Apr 1];3(0). Available from: http://www.journalofextracellularvesicles.net/index.php/jev/article/view/24214

305. Lai CP, Mardini O, Ericsson M, Prabhakar S, Maguire CA, Chen JW, et al. Dynamic Biodistribution of Extracellular Vesicles *in Vivo* Using a Multimodal Imaging Reporter. ACS Nano. 2014 Jan 28;8(1):483–94.

306. Grange C, Tapparo M, Bruno S, Chatterjee D, Quesenberry PJ, Tetta C, et al. Biodistribution of mesenchymal stem cell-derived extracellular vesicles in a model of acute kidney injury monitored by optical imaging. Int J Mol Med. 2014 May;33(5):1055–63.

307. Smyth T, Kullberg M, Malik N, Smith-Jones P, Graner MW, Anchordoquy TJ. Biodistribution and delivery efficiency of unmodified tumor-derived exosomes. J Control Release Off J Control Release Soc. 2015 Feb 10;199:145–55.

308. Wiklander OPB, Nordin JZ, O'Loughlin A, Gustafsson Y, Corso G, Mäger I, et al. Extracellular vesicle in vivo biodistribution is determined by cell source, route of administration and targeting. J Extracell Vesicles [Internet]. 2015 Apr 20 [cited 2015 Apr 23];4(0). Available from: http://www.journalofextracellularvesicles.net/index.php/jev/article/view/26316

309. Tian Y, Li S, Song J, Ji T, Zhu M, Anderson GJ, et al. A doxorubicin delivery platform using engineered natural membrane vesicle exosomes for targeted tumor therapy. Biomaterials. 2014 Feb;35(7):2383–90.

310. Loebinger MR, Kyrtatos PG, Turmaine M, Price AN, Pankhurst Q, Lythgoe MF, et al. Magnetic resonance imaging of mesenchymal stem cells homing to pulmonary metastases using biocompatible magnetic nanoparticles. Cancer Res. 2009 Dec 1;69(23):8862–7.

311. Sasportas LS, Kasmieh R, Wakimoto H, Hingtgen S, van de Water JAJM, Mohapatra G, et al. Assessment of therapeutic efficacy and fate of engineered human mesenchymal stem cells for cancer therapy. Proc Natl Acad Sci. 2009 Mar 24;106(12):4822–7.

312. Yang B, Wu X, Mao Y, Bao W, Gao L, Zhou P, et al. DUAL-TARGETED ANTITUMOR EFFECTS AGAINST BRAINSTEM GLIOMA BY INTRAVENOUS DELIVERY OF TUMOR NECROSIS FACTOR-RELATED, APOPTOSIS-INDUCING, LIGAND-ENGINEERED HUMAN MESENCHYMAL STEM CELLS: Neurosurgery. 2009 Sep;65(3):610–24.

313. Grisendi G, Bussolari R, Cafarelli L, Petak I, Rasini V, Veronesi E, et al. Adipose-Derived Mesenchymal Stem Cells as Stable Source of Tumor Necrosis Factor-Related Apoptosis-Inducing Ligand Delivery for Cancer Therapy. Cancer Res. 2010 May 1;70(9):3718–29.

314. Marleau AM, Chen C-S, Joyce JA, Tullis RH. Exosome removal as a therapeutic adjuvant in cancer. J Transl Med. 2012;10:134.

315. Mincheva-Nilsson L, Nagaeva O, Chen T, Stendahl U, Antsiferova J, Mogren I, et al. Placenta-derived soluble MHC class I chain-related molecules down-regulate NKG2D receptor on peripheral blood mononuclear cells during human pregnancy: a possible novel immune escape mechanism for fetal survival. J Immunol Baltim Md 1950. 2006 Mar 15;176(6):3585–92.

316. Jang SC, Kim OY, Yoon CM, Choi D-S, Roh T-Y, Park J, et al. Bioinspired Exosome-Mimetic Nanovesicles for Targeted Delivery of Chemotherapeutics to Malignant Tumors. ACS Nano. 2013 Sep 24;7(9):7698–710.

317. Jo W, Kim J, Yoon J, Jeong D, Cho S, Jeong H, et al. Large-scale generation of cell-derived nanovesicles. Nanoscale. 2014 Oct 21;6(20):12056–64.

318. De La Peña H, Madrigal JA, Rusakiewicz S, Bencsik M, Cave GWV, Selman A, et al. Artificial exosomes as tools for basic and clinical immunology. J Immunol Methods. 2009 May 31;344(2):121–32.

319. Kooijmans SAA, Vader P, van Dommelen SM, van Solinge WW, Schiffelers RM. Exosome mimetics: a novel class of drug delivery systems. Int J Nanomedicine. 2012;7:1525–41.

320. Jeong D, Jo W, Yoon J, Kim J, Gianchandani S, Gho YS, et al. Nanovesicles engineered from ES cells for enhanced cell proliferation. Biomaterials. 2014 Nov;35(34):9302–10.

321. Takahashi K, Yamanaka S. Induction of pluripotent stem cells from mouse embryonic and adult fibroblast cultures by defined factors. Cell. 2006 Aug 25;126(4):663–76.

322. Takahashi K, Tanabe K, Ohnuki M, Narita M, Ichisaka T, Tomoda K, et al. Induction of pluripotent stem cells from adult human fibroblasts by defined factors. Cell. 2007 Nov 30;131(5):861–72.

323. Malik N, Rao MS. A review of the methods for human iPSC derivation. Methods Mol Biol Clifton NJ. 2013;997:23–33.

324. Mi H, Muruganujan A, Thomas PD. PANTHER in 2013: modeling the evolution of gene function, and other gene attributes, in the context of phylogenetic trees. Nucleic Acids Res. 2013 Jan;41(Database issue):D377–86.

325. Skog J, Würdinger T, van Rijn S, Meijer DH, Gainche L, Sena-Esteves M, et al. Glioblastoma microvesicles transport RNA and proteins that promote tumour growth and provide diagnostic biomarkers. Nat Cell Biol. 2008 Dec;10(12):1470–6.

326. Schwille P. Fluorescence correlation spectroscopy and its potential for intracellular applications. Cell Biochem Biophys. 2001;34(3):383–408.

327. Sezgin E, Schwille P. Fluorescence techniques to study lipid dynamics. Cold Spring Harb Perspect Biol. 2011 Nov;3(11):a009803.

328. Hink MA, Griep RA, Borst JW, van Hoek A, Eppink MHM, Schots A, et al. Structural Dynamics of Green Fluorescent Protein Alone and Fused with a Single Chain Fv Protein. J Biol Chem. 2000 Jun 9;275(23):17556–60.

329. Webber J, Clayton A. How pure are your vesicles? J Extracell Vesicles. 2013;2.

330. Ghossoub R, Lembo F, Rubio A, Gaillard CB, Bouchet J, Vitale N, et al. Syntenin-ALIX exosome biogenesis and budding into multivesicular bodies are controlled by ARF6 and PLD2. Nat Commun [Internet]. 2014 Mar 18 [cited 2014 Jul 17];5. Available from: http://www.nature.com/doifinder/10.1038/ncomms4477

331. Ostrowski M, Carmo NB, Krumeich S, Fanget I, Raposo G, Savina A, et al. Rab27a and Rab27b control different steps of the exosome secretion pathway. Nat Cell Biol. 2010 Jan;12(1):19–30; sup pp 1–13.

332. Pfeffer SR. Two Rabs for exosome release. Nat Cell Biol. 2010 Jan;12(1):3–4.

333. De Jong OG, Verhaar MC, Chen Y, Vader P, Gremmels H, Posthuma G, et al. Cellular stress conditions are reflected in the protein and RNA content of endothelial cell-derived exosomes. J Extracell Vesicles [Internet]. 2012 Apr 16 [cited 2012 Dec 13];1(0). Available from: http://www.journalofextracellularvesicles.net/index.php/jev/article/view/18396

334. Philips M-A, Vikeså J, Luuk H, Jønson L, Lilleväli K, Rehfeld JF, et al. Characterization of MYG1 gene and protein: subcellular distribution and function. Biol Cell Auspices Eur Cell Biol Organ. 2009 Jun;101(6):361–73.

335. Alexander JK, Cox GM, Tian J-B, Zha AM, Wei P, Kigerl KA, et al. Macrophage migration inhibitory factor (MIF) is essential for inflammatory and neuropathic pain and enhances pain in response to stress. Exp Neurol. 2012 Aug;236(2):351–62.

336. Cheong AWY, Lee Y-L, Liu W-M, Yeung WSB, Lee K-F. Oviductal microsomal epoxide hydrolase (EPHX1) reduces reactive oxygen species (ROS) level and enhances preimplantation mouse embryo development. Biol Reprod. 2009 Jul;81(1):126–32.

337. Steele FR, Chader GJ, Johnson LV, Tombran-Tink J. Pigment epithelium-derived factor: neurotrophic activity and identification as a member of the serine protease inhibitor gene family. Proc Natl Acad Sci U S A. 1993 Feb 15;90(4):1526–30.

338. Crawford SE, Stellmach V, Ranalli M, Huang X, Huang L, Volpert O, et al. Pigment epithelium-derived factor (PEDF) in neuroblastoma: a multifunctional mediator of Schwann cell antitumor activity. J Cell Sci. 2001 Dec;114(Pt 24):4421–8.

339. Samkharadze T, Erkan M, Reiser-Erkan C, Demir IE, Kong B, Ceyhan GO, et al. Pigment Epithelium-Derived Factor Associates With Neuropathy and Fibrosis in Pancreatic Cancer. Am J Gastroenterol. 2011 May;106(5):968–80.

340. Bard MP, Hegmans JP, Hemmes A, Luider TM, Willemsen R, Severijnen L-AA, et al. Proteomic analysis of exosomes isolated from human malignant pleural effusions. Am J Respir Cell Mol Biol. 2004 Jul;31(1):114–21.

341. Shelke GV, Lässer C, Gho YS, Lötvall J. Importance of exosome depletion protocols to eliminate functional and RNA-containing extracellular vesicles from fetal bovine serum. J Extracell Vesicles [Internet]. 2014 Sep 30 [cited 2014 Nov 19];3(0).

Available from:
http://www.journalofextracellularvesicles.net/index.php/jev/article/view/24783

342. Momen-Heravi F, Balaj L, Alian S, Mantel P-Y, Halleck AE, Trachtenberg AJ, et al. Current methods for the isolation of extracellular vesicles. Biol Chem. 2013 Oct 1;394(10):1253–62.

343. Lamparski HG, Metha-Damani A, Yao J-Y, Patel S, Hsu D-H, Ruegg C, et al. Production and characterization of clinical grade exosomes derived from dendritic cells. J Immunol Methods. 2002 Dec 15;270(2):211–26.

344. Merchant ML, Powell DW, Wilkey DW, Cummins TD, Deegens JK, Rood IM, et al. Microfiltration isolation of human urinary exosomes for characterization by MS. Proteomics Clin Appl. 2010 Jan;4(1):84–96.

345. Grant R, Ansa-Addo E, Stratton D, Antwi-Baffour S, Jorfi S, Kholia S, et al. A filtration-based protocol to isolate human plasma membrane-derived vesicles and exosomes from blood plasma. J Immunol Methods. 2011 Aug 31;371(1-2):143–51.

346. Maruyama T, Katoh S, Nakajima M, Nabetani H. Mechanism of bovine serum albumin aggregation during ultrafiltration. Biotechnol Bioeng. 2001 Oct 20;75(2):233–8.

347. Chollet P, Favrot MC, Hurbin A, Coll J-L. Side-effects of a systemic injection of linear polyethylenimine-DNA complexes. J Gene Med. 2002 Feb;4(1):84–91.

348. Verbaan FJ, Oussoren C, van Dam IM, Takakura Y, Hashida M, Crommelin DJ, et al. The fate of poly(2-dimethyl amino ethyl)methacrylate-based polyplexes after intravenous administration. Int J Pharm. 2001 Feb 19;214(1-2):99–101.

349. Ratajczak J, Miekus K, Kucia M, Zhang J, Reca R, Dvorak P, et al. Embryonic stem cell-derived microvesicles reprogram hematopoietic progenitors: evidence for horizontal transfer of mRNA and protein delivery. Leuk Off J Leuk Soc Am Leuk Res Fund UK. 2006 May;20(5):847–56.

350. Katsman D, Stackpole EJ, Domin DR, Farber DB. Embryonic stem cell-derived microvesicles induce gene expression changes in Müller cells of the retina. PloS One. 2012;7(11):e50417.

351. Eitan E, Zhang S, Witwer KW, Mattson MP. Extracellular vesicle–depleted fetal bovine and human sera have reduced capacity to support cell growth. J Extracell Vesicles [Internet]. 2015 Mar 26 [cited 2015 Apr 18];4(0). Available from: http://www.journalofextracellularvesicles.net/index.php/jev/article/view/26373

352. Schulz TC, Noggle SA, Palmarini GM, Weiler DA, Lyons IG, Pensa KA, et al. Differentiation of human embryonic stem cells to dopaminergic neurons in serum-free suspension culture. Stem Cells Dayt Ohio. 2004;22(7):1218–38.

353. Garcia-Gonzalo FR, Izpisúa Belmonte JC. Albumin-Associated Lipids Regulate Human Embryonic Stem Cell Self-Renewal. Rutherford S, editor. PLoS ONE. 2008 Jan 2;3(1):e1384.

354. Mathivanan S, Lim JWE, Tauro BJ, Ji H, Moritz RL, Simpson RJ. Proteomics Analysis of A33 Immunoaffinity-purified Exosomes Released from the Human Colon Tumor Cell Line LIM1215 Reveals a Tissue-specific Protein Signature. Mol Cell Proteomics. 2010 Feb 1;9(2):197–208.

355. Théry C, Amigorena S, Raposo G, Clayton A. Isolation and characterization of exosomes from cell culture supernatants and biological fluids. Curr Protoc Cell Biol Editor Board Juan Bonifacino Al. 2006 Apr;Chapter 3:Unit 3.22.

356. Koivisto H, Hyvärinen M, Strömberg A-M, Inzunza J, Matilainen E, Mikkola M, et al. Cultures of human embryonic stem cells: serum replacement medium or serum-containing media and the effect of basic fibroblast growth factor. Reprod Biomed Online. 2004 Jan;9(3):330–7.

357. Wang X, Jauch R. OCT4: A penetrant pluripotency inducer. Cell Regen. 2014;3(1):6.

358. Barrès C, Blanc L, Bette-Bobillo P, André S, Mamoun R, Gabius H-J, et al. Galectin-5 is bound onto the surface of rat reticulocyte exosomes and modulates vesicle uptake by macrophages. Blood. 2010 Jan 21;115(3):696–705.

359. Fevrier B, Vilette D, Archer F, Loew D, Faigle W, Vidal M, et al. Cells release prions in association with exosomes. Proc Natl Acad Sci U S A. 2004 Jun 29;101(26):9683–8.

360. Schofield R. The relationship between the spleen colony-forming cell and the haemopoietic stem cell. Blood Cells. 1978;4(1-2):7–25.

361. Levenberg S, Golub JS, Amit M, Itskovitz-Eldor J, Langer R. Endothelial cells derived from human embryonic stem cells. Proc Natl Acad Sci U S A. 2002 Apr 2;99(7):4391–6.

362. Siu CW, Moore JC, Li RA. Human embryonic stem cell-derived cardiomyocytes for heart therapies. Cardiovasc Hematol Disord Drug Targets. 2007 Jun;7(2):145–52.

363. Jensen J, Hyllner J, Björquist P. Human embryonic stem cell technologies and drug discovery. J Cell Physiol. 2009 Jun;219(3):513–9.

364. Urbach A, Bar-Nur O, Daley GQ, Benvenisty N. Differential Modeling of Fragile X Syndrome by Human Embryonic Stem Cells and Induced Pluripotent Stem Cells. Cell Stem Cell. 2010 May;6(5):407–11.

365. Mou H, Zhao R, Sherwood R, Ahfeldt T, Lapey A, Wain J, et al. Generation of multipotent lung and airway progenitors from mouse ESCs and patient-specific cystic fibrosis iPSCs. Cell Stem Cell. 2012 Apr 6;10(4):385–97.

366. Thomson JA, Itskovitz-Eldor J, Shapiro SS, Waknitz MA, Swiergiel JJ, Marshall VS, et al. Embryonic stem cell lines derived from human blastocysts. Science. 1998 Nov 6;282(5391):1145–7.

367. McLaren A. Ethical and social considerations of stem cell research. Nature. 2001 Nov 1;414(6859):129–31.

368. Zhao T, Zhang Z-N, Rong Z, Xu Y. Immunogenicity of induced pluripotent stem cells. Nature. 2011 Jun 9;474(7350):212–5.

369. Okita K, Yamanaka S. Induced pluripotent stem cells: opportunities and challenges. Philos Trans R Soc Lond B Biol Sci. 2011 Aug 12;366(1575):2198–207.

370. Fusaki N, Ban H, Nishiyama A, Saeki K, Hasegawa M. Efficient induction of transgene-free human pluripotent stem cells using a vector based on Sendai virus, an RNA virus that does not integrate into the host genome. Proc Jpn Acad Ser B Phys Biol Sci. 2009;85(8):348–62.

371. Warren L, Manos PD, Ahfeldt T, Loh Y-H, Li H, Lau F, et al. Highly efficient reprogramming to pluripotency and directed differentiation of human cells with synthetic modified mRNA. Cell Stem Cell. 2010 Nov 5;7(5):618–30.

372. Kim D, Kim C-H, Moon J-I, Chung Y-G, Chang M-Y, Han B-S, et al. Generation of human induced pluripotent stem cells by direct delivery of reprogramming proteins. Cell Stem Cell. 2009 Jun 5;4(6):472–6.

373. Stadtfeld M, Nagaya M, Utikal J, Weir G, Hochedlinger K. Induced pluripotent stem cells generated without viral integration. Science. 2008 Nov 7;322(5903):945–9.

374. Xu X, Zhong Z. Disease modeling and drug screening for neurological diseases using human induced pluripotent stem cells. Acta Pharmacol Sin. 2013 Jun;34(6):755–64.

375. Miura K, Okada Y, Aoi T, Okada A, Takahashi K, Okita K, et al. Variation in the safety of induced pluripotent stem cell lines. Nat Biotechnol. 2009 Aug;27(8):743–5.

376. Boulting GL, Kiskinis E, Croft GF, Amoroso MW, Oakley DH, Wainger BJ, et al. A functionally characterized test set of human induced pluripotent stem cells. Nat Biotechnol. 2011 Mar;29(3):279–86.

377. Gutierrez-Aranda I, Ramos-Mejia V, Bueno C, Munoz-Lopez M, Real PJ, Mácia A, et al. Human Induced Pluripotent Stem Cells Develop Teratoma More Efficiently and Faster Than Human Embryonic Stem Cells Regardless the Site of Injection. STEM CELLS. 2010 Sep;28(9):1568–70.

378. Chin MH, Mason MJ, Xie W, Volinia S, Singer M, Peterson C, et al. Induced pluripotent stem cells and embryonic stem cells are distinguished by gene expression signatures. Cell Stem Cell. 2009 Jul 2;5(1):111–23.

379. Marchetto MCN, Yeo GW, Kainohana O, Marsala M, Gage FH, Muotri AR. Transcriptional signature and memory retention of human-induced pluripotent stem cells. PloS One. 2009;4(9):e7076.

380. Deng J, Shoemaker R, Xie B, Gore A, LeProust EM, Antosiewicz-Bourget J, et al. Targeted bisulfite sequencing reveals changes in DNA methylation associated with nuclear reprogramming. Nat Biotechnol. 2009 Apr;27(4):353–60.

381. Doi A, Park I-H, Wen B, Murakami P, Aryee MJ, Irizarry R, et al. Differential methylation of tissue- and cancer-specific CpG island shores distinguishes human induced pluripotent stem cells, embryonic stem cells and fibroblasts. Nat Genet. 2009 Dec;41(12):1350–3.

382. Kim K, Zhao R, Doi A, Ng K, Unternaehrer J, Cahan P, et al. Donor cell type can influence the epigenome and differentiation potential of human induced pluripotent stem cells. Nat Biotechnol. 2011 Nov 27;29(12):1117–9.

383. Lister R, Pelizzola M, Kida YS, Hawkins RD, Nery JR, Hon G, et al. Hotspots of aberrant epigenomic reprogramming in human induced pluripotent stem cells. Nature. 2011 Mar 3;471(7336):68–73.

384. Ohi Y, Qin H, Hong C, Blouin L, Polo JM, Guo T, et al. Incomplete DNA methylation underlies a transcriptional memory of somatic cells in human iPS cells. Nat Cell Biol. 2011 May;13(5):541–9.

385. Hu B-Y, Weick JP, Yu J, Ma L-X, Zhang X-Q, Thomson JA, et al. Neural differentiation of human induced pluripotent stem cells follows developmental principles but with variable potency. Proc Natl Acad Sci U S A. 2010 Mar 2;107(9):4335–40.

386. Yamanaka S. Induced pluripotent stem cells: past, present, and future. Cell Stem Cell. 2012 Jun 14;10(6):678–84.

387. Davies TJ, Fairchild PJ. Optimization of Protocols for Derivation of Mouse Embryonic Stem Cell Lines from Refractory Strains, Including the Non Obese Diabetic Mouse. Stem Cells Dev. 2012 Jul;21(10):1688–700.

388. Carpenter L, Malladi R, Yang C-T, French A, Pilkington KJ, Forsey RW, et al. Human induced pluripotent stem cells are capable of B-cell lymphopoiesis. Blood. 2011 Apr 14;117(15):4008–11.

389. Silk KM, Tseng S-Y, Nishimoto KP, Lebkowski J, Reddy A, Fairchild PJ. Differentiation of dendritic cells from human embryonic stem cells. Methods Mol Biol Clifton NJ. 2011;767:449–61.

390. Silk KM, Silk JD, Ichiryu N, Davies TJ, Nolan KF, Leishman AJ, et al. Cross-presentation of tumour antigens by human induced pluripotent stem cell-derived CD141(+)XCR1+ dendritic cells. Gene Ther. 2012 Oct;19(10):1035–40.

391. Tseng S-Y, Nishimoto KP, Silk KM, Majumdar AS, Dawes GN, Waldmann H, et al. Generation of immunogenic dendritic cells from human embryonic stem cells without serum and feeder cells. Regen Med. 2009 Jul;4(4):513–26.

392. Graumann J, Hubner NC, Kim JB, Ko K, Moser M, Kumar C, et al. Stable Isotope Labeling by Amino Acids in Cell Culture (SILAC) and Proteome Quantitation of Mouse Embryonic Stem Cells to a Depth of 5,111 Proteins. Mol Cell Proteomics. 2007 Dec 3;7(4):672–83.

393. Munoz J, Low TY, Kok YJ, Chin A, Frese CK, Ding V, et al. The quantitative proteomes of human-induced pluripotent stem cells and embryonic stem cells. Mol Syst Biol. 2014 Apr 16;7(1):550–550.

394. Phanstiel DH, Brumbaugh J, Wenger CD, Tian S, Probasco MD, Bailey DJ, et al. Proteomic and phosphoproteomic comparison of human ES and iPS cells. Nat Methods. 2011 Sep 11;8(10):821–7.

395. Ginis I, Luo Y, Miura T, Thies S, Brandenberger R, Gerecht-Nir S, et al. Differences between human and mouse embryonic stem cells. Dev Biol. 2004 May 15;269(2):360–80.

396. Schnerch A, Cerdan C, Bhatia M. Distinguishing between mouse and human pluripotent stem cell regulation: the best laid plans of mice and men. Stem Cells Dayt Ohio. 2010 Mar 31;28(3):419–30.

397. Narsinh KH, Plews J, Wu JC. Comparison of human induced pluripotent and embryonic stem cells: fraternal or identical twins? Mol Ther J Am Soc Gene Ther. 2011 Apr;19(4):635–8.

398. Stadtfeld M, Hochedlinger K. Induced pluripotency: history, mechanisms, and applications. Genes Dev. 2010 Oct 15;24(20):2239–63.

399. Maherali N, Sridharan R, Xie W, Utikal J, Eminli S, Arnold K, et al. Directly reprogrammed fibroblasts show global epigenetic remodeling and widespread tissue contribution. Cell Stem Cell. 2007 Jun 7;1(1):55–70.

400. Okita K, Ichisaka T, Yamanaka S. Generation of germline-competent induced pluripotent stem cells. Nature. 2007 Jul 19;448(7151):313–7.

401. Mikkelsen TS, Hanna J, Zhang X, Ku M, Wernig M, Schorderet P, et al. Dissecting direct reprogramming through integrative genomic analysis. Nature. 2008 Jul 3;454(7200):49–55.

402. Osafune K, Caron L, Borowiak M, Martinez RJ, Fitz-Gerald CS, Sato Y, et al. Marked differences in differentiation propensity among human embryonic stem cell lines. Nat Biotechnol. 2008 Mar;26(3):313–5.

403. Ward CM, Barrow KM, Stern PL. Significant variations in differentiation properties between independent mouse ES cell lines cultured under defined conditions. Exp Cell Res. 2004 Feb 15;293(2):229–38.

404. Narsinh KH, Sun N, Sanchez-Freire V, Lee AS, Almeida P, Hu S, et al. Single cell transcriptional profiling reveals heterogeneity of human induced pluripotent stem cells. J Clin Invest. 2011 Mar;121(3):1217–21.

405. Boué S, Paramonov I, Barrero MJ, Izpisúa Belmonte JC. Analysis of Human and Mouse Reprogramming of Somatic Cells to Induced Pluripotent Stem Cells. What Is in the Plate? Dopazo J, editor. PLoS ONE. 2010 Sep 17;5(9):e12664.

406. Kurts C. CD11c: not merely a murine DC marker, but also a useful vaccination target. Eur J Immunol. 2008 Aug;38(8):2072–5.

407. Chen G, Gulbranson DR, Hou Z, Bolin JM, Ruotti V, Probasco MD, et al. Chemically defined conditions for human iPSC derivation and culture. Nat Methods. 2011 May;8(5):424–9.

408. Beers J, Gulbranson DR, George N, Siniscalchi LI, Jones J, Thomson JA, et al. Passaging and colony expansion of human pluripotent stem cells by enzyme-free dissociation in chemically defined culture conditions. Nat Protoc. 2012 Oct 25;7(11):2029–40.

409. Wang Y, Chou B-K, Dowey S, He C, Gerecht S, Cheng L. Scalable expansion of human induced pluripotent stem cells in the defined xeno-free E8 medium under adherent and suspension culture conditions. Stem Cell Res. 2013 Nov;11(3):1103–16.

410. Pegtel DM, Cosmopoulos K, Thorley-Lawson DA, van Eijndhoven MAJ, Hopmans ES, Lindenberg JL, et al. Functional delivery of viral miRNAs via exosomes. Proc Natl Acad Sci U S A. 2010 Apr 6;107(14):6328–33.

411. Nolte-'t Hoen ENM, Buermans HPJ, Waasdorp M, Stoorvogel W, Wauben MHM, 't Hoen PAC. Deep sequencing of RNA from immune cell-derived vesicles uncovers the selective incorporation of small non-coding RNA biotypes with potential regulatory functions. Nucleic Acids Res. 2012 Oct 1;40(18):9272–85.

412. Nair R, Santos L, Awasthi S, von Erlach T, Chow LW, Bertazzo S, et al. Extracellular Vesicles Derived from Preosteoblasts Influence Embryonic Stem Cell Differentiation. Stem Cells Dev. 2014 Jul 15;23(14):1625–35.

413. Zhang J, Guan J, Niu X, Hu G, Guo S, Li Q, et al. Exosomes released from human induced pluripotent stem cells-derived MSCs facilitate cutaneous wound healing by promoting collagen synthesis and angiogenesis. J Transl Med [Internet]. 2015 Dec [cited 2015 Apr 18];13(1). Available from: http://www.translational-medicine.com/content/13/1/49

Chapter 8: Appendix

Appendix 8.1 Conferences and Seminar presentations

Year: 2012

Name of conference: International Society for Extracellular Vesicles (ISEV) 2012
Location of conference: Gothenburg, Sweden.
Date of conference: 18th-21st April 2012

- Abstract 1 accepted for oral presentation

"Characterisation of exosomes isolated from dendritic cells differentiatied from human iPS cells"
Lee Y, Li J, Gardiner C, Leishman A, Davies T, EL Andaloussi S, Sargent I, Fairchild P, Wood MJ

- Abstract 2 accepted for oral presentation

"Characterisation of exosomes secreted from neuronal sources"
Li J, **Lee Y**, Gardiner C, EL Andaloussi S, Lakhal-Littleton S, Sargent I, Wood MJ

Year: 2013

Name of conference: International Society for Extracellular Vesicles (ISEV) 2013
Location of conference: Boston, USA
Date of conference: 17th- 20th April 2013

- Abstract 1 accepted for poster presentation

" Characterisation fo exosomes from human induced pluripotent stem cells (hiPSCs) and dendritic cells differentiated from hiPSC (hiPSC-DCs)"
Lee Y, Leishman A, Sachamitr P, Davies T, EL Andaloussi S, Fairchild P, Wood MJ

- Abstract 2 accepted for poster presentation

"LC purification of exosomes: way forward or dead end?"
Nordin, JZ, **Lee Y**, Wiklander OPB, Vader P, Smith Ed, EL Andaloussi S

- Abstract 3 accepted for poster presentation

"Exosomes for delivery of small RNAs to tumours"
Vader P, Nordin JZ, Wiklander O, **Lee Y**, Roberts T, Seow Y, El Andaloussi S, Wood MJ

- Abstract 4 accepted for poster presentation

"Characterisation of exosomes secreted from in vitro neuronal cell lines"
Li J, **Lee Y**, Vader P, EL Andaloussi S, Mager I, Gardiner C, Sargent I, Wood MJ

Year: 2014

Name of conference: International Society for Extracellular Vesicles (ISEV) 2014
Location of conference: Rotterdam, Netherlands
Date of conference: 30th April- 3rd May 2014

- Abstract 1 accepted for poster presentation

"Characterisation of extracellular vesicles (EVs) from the secretome of human induced pluripotent stem cells (iPSCs) during the differentiation into dendritic cells (DCs)"
Lee Y, Leishman A, Sachamitr P, Davies T, EL Andaloussi S, Fairchild P, Wood MJ

- Abstract 2 accepted for oral presentation

"Ultrafiltraton and size exclusion liquid chromatography enable high yield isolation of pure exosomes that retain their biophysical properties"
EL Andaloussi S, Nordin JZ, **Lee Y**, Vader P, Johansson H, Gardiner C, Heusermann W, Wiklander O, Mager, Wood MJ

- Abstract 3 accepted for poster presentation

"Characterisation fo proteomic and RNA profiles of extracellular vesicles and non-vesicular secreted material"
Mager I, **Lee Y**, Sork H, Nordin J, Heldring N, Wiklander O, Vader P, Johansson H, Lethio J, Le Blanc K, EL Andaloussi S, Wood MJ

- Abstract 4 accepted for poster presentation

"Extracellular vesicles for delivery of small RNAs"
Vader P, **Lee Y**, Mager I, EL Andaloussi S, Wood MJ

- Abstract 5 accepted for poster presentation

"Biodistribution of exosomes: evaluation of different cell sources, does and time points"
Wiklander O, Nordin J, O'Loughlin A, **Lee Y**, Alvarez-Erviti L, Mager I, Vader P, Smith Ed, Wood MJ, EL Andaloussi S

Year: 2015

Name of conference: International Society for Extracellular Vesicles (ISEV) 2015
Location of conference: North Bethesda, Washington DC, USA
Date of conference: 23rd April- 26th April 2015

- Abstract 1 accepted for poster presentation

"Investigation on how different purification methodologies can affect the characterization of extracellular vesicles from pluripotent stem cell sources"
Lee Y, Mager I, Wood MJ, EL Andaloussi S

- Abstract 2 accepted for poster presentation

"Characterization and functional evaluation of distinct subpopulations of extracellular vesicles released by melanoma cells"
Vader P, Willms E, Johansson H, Mäger I, **Lee Y**, Lehtio J, EL Andaloussi S, Wood MJ

Appendix 8.2 Manuscripts accepted for publication

Year 2012

Title of review: Exosomes and microvesicles: extracellular vesicles for genetic information transfer and gene therapy.
List of authors: **Lee Y**, EL Andaloussi S, Wood MJ
Name of journal: Human Molecular Genetics, Vol 21(R1): R125-34
doi: 10.1093/hmg/dds317 Epub on Aug 7, 2012

Title of paper: Exosome-mediated delivery of siRNA in vitro and in vivo
List of authors: EL-Andaloussi S*, **Lee Y***, Lakhal-Littleton S*, Li J, Seow Y, Gardiner C, Alvarez-Erviti L, Sargent IL, Wood MJ
Name of journal: Nature Protocols, 7(12): 2112-26
doi: 10.1038/nprot.2012.131 Epub on Nov 15, 2012
* co-1st author

Year 2014

Title of paper: Correlating In Vitro Splice Switching Activity With Systemic In Vivo Delivery Using Novel ZEN-modified Oligonucleotides
List of authors: Hammond SM, McClorey G, Nordin JZ, Godfrey C, Stenler S, Lennox KA, Smith CI, Jacobi AM, Varela MA, **Lee Y**, Behlke MA, Wood MJ, EL Andaloussi S
Name of journal: Molecular Therapy Nucleic Acids
2014 Nov 25;3:e212. doi: 10.1038/mtna.2014.63

Year 2015

Title of paper: Serum-free culturing conditions alter the quantity and protein composition of neuroblastoma-derived extracellular vesicles
List of authors: Li J*, **Lee Y***, Johansson H, Mager I, Vader P, Nordin JZ, Wikander O, Lehtio J, EL Andaloussi S, Wood MJ
Name of journal: Journal of Extracellular Vesicles (JEV)
Manuscript accepted on 15th April 2015
* co-1st author

Title of paper: Ultrafiltration with size-exclusion liquid chromatography for high yield isolation of extracellular vesicles preserving intact biophysical and functional properties
List of authors: Nordin JZ*, **Lee Y***, Vader P, Mager I, Johansson H, Heusermann W, Wiklander O, Hallbrink M, Seow Y, Bultema, J, Gilthorpe J, Davies T, Fairchild P, Gabrielsson S, Meisner-Kober N, Lehtio J, Smith CI, Wood MJ, EL Andaloussi S
Name of journal: Nanomedicine: Nanotechnology, Biology and Medicine (NBM)
2015 Feb 4. pii: S1549-9634(15)00027-1. doi: 10.1016/j.nano.2015.01.003
* co-1st author

Title of paper: Extracellular vesicle in vivo biodistribution is determined by cell source, route of administraiton and targeting
List of authors: Wiklander OPB, Nordin JZ, O'Loughlin A, Gustafsson Y, Mager I, Vader P, **Lee Y**, Corso G, Sork H, Seow Y, Heldring N, Alvarez-Erviti L, Smith CI, Le Blanc K, Macchiarini P, Jungebluth P, Wood MJ, EL Andaloussi S
Name of journal: Journal of Extracellular Vesicles (JEV)
Manuscript accepted on 20th March 2015, 10.3402/jev.v4.26316